



HAL
open science

Synthesis of enantiopure 3,4-dihydro-2H-1,4-benzoxazine analogues for potential biological applications

Hong-Ngoc Pham

► **To cite this version:**

Hong-Ngoc Pham. Synthesis of enantiopure 3,4-dihydro-2H-1,4-benzoxazine analogues for potential biological applications. Chemical and Process Engineering. Université de Lorraine, 2020. English. NNT : 2020LORR0186 . tel-03176568

HAL Id: tel-03176568

<https://hal.univ-lorraine.fr/tel-03176568v1>

Submitted on 22 Mar 2021

HAL is a multi-disciplinary open access archive for the deposit and dissemination of scientific research documents, whether they are published or not. The documents may come from teaching and research institutions in France or abroad, or from public or private research centers.

L'archive ouverte pluridisciplinaire **HAL**, est destinée au dépôt et à la diffusion de documents scientifiques de niveau recherche, publiés ou non, émanant des établissements d'enseignement et de recherche français ou étrangers, des laboratoires publics ou privés.



AVERTISSEMENT

Ce document est le fruit d'un long travail approuvé par le jury de soutenance et mis à disposition de l'ensemble de la communauté universitaire élargie.

Il est soumis à la propriété intellectuelle de l'auteur. Ceci implique une obligation de citation et de référencement lors de l'utilisation de ce document.

D'autre part, toute contrefaçon, plagiat, reproduction illicite encourt une poursuite pénale.

Contact : ddoc-theses-contact@univ-lorraine.fr

LIENS

Code de la Propriété Intellectuelle. articles L 122. 4

Code de la Propriété Intellectuelle. articles L 335.2- L 335.10

http://www.cfcopies.com/V2/leg/leg_droi.php

<http://www.culture.gouv.fr/culture/infos-pratiques/droits/protection.htm>



UNIVERSITÉ
DE LORRAINE

SIMPPÉ



DISSERTATION

Doctoral School: **SIMPPÉ**

Specialty: **Génie des Procédés, des Produits et des Molécules**

SYNTHESIS OF ENANTIOPURE 3,4-DIHYDRO- 2H-1,4-BENZOXAZINE ANALOGUES FOR POTENTIAL BIOLOGICAL APPLICATIONS

To obtain the degree of
Doctor of Philosophy

Presented by

Hong-Ngoc PHAM

Dissertation defense: **the 10th December, 2020**

Jury Members

Claude TAILLEFUMIER	Prof., Université Clermont Auvergne	Reviewer
Sylvain ROUTIER	Prof., Université d'Orléans	Reviewer
Céline FROCHOT	DR, Université de Lorraine	Examinator (President of Jury)
Maud LARREGOLA	MC, Université de Cergy-Pontoise	Examinator
Samir ACHERAR	MC-HDR, Université de Lorraine	Thesis Director
Axelle ARRAULT	MC, Université de Lorraine	Thesis Co-director

To my family,
and my uncle Tuan-Dung VO

ACKNOWLEDGEMENTS

First and foremost, I would like to express my extremely grateful to my two supervisors Dr. Samir ACHERAR and Dr. Axelle ARRAULT for all your supports and encouragements that you gave me throughout these years. I can still recall all the difficulties we have had for the first two years. I really appreciate your patience for leading me the way step-by-step to this success I achieved today. I am considered myself as a lucky person for having you as my PhD supervisors.

I would like to thank Prof. Sylvain ROUTIER, Prof. Claude TAILLEFUMIER, Dr. Céline FROCHOT and Dr. Maud LARREGOLA for the acceptance to be as part of my dissertation jury. The discussion we had and your suggestions made my research so much richer.

I want to send my big thanks to each and every members of Laboratoire de Chimie-Physique Macromoléculaire (LCPM): Prof. Alain DURAND, Dr. Marie-Christine AVERLANT-PETIT, Dr. Jacques BODIGUEL, Dr. Guillaume PICKAERT, Dr. Loïc STEFAN for their kindness, supports and a pleasant working environment. Additionally, I would like to give a special thank Monsieur Olivier FABRE for the NMR analyses and Madame Mathilde ACHARD for analysis of mass spectroscopy et her guidance for the use of all equipments and devices in the laboratory.

Futhermore, I greatly appreciated Dr. Nicolas VANTHUYNE at “Plateforme de Chromatographie Chirale” in Aix-Marseille University for his support on HPLC enantioseparation part, also I want to thank Dr. Emmanuel WENGER (CRM2) for the X-Ray diffraction measurements.

I would also like to thank Ministry of Education and Training of Vietnam (MOET) and Vietnam-France University (University of Science and Technology of Hanoi – USTH) for the financial support and giving me a chance to do my PhD in France.

Especially, I want to express my gratefulness to Tany SAHYOUN, Olga OVDIICHUK and Tristan GIRAUD who are truly good friends and colleagues, not only because of their supports in work but also for all moment we shared together in daily life, as a friend. I cannot get to this step if I don't have you all beside me to encourage me through difficulties and stresses. I don't have many friends in life but thanks Gods for giving me the most valuable ones. I will never

forget you all and I can guarantee that we will reunite one day not so far. Deep inside my heart, I do appreciate to everything you've done for me since the first time I was alone coming to France and start getting to know a new environment, new culture, new language.

Additionally, I also would like to thank Géraldine RANGEL, Amina BEN-MIHOUB, Lison THEVENART-BRIOUX, Mohamed IBRAHIM for cheering me all the time, especially Amina who always has positive vibe and she transfer it to me to raise me up every Monday morning.

I send a big thank to my best friend in Vietnam, Thi-Ngoc-Mai NGUYEN who also always cheer me up through the most difficult time when I am unfamiliar to France, despite of the distance 6 hours, she always be there for me.

I want to give a huge hug and appreciation to my boyfriend, Bao-Trung DOAN for always beside me, supporting me, encouraging me, making me laugh, listening to all my problems even they are small or big. He is also a big energy source pushing me move forward. Even we have been in a long-distance relationship but he is one of my motivation to finish this work. Thank you so much!

At last, I am extremely grateful to all members in my family for always support, encourage me and care about me. I am thankful for all the things they have done for me, they are my big motivation, my huge energy source where I can always be fully charged after each exhausted working day. Thank all my cousins, my little brother for always making me laugh. A thank will be not enough to describe my appreciation for you.

I want to dedicate this thesis to my uncle Tuan-Dung VO, he passed away on my birthday in 2018. At that moment, my work also seemed not so good with many difficulties and I could say that it was the hardest time I have ever had in my life. For me, he was and always be my second dad! I just wanna say I love him so much and we do miss you, uncle Dung. Even he could not see how I successfully reached to this step but I know he would be proud of me in the other world.

Table of Contents

LIST OF ABBREVIATIONS	1
RÉSUMÉ DÉTAILLÉ.....	4
CHAPTER I	11
1. General introduction.....	12
1.1. Pseudopeptides.....	12
1.2. Optical active compound (enantiomer).....	14
1.3. Chiral High-Resolution Liquid Chromatography	17
1.4. Determination of optical value, absolute configuration and enantiomeric purity.....	19
2. 1,4-benzoxazines as potential scaffold for therapeutic applications	21
3. Synthetic routes for 1,4-benzoxazine derivatives	27
3.1. Synthetic routes for racemate 1,4-benzoxazine derivatives.....	27
3.2. Synthetic routes for chiral 1,4-benzoxazine derivatives	29
REFERENCES	36
CHAPTER II.....	45
1. Synthetic plan.....	46
2. Obtainment of chiral ethyl 2,3-dibromopropionate (<i>S</i>)-1 and (<i>R</i>)-1	47
2.1. <i>Via</i> enantioselective synthesis.....	47
2.2. <i>Via</i> preparative HPLC enantioseparation of commercially available <i>rac</i> -1 on multigram scale.....	51
2.2.1. Analytical HPLC enantioseparation	51
2.2.2. <i>Via</i> preparative HPLC enantioseparation of <i>rac</i> -1 on multigram scale.....	53
2.3. Optical rotation value of (<i>S</i>)-1 and (<i>R</i>)-1	54
2.4. Racemization during enantioselective synthesis of (<i>S</i>)-1.....	55
2.4.1. Synthesis condition of (<i>S</i>)-1 (Method C).....	56

3. Obtainment of chiral ethyl 3,4-dihydro-2 <i>H</i> -1,4-benzoxazine-2-carboxylate.....	57
3.1. Obtainment of (<i>R</i>)-2 <i>via</i> enantioselective synthesis.....	59
3.2. Obtainment of (<i>S</i>)-2 and (<i>R</i>)-2 <i>via</i> preparative HPLC enantioseparation of racemate on multigram scale	59
3.2.1. Analytical chiral HPLC	59
3.2.2. Preparative HPLC enantioseparation of <i>rac</i> -2 on multigram scale.....	61
3.3. Absolute configuration (AC) and optical rotation value determination.....	62
3.3.1. Computational chemistry for AC determination	62
3.3.2. Optical rotation values.....	64
3.4. Racemization during enantioselective synthesis of (<i>R</i>)-2	65
4. Synthesis of chiral pseudopeptide bearing 1,4-benzoxazine moiety	68
4.1. Elongation of <i>N</i> -terminal extremity (synthesis of pseudodipeptides).....	68
4.1.1. Coupling with Boc-protected α -amino acids	68
4.1.2. Coupling with Fmoc-protected α -amino acids	70
4.2. Elongation of <i>C</i> -terminal extremity (synthesis of pseudodipeptides).....	71
4.3. Elongation of <i>C</i> - and <i>N</i> -terminal extremities (synthesis of pseudotripeptides)	71
CHAPTER III	77
1. General introduction.....	78
2. Conformational study of 1,4-benzoxazine-based pseudodipeptides	79
2.1. Conformational study of (<i>S</i>)-2, (<i>R</i>)-2 and <i>rac</i> -16 as reference models.....	79
2.1.1. Solution state analysis of (<i>S</i>)-2, (<i>R</i>)-2 and <i>rac</i> -16	79
2.1.2. Solid state analysis of <i>rac</i> -16.....	83
2.2. Solution state analysis of compounds (<i>S,S</i>)- and (<i>R,S</i>)-9, -10.....	84
2.3. Conformational study of compounds (<i>S,S</i>)- and (<i>R,S</i>)-11, -12	89
2.3.1. Solution state analysis of compounds (<i>S,S</i>)- and (<i>R,S</i>)-11, -12	89
2.3.2. Solid state analysis of compounds (<i>S,S</i>)-11, (<i>R,S</i>)-11 and (<i>S,S</i>)-12.....	95
3. Conformational study of 1,4-benzoxazine-based pseudotripeptides.....	101

3.1. Conformational study of (S,S)- and (R,S)-8 as reference models	101
3.2. Conformational study of (S,S,S)-13, -14 and (S,R,S)-13, -14.....	102
3.2.1. Solution state analysis of (S,S,S)-13, -14 and (S,R,S)-13, -14	102
3.2.2. Solid state analysis of compound (S,R,S)-13	106
3.3. Conformational study of (S,S,S)- and (S,R,S)-15	108
4. Conclusion.....	111
REFERENCE.....	114
GENERAL CONCLUSIONS AND PERSPECTIVES	115
1. General conclusions	116
2. Perspectives.....	120
EXPERIMENTAL PART	124
APPENDIX 1.....	151
APPENDIX 2.....	153
APPENDIX 3.....	161

LIST OF ABBREVIATIONS

Å	Ångström
AA	Amino acid
ADH	AntiDiuretic Hormone
Ala	Alanine
Bn	Benzyl
Boc	<i>tert</i> -butyloxycarbonyl
CD	Circular dichroism
COSY	CORrelated SpectroscopY
CSP	Chiral Stationary Phase
DCC	DiCyclohexylCarbodiimide
DMF	<i>N,N</i> -DiMethylFornamide
DMSO	DiMethylSulfOxide
ECD	Electronic Circular Dichroism
EDCI	<i>N</i> -Ethyl- <i>N'</i> -(3-Dimethylamiopropyl)CarbodiImide hydrochloride
ee	Enantiomeric excess
Equiv.	Equivalent
ESI	ElectroSpray Ionization
Et ₂ O	Diethyl ether
EtOAc	Ethyl acetate
EtOH	Ethanol
Fmoc	Fluorenylmethoxycarbonyl
FTIR	Fourier-Transform InfraRed spectroscopy
g	Gram
h	Hour
HMBC	Heteronuclear Multiple Bond Correlation spectroscopy

HOBt	1-HydrOxyBenzotriazole
HPLC	High-Performance Liquid Chromatography
HRMS	High Resolution Mass Spectroscopy
HSQC	Heteronuclear Single Quantum Coherence spectroscopy
Hz	Hertz
L	Liter
LC-MS	Liquid Chromatography–Mass Spectrometry
M	Mole
MCT	Mercury-Cadmium-Telluride
Me	Methyl
MeCN	Acetonitrile
MeOH	Methanol
mg	Miligram
MHz	MegaHertz
min	Minute
mL	Milliliter
mM	Millimole
mp	Melting point
nm	Nanometer
NMM	4-methylmorpholine
NMP	<i>N</i> -Methyl-2-Pyrrolidone
NMR	Nuclear Magnetic Resonance
PE	Petroleum ether
Phe	Phenylalanine
ppm	Parts per million
RMS	Root-Mean-Square
RT/rt	Room Temperature

TD-DFT	Time-Dependent Density Functional Theory
TEA	TriEthylAmine
Tf ₂ O	Trifluoromethanesulfonic
TFA	TriFluoroacetic Acid
THF	TetraHydroFuran
TLC	Thin-Layer Chromatography
TMS	TetraMethylSilane
UV	UltraViolet
v/v	Volumn/volumn

RÉSUMÉ DÉTAILLÉ

Les peptides, chaînes comprenant 2 à 50 acides aminés environ, possèdent un grand potentiel pour la chimie médicinale. Les chaînes plus longues de peptides forment les protéines, qui jouent indéniablement un rôle important au sein du corps humain. Ainsi, les peptides fonctionnalisés peuvent être des hormones, des neuro-transmetteurs, des agents thérapeutiques, *etc...* Le terme « pseudopeptide » quant à lui, désigne des analogues de peptides dont une partie des liaisons peptidiques qui le composent sont modifiées dans le but d'augmenter la biodisponibilité et/ou de diminuer la dégradation par des protéases des peptides naturels utilisés en médecine. Par conséquent, la synthèse de tels composés pseudopeptidiques est un objectif fortement intéressant en matière de drug design.

En raison des nombreuses possibilités d'application des hétérocycles, les molécules comportant ces cycles sont au cœur du développement de nouveaux médicaments. La combinaison d'hétérocycles avec des acides aminés est une des nombreuses approches que l'on peut avoir dans la formation de pseudopeptides, où le cœur hétérocyclique sert de structure rigide liée aux acides α -aminés pour recréer des systèmes imitant des α -, β -, ou γ -turn. Parmi la grande variété de composés hétérocycliques, la 3,4-dihydro-2*H*-1,4-benzoxazine et ses dérivés ont été dépeints comme des candidats prometteurs pour de nombreuses applications thérapeutiques. Cette classe fascinante de composés hétérocycliques présente différentes propriétés intéressantes en biologie, comme par exemple une capacité anti-bactérienne, de protection du système cardio-vasculaire, ou contre l'hypertension. De plus, la molécule qui nous intéresse, le 3,4-dihydro-2*H*-1,4-benzoxazine-2-carboxylate d'éthyle **2**, comporte un atome d'azote (Figure 1) ; sa structure est proche de celle d'un acide β -aminé, avec un groupe ester lié au carbone α et un groupe amine lié au carbone β . Par conséquent, c'est un atout intéressant pour la chimie médicinale puisqu'il peut permettre de mimer un β -turn qui joue un rôle important dans divers systèmes de reconnaissance biologique.

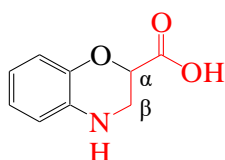


Figure 1 3,4-dihydro-2*H*-1,4-benzoxazine-2-carboxylate d'éthyle **2** comme analogue d'acide β -aminé

La synthèse énantiosélective est devenue un sujet phare de la recherche en pharmacochimie étant donnée la sélectivité des récepteurs biologiques et la différence d'activité des

énantiomères. De nombreux composés chiraux, où un énantiomère présente une meilleure activité pharmacologique qu'un autre, ont été reportés comme c'est le cas par exemple pour la levofloxacinine ou la thalidomide. Dans cette thèse, l'objectif était la synthèse de nouveaux analogues à motif 3,4-dihydro-2*H*-1,4-benzoxazinique sous forme énantiopure pouvant avoir des activités biologiques intéressantes (anti-angiogénique, anti-bactérien, anti-cancéreux,...) des pseudodipeptides et pseudotriptides capables d'imiter une structure β -turn, en se basant sur le composé **2**, et d'étudier leurs conformations.

Le premier chapitre introduit les applications thérapeutiques des dérivés de la 3,4-dihydro-2*H*-1,4-benzoxazine, les techniques de synthèse de ces composés sous forme racémique ou énantiopure qui ont déjà été décrites dans la littérature, ainsi que la stratégie pour produire ces énantiomères. La forme racémique du composé **2** est facilement obtenue par une réaction de double substitution nucléophile du 2-aminophénol sur le 2,3-dibromopropionate d'éthyle **1**, commerciaux, en présence de K_2CO_3 sous reflux d'acétone. Le second chapitre décrit la méthodologie d'obtention des deux énantiomères purs de **1** et **2** suivant deux stratégies : (i) par synthèse énantiosélective et (ii) par séparation énantiomérique par HPLC d'un racémique. Une fois les deux énantiomères **2** obtenus, différents acides α -aminés sont ajoutés en position C- et N-terminale afin de former de nouveaux pseudopeptides énantiopurs à motif 3,4-dihydro-2*H*-1,4-benzoxazinique. Le troisième chapitre reporte l'analyse conformationnelle des pseudo-dipeptides et -triptides synthétisés, par analyses spectroscopiques (IR, RMN) et diffraction des rayons X.

Tout d'abord, pour obtenir le 3,4-dihydro-2*H*-1,4-benzoxazine-2-carboxylate d'éthyle **2** sous forme énantiopure afin de l'utiliser comme base de la synthèse de pseudopeptides analogues, l'obtention des deux énantiomères du 2,3-dibromopropionate d'éthyle **1** a été étudiée, et ce, par deux stratégies : par synthèse énantiosélective et par séparation énantiomérique par HPLC du composé racémique commercial.

Au début, des difficultés pour obtenir un produit énantiopur lors de la synthèse énantiosélective de (*S*)-**1** ont été rencontrées, à cause notamment de la dégradation rapide de (*S*)-**1** pendant l'étape de purification par chromatographie flash sur gel de silice, produisant de très faibles rendements. Après plusieurs essais pour éviter cette dégradation, l'énantiomère (*S*)-**1** a été obtenu en trois étapes (59% de rendement global) à partir de la (*S*)-serine, après une rapide purification sur colonne avec une très faible hauteur de silice. Néanmoins, les équipements du laboratoire ne permettant pas de vérifier la pureté énantiomérique de nos composés chiraux,

une collaboration avec un autre laboratoire plus qualifié dans ce domaine a été engagée et plus particulièrement avec un collègue de la “Plateforme de chromatographie chirale” de l’Université d’Aix-Marseille.

Afin de déterminer les meilleures conditions de séparation énantiomérique du composé **1** racémique (*rac-1*), plusieurs phases stationnaires chirales (CSP) ont été testées. La meilleure séparation des deux énantiomères a été obtenue sur une colonne préparative Chiralpak AD-H avec un excès énantiomérique (ee) élevé ($ee \geq 99.5\%$) à l’échelle du multi-gramme (5 g). En se basant sur les données enregistrées, l’ee du composé (*S-1*) précédemment synthétisé a été examiné. Les résultats étaient peu satisfaisants puisque l’ee de (*S-1*) n’atteignait que 17 à 36% ce qui signifie que (*S-1*) s’était racémisé pendant la synthèse énantiosélective. Après plusieurs essais pour en chercher la cause, il s’est avéré que ce processus de racémisation avait lieu pendant la bromation de l’intermédiaire (*S*)-glycérate d’éthyle en présence de CBr_4 et PPh_3 . La quantification du processus de racémisation (l’influence du temps de réaction et de la stoechiométrie des réactifs) a permis d’atteindre des $ee \approx 9-50\%$ et de conclure qu’un temps de réaction plus long induisait un rendement plus élevé pour la synthèse de (*S-1*), accompagné d’un plus faible ee. A l’inverse, l’utilisation d’une quantité plus faible de réactifs améliore le ee du produit mais avec un rendement moindre. L’anhydride triflique a été utilisé pour remplacer l’atome de brome par un groupement triflate, meilleur groupe partant mais, à nouveau, la β -élimination a eu lieu. Par conséquent, les deux énantiomères **1** obtenus par séparation énantiomérique par HPLC à l’échelle du gramme (5 g) ont été utilisés pour synthétiser les énantiomères correspondants du composé **2**, sous formes énantio-pures, *via* une double $\text{S}_{\text{N}}2$ avec le 2-aminophénol.

Les deux énantiomères (*S*)- and (*R*)-3,4-dihydro-2*H*-1,4-benzoxazine-2-carboxylate d’éthyle **2** n’étant pas décrits dans la littérature, ils ont été séparés par HPLC préparative chirale sur colonne Lux-Cellulose-2[®] à partir du composé **2** racémique (*rac-2*), synthétisé à l’échelle de quelques grammes (12 g). La pureté énantiomérique du (*R-2*) précédemment synthétisé de façon énantiosélective a été ensuite vérifiée. Malheureusement, lors de l’étape de double $\text{S}_{\text{N}}2$, malgré les conditions douces, le composé (*R-2*) synthétisé s’est partiellement racémisé ($ee \approx 55\%$ ou 66%). La raison de cette racémisation a pu être prédite à partir du mécanisme supposé reporté dans la littérature, impliquant la déhydrobromation du composé dibromé **1**. La formation inévitable du 2-bromoacrylate d’éthyle **5** par élimination a été identifiée comme étant la cause de la racémisation de **2** dans ces conditions (Schema 1). La formation de **5** à partir de (*R-1*) en présence de K_2CO_3 sous reflux d’acétone a été étudiée (Schema 1, étape 1)

et l'avancement de la réaction a été suivi par HPLC analytique classique sur colonne achirale. Les résultats montrent que 57% de **5** sont formés rapidement après 2 heures, suivie d'une formation plus lente de **5** pendant la suite de la réaction (atteignant un taux maximal de conversion de 93% en 16 heures).

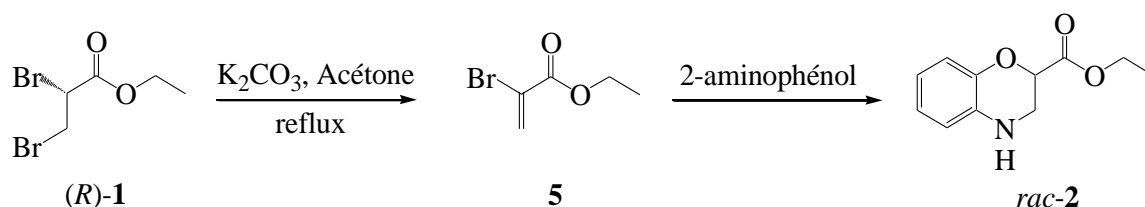


Schéma 1 Obtention du composé **2** sous forme racémique

Suite à ce résultat prouvant la racémisation, les deux énantiomères du composé **2** ont été isolés par HPLC préparative chirale avec une excellente pureté énantiomérique ($ee \geq 99.5\%$) à partir de *rac*-**2** à l'échelle de quelques grammes (12 g). Ces deux énantiomères ont ensuite été utilisés comme briques moléculaires dans l'étape suivante pour le développement de nouveaux pseudopeptides à motif 3,4-dihydro-2*H*-1,4-benzoxazinique (Schéma 2).

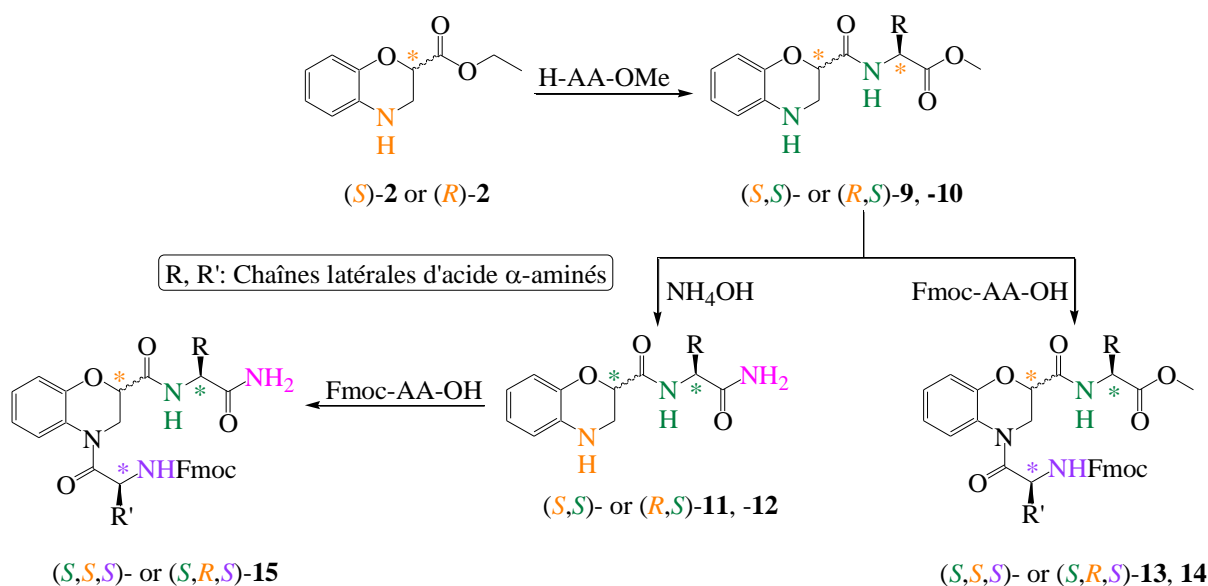


Schéma 2 Obtention de nouveaux pseudopeptides à motif 3,4-dihydro-2*H*-1,4-benzoxazinique.

Ensuite, les extrémités C- et N-terminales des composés (*S*)-**2** et (*R*)-**2** ont été modifiées par réaction de couplage peptidique avec un acide α -aminé afin de former de nouveaux analogues pseudopeptidiques énantiopures à motif 3,4-dihydro-2*H*-1,4-benzoxazinique. Dans ce travail, nous avons choisi d'utiliser arbitrairement une alanine et/ou une phénylalanine. La synthèse des nouveaux pseudopeptides commence par la saponification du groupement ester éthylique en présence de LiOH dans l'EtOH/H₂O (8/2, v/v) pour générer l'acide carboxylique

correspondant, puis par le couplage peptidique avec le chlorhydrate d'ester méthylique d'alanine ou de phénylalanine en présence de HOBt, TEA et EDCI comme agents de couplage. A cause de la faible réactivité du proton NH du motif 3,4-dihydro-2*H*-1,4-benzoxazinique, l'insertion de l'acide α -aminé sur l'extrémité C-terminale ne nécessite pas une protection Boc ou Fmoc sur ce NH. Les quatre molécules (*S,S*)- et (*R,S*)-**9**, -**10** ont été obtenues comme diastéréoisomères purs grâce à l'utilisation de HOBt. Ensuite, afin de favoriser la formation de liaisons hydrogène intramoléculaires, une amidation du groupement ester méthylique des composés (*S,S*)- et (*R,S*)-**9**, -**10** a été réalisée avec l'utilisation d'une solution d'ammonium 35% pour former les pseudodipeptides (*S,S*)- et (*R,S*)-**11**, -**12** (Schéma 3).

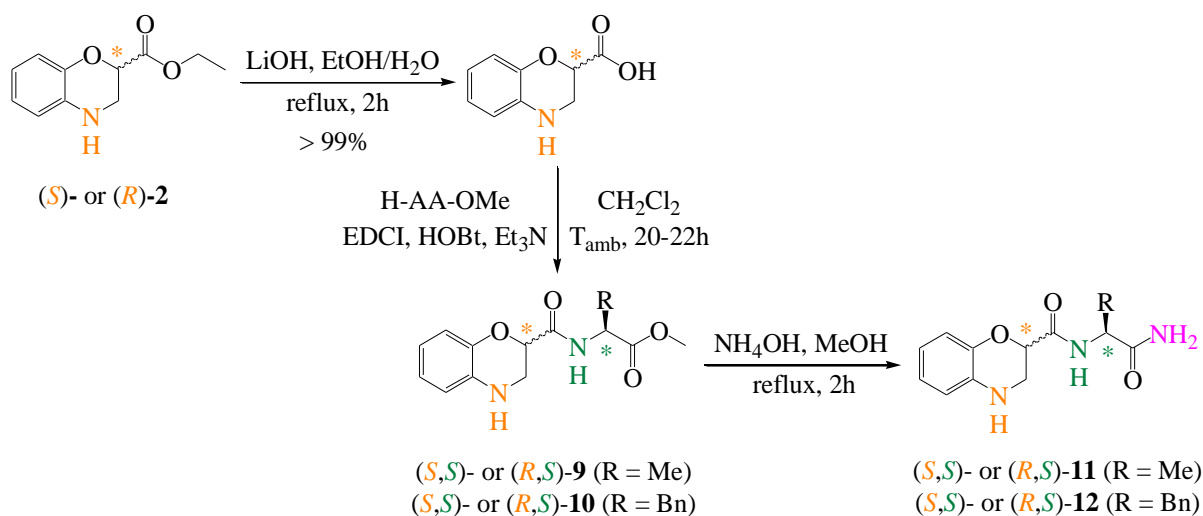


Schéma 3 Élongation de l'extrémité C-terminale des composés (*S*)-**2** et (*R*)-**2**

Pour obtenir les pseudotripeptides, l'extrémité N-terminale est mise en réaction avec la Fmoc-alanine sous forme de chlorure d'acide (Fmoc-Ala-Cl) *via* un couplage peptidique. Les chlorures d'acide sont connus pour être très réactifs et la Fmoc-Ala-Cl a été obtenue par chloration de la Fmoc-Ala-OH par du SOCl₂. La réaction entre les pseudodipeptides (*S,S*)- et (*R,S*)-**9**, -**10** et -**11** et la Fmoc-Ala-Cl en présence de la base NaHCO₃ génère les pseudotripeptides (*S,S,S*)- et (*S,R,S*)-**13**, -**14**, -**15** correspondants (Schéma 4).

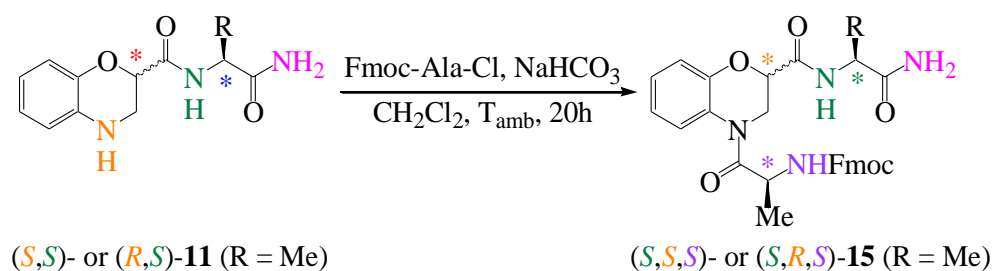
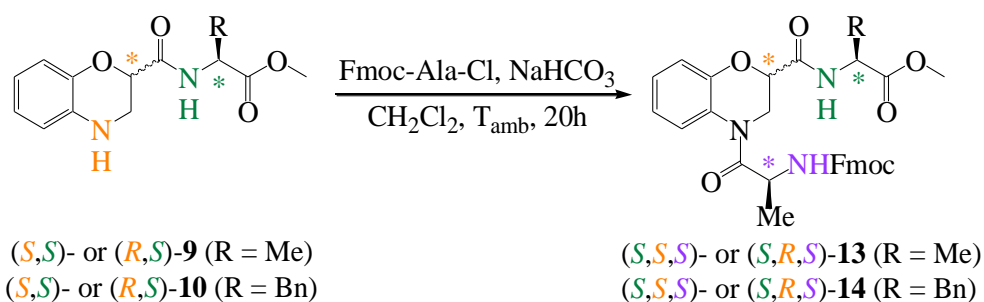


Schéma 4 Élongation de l'extrémité *N*-terminale de (S,S) - et (R,S) - **9**, **-10**, **-11**

Enfin, l'étude conformationnelle des différents pseudo-peptides précédemment obtenus a été méticuleusement réalisée par spectroscopies RMN et FTIR. De plus, les cristaux des composés (S,S) -**11**, (R,S) -**11**, (S,S) -**12** et (S,R,S) -**13** ont été obtenus avec succès dans différents mélanges de solvants ; ces cristaux ont été analysés par diffraction des rayons X. Pour les composés **11** à **14**, les résultats montrent qu'en solution ($CDCl_3$), une seule liaison hydrogène intramoléculaire est formée entre le proton NH de l'amide secondaire et un doublet non-liant de l'oxygène du cycle 3,4-dihydro-2*H*-1,4-benzoxazinique formant ainsi un pseudocycle en C_5 . L'analyse des cristaux par diffraction aux rayons X de (S,S) -**11**, (R,S) -**11**, (S,S) -**12** et (S,R,S) -**13** est en accord avec les données acquises en solution, c'est-à-dire formation du pseudocycle en C_5 . De plus, si (S,S,S) -**15** et (S,R,S) -**15** forment un pseudocycle en C_5 , ils contiennent probablement un pseudocycle C_7 supplémentaire impliquant le proton NH de l'amide primaire et le groupe C=O de l'amide secondaire (Figure 2). Cependant, la conformation en C_5 semble prédominante dans l'ensemble des pseudo-peptides que nous avons synthétisés.

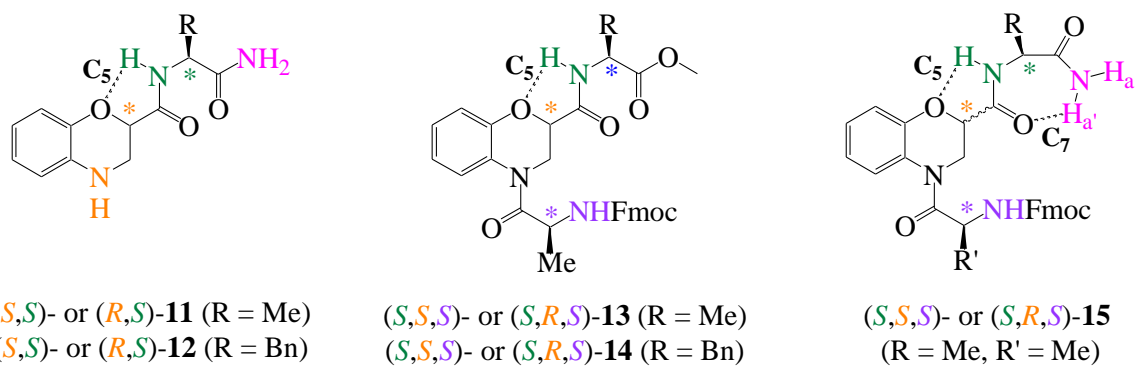


Figure 2 Conformations possibles dans les pseudo-dipeptides et -tripeptides.

CHAPTER I

BIBLIOGRAPHY

Among diversity of heterocyclic compounds, 3,4-dihydro-2*H*-1,4-benzoxazine and its derivatives were described as promising candidates for many choices of therapeutic applications. This fascinating class of heterocyclic compounds exhibits various biological properties such as antibacterial, cardiovascular protector, anti-hypertensive or anti-angiogenesis so that it can be a favorable core for medicinal chemistry. In this thesis, we reported the synthetic routes and conformational analysis of novel enantiopure 3,4-dihydro-2*H*-1,4-benzoxazine analogues as scaffold for pseudopeptides and for potential biological applications.

1. General introduction

1.1. Pseudopeptides

Peptide, a chain consisting of 2 to 50 amino acids that bind to each other *via* covalent chemical bonds (amide bonds) which is formed between carboxylic group of one amino acid and amino group of the other amino acid, is being a potential target for medicinal chemistry. A chain of peptides forms oligopeptide and a longer one, protein. Enzymes are required for thousands of chemical reactions within human body, for examples: i) hormones like insulin or ADH (AntiDiuretic Hormone) act as signal transmitters to delivery information between cells; ii) antibody that helps to protect our body from foreign harmful particles or iii) energy source needed for human body, *etc.*, are proteins. Proteins play an undeniable important role to human, peptide also. Peptides play various functions as hormones, neurotransmitters, infection treatments, *etc.*¹ However, their limitations such as low bioavailability, instability due to proteolysis, poor selectivity because of the conformational flexibility² brought troubles. Those constraints prompt science to search for solutions, hence peptide-based drugs have been developed and marketed for various therapeutics. Peptide-based compounds could be divided as modified peptides, pseudopeptides and peptidomimetics. The term “pseudopeptide” are peptide analogues that its amide bonds have been adjusted but the structure still maintains a partial part of natural one³. These backbone-modified peptides are essential used to eliminate the low bioavailability and/or to avoid degradation problems by protease.

Many biological processes, such as the process of cellular differentiation where a normal cell might be adjusted/changed to mutated cell, are catalyzed by two or more proteins interacting with each other. The study of the interactions between proteins helps us better understand the mechanisms and finding the way to control or inhibit their activity⁴. To intervene the protein-protein interaction, managing its bonds would be a solution. There are four stages of protein

folding in which secondary structures are most important (e.g. α -helices and β -sheets). The secondary protein shape is formed *via* peptide bond between amino group of one amino acid and carboxyl group of another, this type of peptide bond can generate different types of turn (Figure 1.1) which β -turn plays an important role in various biological recognition systems^{3,5}. Therefore, obtainment of pseudopeptide compounds containing intramolecular hydrogen bonds (H-bonds) that mimic protein-turn (like β -turn) is an interesting target for drug design. Those compounds can give “deceive” signals to interfere protein-protein interactions then the diseases will be cured.

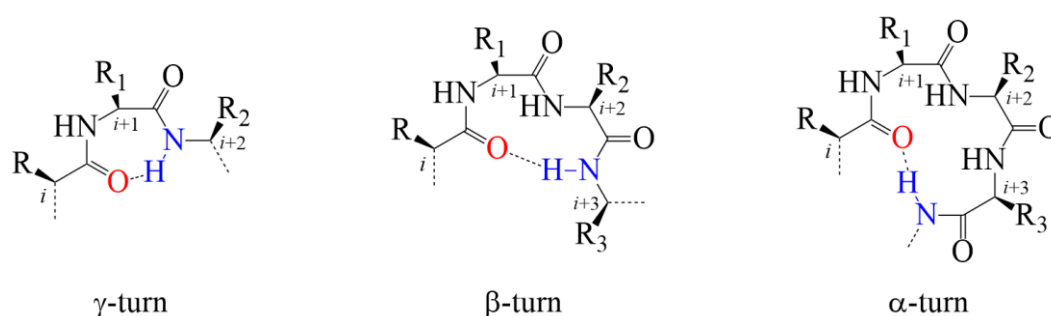


Figure 1.1 Three types of peptide turn

Due to the extraordinary diversity and multi-functions of heterocycles, heterocycle-based molecules are becoming key structures in development of new drugs with two third of marketed drugs containing heterocycles⁶. The combination of heterocycles and amino acids is one among various approaches for pseudopeptide designs with heterocyclic core used as rigid frame attaching to α -amino acids to create α -, β - or γ -turn mimetics. The α -turn is formed when there is a hydrogen bond between the i and $(i+4)$ residues, β -turn will be formed between i and $(i+3)$ residues and γ -turn will be formed between i and $(i+2)$ residues. In addition, an extensive part of heterocyclic framework containing nitrogen atom contributes remarkable applications as medicines, pharmaceuticals or agrochemicals. *N*-heterocycles are attractive scaffold for drug development especially for bioactive compounds consisting of amino acids/peptides⁷. Interestingly, our selected heterocycle ethyl 3,4-dihydro-2*H*-1,4-benzoxazine-2-carboxylate encloses nitrogen atom (Figure 1.2). With carboxylic group attaches to α -carbon and amine group attaches to β -carbon, its structure simulates β -amino acid that makes this heterocyclic molecule more inquisitive to study.

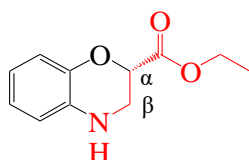


Figure 1.2 Ethyl 3,4-dihydro-2*H*-1,4-benzoxazine-2-carboxylate as amino acid analogue

1.2. Optical active compound (enantiomer)

In 1815⁸, the term of “optical activity” was discovered by a French physicist Jean-Baptiste Biot that used to describe organic chemicals capable of rotating the plane of polarized light even in solution or at liquid state. Those chemicals are called “optically active compounds” or “chiral compounds”. The first chiral discovered molecule, sodium ammonium tartrate, was separated by a French chemist Louis Pasteur in 1848⁸ from racemate of para-tartaric acid in quantity by crystallization. This achievement is the first step to open a new era for organic and medicinal chemistry.

Chiral molecule is defined as a molecule which cannot be superimposed on its image. The simplest model to explain chirality property in molecule is right- and left-hand (Figure 1.3), the two mirror images of a chiral molecule are called enantiomers. A chiral center of enantiomer is an asymmetric carbon (a sp^3 -hybridized carbon atom) that links to four different groups. Chiral molecule containing more than one asymmetric carbon can be a diastereoisomer and is also not mirror image. Two enantiomers have the same molecular formula, exactly same chemical and physical properties but may have different biological activities.

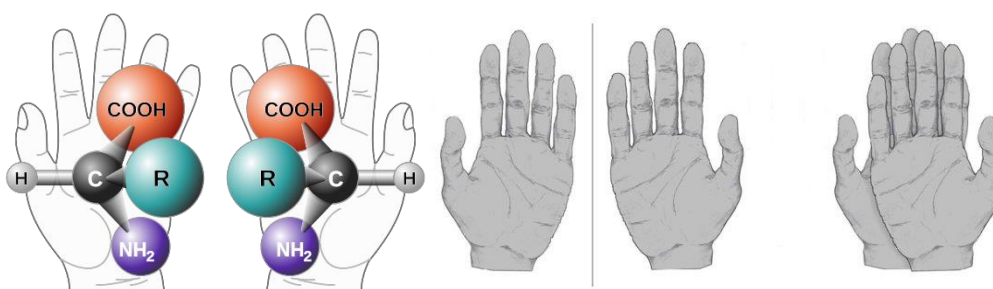


Figure 1.3 Chiral compounds are presented by hand-model*

Due to receptor selectivity and differences in biological and pharmacological activities, many chiral compounds have been reported with one of its enantiomer exhibiting better pharmacological activities than the other such as levofloxacin¹⁰ or number of β -blockers¹¹. In addition, one enantiomer in a racemate releases biological effect while the other causes toxicity

* Images were taken from Wikipedia and reference⁹

like the famous case of a chiral drugs called thalidomide¹². Thalidomide was discovered in 1953 and commercialized in 1956 for several indications. In 1958, it was used as a sedative and a morning-sickness remedy for pregnant woman. Unfortunately, (*R*)-enantiomer had the desired therapeutic effect but (*S*)-enantiomer causes many miscarriages, birth defect¹² with more than 10,000 children were born with severe physical handicap¹³. The hypothesis that one enantiomer of thalidomide caused fetal malformation is still under debate, it seems the racemization of interesting enantiomer occurred during absorption and metabolism in human body. However, there were no strong evidence to confirm its mechanism¹⁴. In the case of Ibuprofen, used as an inflammatory treatment, it has been proven that *in vitro* only (*S*)-isomer is active and after absorption *via* oral administration, one-third of (*R*)-isomer is converted to active form¹⁵. The pain relief medicine as naproxen also is marketed only as single enantiomer^{16,17}. Another example is quinine – an alkaloid which is extracted from quinine tree. Quinine has been known as a very effective treatment for malaria¹⁸ disease but it can induce toxicity for cardiovascular system. However, one of its enantiomers, quinidine has been reported that not only containing similar effect as anti-malarial medicine as quinine, it also creates much lower damage on heart and blood vessels. Quinidine is used as a treatment for few types of arrhythmia diseases¹⁸.

The Easson and Stedman¹⁹ model (Figure 1.4) simply explained the relationship between chiral drug and a specific drug receptor. One enantiomeric compound is well-binding to the receptor to release pharmacological activity but its mirror-image which presents different spatial arrangement of atoms or functional groups is blocked out of the drug receptor leading to no effects or in some cases it even causes toxicity. Since essential biomolecules needed for human body are appeared as enantiomerically pure and to date, approximately 56% of marketed medicines are used in enantiomeric form^{11,20}, chemists are raising an awareness about the obtainment of different chiral active molecules. There are various approaches to achieve chiral compounds that can be mainly divided into two approaches: enantioselective synthesis (or asymmetric synthesis) or enantioseparation of racemic mixture (racemate resolution).

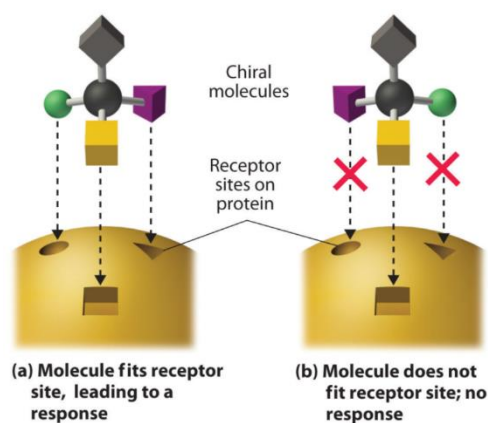


Figure 1.4 Easson and Stedman model – Three-points interaction of chiral drug and receptor[†]

A published review article by Sachine Mane generally introduced various approaching methods to obtain enantiomerically compounds²². Enantioselective synthesis presents a type of reaction using a new chiral compound created after addition of chiral auxiliary, catalysts, reagents or substrates. Chiral auxiliaries can be derived from nature source such as amino acids or carbohydrates²³. They assist the achiral compound to participate in stereoselective process to attain a chiral compound before to be certainly removed and recycled. Chiral catalysts including metal-, organo-catalysts, organometallic complexes, ligands and enzymes are all used to accelerate stereoselective reaction from non-chiral compound to achieve an outcome of optical active compound. An advantage of chiral catalysts is low priced but complicated structure. Unlike chiral catalysts or chiral auxiliaries, chiral reagents involved to asymmetric reaction to bind with achiral starting material to generate diastereoisomers which can be separate by normal-phase column chromatography or by chiral column chromatography for enantiomers. Chiral substrate or chiral pool is the most common method to synthesize optical active compound by modifying structure of available and/or commercially enantiopure starting molecule to desired one. However, due to some limitations like eco-unfriendly (metal catalysis), high-priced and complex structure, even enantioselective synthesis is common method for obtainment of chiral active compounds, the other technique called racemate resolution is preferable.

Several racemate resolution methods to achieve enantiopure molecules were also listed in the same reviewed article mentioned above^{22,24} which are divided into direct and indirect methods. In general, indirect approaches are trying to collect pure enantiomer *via* crystallization or conversion of enantiomers to diastereoisomers which can be separated by non-chiral column

[†] Image was taken from the reference²¹

chromatography. Few selected examples of indirect approaches are mechanical resolution, kinetic resolution or diastereomeric resolution. Mechanical resolution is crystallization of one enantiomer out of the racemic mixture. This method has limited application because it is time-consuming and there are few enantiomers that are mechanically separable *via* crystallization. Kinetic resolution bases on different reactivity between two enantiomers with chiral catalysts such as enzymes to distinguish them, one enantiomer can be quickly reacted to form chiral complexes and the other does not. Kinetic resolution is the most effective way because the obtained chiral complexes always exist in high enantiomeric purity. However, it is hardly to recover single pure enantiomer from reaction mixture. Diastereomeric resolution is commonly applied for enantioseparation. It is allowed to separate diastereoisomeric mixture by one or several columns. Even this method is easy to use but it requires screening for suitable chiral bases to form diastereoisomeric mixture. If two diastereoisomers having very similar resolution on column and numerous columns are needed for separation, it may cause the loss in yield. To the contrary, the typical direct approaches are using of chiral stationary phases (CSPs) or chiral mobile phase additives, herein we only discussed about enantioseparation by High-Resolution Liquid Chromatography (HPLC) using CSPs of enantiomers from racemic mixture.

1.3. Chiral High-Resolution Liquid Chromatography

HPLC is developed from conventional liquid chromatography. A HPLC system (Figure 1.5) includes a column (stationary phase), solvent reservoir (mobile phase), injector system and detector. The column is made of stainless steel containing absorbent material (silica gel) with the length can be up to 25 cm and 4.5 – 5 mm of internal diameter. Normally two reservoirs can keep 1 – 2 litres of solvents are attached to HPLC system *via* a high-pressure pump that leads solvents into the column with high pressure. Before the solvent get in the column, it will pass a pre-column to remove impurities in the solvent and to saturate the mobile phase with the stationary phase. The separation is called isocratic elution when HPLC system runs with consistent of solvent mixture, if composition of mobile phase changes while system is running, the separation is called gradient elution. The sample is introduced to the column *via* the injector system. Outcome of the column is attached to the detector connected to a computer for information collecting and that has various wavelengths to detect if samples are eluting out of column. There is diversity of detectors such as ultraviolet (UV) detector, infrared (IR) detector, mass spectrometer or evaporative light scattering (ELS) detector that commonly used for high molecular weight analytes. The HPLC is also divided into different types such as normal phase chromatography, reversed phase chromatography, ion chromatography, size exclusion

chromatography depending on characteristic of sample. To fully understand HPLC results, important parameters like the retention time (Rt), the retention or capacity factor (k), the selectivity or separation factor (α), the resolution factor (R_s) and efficiency (N) are needed to be studied.

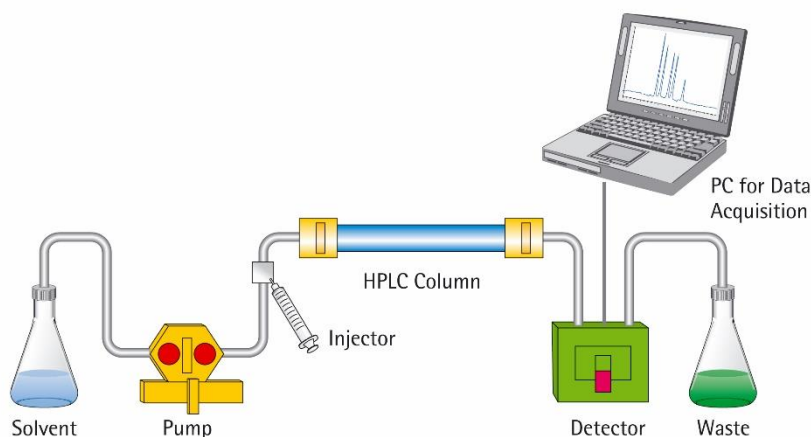


Figure 1.5 General HPLC system components[‡]

Retention time Rt is the time taken for a chemical component elutes out of the column starting from the injection time. The retention (capacity) factor $k_i = (Rt_i - Rt_0) / Rt_0$ expresses the relation between the time of analyte spends in the stationary phase and in the mobile phase. The k value should be between 1 and 10 for the good separation. The selectivity (separation) factor α defines how chromatographic system differentiates sample components, it is quotient of k values of two components ($\alpha = k_2 / k_1$ with $k_2 > k_1$). If $\alpha = 1$, all components are eluting at the same time then no separation occurs, therefore, the greater of α value gives the better separation. One of the most important parameters is the resolution factor R_s that determines how well two components are separated in a chromatographic system. It is calculated by the following formula $R_s = 1.18 (Rt_2 - Rt_1) / (w_1 + w_2)$ where Rt is retention time of chemical component and w is peak width. If the resolution value more differ than 1.5, the elution peaks are well-separated^{25,26}.

The fundamental of chiral HPLC is completely the same as normal HPLC but it uses at least one chiral factor. Enantioseparation system by chiral HPLC can be accomplished *via* three approaches: (a) chiral mobile phase, non-chiral stationary phase; (b) non-chiral mobile phase, chiral liquid stationary phase and (c) non-chiral mobile phase, chiral solid stationary phase²⁵. This work only mentioned the third method. Instead of using normal type of stationary phases

[‡] Image was taken from [Toppr](#)

like silica or alumina, chiral HPLC uses various types of chiral stationary phases (CSPs) such as Brush-type, synthetic polymer-based, natural polymer-based, *etc.* The most common CSPs like cellulose-based, amylose-based, polyacrylamide-based phases, crosslinked diallyltartardiamide, pirkle and chirobiotic phases are exploited especially for preparative chiral HPLC. Even CSPs are widely used for separation of two enantiomers, they are quite expensive and selectively for specific type of enantiomers. To start processing enantioseparation of two enantiomers, a number of CSPs will be screened and proper mobile phase will be examined. This action helps user to optimize the conditions as well as to reach the most efficient parameters in analytical system before applying to preparative chiral HPLC in multi-gram scale. Chiral HPLC can provide throughput enantiomers in high purity and the system is easy to perform, therefore, chiral HPLC is being an effective technique in medicinal chemistry^{25,27-31}. Once the enantioseparation finishes, optical rotation value, enantiomeric purity and absolute configuration of both enantiomers should be taken.

1.4. Determination of optical value, absolute configuration and enantiomeric purity

A specific property of optical active compound is optical rotation value which is measured by polarimeter. The optical value is calculated by the following Biot's law equation: $[\alpha]_{\lambda}^T = \alpha / lc$ where $[\alpha]_{\lambda}^T$ is the optical rotation value (in degrees), λ (nm) the wavelength of light source for observation (normally used halogen lamp such as sodium lamp (D) has $\lambda = 589$ nm), T the temperature (in degree Celsius), α the observed rotation value on device, l the path length of the sample tube (in decimeters) and c the concentration of sample solution (g/100mL). Enantiomer has ability to rotate the plane-polarized light and two enantiomers will rotate the plane of polarization but in opposite directions. Racemic mixture is optically inactive and cannot rotate the plane-polarized light, thus it gives the value of zero.

Among various techniques to determine absolute configuration and optical purity of enantiomerically pure, X-ray crystallography is commonly applied. X-ray interprets the crystal formed between a pure enantiomer and a known absolute configuration derivatizing agent to reveal the configuration of that enantiomer.

Another widely used method is circular dichroism (CD) spectroscopy which shows difference of absorption of left and right circularly polarized light by a substance (enantiomer). To simply comprehend, two enantiomers have opposite chiral features thus will be absorbed differently by left and right circularly polarized light. The detector of CD system will detect and record

two spectra with exactly same signals but in opposite sign^{32,33} (Figure 1.6). Even CD spectra of two enantiomers are mirror-image but they do not indicate specific absolute configuration of enantiomers.

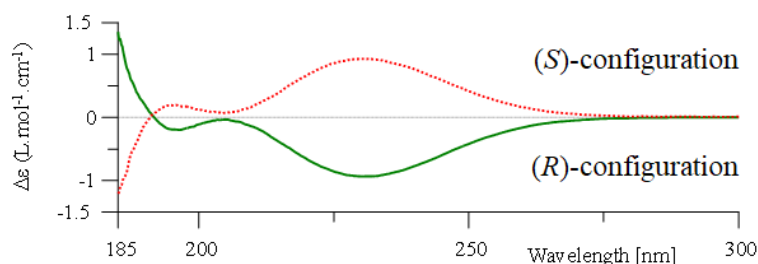


Figure 1.6 An example of CD spectra of ethyl 2,3-dibromopropionate enantiomers

In addition, NMR is reported as an efficient tool for either absolute configuration or enantiomeric purity determination. The term “enantiomeric purity” or “enantiomeric excess” (ee) presents the quantification of one enantiomer over the other. If $ee \approx 100\%$, compound is enantiomerically pure and in reverse, racemic mixture has $ee = 0\%$. Plus, chiral centers of diastereoisomer may cause different resonances in electromagnetic field due to spatial arrangement of atoms hence they will slightly affect to chemical shifts on ^1H NMR. To apply NMR techniques for absolute configuration, both enantiomers first have to be coupled with an auxiliary chiral reagent to convert them into diastereoisomers. Secondly, analysis of NMR spectra then can specify the absolute configuration of original enantiomer based on given NMR signals of the auxiliary chiral reagent^{34,35}. NMR techniques are also used to examine the purity of diastereoisomer. If a diastereoisomer is not pure and NMR shows presence of the other diastereoisomer, ^1H NMR can reveal signals of both and base on given number of protons, the ratio between two diastereoisomers can be calculated. This technique has high sensibility and the accuracy can reach 95%. Other methods for examination of enantiomeric excess are described in the literature and used chiral HPLC, gas chromatography or capillary electrophoresis^{36–38}.

In this thesis, our chiral (*R*)- and (*S*)-ethyl 3,4-dihydro-2*H*-1,4-benzoxazine-2-carboxylate as starting scaffold were obtained *via* two strategies: enantioselective synthesis and preparative enantioseparation of racemate by chiral HPLC. The absolute configuration and/or optical purity of each chiral compounds were determined by either electronic circular dichroism (ECD) spectroscopy or chiral HPLC with UV and CD detection, their optical values were measured by polarimeter.

2. 1,4-benzoxazines as potential scaffold for therapeutic applications

A few biopharmacological activities of 1,4-benzoxazine derivatives were collected from available literature and mentioned below. By attaching imidazoline ring to 1,4-benzoxazine scaffold, 29 different imidazolinic derivatives were generated³⁹ for testing *in vivo* their effects on binding with imidazoline binding sites (IBS) and adrenergic receptors to evaluate the ability of blood pressure reduction. One of those compounds showed highly potential for antihypertensive effect. Based on previous described benzoxazine-based molecules that possess a substantial properties to prevent neurons degeneration⁴⁰⁻⁴², in 2005, a new derivative (Figure 1.7A) was developed. It is aiming to inhibit oxidative stress-mediated neuronal degeneration⁴³ in order to protect brain damage. This compound then impressively exhibited neuroprotective activity without leaving cytotoxicity in *in vivo* test. With the same desire on neurodegenerative protection discovery, a series of 1,4-benzoxazine analogues were synthesized⁴⁴. Among 21 designed molecules had similarly chemical structure, only compound marked as HSB-13 (Figure 1.7B) expressed a significant neuroprotective activity against degeneration.

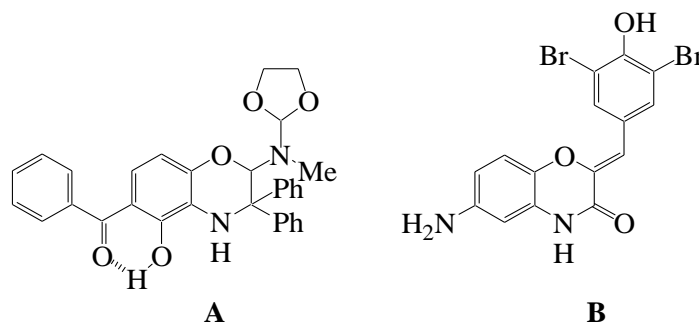


Figure 1.7 1,4-benzoxazine derivatives containing neuroprotective activity

Additionally, a novel 1,4-benzoxazine analogue was designed by La et al.⁴⁵ as a powerful compound that can inhibit angiogenesis process (Figure 1.8A). This compound binds to kinase insert domain receptor (KDR) to inactivate tyrosine kinase activity inside cell membrane, then block the process of forming new blood vessels to “raise” existed tumour. With the same mechanism, Honda’s team developed a new molecule also bearing this framework⁴⁶ prohibited the tyrosine kinases and produced a comparatively high inhibitory activities against KDR (Figure 1.8B).

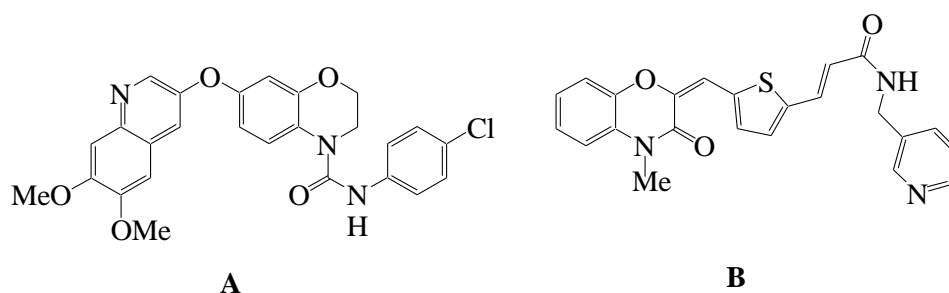


Figure 1.8 1,4-benzoxazine derivatives developed by La et al (**A**) and Honda et al (**B**) containing anti-angiogenesis activity

Although those two molecules have revealed a good capability of angiogenesis restraint to stop the tumours being metastasis, their mechanism of action can lead to another health issue. The using of angiogenesis inhibitor in cancer patients may prevent the growth and regeneration of new blood vessels that can cause blood clotting disorder. This phenomenon affects to blood circulation system in human body then brings out thrombosis. In 2012, a study of the dual activity on thrombotic inhibitory and glycoprotein IIb/IIIa receptor antagonistic of several fluorinated 3,4-dihydro-2*H*-1,4-benzoxazine was reported⁴⁷. Their findings indicated a promising compound (Figure 1.9A) which was highly satisfied for their aim. Furthermore, they also successfully developed another structurally similar compound (Figure 1.9B) containing not only dual antithrombin but combining with anti-angiogenesis activity by transfer carboxylic group to ethyl ester one⁴⁸.

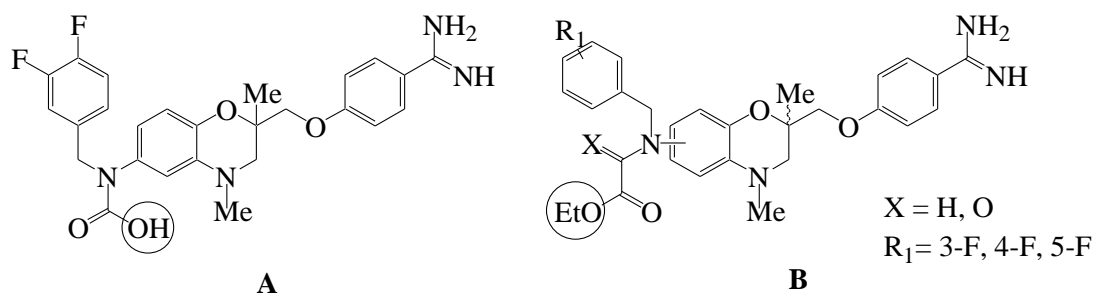


Figure 1.9 1,4-benzoxazine derivatives containing antithrombotic activity (**A**) and dual anti-thrombin and anti-angiogenesis activities (**B**)

Aiming to find out a treatment for cardiovascular diseases which preferably target to the causes than only deal with its symptoms, a series of 1,4-benzoxazine derivatives was synthesized bearing different types of antianginal calcium antagonists⁴⁹. It indicated that the most potent compound should bear benzyl group on nitrogen atom of 1,4-benzoxazine moiety. In addition, heterocyclic framework should be distanced from amine function by three methylene groups to reach prominent effect as intracellular calcium blocker (Figure 1.10).

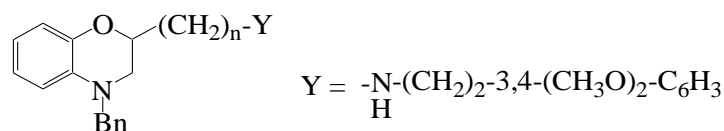


Figure 1.10 1,4-benzoxazine derivative containing intracellular calcium antagonist activity

To devise a new class of analogues bearing aminoamide functionality of lidocaine, a medicine used for treatment of arrhythmias when ischemia-reperfusion occurs, 5,6,8-trimethyl-1,4-benzoxazine has been involved to design next generation of antiarrhythmic drugs (Figure 1.11). Among various synthesized molecules, two of them highlighted a remarkable effect on arrhythmias and showed less complications⁵⁰. During this study, the authors described enantioseparation of 1,4-benzoxazine analogues by chiral HPLC system which is one way among variety of methods to approach chiral 1,4-benzoxazines.

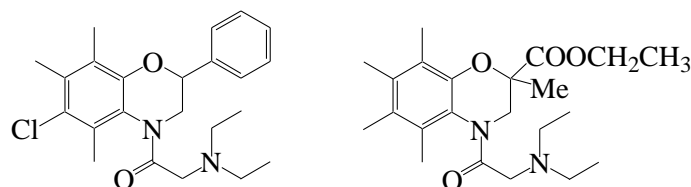


Figure 1.11 1,4-benzoxazine derivatives against arrhythmias

Moreover, 1,4-benzoxazine moiety was exploited as a dual-acting factor⁵¹ for treatment of thrombosis. The scaffold was designed to bear both thromboxane A₂ (TXA₂) antagonist and prostacyclin (PGI₂) agonist which have opposite activities on platelet aggregation (Figure 1.12). The pharmacological study on these 3,4-dihydro-2*H*-1,4-benzoxazine series also showed no side effects on blood pressure and heart rate. Hence, it is potential medicine for antithrombin and cardiovascular field.

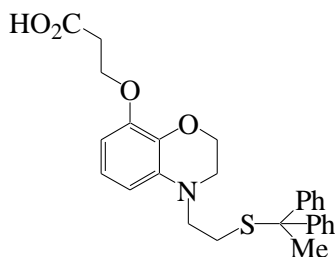


Figure 1.12 1,4-benzoxazine derivative inhibits TXA₂ and activates PGI₂

By adding serotonin (5-HT) component to 1,4-benzoxazine framework, a series of new 3,4-dihydro-2*H*-1,4-benzoxazine derivatives was developed (Figure 1.13) as serotonin 1A receptor (5-HT_{1A}) agonists. These compounds can bind to 5-HT_{1A} to increase 5-HT level in the brain and help reducing depressant symptoms. They also are selective serotonin reuptake inhibitors

(SSRIs) which will block serotonin to be reabsorbed to neurons and keep them working as neurotransmitter⁵². Another 1,4-benzoxazine analogue that contains same effect as anti-depressant drug was also reported⁵³.

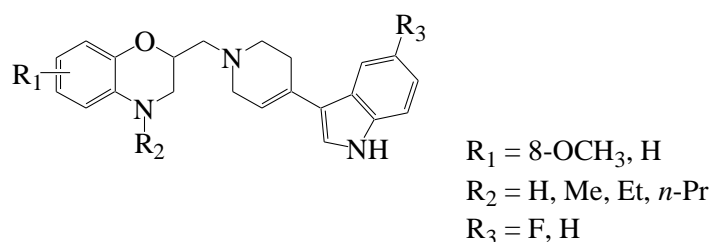


Figure 1.13 3,4-dihydro-2*H*-benzo[1,4]oxazine derivatives incorporate dual SSRI and 5-HT_{1A} receptor activities

A research on synthesizing of 2,2-dimethyl-3,4-dihydro-2*H*-1,4-benzoxazines (Figure 1.14) acting as isosteres of their chroman counterparts to investigate their inhibiting effect on the glucose-induced insulin and myorelaxant activity was reported⁵⁴. It figured out the benzoxazine substitutes were less active in releasing insulin from rat pancreatic but considerably potential as myorelaxants.

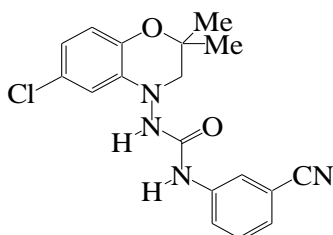


Figure 1.14 2,2-dimethyl-3,4-dihydro-2*H*-1,4-benzoxazine derivative containing muscle relaxant activity

Transient receptor potential vanilloid-1 (TRPV1) locates on sensory neurons. It can be activated by high temperature ($\geq 42^\circ\text{C}$) or capsaicin (compound that be found in hot chilly) and other endogenous lipids. When TRPV1 is activated, it will generate the feeling of pain or burning sensation and in longer time may cause peripheral neuropathy, asthma or temporary deaf. Therefore, TRPV1 becomes an attractive target for treatment of pain⁵⁵. A series of cooperative piperidine carboxamides with 1,4-benzoxazin-3-one have been synthesized as TRPV1 inhibitors. One molecule among them exhibited significant inhibitory activity (Figure 1.15)⁵⁶.

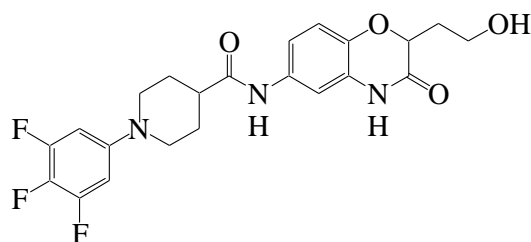


Figure 1.15 1,4-benzoxazine derivative inactivating TRPV1

Methotrexate (MTX) is an antifolate used to treat leukemia and other types of cancer such as breast cancer, lung cancer. It is also one of the most effective drugs for arthritis treatment but long-term treatment with MTX causes severe side effects like nausea, vomiting or even hair loss. In order to enhance the bioactivity and avoid side effects of MTX, its derivatives conjugated with 1,4-benzoxazine and 1,4-benzothiazine scaffold were synthesized. They were examined to measure *in vitro* inhibitory proliferation activity towards human synovial cells (hSC) and human peripheral blood mononuclear cells (hPBMC), and through *in vivo* tests on ability to inhibit arthritis on rat model. The results were impressive to MTX conjugated with 1,4-benzothiazine moiety and sufficient to the one with 1,4-benzoxazine moiety. Antiproliferative inhibitory effect of MTX-based 1,4-benzoxazine derivatives (Figure 1.16) were similar to MTX itself and strongly inhibited the development of disease in arthritic rat model⁵⁷.

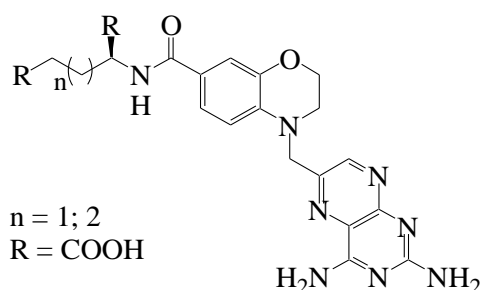


Figure 1.16 MTX derivative bearing 1,4-benzoxazine scaffold for arthritis treatment

Levofloxacin or (–)-ofloxacin is very known as antibiotic having 1,4-benzoxazine core that had been discovered by Daiichi Seiyaku Company in Tokyo by separating two enantiomers of ofloxacin. It was first approved for marketing in 1993 in Japan and the US Food and Drug Administration (FDA) authorized use of levofloxacin in the United States in 1996^{58,59}. Levofloxacin (Figure 1.17) was reported with inhibitory activity 8 to 128 times more potent compare to the other enantiomer⁶⁰. In 2010, various 1,4-benzoxazine analogues were generated specially focus on inhibition of strain of tuberculosis (*M. tuberculosis* H37Rv). They showed a promising antibacterial property with low IC₅₀ values against *M. tuberculosis* bacterium⁶¹.

Furthermore, different molecules bearing 1,4-benzoxazine scaffold that contain favorable antimicrobial activity^{62,63} were described.

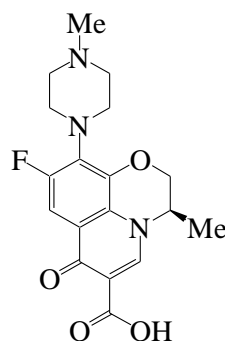


Figure 1.17 Levofloxacin – antibacterial drug

The 2*H*-1,4-benzoxazine-2-carboxylic building block (1,4-benzoxazin-3-one) as perspective peptidomimetics for serine protease inhibitors (Figure 1.18A) and also several proline containing same general formula (Figure 1.18B) as fibrinogen receptor antagonists were synthesized^{64,65}. In addition, the synthesis of potent immunostimulatory compounds-based muramyl dipeptide with retro-inverso formula was showed up (Figure 1.18C). Even the synthesized compound were inactive for immunostimulant activity, it convinced a hypothesis that intramolecular peptide bond is crucial for immunorestitution⁶⁶.

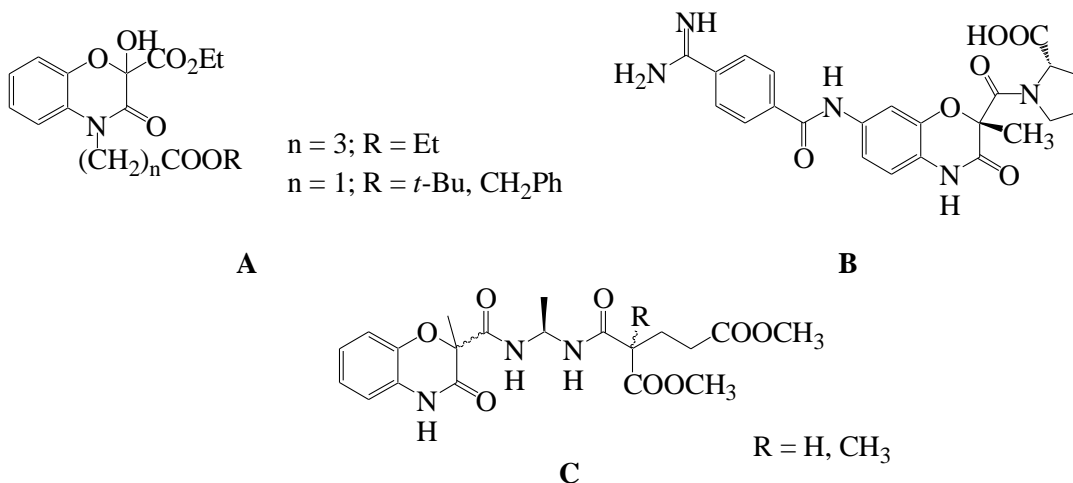


Figure 1.18 1,4-benzoxazine derivatives as peptidomimetics

Not only be useful in many pharmaceutical fields, this amazing heterocyclic skeleton also be a target in agricultural chemistry. Based on the previous research on phytotoxicity of benzoxazinones for weed control on barnyardgrass⁶⁷, the potential candidate has been continuing generated as a novel model for herbicide in specific rice plants *Oryza sativa* – *Echinochloa crus-galli*. By upgrading its lipophilicity *via* screening of different hydrocarbon

chains at C-2 position to find the most favourable one that make the designed molecule's *logP* value stable between 1 and 2.⁶⁸ The best candidate was the 2-ethyl-substituted compound (Figure 1.19).

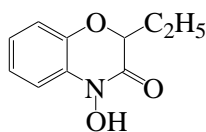


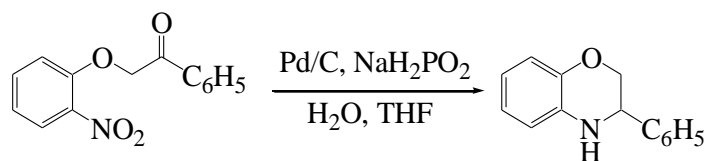
Figure 1.19 1,4-benzoxazin-3-one as new herbicide model

Due to those applications, 3,4-dihydro-2*H*-1,4-benzoxazine is a certain attractive target to develop therapeutic molecules. Even 1,4-benzoxazine scaffold have many potential medical applications, its synthetic route is not complicated. Many different strategies to afford 1,4-benzoxazine derivatives by ring closure have been collected in a review written by Ilaš⁶⁹. Herein are listed few selected strategies to approach 1,4-benzoxazine scaffold.

3. Synthetic routes for 1,4-benzoxazine derivatives

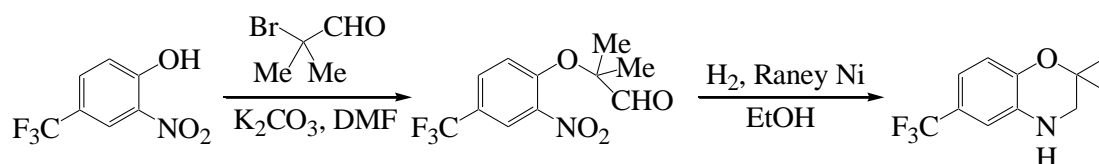
3.1. Synthetic routes for racemate 1,4-benzoxazine derivatives

Metal-catalysts is commonly used in various reactions to increase reaction rate and to improve the effect of activating reactants. In 1979, Battistoni et al. performed the synthesis of racemic 3-phenyl-2*H*-1,4-benzoxazine (Scheme 1.1)⁷⁰ by reduction of 2-(2-nitrophenoxy)acetophenone using sodium phosphinite in the presence of palladium on charcoal.



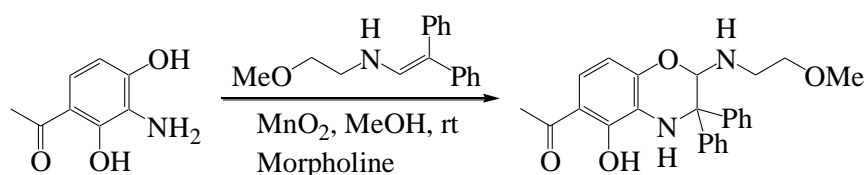
Scheme 1.1 Synthesis of racemic 3-phenyl-2*H*-1,4-benzoxazine

The preparation of intermediate 3,4-dihydro-2,2-dimethyl-6-trifluoromethyl-2*H*-1,4-benzoxazine was realized by substitution of 2-nitro-4-trifluoromethylphenol with 2-bromoisobutyraldehyde in the presence of potassium carbonate, followed by hydrogenation step in the presence of Raney nickel to complete ring closure (Scheme 1.2). This intermediate compound was modified *via* multi-steps to achieve 1,4-benzoxazine derivative possessing effect as potassium channel activator⁷¹.



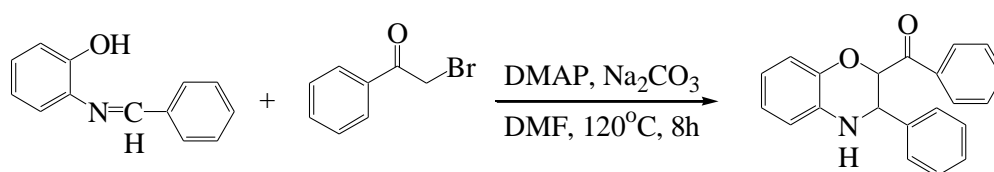
Scheme 1.2 Synthesis of intermediate 3,4-dihydro-2,2-dimethyl-6-trifluoromethyl-2H-1,4-benzoxazine

Oxidation of different *ortho*-aminophenol *via* inverse-electron-demand Diels-Alder reaction by using manganese dioxide (MnO_2) and enamine with 1.5 equivalents of morpholine can generate also racemic 1,4-benzoxazine derivatives in good yield⁷². One of those molecules that bearing 1,4-benzoxazine framework showed significant neuroprotective activity (Scheme 1.3).



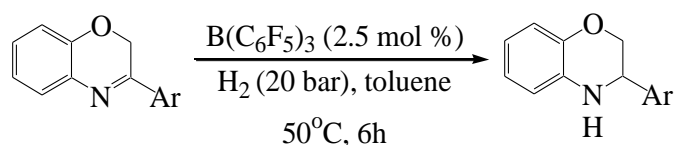
Scheme 1.3 Synthesis of racemic [3,3-diphenyl-5-hydroxy-2-(2-methoxy)ethylamino-3,4-dihydro-2H-1,4-benzoxazine-6-yl](methyl)methanone as potential neuroprotective treatment

Although using metal-catalyzed is known, this method is partially expensive and a metal-free synthetic route will be more persuasive. The cycloaddition between *o*-phenol imine (Shiff base) and α -halo ketone can give 1,4-benzoxazine derivative⁷³ (Scheme 1.4). To optimize the efficiency of this reaction, 4-dimethylaminopyridine (4-DMAP) was used as a catalyst to increase the yield.



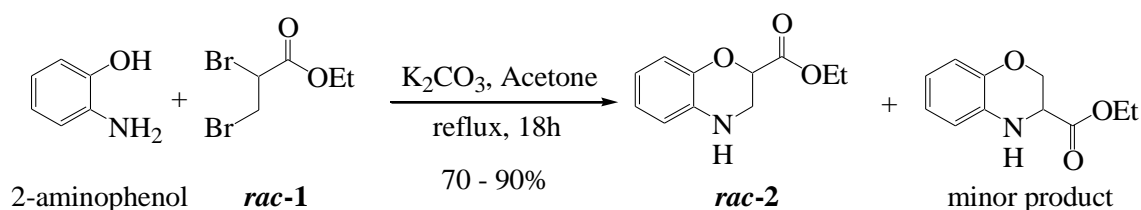
Scheme 1.4 Synthesis of racemic phenyl-(3-phenyl-3,4-dihydro-2H-1,4-benzoxazin-2-yl)-methanone

Another metal-free method was reported by Wei et al. which was simply hydrogenation of diverse 3-substituted-2H-1,4-benzoxazines in the presence of tris(pentafluorophenyl)borane ($\text{B}(\text{C}_6\text{F}_5)_3$) under hydrogen in toluene to produce 3,4-dihydro-2H-1,4-benzoxazine derivatives in excellent conversion⁷⁴ (Scheme 1.5). In this report, chiral borane catalysts were also prepared *in situ* by hydroboration of Piers' borane ($\text{BH}(\text{C}_6\text{F}_5)_2$) with different chiral dienes to examine for the asymmetric hydrogenation of 1,4-benzoxazine but the results showed poor enantiomeric excess (~30%).



Scheme 1.5 Metal-free hydrogenation of 3-substituted-2*H*-1,4-benzoxazines

Among the different synthetic routes, the most commonly used method for the synthesis of racemate 1,4-benzoxazine is a double nucleophilic substitution of racemic ethyl 2,3-dibromopropionate **rac-1** by 2-aminophenol^{75–78}. This strategy allows to obtain racemic ethyl 3,4-dihydro-2*H*-1,4-benzoxazine-2-carboxylate **rac-2** in high yield (70-90%) (Scheme 1.6).

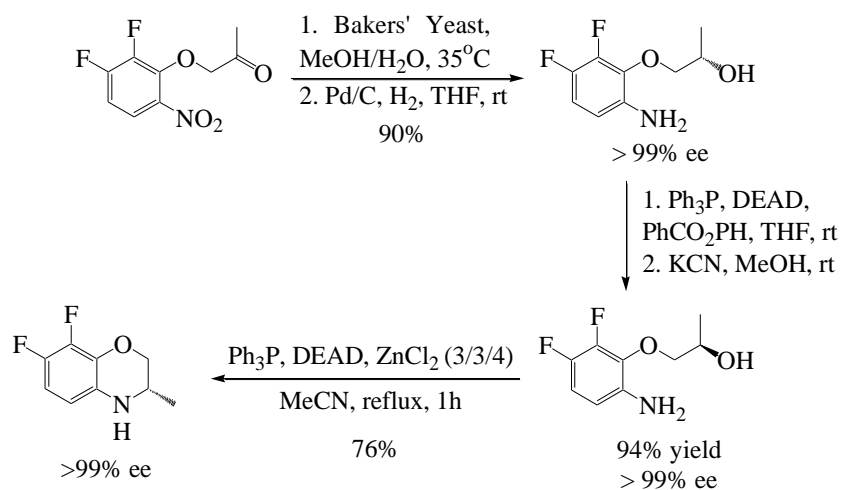
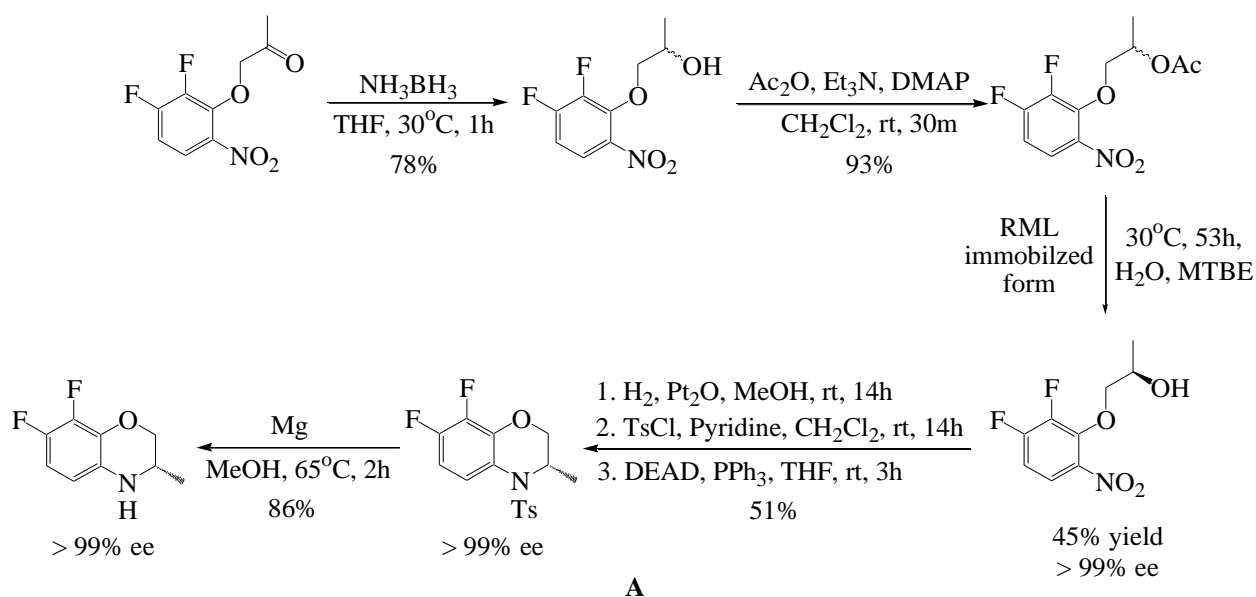


Scheme 1.6 Synthesis of racemic ethyl 3,4-dihydro-2*H*-1,4-benzoxazine-2-carboxylate **rac-2**

However, due to the differences in biological activities of two enantiomers, our concern was on the enantiopure ethyl 3,4-dihydro-2*H*-1,4-benzoxazine-2-carboxylates (**R**)- and (**S**)-**2**. Unfortunately, there were not many reports in the available literature brought up an effortless and straightforward procedure to obtain chiral 1,4-benzoxazine derivatives.

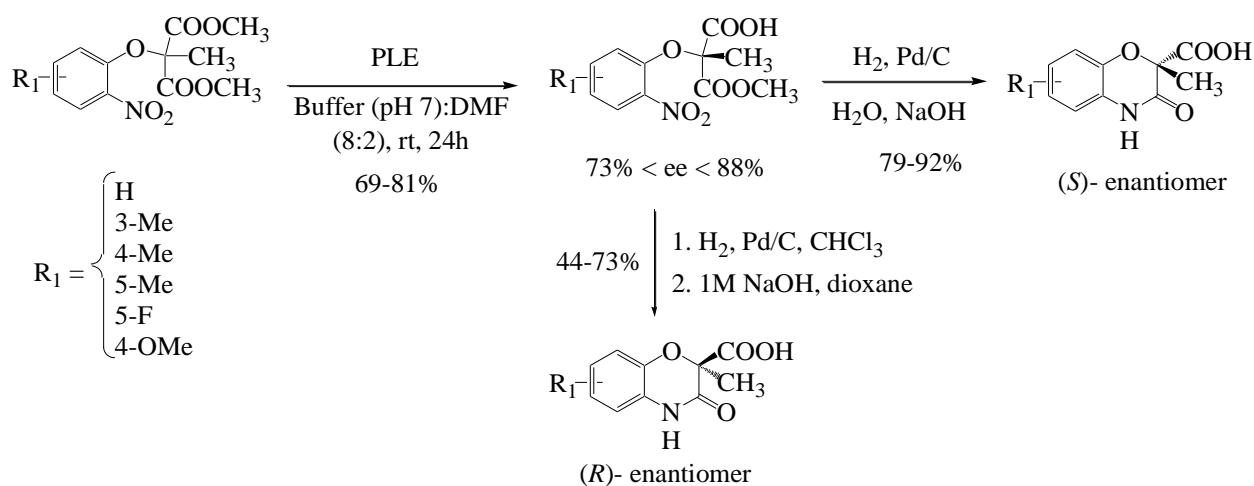
3.2. Synthetic routes for chiral 1,4-benzoxazine derivatives

An enantioselective synthesis of Levofloxacin precursor was presented by López-Iglesias et al. used enzyme-catalyzed like *Rhizomucor miehei* lipase (RML) and dehydrogenase enzyme ADH-A. Despite of good yield and rich enantiomeric excess of final compound, this method took long time and needed multi-steps to proceed⁷⁹ (Scheme 1.7A). Another method to acquire precursor of levofloxacin and to enhance properties of synthetic process (yield, enantiomeric excess, *etc.*) was the use of Bakers' Yeast to obtain enantiomer of intermediate compound. The intermediate then formed ring closure *via* an intramolecular Mitsunobu cyclization reaction in the presence of zinc chloride to eliminate unexpected by-product⁸⁰ (Scheme 1.7B).



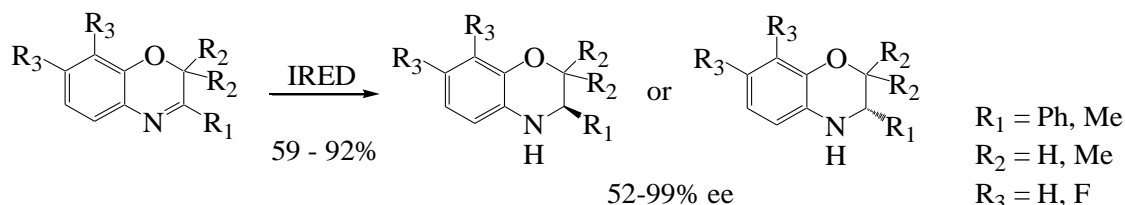
Scheme 1.7 Synthesis of Levofloxacin precursor

With similarly principle of using enzyme catalyst, Breznik et al. employed useful pig liver esterase (PLE) to obtain chiral intermediate⁸¹. Palladium on charcoal as catalyst then was used to make cyclization for obtainment of both enantiomers of 2-methyl-3-oxo-3,4-dihydro-2*H*-1,4-benzoxazine-2-carboxylic acid in good yield. The major product was produced depending on solvent (Scheme 1.8).



Scheme 1.8 Synthesis of (*S*)- and (*R*)-2-methyl-3-oxo-3,4-dihydro-2*H*-1,4-benzoxazine-2-carboxylic acids via PLE

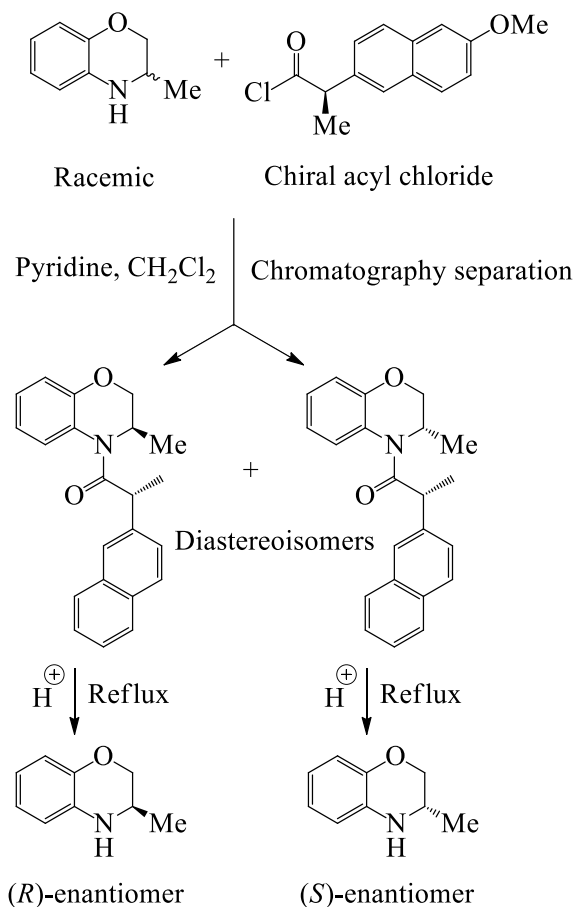
In order to identify a simple route for enantioselective synthesis of 3,4-dihydro-2*H*-1,4-benzoxazines, Zumbrägel et al. employed imine reductases (IREDs). IREDs are helpful biocatalyst using for asymmetric synthesis of chiral amines by reduction of imines. In this case, IRED catalyzed the reduction of 2*H*-1,4-benzoxazines under mild conditions^{82,83}. The outcomes expressed a good conversion based on type of IRED and high enantiomeric excess of 3,4-dihydro-2*H*-1,4-benzoxazines (Scheme 1.9).



Scheme 1.9 Synthesis of (*R*)- or (*S*)-3,4-dihydro-2*H*-1,4-benzoxazines using IRED

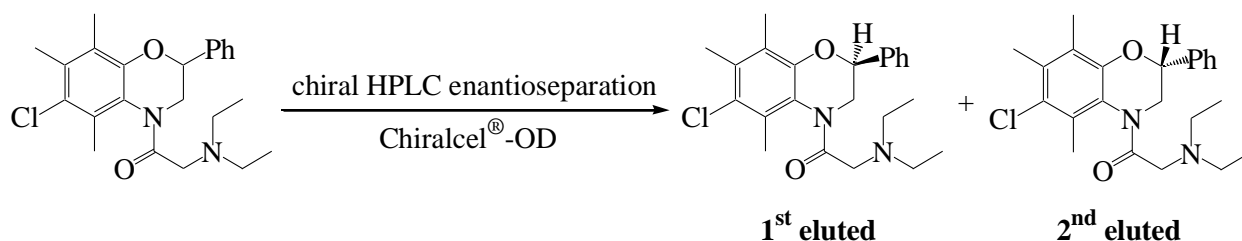
As mentioned above, the separation and purification of enantiomers from its racemic form by racemate resolution methods are commonly used. To obtain pure (*R*)- and (*S*)-2,3-dihydro-3-methyl-4*H*-1,4-benzoxazine, a process was revealed by reacting its racemate with chiral acyl chloride to create mixture of two diastereoisomers then easy be separated by achiral column. While two enantiomers are identical in term of chemical and physical properties, diastereoisomers are not so their separation should not be a concern. Pure enantiomers of 1,4-benzoxazine were obtained after hydrolysis by heating each single diastereoisomer under reflux in very acidic environment and purification by column chromatography. The desired enantiomers were recovered in moderate yield but high enantiomeric excess ($\geq 99\%$)^{84,85}

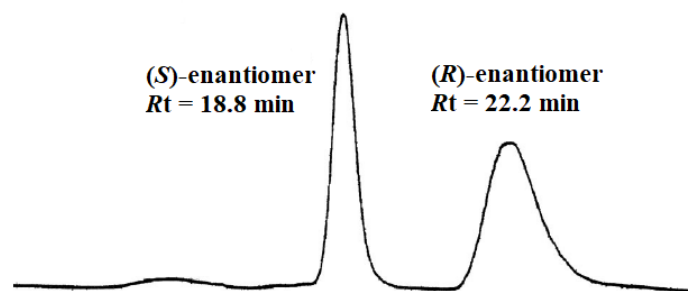
(Scheme 1.10). Similar approaches also were mentioned in other articles for their particular purposes⁸⁶⁻⁸⁸.



Scheme 1.10 Separation of (*R*)- and (*S*)-2,3-dihydro-3-methyl-4*H*-1,4-benzoxazine by kinetic resolution

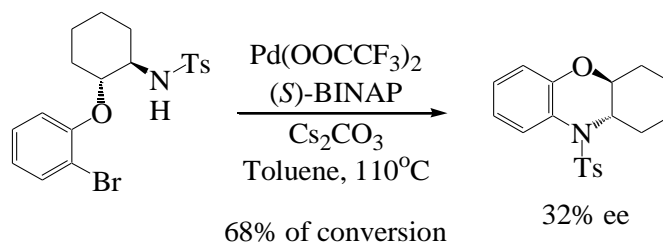
Koini et al.⁵⁰ reported before about using chiral HPLC to separate two enantiomers from synthesized racemic mixture of a 1,4-benzoxazine analogue. Chiralcel[®]-OD as chiral stationary phase and a mixture of hexane/2-propanol (90/10, v/v) as mobile phase were applied. The first eluted fraction was indicated as (*S*)-enantiomer and the second one was (*R*)-enantiomer with retention time was 18.8 min and 22.2 min, respectively (Scheme 1.11).





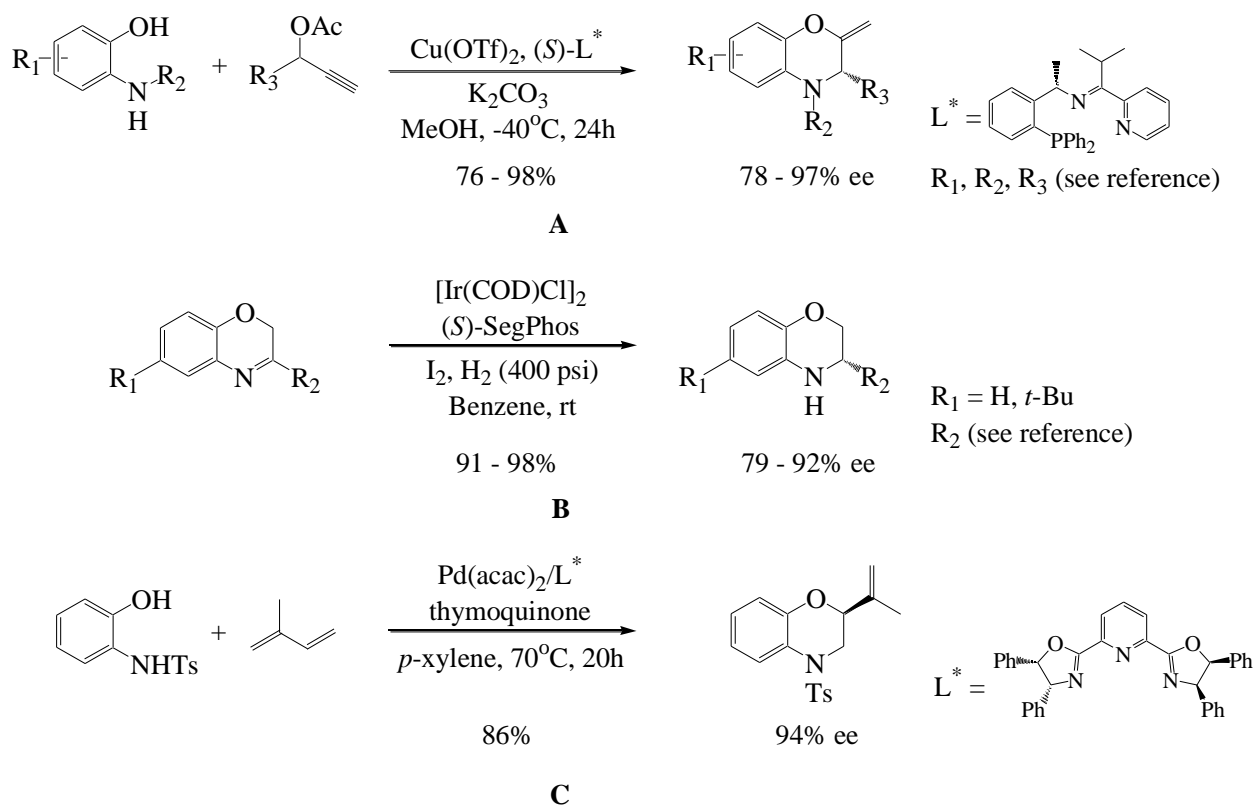
Scheme 1.11 Separation of (*S*)- and (*R*)-1,4-benzoxazine derivative by chiral HPLC on Chiralcel[®]-OD

Employed the kinetic resolution method, Rao et al. did a little more complicated work by using palladium complex as catalyst together with chiral ligand⁸⁹. *Via* screening of various solvents, bases and changing of other parameters, it turned out that (*S*)-BINAP as chiral ligand, Pd(OOCCF₃)₂ as palladium source in the presence of Cs₂CO₃ in toluene under reflux gave the best result of 68% of conversion. However, the enantiomeric excess of product only reached 32% (Scheme 1.12).



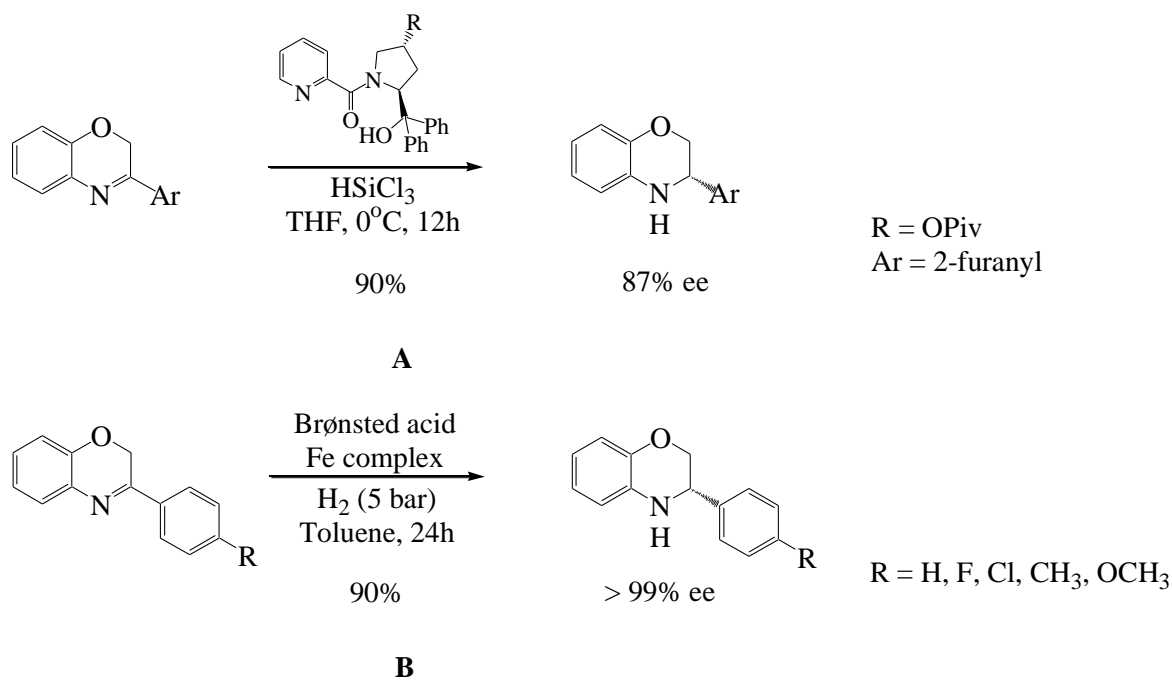
Scheme 1.12 Synthesis of optical active 1,4-benzoxazine derivative

In term of asymmetric synthesis, organometallic complexes are known as effective and high reactivity reagents. Few examples described enantioselective synthesis of 1,4-benzoxazine ring such as using copper-catalyzed⁹⁰ to form [4+2] cycloaddition reaction between 2-aminophenol and various propargylic esters to obtain 1,4-benzoxazine enantiomer in excellent yield (Scheme 1.13A) or employment of iridium-catalyzed⁹¹ to hydrogenate 3-aryl-2*H*-1,4-benzoxazines *via* one step reaction (Scheme 1.13B). Similarly, mechanism using palladium-catalysis⁹² to develop series of chiral 1,4-benzoxazine *via* asymmetric amino hydroxylation, gave very good yield and rich enantiomeric excess (Scheme 1.13C).



Scheme 1.13 Synthesis of chiral 1,4-benzoxazine derivatives using organometallic and chiral ligands

Besides organometallic, organic catalysts also are common reagents used for enantioselective synthesis of chiral active compounds because they are environmentally friendly, less toxic and low-cost⁹³ compare to metals. Screening of different Lewis bases to develop straightforward way to obtain chiral substituted 1,4-benzoxazine by hydrosilylation, Jiang et al.⁹⁴ successfully afforded enantioenriched products in moderate enantiomeric excess of products (Scheme 1.14A). A similarly method was applied by Liu et al.⁹⁵. With the ambition of not using noble metals as others, Fleischer et al.⁹⁶ employed iron complex and Brønsted acid to hydrogenate 4-substituted-2*H*-1,4-benzoxazines (Scheme 1.14B).



Scheme 1.14 Synthesis of chiral 1,4-benzoxazine derivatives using organic catalysts

Using phase-transfer-catalyzed⁹⁷ or Brønsted acid cooperated with non-metal catalyze⁹⁸ to achieve enantioenriched 1,4-benzoxazine also were reported.

However, all the mentioned methods require multi-steps or expensive reagents to succeed. Thus, the essential of designing a straightforward way, using inexpensive reagents and uncomplicated manipulations to acquire directly chiral molecules bearing 1,4-benzoxazine core is accelerating us to engage in this subject. Herein we reported the synthesis routes and conformational behaviour analysis of new chiral 3,4-dihydro-2*H*-1,4-benzoxazine derivatives as new pseudopeptides for potential biological activities. To achieve the goals, it was considered to try to obtain both (*R*)- and (*S*)-ethyl 3,4-dihydro-2*H*-1,4-benzoxazine-2-carboxylates *via* two strategies: enantioselective synthesis and enantioseparation of racemate by chiral HPLC. After this first aim, different α -amino acids could be coupled at the *C*- and/or *N*-terminal extremities of 1,4-benzoxazine core in order to form pseudopeptide analogues. Finally, structure analysis will be realized on the obtained compounds by using different techniques (NMR experiments, IR, X-Ray crystallography, *etc.*).

REFERENCES

- (1) Fosgerau, K.; Hoffmann, T. Peptide Therapeutics: Current Status and Future Directions. *Drug Discovery Today* **2015**, *20* (1), 122–128.
- (2) Haggag, Y. A. Peptides as Drug Candidates: Limitations and Recent Development Perspectives. *BJSTR* **2018**, *8* (4), 6659–6662.
- (3) Trabocchi, A.; Guarna, A. *Peptidomimetics in Organic and Medicinal Chemistry: The Art of Transforming Peptides in Drugs*; John Wiley & Sons, Ltd: Chichester, UK, 2014.
- (4) Lee, A. C.-L.; Harris, J. L.; Khanna, K. K.; Hong, J.-H. A Comprehensive Review on Current Advances in Peptide Drug Development and Design. *IJMS* **2019**, *20* (10), 2383.
- (5) Suat, K.; Jois, S. Design of Beta-Turn Based Therapeutic Agents. *Curr. Pharm. Des.* **2003**, *9* (15), 1209–1224.
- (6) Dua, R.; Shrivastava, S.; Sonwane, S. K.; Srivastava, S. K. Pharmacological Significance of Synthetic Heterocycles Scaffold: A Review. **2011**, 25.
- (7) Wang, M.; Rakesh, K. P.; Leng, J.; Fang, W.-Y.; Ravindar, L.; Channe Gowda, D.; Qin, H.-L. Amino Acids/Peptides Conjugated Heterocycles: A Tool for the Recent Development of Novel Therapeutic Agents. *Bioorganic Chemistry* **2018**, *76*, 113–129.
- (8) *Drug Stereochemistry: Analytical Methods and Pharmacology*, 2nd ed., revised and expanded.; Wainer, I. W., Ed.; Clinical pharmacology; M. Dekker: New York, 1993.
- (9) Karras, M. Synthesis of Enantiomerically Pure Helical Aromatics Such as NHC Ligands and Their Use in Asymmetric Catalysis, Universität Potsdam, 2018.
- (10) Gascón, A. R.; Campo, E.; Hernández, R. M.; Calvo, B.; Errasti, J.; Muñoz, J. L. P. Pharmacokinetics of Ofloxacin Enantiomers after Intravenous Administration for Antibiotic Prophylaxis in Biliary Surgery. *The Journal of Clinical Pharmacology* **2000**, *40* (8), 869–874.
- (11) Nguyen, L. A.; He, H.; Pham-Huy, C. Chiral Drugs: An Overview. *International Journal of Biomedical Science* **2006**, *2*, 85–100.
- (12) Tokunaga, E.; Yamamoto, T.; Ito, E.; Shibata, N. Understanding the Thalidomide Chirality in Biological Processes by the Self-Disproportionation of Enantiomers. *Sci Rep* **2018**, *8* (1), 17131.
- (13) Yashiro, K.; Miyagawa, S.; Sawa, Y. A Lesson From the Thalidomide Tragedy — *The Past Is Never Dead. It's Not Even Past*. William Faulkner, From “Requiem for a Nun” —. *Circ J* **2018**, *82* (9), 2250–2252.
- (14) Ridings, J. E. The Thalidomide Disaster, Lessons from the Past. In *Teratogenicity Testing*; Barrow, P. C., Ed.; Humana Press: Totowa, NJ, 2013; Vol. 947, pp 575–586.

- (15) Geisslinger, G.; Stock, K.-P.; Bach, G. L.; Loew, D.; Brune, K. Pharmacological Differences between R(-)- and S(+)-Ibuprofen. *Agents and Actions* **1989**, *27* (3–4), 455–457.
- (16) Pirkle, W. H.; Welch, C. J.; Lamm, B. Design, Synthesis, and Evaluation of an Improved Enantioselective Naproxen Selector. *J. Org. Chem.* **1992**, *57* (14), 3854–3860.
- (17) Kean, W. F.; Lock, C. J. L.; Rischke, J.; Butt, R.; Watson Buchanan, W.; Howard-Lock, H. Effect of R and S Enantiomers of Naproxen on Aggregation and Thromboxane Production in Human Platelets. *Journal of Pharmaceutical Sciences* **1989**, *78* (4), 324–327.
- (18) Kluska, M.; Marciniuk-Kluska, A.; Prukała, D.; Prukała, W. Analytics of Quinine and Its Derivatives. *Critical Reviews in Analytical Chemistry* **2016**, *46* (2), 139–145.
- (19) Easson, L. H.; Stedman, E. Studies on the Relationship between Chemical Constitution and Physiological Action: Molecular Dissymmetry and Physiological Activity. *Biochem J* **1933**, *27* (4), 1257–1266.
- (20) Agranat, I.; Caner, H.; Caldwell, J. Putting Chirality to Work: The Strategy of Chiral Switches. *Nat Rev Drug Discov* **2002**, *1* (10), 753–768.
- (21) Hamidi, S.; Jouyban, A. Pre-Concentration Approaches Combined with Capillary Electrophoresis in Bioanalysis of Chiral Cardiovascular Drugs. *Pharm Sci* **2015**, *21* (4), 229–243.
- (22) Mane, S. Racemic Drug Resolution: A Comprehensive Guide. *Anal. Methods* **2016**, *8* (42), 7567–7586.
- (23) Diaz-Muñoz, G.; Miranda, I. L.; Sartori, S. K.; Rezende, D. C.; Alves Nogueira Diaz, M. Use of Chiral Auxiliaries in the Asymmetric Synthesis of Biologically Active Compounds: A Review. *Chirality* **2019**, *31* (10), 776–812.
- (24) Fogassy, E.; Nógrádi, M.; Kozma, D.; Egri, G.; Pálovics, E.; Kiss, V. Optical Resolution Methods. *Org. Biomol. Chem.* **2006**, *4* (16), 3011–3030.
- (25) Meyer, V. R. *Practical High-Performance Liquid Chromatography*, 5th Edition.; John Wiley & Sons, Ltd, 2010.
- (26) LC-GC magazine; Crawford Scientific. Theory of HPLC Chromatographic Parameters <https://www.chromacademy.com/hplc-training.html>.
- (27) Francotte, E. R. Enantioselective Chromatography as a Powerful Alternative for the Preparation of Drug Enantiomers. *Journal of Chromatography A* **2001**, *906* (1–2), 379–397.

- (28) Andersson, S.; Allenmark, S. G. Preparative Chiral Chromatographic Resolution of Enantiomers in Drug Discovery. *Journal of Biochemical and Biophysical Methods* **2002**, *54* (1–3), 11–23.
- (29) Okamoto, Y.; Kawashima, M.; Hatada, K. Useful Chiral Packing Materials for High-Performance Liquid Chromatographic Resolution of Enantiomers: Phenylcarbamates of Polysaccharides Coated on Silica Gel. *Journal of the American Chemical Society* **1984**, *106*, 5357–5359.
- (30) Zhang, Y.; Yao, S.; Zeng, H.; Song, H. Chiral Separation of Pharmaceuticals by High Performance Liquid Chromatography. *CPA* **2010**, *6* (2), 114–130.
- (31) Leek, H.; Andersson, S. Preparative Scale Resolution of Enantiomers Enables Accelerated Drug Discovery and Development. *Molecules* **2017**, *22* (1), 158.
- (32) Roussel, C.; Rio, A. D.; Pierrot-Sanders, J.; Piras, P.; Vanthuyne, N. Chiral Liquid Chromatography Contribution to the Determination of the Absolute Configuration of Enantiomers. *Journal of Chromatography A* **2004**, *1037* (1–2), 311–328.
- (33) Berova, N.; Bari, L. D.; Pescitelli, G. Application of Electronic Circular Dichroism in Configurational and Conformational Analysis of Organic Compounds. *Chem. Soc. Rev.* **2007**, *36* (6), 914.
- (34) Dale, J. A.; Mosher, H. S. Nuclear Magnetic Resonance Enantiomer Regents. Configurational Correlations via Nuclear Magnetic Resonance Chemical Shifts of Diastereomeric Mandelate, O-Methylmandelate, and .Alpha.-Methoxy-.Alpha.-Trifluoromethylphenylacetate (MTPA) Esters. *J. Am. Chem. Soc.* **1973**, *95* (2), 512–519.
- (35) Seco, J. M.; Quiñoá, E.; Riguera, R. Boc-Phenylglycine: The Reagent of Choice for the Assignment of the Absolute Configuration of α -Chiral Primary Amines by ^1H NMR Spectroscopy. *J. Org. Chem.* **1999**, *64* (13), 4669–4675.
- (36) Leung, D.; Kang, S. O.; Anslyn, E. V. Rapid Determination of Enantiomeric Excess: A Focus on Optical Approaches. *Chem. Soc. Rev.* **2012**, *41* (1), 448–479.
- (37) Lewis, R. J.; Bernstein, M. A.; Chang, H.-F.; Chapman, D.; Pemberton, N. Enantiomeric Purity Determination by NMR: Proving the Purity of a Single Enantiomer. *Tetrahedron: Asymmetry* **2013**, *24* (13–14), 866–870.
- (38) Parker, David. NMR Determination of Enantiomeric Purity. *Chem. Rev.* **1991**, *91* (7), 1441–1457.
- (39) Touzeau, F.; Arrault, A.; Guillaumet, G.; Scalbert, E.; Pfeiffer, B.; Rettori, M.-C.; Renard, P.; Mérour, J.-Y. Synthesis and Biological Evaluation of New 2-(4,5-Dihydro-1 *H* -

- Imidazol-2-Yl)-3,4-Dihydro-2 H -1,4-Benzoxazine Derivatives. *J. Med. Chem.* **2003**, *46* (10), 1962–1979.
- (40) LARGERON, M.; DUPUY, H.; FLEURY, M.-B. Novel 1,4-Benzoxazine Derivatives of Pharmacological Interest. Electrochemical and Chemical Syntheses. *Tetrahedron* **1995**, *51* (17), 4953–4968.
- (41) FLEURY, M.-B.; MAURETTE, J.-M.; COLOMBES, G.; LARGERON, M. Benzoxazine Derivatives, Methods for Obtaining Same, and Their Use as Drugs. 5804580, 1998.
- (42) LARGERON, M.; MESPLES, B.; GRESSENS, P.; CECHELLI, R.; SPEDDING, M.; LE RIDANT, A.; FLEURY, M.-B. The Neuroprotective Activity of 8-Alkylamino-1,4-Benzoxazine Antioxidants. *European Journal of Pharmacology* **2001**, *424* (3), 189–194.
- (43) BLATTES, E.; LOCKHART, B.; LESTAGE, P.; SCHWENDIMANN, L.; GRESSENS, P.; FLEURY, M.-B.; LARGERON, M. Novel 2-Alkylamino-1,4-Benzoxazine Derivatives as Potent Neuroprotective Agents: Structure–Activity Relationship Studies. *Journal of Medicinal Chemistry* **2005**, *48* (4), 1282–1286.
- (44) WANG, L.; ANKATI, H.; AKUBATHINI, S. K.; BALDERAMOS, M.; STOREY, C. A.; PATEL, A. V.; PRICE, V.; KRETZSCHMAR, D.; BIEHL, E. R.; D’MELLO, S. R. Identification of Novel 1,4-Benzoxazine Compounds That Are Protective in Tissue Culture and in Vivo Models of Neurodegeneration. *Journal of Neuroscience Research* **2010**, 1970–1984.
- (45) LA, D. S.; BELZILE, J.; BREADY, J. V.; COXON, A.; DEMELFI, T.; DOERR, N.; ESTRADA, J.; FLYNN, J. C.; FLYNN, S. R.; GRACEFFA, R. F.; HARRIMAN, S. P.; LARROW, J. F.; LONG, A. M.; MARTIN, M. W.; MORRISON, M. J.; PATEL, V. F.; ROVETO, P. M.; WANG, L.; WEISS, M. M.; WHITTINGTON, D. A.; TEFFERA, Y.; ZHAO, Z.; POLVERINO, A. J.; HARMANGE, J.-C. Novel 2,3-Dihydro-1,4-Benzoxazines as Potent and Orally Bioavailable Inhibitors of Tumor-Driven Angiogenesis [¶]. *J. Med. Chem.* **2008**, *51* (6), 1695–1705.
- (46) HONDA, T.; TERAOKA, T.; AONO, H.; BAN, M. Synthesis of Novel 1,4-Benzoxazin-3-One Derivatives as Inhibitors against Tyrosine Kinases. *Bioorg. Med. Chem* **2009**, *17* (2), 699–708.
- (47) ILIĆ, M.; KIKELJ, D.; ILAŠ, J. Fluorinated Dual Antithrombotic Compounds Based on 1,4-Benzoxazine Scaffold. *European Journal of Medicinal Chemistry* **2012**, *50*, 255–263.
- (48) ILIĆ, M.; ILAŠ, J.; DUNKEL, P.; MÁTYUS, P.; BOHÁČ, A.; LIEKENS, S.; KIKELJ, D. Novel 1,4-Benzoxazine and 1,4-Benzodioxine Inhibitors of Angiogenesis. *European Journal of Medicinal Chemistry* **2012**, *58*, 160–170.

- (49) Bourlot, A.-S.; Sánchez, I.; Dureng, G.; Guillaumet, G.; Massingham, R.; Monteil, A.; Winslow, E.; Pujol, M. D.; Mérour, J.-Y. New Substituted 1,4-Benzoxazine Derivatives with Potential Intracellular Calcium Activity. *J. Med. Chem.* **1998**, *41* (17), 3142–3158.
- (50) Koini, E. N.; Papazafiri, P.; Vassilopoulos, A.; Koufaki, M.; Horváth, Z.; Koncz, I.; Virág, L.; Papp, G. J.; Varró, A.; Calogeropoulou, T. 5,7,8-Trimethyl-Benzopyran and 5,7,8-Trimethyl-1,4-Benzoxazine Aminoamide Derivatives as Novel Antiarrhythmics against Ischemia–Reperfusion Injury. *Journal of Medicinal Chemistry* **2009**, *52* (8), 2328–2340.
- (51) Ohno, M.; Tanaka, Y.; Miyamoto, M.; Takeda, T.; Hoshi, K.; Yamada, N.; Ohtake, A. Development of 3,4-Dihydro-2H-Benzo[1,4]Oxazine Derivatives as Dual Thromboxane A₂ Receptor Antagonists and Prostacyclin Receptor Agonists. *Bioorganic & Medicinal Chemistry* **2006**, *14* (6), 2005–2021.
- (52) Zhou, D.; Harrison, B. L.; Shah, U.; Andree, T. H.; Hornby, G. A.; Scerni, R.; Schechter, L. E.; Smith, D. L.; Sullivan, K. M.; Mewshaw, R. E. Studies toward the Discovery of the next Generation of Antidepressants. Part 5: 3,4-Dihydro-2H-Benzo[1,4]Oxazine Derivatives with Dual 5-HT_{1A} Receptor and Serotonin Transporter Affinity. *Bioorganic & Medicinal Chemistry Letters* **2006**, *16* (5), 1338–1341.
- (53) Ward, S. E.; Johnson, C. N.; Lovell, P. J.; Scott, C. M.; Smith, P. W.; Stemp, G.; Thewlis, K. M.; Vong, A. K.; Watson, J. M. Studies on a Series of Potent, Orally Bioavailable, 5-HT₁ Receptor Ligands. *Bioorganic & Medicinal Chemistry Letters* **2007**, *17* (18), 5214–5217.
- (54) Pirotte, B.; Florence, X.; Goffin, E.; Lebrun, P. 2,2-Dimethyl-3,4-Dihydro-2H-1,4-Benzoxazines as Isosteres of 2,2-Dimethylchromans Acting as Inhibitors of Insulin Release and Vascular Smooth Muscle Relaxants. *Medicinal Chemistry Communications* **2019**, *10* (3), 431–438.
- (55) Brito, R.; Sheth, S.; Mukherjea, D.; Rybak, L.; Ramkumar, V. TRPV1: A Potential Drug Target for Treating Various Diseases. *Cells* **2014**, *3* (2), 517–545.
- (56) Cheung, W. S.; Calvo, R. R.; Tounge, B. A.; Zhang, S.-P.; Stone, D. R.; Brandt, M. R.; Hutchinson, T.; Flores, C. M.; Player, M. R. Discovery of Piperidine Carboxamide TRPV1 Antagonists. *Bioorganic & Medicinal Chemistry Letters* **2008**, *18* (16), 4569–4572.
- (57) Matsuoka, H.; Ohi, N.; Mihara, M.; Suzuki, H.; Miyamoto, K.; Maruyama, N.; Tsuji, K.; Kato, N.; Akimoto, T.; Takeda, Y.; Yano, K.; Kuroki, T. Antirheumatic Agents: Novel Methotrexate Derivatives Bearing a Benzoxazine or Benzothiazine Moiety. *J. Med. Chem.* **1997**, *40* (1), 105–111.

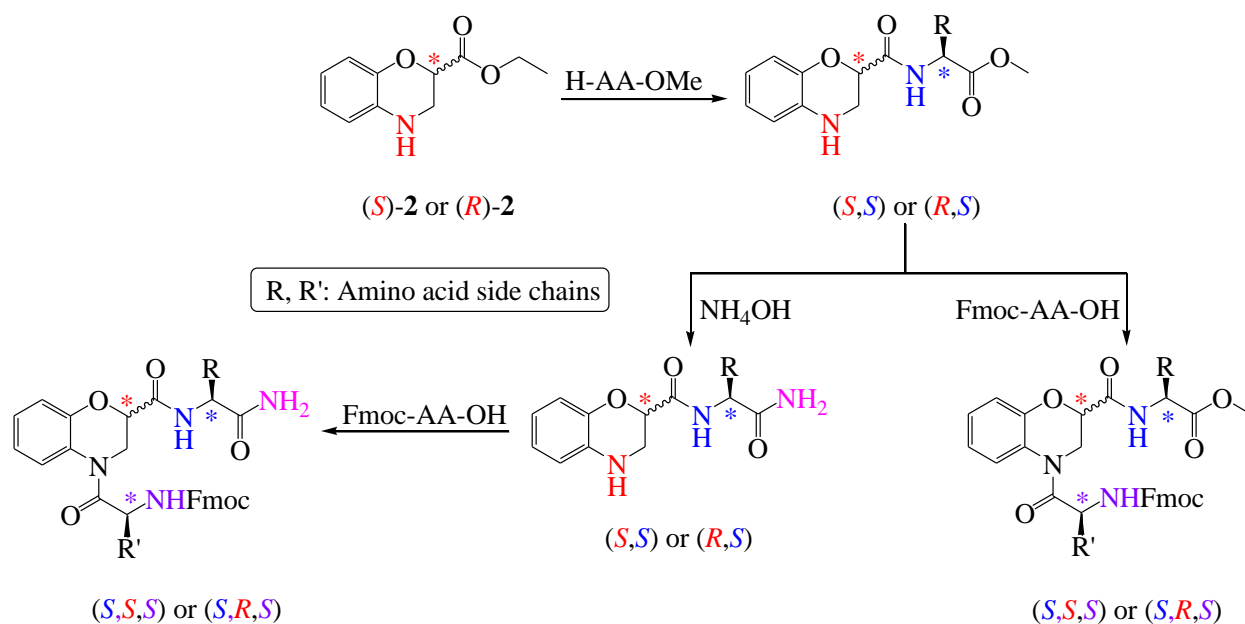
- (58) Sneader, W. *Drug Discovery: A History*; John Wiley & Sons, Ltd, 2005.
- (59) M Bush, L.; Chaparro-Rojas, F.; Okeh, V.; Etienne, J. Cumulative Clinical Experience from over a Decade of Use of Levofloxacin in Urinary Tract Infections: Critical Appraisal and Role in Therapy. *IDR* **2011**, 177–189.
- (60) Hayakawa, I.; Atarashi, S.; Yokohama, S.; Imamura, M.; Sakano, K.; Furukawa, M. Synthesis and Antibacterial Activities of Optically Active Ofloxacin. *Antimicrobial Agents and Chemotherapy* **1986**, 29 (1), 163–164.
- (61) Li, X.; Liu, N.; Zhang, H.; Knudson, S. E.; Slayden, R. A.; Tonge, P. J. Synthesis and SAR Studies of 1,4-Benzoxazine MenB Inhibitors: Novel Antibacterial Agents against Mycobacterium Tuberculosis. *Bioorganic & Medicinal Chemistry Letters* **2010**, 20 (21), 6306–6309.
- (62) Pamerla, M.; Rama Sekhara Reddy, D.; Sreenivasa Rao, B.; Bodipati, N.; Murthy, Y. L. N. Antimicrobial Evaluation of 1,4-Benzoxazine Derivatives. *Medicinal Chemistry Research* **2015**, 24 (2), 611–615.
- (63) Alper-Hayta, S.; Akı-Sener, E.; Tekiner-Gulbas, B.; Yıldız, I.; Temiz-Arpacı, O.; Yalcın, I.; Altanlar, N. Synthesis, Antimicrobial Activity and QSARs of New Benzoxazine-3-Ones. *European Journal of Medicinal Chemistry* **2006**, 41 (12), 1398–1404.
- (64) Štefanič, P.; Turnšek, K.; Kikelj, D. Synthesis of Alkyl 4-Alkyl-2-Hydroxy-3-Oxo-3,4-Dihydro-2H-1,4-Benzoxazine-2-Carboxylates as Peptidomimetic Building Blocks. *Tetrahedron* **2003**, 59 (36), 7123–7129.
- (65) Štefanič, P.; Simončič, Z.; Breznik, M.; Plavec, J.; Anderluh, M.; Addicks, E.; Giannis, A.; Kikelj, D. Conformationally Tailored N-[(2-Methyl-3-Oxo-3,4-Dihydro-2H-1,4-Benzoxazin-2-yl)Carbonyl]Proline Templates as Molecular Tools for the Design of Peptidomimetics. Design and Synthesis of Fibrinogen Receptor Antagonists. *Org. Biomol. Chem.* **2004**, 2 (10), 1511–1517.
- (66) Tratar, F.; Marc, G.; Sollner, M.; Kikelj, D. Synthesis of the Retro-Inverso Peptide Analogues of N-Acetylmuramyl-L-Alanyl-D-Isoglutamine (MDP). *Arkivoc* **2001**, 2001 (5), 7.
- (67) Macías, F. A.; Chinchilla, N.; Varela, R. M.; Oliveros-Bastidas, A.; Marín, D.; Molinillo, J. M. G. Structure–Activity Relationship Studies of Benzoxazinones and Related Compounds. Phytotoxicity on *Echinochloa Crus-Galli* (L.) P. Beauv. *J. Agric. Food Chem.* **2005**, 53 (11), 4373–4380.
- (68) Macías, F. A.; Chinchilla, N.; Varela, R. M.; Molinillo, J. M. G.; Marín, D.; De Siqueira, J. M. Modified Benzoxazinones in the System *Oryza Sativa* – *Echinochloa Crus-Galli* :

- An Approach to the Development of Biorational Herbicide Models. *J. Agric. Food Chem.* **2008**, *56* (21), 9941–9948.
- (69) Ilaš, J.; Anderluh, P. Š.; Dolenc, M. S.; Kikelj, D. Recent Advances in the Synthesis of 2H-1,4-Benzoxazin-3-(4H)-Ones and 3,4-Dihydro-2H-1,4-Benzoxazines. *Tetrahedron* **2005**, *61* (31), 7325–7348.
- (70) Battistoni, P.; Bruni, P.; Fava, G. A General Method for the Synthesis of 3-Phenyl-2H-1,4-Benzoxazines and 3-Phenyl-2H-3,4-Dihydro-1,4-Benzoxazines. *Synthetic Communications* **1979**, No. 3, 220–221.
- (71) Matsumoto, Y.; Tsuzuki, R.; Matsuhisa, A.; Takayama, K.; Yoden, T.; Uchida, W.; Asano, M.; Fujita, S.; Yanagisawa, I.; Fujikura, T. Novel Potassium Channel Activators: Synthesis and Structure-Activity Relationship Studies of 3,4-Dihydro-2H-1,4-Benzoxazine Derivatives. *Chemical and Pharmaceutical Bulletin* **1996**, *44* (1), 103–114.
- (72) Nguyen, K. M. H.; Schwendimann, L.; Gressens, P.; Langeron, M. Regiospecific Synthesis of Neuroprotective 1,4-Benzoxazine Derivatives through a Tandem Oxidation–Diels–Alder Reaction. *Org. Biomol. Chem.* **2015**, *13* (12), 3749–3756.
- (73) Wang, C.; He, X.; Liu, X.; Shang, Y. DMAP-Catalyzed Cyclization of Schiff Bases with α -Halo Ketones: Synthesis of 1,4-Benzoxazines. *Synthetic Communications* **2017**, *47* (9), 878–885.
- (74) Wei, S.; Feng, X.; Du, H. A Metal-Free Hydrogenation of 3-Substituted 2H-1,4-Benzoxazines. *Org. Biomol. Chem.* **2016**, *14* (34), 8026–8029.
- (75) Chioccare, F.; Prota, G.; Thomson, R. H. New Benzoxazine and Benzothiazine Dyes. *Tetrahedron* **1976**, *32* (12), 1407–1409.
- (76) Butler, R. C. M.; Chapleo, C. B.; Myers, P. L.; Welbourn, A. P. Synthesis of 2-(2-Imidazolyl) Substituted 2,3-Dihydro-4H-1,4-Benzothiazine and 3,4-Dihydro-2H-1,4-Benzoxazines. *J. Heterocycl. Chem.* **1985**, *22*, 177.
- (77) Bartsch, H. Studies on the Chemistry of 1,4-Oxazines, XV [1]: Synthesis of Ethyl 3,4-Dihydro-4-Tosyl-2H-1,4-Benzoxazine-3- Carboxylate. *Monatshefte für Chemie* **1987**, *118*, 273–276.
- (78) Sánchez, I.; López, N.; Pujol, M. D. New Synthesis of Methylfuro[3,4-b][1,4]Benzoxazine as an Intermediate in the Preparation of Polycyclic Compounds. *Arkivoc* **2006**, No. 1, 81–88.
- (79) López-Iglesias, M.; Busto, E.; Gotor, V.; Gotor-Fernández, V. Chemoenzymatic Asymmetric Synthesis of 1,4-Benzoxazine Derivatives: Application in the Synthesis of a Levofloxacin Precursor. *The Journal of Organic Chemistry* **2015**, *80* (8), 3815–3824.

- (80) Kang, S. B.; Ahn, E. J.; Kim, Y. A Facile Synthesis of (S)-(-)-7,8-Difluoro-3,4-Dihydro-3-Methyl-2H-1,4-Benzoxazine by Zinc Chloride Assisted Mitsunobu Cyclization Reaction. *Tetrahedron Letters* **1996**, *37*, 9317–9320.
- (81) Breznik, M.; Hrast, V.; Mrcina, A.; Kikelj, D. Stereoselective Synthesis of (R)- and (S)-2-Methyl-3-Oxo-3,4-Dihydro-2H-1,4-Benzoxazine-2-Carboxylic Acids, -Carboxylates and -Carboxamides. *Tetrahedron: Asymmetry* **1999**, *10* (1), 153–167.
- (82) Mangas-Sanchez, J.; France, S. P.; Montgomery, S. L.; Aleku, G. A.; Man, H.; Sharma, M.; Ramsden, J. I.; Grogan, G.; Turner, N. J. Imine Reductases (IREDs). *Current Opinion in Chemical Biology* **2017**, *37*, 19–25.
- (83) Zumbrägel, N.; Machui, P.; Nonnhoff, J.; Gröger, H. Enantioselective Biocatalytic Reduction of 2 H -1,4-Benzoxazines Using Imine Reductases. *J. Org. Chem.* **2019**, *84* (3), 1440–1447.
- (84) Charushin, V. N.; Krasnov, V. P.; Levit, G. L.; Korolyova, M. A.; Kodess, M. I.; Chupakhin, O. N.; Kim, M. H.; Lee, H. S.; Park, Y. J.; Kim, K.-C. Kinetic Resolution of (±)-2,3-Dihydro-3-Methyl-4H-1,4-Benzoxazines with (S)-Naproxen. *Tetrahedron: Asymmetry* **1999**, *10* (14), 2691–2702.
- (85) Slepukhin, P. A.; Gruzdev, D. A.; Chulakov, E. N.; Levit, G. L.; Krasnov, V. P.; Charushin, V. N. Structures of the Racemate and (S)-Enantiomer of 7,8-Difluoro-3-Methyl-2,3-Dihydro-4H-[1,4]Benzoxazine. *Russian Chemical Bulletin* **2011**, *60* (5), 955–960.
- (86) Chulakov, E. N.; Gruzdev, D. A.; Levit, G. L.; Sadretdinova, L. Sh.; Krasnov, V. P.; Charushin, V. N. 2-Arylpropionyl Chlorides in Kinetic Resolution of Racemic 3-Methyl-2,3-Dihydro-4H-[1,4]Benzoxazines. *Russ Chem Bull* **2011**, *60* (5), 948–954.
- (87) Korolyova, M. A.; Vakarov, S. A.; Kozhevnikov, D. N.; Gruzdev, D. A.; Levit, G. L.; Krasnov, V. P. Mutual Kinetic Resolution of Racemic 3,4-Dihydro-3-Methyl-2 H -[1,4]Benzoxazines with Acyl Chlorides of Racemic O -Phenyllactic Acids and DFT Modelling of Transition States: Mutual Kinetic Resolution of Racemic 3,4-Dihydro-3-Methyl-2H-[1,4]Benzoxazines with Acyl Chlorides of Racemic O-Phenyllactic Acids and DFT Modelling o. *Eur. J. Org. Chem.* **2018**, *2018* (33), 4577–4585.
- (88) Vakarov, S. A.; Gruzdev, D. A.; Sadretdinova, L. Sh.; Kodess, M. I.; Tumashov, A. A.; Gorbunov, E. B.; Levit, G. L.; Krasnov, V. P. Mutual Kinetic Resolution of 3-Methyl-3,4-Dihydro-2H-1,4-Benzoxazines and 2-Alkoxyacyl Chlorides. *Chemistry of Heterocyclic Compounds* **2018**, *54* (4), 437–446.

- (89) Koteswar Rao, R.; Sekar, G. Synthesis of Optically Active 1,4-Benzoxazine Derivatives Using Palladium-Catalyzed Coupling Kinetic Resolution. *Tetrahedron: Asymmetry* **2011**, *22* (9), 948–954.
- (90) Liu, Z.-T.; Wang, Y.-H.; Zhu, F.-L.; Hu, X.-P. Enantioselective Copper-Catalyzed Formal [4 + 2] Cycloaddition of o-Aminophenol Derivatives with Propargylic Esters for Synthesis of Optically Active 3,4-Dihydro-2H-1,4-Benzoxazines. *Organic Letters* **2016**, *18* (5), 1190–1193.
- (91) Gao, K.; Yu, C.-B.; Wang, D.-S.; Zhou, Y.-G. Iridium-Catalyzed Asymmetric Hydrogenation of 3-Substituted 2H-1,4-Benzoxazines. *Advanced Synthesis & Catalysis* **2012**, *354* (2–3), 483–488.
- (92) Shen, H.-C.; Wu, Y.-F.; Zhang, Y.; Fan, L.-F.; Han, Z.-Y.; Gong, L.-Z. Palladium-Catalyzed Asymmetric Aminohydroxylation of 1,3-Dienes. *Angewandte Chemie International Edition* **2018**, *57* (9), 2372–2376.
- (93) Oliveira, V.; Cardoso, M.; Forezi, L. Organocatalysis: A Brief Overview on Its Evolution and Applications. *Catalysts* **2018**, *8* (12), 605.
- (94) Jiang, Y.; Liu, L.-X.; Yuan, W.-C.; Zhang, X.-M. Lewis Base Organocatalyzed Enantioselective Hydrosilylation of 1,4-Benzoxazines. *Synlett* **2012**, *23*, 1797–1800.
- (95) Liu, X.-W.; Wang, C.; Yan, Y.; Wang, Y.-Q.; Sun, J. An Organocatalyst Bearing Stereogenic Carbon and Sulfur Centers as an Efficient Promoter for Enantioselective Hydrosilylation of 1,4-Benzoxazines. *J. Org. Chem.* **2013**, *78* (12), 6276–6280.
- (96) Fleischer, S.; Zhou, S.; Werkmeister, S.; Junge, K.; Beller, M. Cooperative Iron-Brønsted Acid Catalysis: Enantioselective Hydrogenation of Quinoxalines and 2H-1,4-Benzoxazines. *Chemistry - A European Journal* **2013**, *19* (16), 4997–5003.
- (97) Pawliczek, M.; Shimazaki, Y. Phase-Transfer-Catalysed Asymmetric Synthesis of 2,2-Disubstituted 1,4-Benzoxazin-3-Ones. *Chemical Communications* **2016**, *52* (1), 64–67.
- (98) Rueping, M.; Stoeckel, M.; Sugiono, E.; Theissmann, T. Asymmetric Metal-Free Synthesis of Fluoroquinolones by Organocatalytic Hydrogenation. *Tetrahedron* **2010**, *66* (33), 6565–6568.

CHAPTER II
SYNTHESIS OF ENANTIOPURE
3,4-DIHYDRO-2*H*-1,4-BENZOXAZINE
ANALOGUES



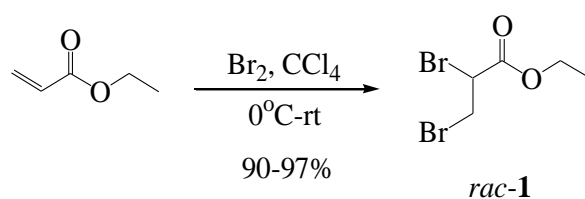
Scheme 2.1 Synthetic plan for obtainment of chiral 1,4-benzoxazine pseudopeptide analogues

2. Obtainment of chiral ethyl 2,3-dibromopropionate (*S*)-1 and (*R*)-1

2.1. Via enantioselective synthesis

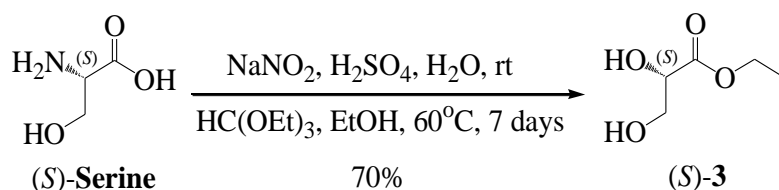
Racemic ethyl 2,3-dibromopropionate *rac*-1 is a key intermediate used in the synthesis of different heterocycles, especially benzoheterocycles. Among those heterocycles, we could mention aziridine-2-carboxylates¹, 1,4-benzodioxans², 1,4-benzoxathians³ and certainly 1,4-benzoxazine^{4,5}. Some of these compounds display interesting biological activities with antihepatotoxic⁶, anti-angiogenesis^{7,8} or anti-hypertensive^{9,10} properties. However, despite of overwhelming interest, only *rac*-1 is commercially available at low price, the optically pure enantiomers (*S*)-1 and (*R*)-1 and their corresponding carboxylic acids or other related esters have never been described in the literature. Therefore, we wished first to achieve enantiomerically pure of 1 then to engage it by a double substitution reaction with 2-aminophenol to obtain enantiopure (*R*)-2 and (*S*)-2.

Compound *rac*-1 could be easily obtained by an elementary reaction of bromination of ethyl acrylate in carbon tetrachloride^{11,12} (Scheme 2.2).



Scheme 2.2 Synthesis of racemic ethyl 2,3-dibromopropionate *rac*-1

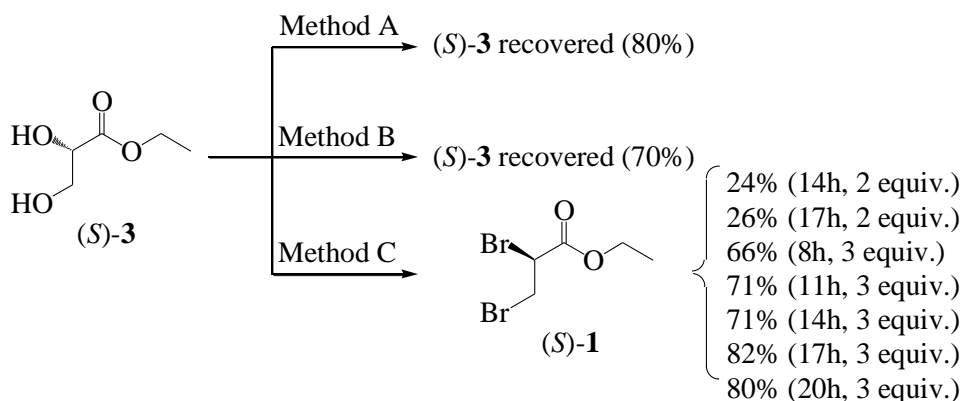
The enantioselective synthesis of (*S*)-**1** is based on brominating reaction starting from enantiomerically pure (*S*)-Ethyl glycerate (*S*)-**3**. (*S*)-**3** was obtained in 70% overall yield from (*S*)-Serine in two steps following the procedure that previously described by Mukaiyama et al.¹³ (Scheme 2.3). First step was taken 5 days for deamination of commercially available amino acid (*S*)-serine in highly acidic environment to generate (*S*)-glyceric acid. Second step took one day for esterification of glyceric acid by triethyl orthoformate in ethanol under reflux to obtain (*S*)-**3**. Including treatment and purification of crude mixture, this reaction took approximately 7 days to complete that was peculiarly long. A similar method was applied by Jervis et al.¹⁴ using solution of sodium nitrite and hydrochloric acid for hydrolysis of (*S*)-serine to convert amine group to hydroxyl then (*S*)-glyceric acid was esterified by *p*-toluenesulfonic acid (*p*-TSA) in ethanol. Their method also required around 5 days to complete but it seemed not effective for us to treat extremely sticky crude mixture that led to low yield (25%) of obtained product. Therefore, method of Mukaiyama was chosen and (*S*)-**3** was then subjected to a double brominating reaction *via* three different methods (Scheme 2.4).



Scheme 2.3 Synthesis of (*S*)-ethyl 2,3-dihydroxypropionate (*S*)-**3**

The optical rotation value of (*S*)-**3**: $[\alpha]_{\text{D}}^{25} = -11.2^\circ$ ($c = 0.05$, CHCl_3) was in agreement with those reported in literature $[\alpha]_{\text{D}}^{23} = -11.6^\circ$ ($c = 1.00$, CHCl_3)¹⁴ and $[\alpha]_{\text{D}}^{15} = -9.1^\circ$ ($c = 1.19$, CHCl_3)¹⁵. The difference might due to the low concentration of solution sample (1.00 in the literature and 0.05 in our case), temperature also could cause a little affect to optical value but the structure of (*S*)-**3** was confirmed by NMR.

The starting material (*S*)-**3** is subjected to a double bromination reaction with *N*-bromosuccinimide (NBS, Method A)¹⁶, phosphorus tribromide (PBr_3 , Method B)¹⁷, or carbon tetrabromide (CBr_4 , Method C)^{18–20} as brominating agents and triphenylphosphine (PPh_3 , Methods A and C) or pyridine (Method B) as co-reagents in CH_2Cl_2 or Et_2O as solvents (Scheme 2.4). (*S*)-**3** is always recovered with no racemization by using Methods A and B. Despite several attempts, only Method C (Appel reaction) with 2 or 3 equivalents of CBr_4 and PPh_3 provides (*S*)-**1** with yields from 24 to 82% (Scheme 2.4). It is also interesting to note that the Method C did not work with 1 equivalent of CBr_4 and PPh_3 . The Appel reaction in Method C proceeds via a $\text{S}_{\text{N}}2$ mechanism with spatial inversion of stereochemistry and affords (*S*)-**1**.



Scheme 2.4 Enantioselective synthesis of (*S*)-ethyl 2,3-dibromopropionate (*S*)-1

Before successfully achieved (*S*)-1 in good yield, the purification step brought some difficult. It seemed that compound (*S*)-1 degraded rapidly during the purification realized through silica gel flash column. To prove that the degradation occurred during purification, a mixture of commercially available *rac*-1, PPh₃ and PPh₃O was prepared to run over flash column. The result was extremely disappointing because only 70% of *rac*-1 was finally recovered. Acidic environment of silica gel could be the cause of the degradation. To bypass this problem, silica was replaced by neutral alumina oxide (Al₂O₃) and commercial *rac*-1 was run over. Unfortunately, 60-80% of *rac*-1 was only obtained after elution. To overcome this issue, purification by column chromatography was avoided and another solution was brought up to eliminate by-product PPh₃O followed reported method. A big part of PPh₃O was easily removed by forming a complex with zinc chloride²¹. After its precipitation in ethanol, the residual solute should contain only (*S*)-1. However, after several times of washing, PPh₃O could not be completely eliminated and a small quantity of (*S*)-1 was lost during filtration of solid.

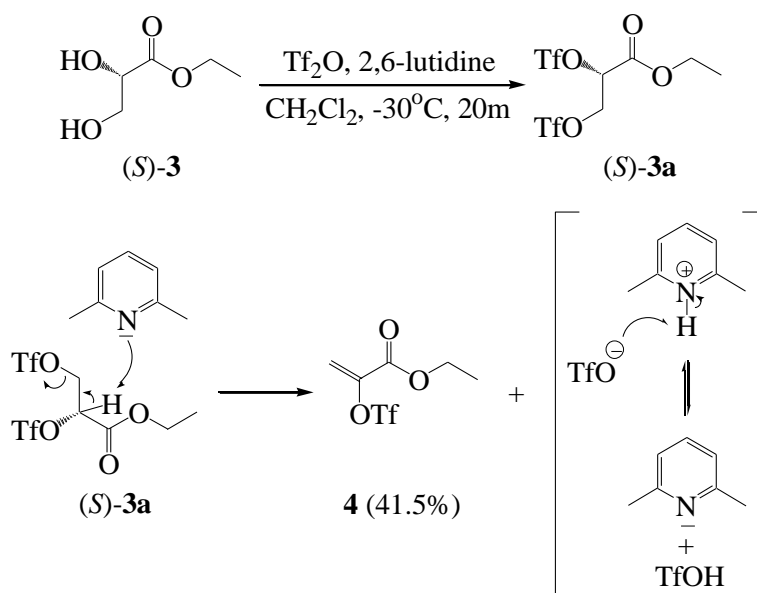
Table 1 Conditions for brominating of (*S*)-3

Method	Reagent	Base	Solvent	Temperature (°C)	Time (h)
A	NBS (1 or 3 equiv.)	PPh ₃ (1 or 3 equiv.)	Et ₂ O or CH ₂ Cl ₂	0 – rt ^a	6 – 12
B	PBr ₃ (1, 3 or 5 equiv.)	Pyridine (1.1 equiv.)	Et ₂ O or CH ₂ Cl ₂	-10 – rt ^a	2 – 24
C	CBR ₄ (2 or 3 equiv.)	PPh ₃ (2 or 3 equiv.)	CH ₂ Cl ₂	rt ^a	8 – 20

^a rt = room temperature

An alternative solution to synthesize (*R*)-2 and (*S*)-2 and to avoid the problem of degradation of (*S*)-1 was applied. Compound (*S*)-3 was reacted with trifluoromethanesulfonic anhydride

(Tf₂O) to replace bromide by triflate, one of the best good leaving group. This solution was tested in parallel with the previous one. Tf₂O (2.2 eq.) as reagent in the presence of 2,6-lutidine (2.2 eq.) in CH₂Cl₂ at -30°C was used^{22,23}. Unfortunately, after formation of the ditriflate compound **3a**, an unexpected β-elimination of the primary triflate group occurred and led to the creation of a conjugated double bond (compound **4**, Scheme 2.5).



Scheme 2.5 β-elimination reaction accompanying the synthesis of (S)-**3a**

Meanwhile, degradation problem of (S)-**1** was solved by a very simple way. After several improvement attempts, the use of a low height of silica gel in the column significantly reduced the degradation of (S)-**1**. Purification was accomplished with non-polar eluent (PE/EtOAc, 9/1, v/v) and generated compound (S)-**1** in 82% of yield (Method C, Table 1). It seemed to strengthen the hypothesis that acidic environment caused by silica was the reason of degradation. The longer (S)-**1** stays on the column, the lower yield is obtained.

To ensure the effectiveness of this strategy in obtaining of enantiomerically pure (S)-**1**, optical purity determination of this compound is a crucial step. For this reason, analytical HPLC enantioseparation of commercially available racemate *rac*-**1** was investigated in order to be able to determine the enantiomeric excess (ee) and the optical rotation value of the synthesized (S)-**1** as a reference.

2.2. Via preparative HPLC enantioseparation of commercially available *rac*-1 on multigram scale

2.2.1. Analytical HPLC enantioseparation

To obtain complete resolution of the racemate *rac*-1, a screening of 14 different chiral stationary phases (CSPs, 250 x 4.6 mm) was undertaken using a mixture of heptane/EtOH (98/2 or 95/5, v/v) as mobile phase with a flow-rate of 1 mL/min under UV and circular dichroism (CD) detection at 254 nm. The chromatographic results of the screening were reported in Table 2. Experimental data indicated that no separation ($\alpha = 1$, entries 1, 3, 4, 6, 9, 10, 12 and 14, Table 2) or no baseline separation ($R_s < 1.5$, entries 2, 11 and 13, Table 2) was obtained for the majority of CSPs. It should be noted that the higher of resolution factor is, the better of baseline separation will be. Baseline separation was observed on Chiralpak AZ-H, Chiralpak IA and Lux-Amylose-1[®] (entries 5, 7 and 8, Table 2), but only Lux-Amylose-1[®] CSP showed a good resolution for *rac*-1 ($R_s > 3$, entries 5a and 5b, Table 2 and Figure 2.2). HPLC chromatogram using Lux-Amylose-1[®] as CSP and heptane/EtOH (95/5, v/v) as mobile phase (entry 5b, Table 2) gave retention times of 4.74 and 5.21 min for (-)-1 and (+)-1 enantiomers, respectively, with a R_s value of 3.13 (Figure 2.2). The circular dichroism detector revealed that the elution order is (-)_{CD254nm}/(+)_{CD254nm} on amylose based CSPs, whereas the (+)_{CD254nm} was the first eluted on the only cellulose based CSP (Chiralcel OD-3). The resolution was worse on immobilized polysaccharide CSPs (Chiralpak IA and IF) than on the corresponding coated CSPs (Lux-Amylose-1[®] and Chiralpak AZ-H).

Table 2 Screening results for analytical HPLC enantioseparation of *rac*-1

Entry	Column	Heptane /EtOH (v/v)	1 st eluted enantiomer		2 nd eluted enantiomer		α^c	R_s^d
			R_{t1}^a	k_1^b	R_{t2}^a	k_2^b		
1	Chiralpak AS-H	98/2	4.08	0.38	–	–	1	0
2	Chiralcel OD-3	98/2	4.46 (+)	0.51	4.57 (-)	0.55	1.07	0.52
3	Lux-Cellulose-2	98/2	4.22	0.43	–	–	1	0
4	Lux-Cellulose-4	98/2	4.10	0.39	–	–	1	0
5a	Lux-Amylose-1	98/2	5.13 (-)	0.74	5.76 (+)	0.95	1.29	3.68
5b	Lux-Amylose-1	95/5	4.74 (-)	0.61	5.21 (+)	0.77	1.26	3.13
6	Lux-Amylose-2	98/2	5.04	0.71	–	–	1	0

7	Chiralpak AZ-H	98/2	5.38 (-)	0.82	5.64 (+)	0.91	1.11	1.28
8	Chiralpak IA	98/2	4.84 (-)	0.64	5.19 (+)	0.76	1.18	1.40
9	Chiralpak IB	98/2	4.20	0.42	–	–	1	0
10	Chiralpak IC	98/2	4.32	0.46	–	–	1	0
11	Chiralpak ID	98/2	4.87 (-)	0.65	5.09 (+)	0.73	1.12	0.76
12	Chiralpak IE	98/2	5.10	0.73	–	–	1	0
13	Chiralpak IF	98/2	5.38 (-)	0.82	5.63 (+)	0.91	1.10	1.04
14	(<i>S,S</i>)-Whelk-O1	98/2	4.72	0.60	–	–	1	0

^a Retention time (min); ^b Retention factor; ^c Enantioselectivity factor; ^d Resolution

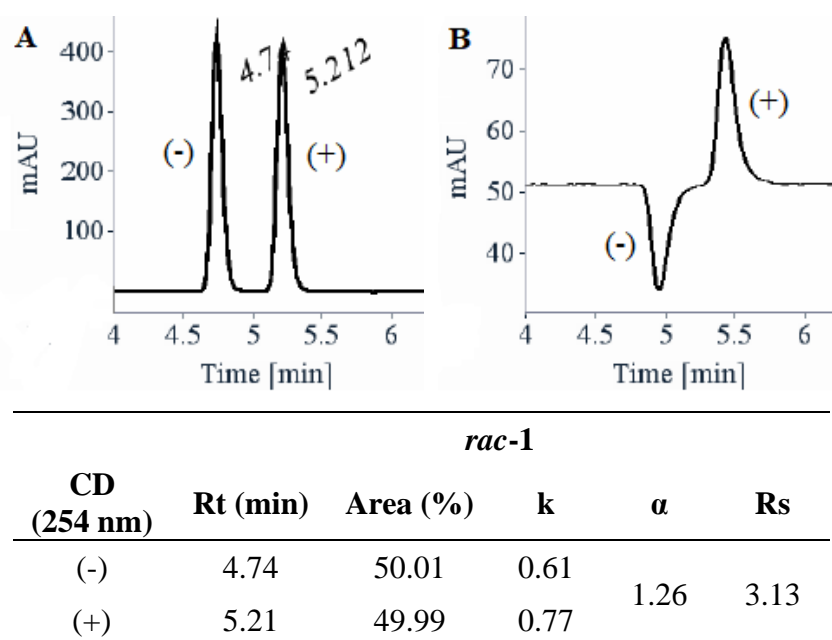
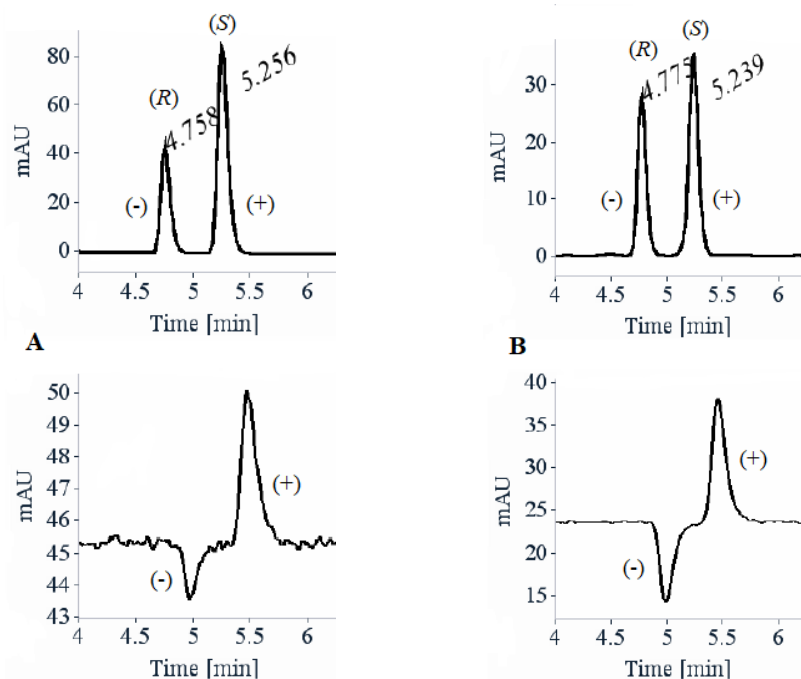


Figure 2.2 Analytical HPLC enantioseparation chromatograms under (A) UV and (B) CD detection (254 nm) and its parameters of commercially *rac-1*

The assignment of the absolute configuration was established by comparing analytical chiral HPLC chromatogram of synthesized (*S*)-**1** and *rac-1* on Lux-Amylose-1[®]. As showed in the Figure 2.3, the major enantiomer in the HPLC chromatograms of (*S*)-**1** was the second eluted enantiomer and following the extension of reaction time, the percentage of the first eluted enantiomer increased that led to decreasing of ee value. Therefore, we can assume that the second eluted enantiomer is (*S*)-**1** and the first one is (*R*)-**1**.



Synthesized compound (S)-1								
	Configuration	CD (254 nm)	Rt (min)	Area (%)	k	α	Rs	ee
A	(R)	(-)	4.76	31.87	0.61	1.28	3.13	36%
	(S)	(+)	5.26	68.13	0.78			
B	(R)	(-)	4.78	41.28	0.62	1.25	3.08	17%
	(S)	(+)	5.24	58.72	0.78			

Figure 2.3 Examples of two analytical HPLC chromatograms of the synthesized (S)-1 after 14h (A) and 17h (B)

2.2.2. Via preparative HPLC enantioseparation of *rac*-1 on multigram scale

Based on the optimized analytical HPLC enantioseparation analytical conditions for commercially available *rac*-1 mentioned above (entry 5b, Table 2), the preparative HPLC enantioseparation of *rac*-1 on multigram scale using Chiralpak AD-H (250 x 10 mm, 5 μ m) was performed. The Chiralpak AD-H column is an alternative of Lux-Amylose-1[®], those two CSPs share the same amylose-based chiral selector which is amylose tris(3,5-dimethylphenylcarbamate) coated on silica. The preparative resolution of *rac*-1 on multigram scale (5g) was successively performed with a mixture of hexane/EtOH (95/5, v/v, 6 L) as mobile phase with a flow-rate of 5 mL/min under UV and CD detection (254 nm). *Rac*-1 was dissolved in 60 mL of hexane/EtOH (95/5, v/v) then the separation was done after one day with stacking injection mode with 1200 times injection of 50 μ L each 1.2 min. The first (2.3g) and the second (2.3g) fractions at a retention time of 4.73 and 5.18 min, respectively, were isolated with ee

higher than 99.5% (Figures 2.4A-B). The separated enantiomers were characterized by optical rotation, electronic circular dichroism (ECD) and UV. (*S*)-**1** has a positive ECD band between 200 and 275 nm (Figure 2.4C) and in reverse, (*R*)-**1** shows opposite values (Figures 2.4C) but same UV spectra for both (Figure 2.4D).

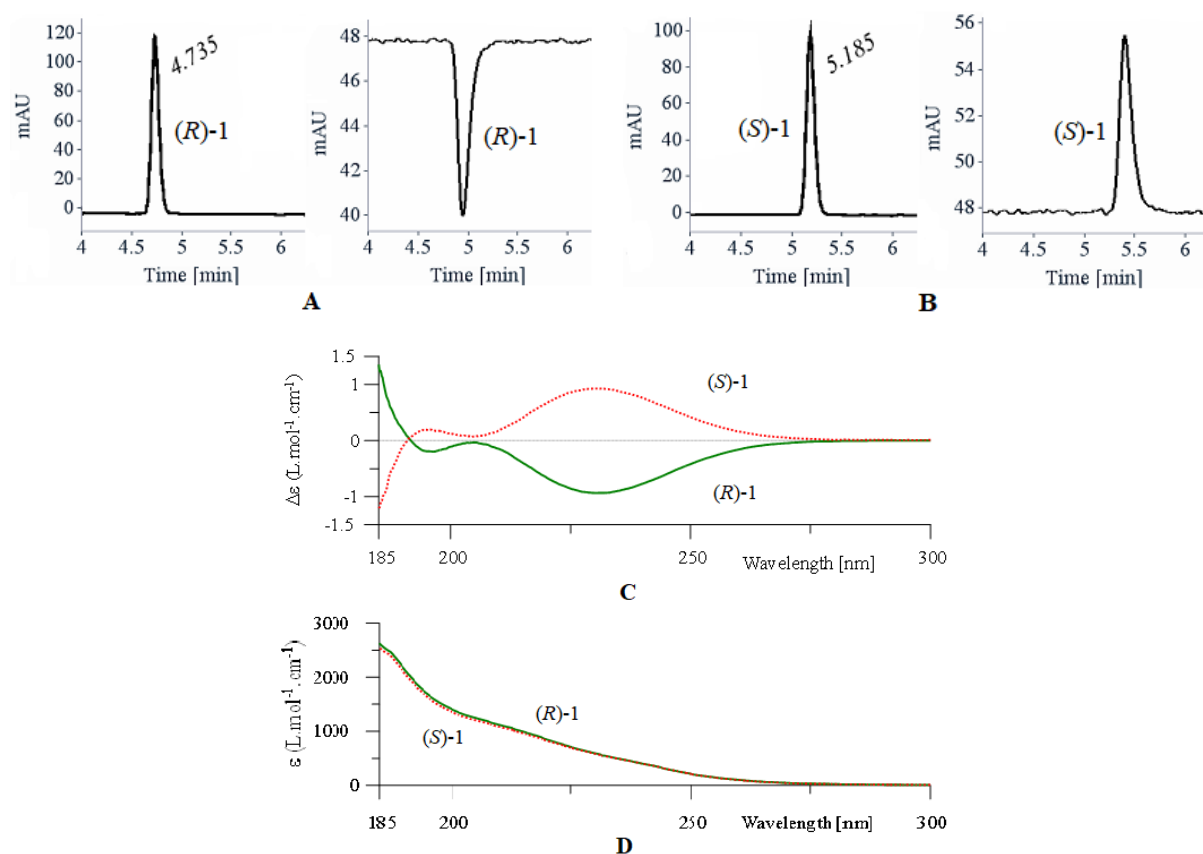


Figure 2.4 Preparative HPLC chromatograms of the separated enantiomers from *rac*-**1** (A, B) under UV (left) and CD (right) detection (254 nm) and their ECD (C) and UV (D) spectra (CH_3CN , $c = 7.2$ mM)

2.3. Optical rotation value of (*S*)-**1** and (*R*)-**1**

Normally, the optical rotation value is measured by a single wavelength at 589 nm of sodium-vapor lamp as the most suitable monochromatic light source. Measurement by other wavelengths requires specialized equipment. In this case, different optical rotation values of (*S*)-**1** and (*R*)-**1** were measured with under various wavelengths: sodium (589 nm) and halogen (365, 405, 436, 546 and 578 nm) lamps (Table 3). Two enantiomerically pure compounds are supposed to have same value of specific rotation $[\alpha]$ but in opposite angles when they are measured at the same conditions (concentration, temperature, wavelength).

Table 3 Optical rotation values of the two separated enantiomers of **1** at different wavelength

λ (nm)	(<i>R</i>)-1 $[\alpha]_{\lambda}^{25}$ (CH ₂ Cl ₂ , <i>c</i> = 3)	(<i>S</i>)-1 $[\alpha]_{\lambda}^{25}$ (CH ₂ Cl ₂ , <i>c</i> = 3)
589	+12	-12
578	+13	-13
546	+14	-14
436	+20	-20
405	+22	-22
365	+22	-22

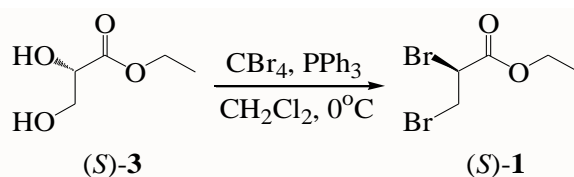
2.4. Racemization during enantioselective synthesis of (*S*)-1

As reported above in Figure 2.3, synthesized compound (*S*)-1 was racemized with low enantiomeric excess of resulted products after a reaction time of 14h and 17h (ee = 17% and 36%). To search for the reason, we hypothesized that two impact factors might cause the racemization: i) purification step and ii) reaction conditions. Firstly, enantiomer (*S*)-1 obtained preparative HPLC enantioseparation was passed through a silica gel column chromatography with the same condition which used during the enantioselective synthesis (*i.e.* PE/EtOAc, 9/1, v/v as eluent). The collected fraction was concentrated under vacuum and checked for the enantiomeric purity. The analytical chiral HPLC chromatograms using Lux-Amylose-1[®] CSP demonstrated that purification did not induce racemization (Table 4) with ee of (*S*)-1 was 100%. Since purification by silica gel was not the source of problem, reaction conditions were brought up to examine.

Table 4 Analytical HPLC parameters of enantiomerically pure (*S*)-1 after purification under UV detection (254 nm)

HPLC chromatograms	Rt (min)	Area (%)	k	α	Rs	ee
	5.23	100	0.77	-	-	100%

2.4.1. Synthesis condition of (S)-1 (Method C)



Scheme 2.6 Method C: Synthesis of ethyl 2,3-dibromopropionate (S)-1

Because the synthesized (S)-1 was not obtained in enantiopure form, its synthesis conditions were examined to find which parameter caused the racemization during the Appel reaction (Scheme 2.6). As we observed earlier (Figure 2.3), the ee of the synthesized (S)-1 decreased when the reaction time was extended from 14h to 17h (Figure 2.3) so several attempts were performed with different conditions (equivalent of CBr₄ and PPh₃, and time reaction) for the Appel reaction (Method C) to find out the reason. The various ee of the synthesized (S)-1 was determined by the analytical HPLC system using Lux-Amylose-1[®] as CSP and heptane/EtOH (95/5, v/v) as mobile phase. Table 5 presented the ee of the synthesized (S)-1 for each attempt and as the showed data, the ee of (S)-1 ranged from around 8% to 50%. These low ee for the (S)-1 showed that a racemization process was carried out during the Appel reaction (Method C). The racemization process (i) occurs quickly (ee ≈ 33% with a reaction time of 8 hours, entry 3), (ii) increases with time (comparison of entries 1/2 or 3/4/5/6/7), and (iii) proceeds more slowly when fewer equivalents of CBr₄ and PPh₃ are used (comparison of entries 1/5 or 2/6). Our difficulties in precipitating of soluble PPh₃ by-product and its presence during the purification process might explain the problem of racemization in the Appel reaction (Method C)^{24,25}.

Table 5 Enantiomeric measurement of the synthesized (S)-1^a (Method C)

Entry	CBr ₄ /PPh ₃ (equiv.)	Time (h)	Yield (%)	Ee (%)
1	2	14	24	49.3
2	2	17	26	35.4
3	3	8	66	33.2
4	3	11	71	29.5
5	3	14	71	36.3
6	3	17	82	17.4
7	3	20	80	8.8

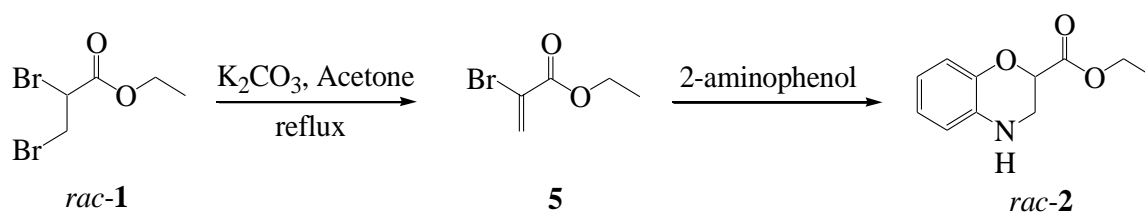
^aUsing Lux-Amylose-1[®] as CSP and heptane/EtOH (95/5, v/v) as mobile phase under UV and CD (254 nm) detection.

To conclude, a longer reaction time gave higher yield of the reaction but with a less measured ee. In addition, the use of the less reagent quantity was profitable for the ee of the product but with a lower yield.

3. Obtainment of chiral ethyl 3,4-dihydro-2*H*-1,4-benzoxazine-2-carboxylate

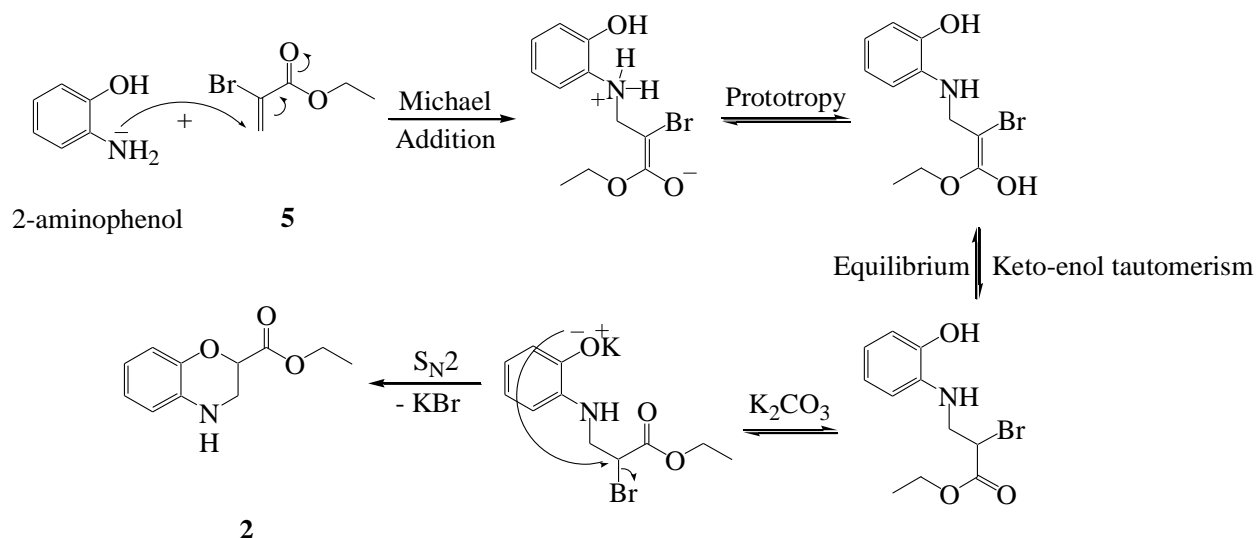
Due to the racemization of our synthesized (*S*)-**1**, we concerned that it could happen to enantioselective synthesis of ethyl 3,4-dihydro-2*H*-1,4-benzoxazine-2-carboxylate (*S*)-**2** and (*R*)-**2** also. Unfortunately, by searching in the literature, we found that during the synthesis of *rac*-**2** or other benzoheterocycles, by substitution of *rac*-**1** and corresponding aminophenol, could cause the racemization. The reason of this problem was because of the formation of an alkyl α -bromoacrylate from dibromo compound **1** in medium base (Scheme 2.7).

The synthesis of 1,4-benzodioxane or 1,4-benzoxathian, which are benzoheterocycles as 1,4-benzoxazine, was reported^{26,27}. Catechol or 2-mercaptophenol was reacted with *rac*-**1** to obtain desired molecules. However, instead of following the normal S_N2 substitution directly, *rac*-**1** was dehydrobrominated to generated ethyl 2-bromoacrylate **5** (Scheme 2.7). Dehydrobromination of *rac*-**1** was reported also by Arrault et al.²⁸ It was found that formation of acrylate compound **5** did not affect to synthesis of desired benzoheterocycle. Based on these findings, we could lose the chirality of (*S*)-**2** and (*R*)-**2** during the enantioselective synthesis.



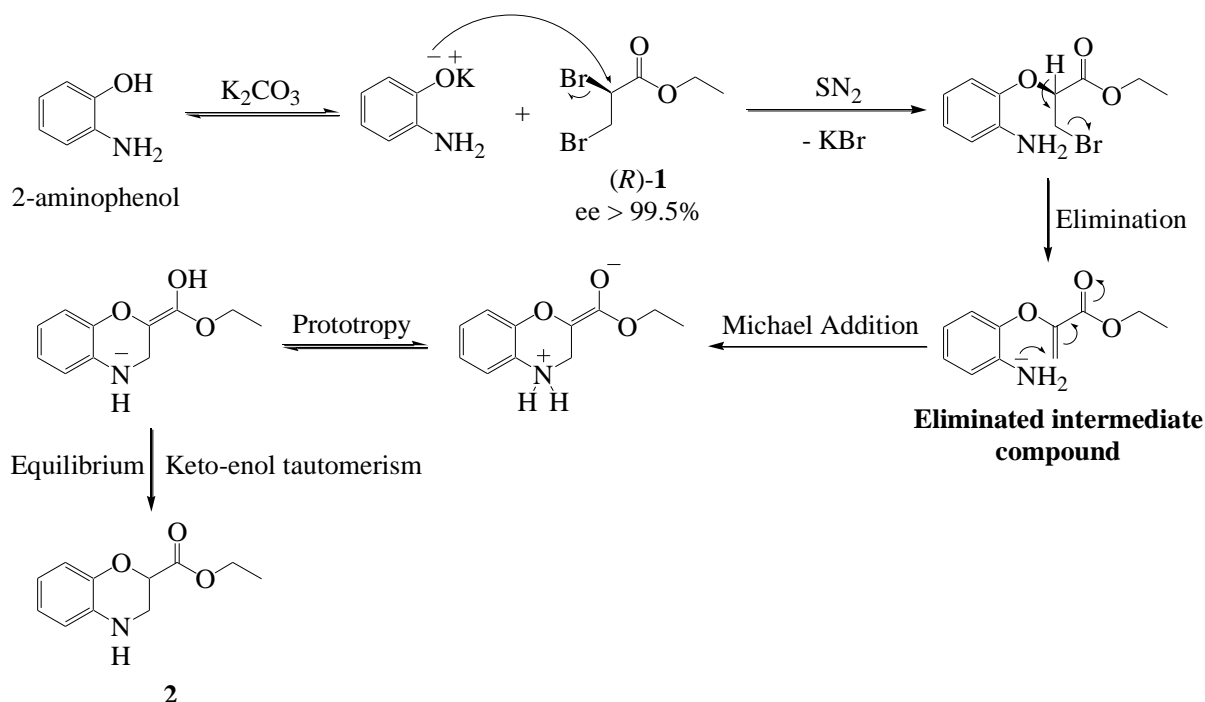
Scheme 2.7 Hypothesized process for obtainment of partial racemized compound **2**

Two possible mechanisms might be advanced as possible explanation for the racemization process that could occur during the enantioselective synthesis of compound **2**. Scheme 2.8 describes the first postulated mechanism for racemization of **2**. In this hypothesis, the chirality could be lost after spontaneous elimination of HBr in the conditions of reaction from the enantiomerically pure compound **1**, as described in the literature²⁷. This postulated mechanism involved a 1,4-Michael addition reaction followed by a cyclization with phenolate anion through a S_N2 reaction.



Scheme 2.8 First postulated mechanism for racemization of **2** from eliminated product **5**

The second postulated mechanism for racemization of compound **2** is depicted in Scheme 2.9. In this case, the chirality could be lost during the synthesis *via* the formation of an eliminated intermediate compound.

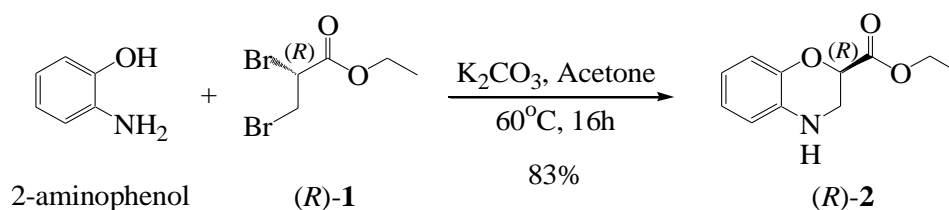


Scheme 2.9 Second postulated mechanism for racemization of **2** from eliminated intermediate compound

However, all synthesized molecules in the literature were in racemate form. Therefore, to determine whether the racemization really occurs and if it occurs, which postulated mechanism it follows and its quantification, the enantioselective synthesis of (*R*)-**2** was firstly performed.

3.1. Obtainment of (*R*)-2 via enantioselective synthesis

(*R*)-2 was prepared from the pure (*R*)-1 obtained by preparative HPLC enantioseparation. Applying the same conditions as reported in the literature^{4,29} for the racemate one (Scheme 2.10), the reaction afforded (*R*)-2 in 83% yield (reaction repeated two times). In order to validate the enantiomeric purity as well as absolute configuration determination of the first synthesized chiral 1,4-benzoxazine (*R*)-2, separation of *rac*-2 by chiral HPLC was brought up.



Scheme 2.10 Enantioselective synthesis of (*R*)-2

3.2. Obtainment of (*S*)-2 and (*R*)-2 via preparative HPLC enantioseparation of racemate on multigram scale

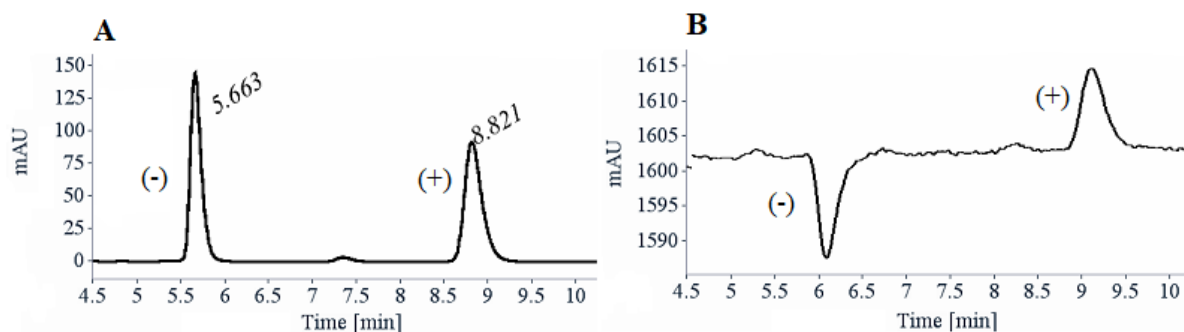
3.2.1. Analytical chiral HPLC

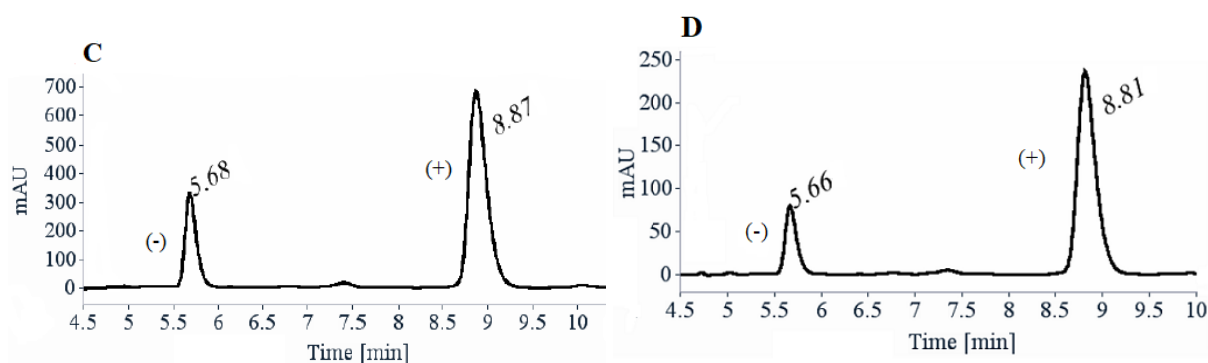
Approximately 12g of *rac*-2 was prepared from commercially *rac*-1 (Scheme 1.7). With the similar procedure as enantioseparation of *rac*-1, a screening of 16 different CSPs (250 x 4.6 mm) was initiated with the mixture of heptane/EtOH (70/30, v/v) as mobile phase and a flow-rate of 1mL/min. UV and CD detection (254 nm) were used to detect the throughput enantiomers. The results of CSPs screening was presented in Table 6. Unlike *rac*-1, the selectivity of CSPs for separation of *rac*-2 was not complicated. Among 16 screened CSPs, only three showed poorly baseline separation which were on Chiralpak AS-H, Chiralpak ID and (*S,S*)-Whelk-O1 ($R_s \leq 1.2$, Table 6, entries 1, 12, 16). Good separation was presented on mostly CSPs (Table 6, entries 6, 7, 9-11, 13, 15) with enantioselective factor α greater than 1. The best CSP for enantioseparation of *rac*-2 was Lux-Cellulose-2[®] ($R_s = 10.09$, $\alpha = 2.16$, Table 6, entry 3). Even Lux-Cellulose-3[®] (Table 6, entry 4) showed similar resolution value ($R_s = 10.06$) and good separation factor ($\alpha = 1.64$) but the retention time of each eluted enantiomer were much longer than on Lux-Cellulose-2[®] so it was not interesting to apply. The analytical chiral HPLC chromatogram (Figure 2.5A) using Lux-Cellulose-2[®] as CSP and heptane/EtOH (70/30, v/v) as mobile phase gave retention times of 5.66 and 8.82 min for (-)-2 and (+)-2, respectively (Table 6, entry 3). The CD detector proved the elution order (Figure 2.5B).

Table 6 Screening results for analytical HPLC enantioseparation of *rac-2*

Entry	Column	Heptane /EtOH (v/v)	1 st eluted enantiomer		2 nd eluted enantiomer		α^c	Rs ^d
			Rt ₁ ^a	k ₁ ^b	Rt ₂ ^a	k ₂ ^b		
1	Chiralpak AS-H	70/30	4.43(-)	0.50	4.66(+)	0.58	1.15	0.82
2	Chiralpak OD-3	70/30	6.32(-)	1.14	7.99(+)	1.71	1.50	6.08
3	Lux-Cellulose-2	70/30	5.66(-)	0.93	8.82(+)	2.01	2.16	10.09
4	Lux-Cellulose-3	70/30	14.56(-)	3.94	22.01(+)	6.46	1.64	10.06
5	Lux-Cellulose-4	70/30	5.23(-)	0.77	7.17(+)	1.43	1.85	8.43
6	Lux-Amylose-1	70/30	6.79(+)	1.30	8.23(-)	1.79	1.37	5.23
7	Lux-Amylose-2	70/30	5.94(-)	1.01	6.79(+)	1.30	1.29	3.89
8	Chiralpak AZ-H	70/30	5.31(-)	0.80	7.02(+)	1.38	1.72	6.38
9	Chiralpak IA	70/30	6.13(+)	1.08	7.25(-)	1.46	1.35	2.85
10	Chiralpak IB	70/30	5.39(-)	0.83	6.00(+)	1.03	1.25	2.60
11	Chiralpak IC	70/30	5.09(-)	0.72	5.77(+)	0.95	1.32	2.90
12	Chiralpak ID	70/30	5.13(-)	0.74	5.44(+)	0.84	1.14	0.98
13	Chiralpak IE	70/30	5.49(-)	0.86	6.00(+)	1.04	1.20	2.30
14	Chiralpak IF	70/30	5.45(-)	0.85	7.21(+)	1.45	1.70	5.60
15	Chiralpak IG	70/30	6.66(-)	1.26	7.36(+)	1.49	1.19	2.46
16	(<i>S,S</i>)-Whelk-O1	70/30	6.90(-)	1.34	7.33(+)	1.49	1.11	1.20

^a Retention time (min); ^b Retention factor; ^c Enantioselectivity factor; ^d Resolution





	Polarimeter detector	Rt (min)	Area (%)	k	α	Rs	ee
A	(-)	5.66	50.63	0.93	2.16	10.09	
	(+)	8.82	49.37	2.01			
C	(-)	5.68	22.74	0.93	2.16	10.68	55%
	(+)	8.87	77.26	2.01			
D	(-)	5.66	17.03	0.92	2.16	10.88	66%
	(+)	8.81	82.97	1.99			

Figure 2.5 Analytical HPLC enantioseparation chromatograms of racemate *rac-2* under (A) UV and (B) CD detection (254 nm) and (C, D) the two synthesized (*R*)-**2** under UV detection (254 nm)

As shown in the Figure 2.5, synthesis of (*R*)-**2** from enantiomerically pure (*R*)-**1** generated again racemization. The major enantiomer was corresponded to second eluted fraction and the ee calculated for the synthesized (*R*)-**2** was \approx 55% and 66%. These data suggested that the second eluted enantiomer was the (*R*)-enantiomer and this result was confirmed by theoretical calculations (see Section 3.3). In parallel, *rac-2* was separated in multi-gram scale (12g) by using preparative HPLC enantioseparation and resulted enantiomers were used directly for the next step of coupling with α -amino acids to generate pseudopeptides. The coupling reactions should not give any racemization and all obtained molecules should be in high enantiomeric purity.

3.2.2. Preparative HPLC enantioseparation of *rac-2* on multigram scale

As the optimal conditions was noted based on analytical chiral HPLC, 12g of *rac-2* was dissolved in 180mL of mixture heptane/EtOH (50/50, v/v) and put on CSP Lux-Cellulose-2[®] (250 x 10 mm) with tris(3-chloro-4-methylphenylcarbamate) coated on silica. Heptane/EtOH (70/30, v/v) was used as the mobile phase with flow rate of 5mL/min under UV detection at 254nm. The first enantiomer fraction (5.7g) was eluted at 5.59 min and the second one (5.6g)

at 8.53 min with $ee \geq 99.5\%$ (Figure 2.6). The ECD and UV spectra were measured also. Under the same conditions, as expected for both enantiomers, the two eluted enantiomers showed opposite values in ECD spectra and exactly same absorption bands in UV spectra (Figure 2.7).

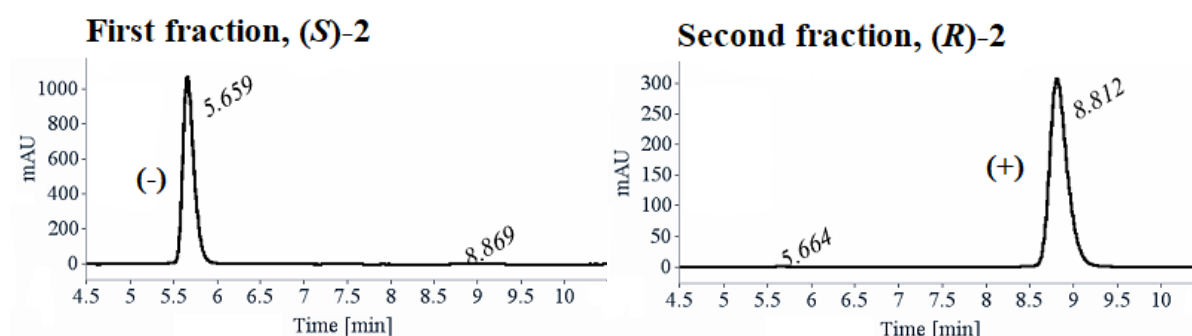


Figure 2.6 Preparative HPLC chromatograms of the separated enantiomers from *rac-2* under UV detection (254 nm)

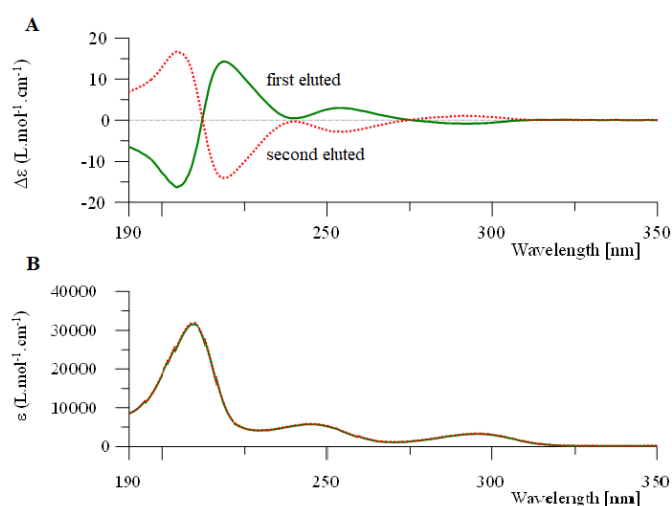


Figure 2.7 ECD (A) and UV (B) spectra of the separated enantiomers from *rac-2* (CH_3CN , $c = 0.6$ mM)

3.3. Absolute configuration (AC) and optical rotation value determination

3.3.1. Computational chemistry for AC determination

To elucidate the absolute configuration of a chiral compound, different chiroptical spectroscopic methods such as optical rotatory dispersion (ORD), electronic circular dichroism (ECD), vibrational circular dichroism (VCD), or Raman optical activity (ROA)³⁰ are applied in which ECD is the most commonly used. ECD or CD is the difference of absorption behaviour of a chiral molecule to left- and right-circular polarized light (CPL) and is measured as molar circular dichroism $\Delta\epsilon$ ($\text{L.mol}^{-1}.\text{cm}^{-1}$) = $\epsilon_L - \epsilon_R$ where ϵ_L and ϵ_R are absorption coefficients of left- and right-CPL, respectively^{31,32}. Measurement of $\Delta\epsilon$ values at different

wavelengths generates CD spectra then base on CD spectra, one can predict the AC of tested chiral molecule. The principle of using CD for AC determination is to compare UV and CD spectra between a chiral molecule (experimental) is needed to clarify the AC and a reference molecule (calculated) which its AC is already known. The more similar they are, the more accurate AC of investigated compound can be assigned. The chiral reference compound should have similar chromophore with tested one, containing substituted groups that do not affect to chromophore^{32,33}. The comparison is generated by applying *ab initio* methods like density functional theory (DFT), time-dependent density functional theory (TD-DFT) or configuration interaction (CI)³⁴. In this work, TD-DFT were applied for AC confirmation of both enantiomers of **2**.

Basically, there are three steps for obtainment of UV and CD spectra of investigated chiral compound and reference to determine AC. First of all, optimization of conformers of tested chiral compound should be done by Boltzmann method or molecular dynamics. Secondly, rotatory and oscillator strengths are calculated. Finally, resulted UV and CD curves of both compounds are drawn to compare³⁴.

The AC was first predicted based on analytical chiral HPLC chromatograms on Lux-Cellulose-2[®] CSP of *rac*-**2** and synthesized (*R*)-**2**. The synthesis of the chiral compound **2** (Scheme 2.6) was performed with (*R*)-**1** (first eluted enantiomer, Figure 2.3) to afford (*R*)-**2** thanks to a S_N2 mechanism. As showed in the Figure 2.5C, the ee measurement for the synthesized (*R*)-**2** was found to be around 55% and 66% with the second eluted enantiomer as the major product. Thanks to these data, we can assume that the first eluted enantiomer on Lux-Cellulose-2[®] CSP was (*S*)-**2** and the second one was (*R*)-**2**. To confirm the prediction, the comparison of the experimental and calculated UV and ECD spectra of (*S*)-**2** was done. The experimental spectra were from the first eluted enantiomer on Lux-Cellulose-2[®] and the calculated were from the DFT and TD-DFT calculations.

DFT and TD-DFT calculations were performed using Gaussian 16 package³⁵, with the default parameters for solvent used in SMD. Spectra were plotted with Specdis v. 1.71³⁶ as sum of Gaussians with σ as half the bandwidth at $1/e$ peak height. Two conformer geometries were found for the (*S*)-enantiomer after a conformational analysis with molecular mechanics and DFT at the SMD(CH₃CN)/B3LYP/6-311G(d,p) level.

Figure 2.8 describes the re-optimization of the conformers to compare the similarity between calculated and experimental (*S*)-**2**. These calculations were performed at the CRCMM (Centre

Régional de Compétences en Modélisation Moléculaire de Marseille). Other figures with different formula for frequency and TD-DFT calculations were presented in experimental part of this thesis. Only one example was taken to discuss here. In all cases, the calculated UV and ECD spectra for (*S*)-**2** are consistent with their experimental data from the first eluted enantiomer on Lux-Cellulose-2[®] in the region of 190-350 nm with a slight shifting of the maximum absorbance peaks. Therefore, the comparison of calculated and experimental UV and ECD spectra also confirmed that the first eluted enantiomer on Lux-Cellulose-2[®] was (*S*)-**2** and the second one was (*R*)-**2**.

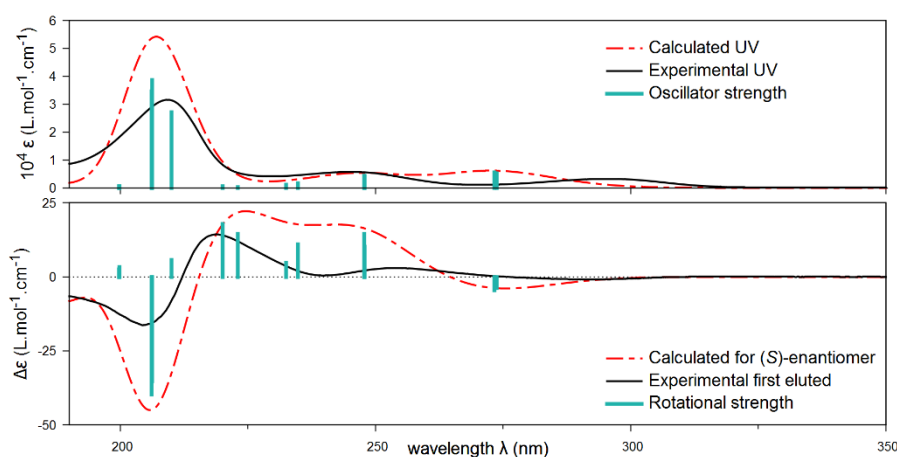


Figure 2.8 Comparison of UV (top) and ECD (bottom) experimental spectra in acetonitrile ($c = 0.6$ mM) for the first eluted enantiomer of **2** on Lux-Cellulose-2[®] and TD-DFT calculated spectra (Boltzmann averages of two conformers, = 0.29 eV, shifted by 16 nm). Vertical bars are oscillator and rotational strengths calculated for the two conformers with arbitrary unit. Frequency calculations at SMD(CH₃CN)/B3LYP-D3/Def2SVP level and TD-DFT calculations at SMD(CH₃CN)/CAMB3LYP-D3/Def2SVP level.

3.3.2. Optical rotation values

The optical rotations values of each enantiomers of **2** were measured by different wavelengths as before with enantiomers of **1** and are presented in the Table 7.

Table 7 Optical rotation values of the two separated enantiomers of **2** at different wavelength

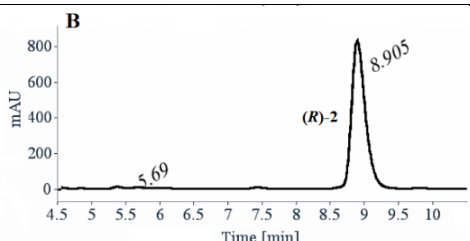
λ (nm)	First eluted (<i>S</i>)- 2 [α] _{λ25} (CH ₂ Cl ₂ , <i>c</i> = 0.2)	Second eluted (<i>R</i>)- 2 [α] _{λ25} (CH ₂ Cl ₂ , <i>c</i> = 0.19)
589	+37	-37
578	+38	-39
546	+43	-44
436	+74	-75
405	+89	-91

3.4. Racemization during enantioselective synthesis of (*R*)-**2**

As mentioned above, the racemization occurred again during the enantioselective synthesis of (*R*)-**2**. Because obtained product was not fully racemized (*ee* \approx 55% and 66%) so in order to quantify this problem and to confirm the cause and mechanism induced the racemization of (*R*)-**2**, the synthesis condition of (*R*)-**2** was examined.

Firstly, to be sure that purification step did not generate racemization, (*R*)-**2** separated by preparative chiral HPLC was also passed through a silica gel column chromatography using PE/EtOAc (3/7, v/v) as eluent. The collected fraction was checked by analytical chiral HPLC (Table 8). Resulted product was obtained as pure enantiomer.

Table 8 Analytical HPLC chromatogram of (*R*)-**2** after purification under UV detection (254 nm)

HPLC chromatograms	Rt (min)	Area (%)	k	α	Rs	ee
	8.90	99.5	2.02	2.17	10.83	99.5%

Secondly, (*R*)-**1** and (*R*)-**2** afforded by preparative HPLC enantioseparation were placed under the conditions as the synthesis of (*R*)-**2**. They were stirred with potassium carbonate in acetone under reflux for 16h. The mixtures were extracted with CH₂Cl₂ and collected organic phases were concentrated under vacuum to be checked for *ee* by running through chiral HPLC with appropriate CSPs (Figure 2.9). Fortunately, (*R*)-**2** was not affected at all by reaction conditions and it was obtained as enantiopure (*ee* > 99.5%). Contrariwise, (*R*)-**1** could not be recovered. We doubted that enantiomer (*R*)-**1** had been affected by potassium carbonate to generate eliminated compound **5** as reported in the literature²⁷ (Scheme 2.7).

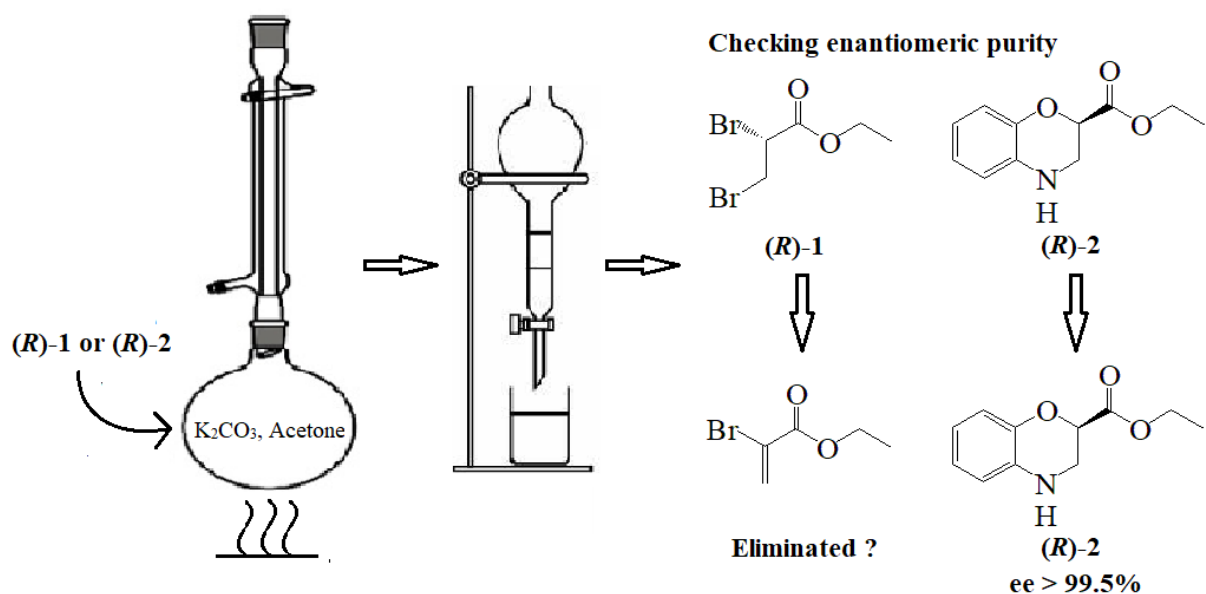
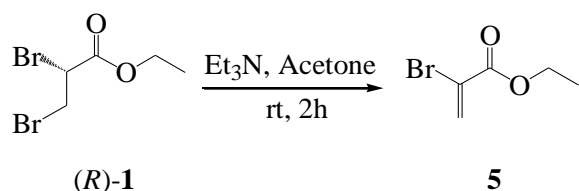


Figure 2.9 Examining synthesis conditions for 1,4-benzoxazine for racemization

To verify this assumption, we decided to synthesize the eliminated compound **5** (Scheme 2.11). To the solution of pure enantiomer $(R)\text{-1}$ in acetone was added 1.1 equiv. of triethylamine. The reaction was stirred at room temperature for 2h then ammonium salt was filtered³⁷. The resulting solution was compound **5** (confirmed by ^1H NMR, Figure 2.10). In parallel, $(R)\text{-1}$ was repeatedly stirred for 16h under synthesis conditions of $(R)\text{-2}$ then the mixture was filtered and sent directly to check by ^1H NMR. Unsurprisingly, two resulted NMR showed the same product which was eliminated compound **5**.



Scheme 2.11 Synthesis of ethyl 2-bromoacrylate **5**

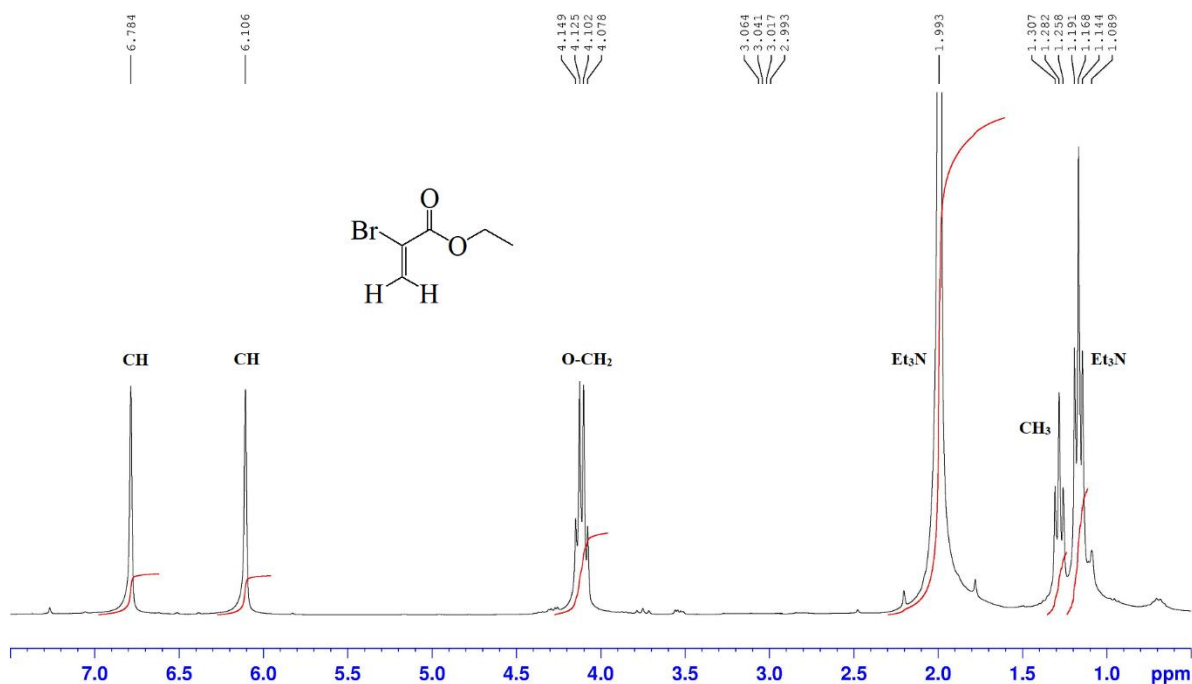


Figure 2.10 ¹H NMR of the synthesized ethyl 2-bromoacrylate **5** (CDCl₃, 300K, 300 MHz)

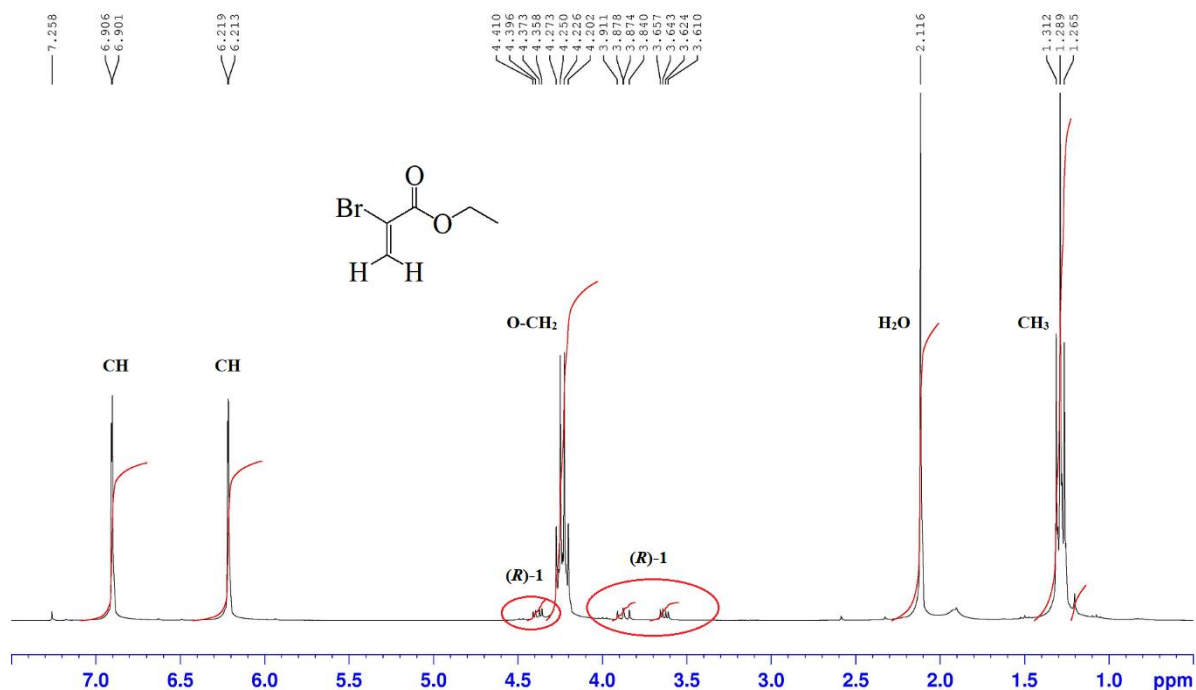


Figure 2.11 ¹H NMR of the resulted product after 16h stirring (*R*)-**1** and K₂CO₃ in refluxed acetone (CDCl₃, 300K, 300 MHz)

Figure 2.11 revealed the trace of enantiomer (*R*)-**1** so it meant that the elimination was not induced fully. To quantify this problem, mixture of enantiomer (*R*)-**1** (1 mmol) and K₂CO₃ (2.2 mmol) in acetone under reflux was stirred and the solution was checked by analytical achiral HPLC each hour. Column Nucleosil silica gel C4 (250 x 4 mm) was applied, CH₃CN/H₂O

(5/95, v/v) was used as the mobile phase with flow rate of 1 mL/min under UV detection at 254 nm. The retention times of (*R*)-**1** and **5** are 9.9 min and 7.8 min, respectively. This work was processed to examine the formation speed of eliminated compound **5**. The result expressed that **5** appeared immediately after 10 min and quickly increased in the first two hours then it was consistently raised in the next seven hours. After 16h stirring under reflux, it reached to 93% while enantiomer (*R*)-**1** only rested around 7% (Figure 2.12). This verification helped to confirm that the dehydrobromination of (*R*)-**1** under medium base caused the partial racemization of the synthesized (*R*)-**2**. The formation of eliminated product **5** did not affect the cyclization of 2-aminophenol to afford **2** as mentioned above (Scheme 2.8). The same mechanism was described in the literature^{27,28}.

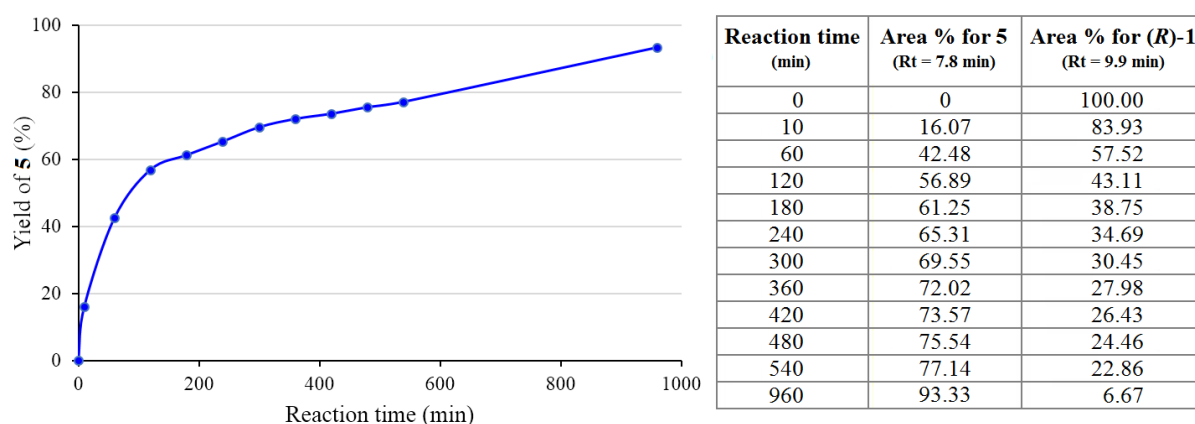


Figure 2.12 Evolution of ethyl 2-bromoacrylate **5** under synthesis conditions of (*R*)-**2**

To conclude, racemization of both synthesized (*R*)-**1** and (*R*)-**2** has been shown to be induced by synthesis conditions. The basic medium of reaction generated eliminated compound **5** from (*R*)-**1** that led to the loss of chirality just before ethyl 3,4-dihydro-2*H*-1,4-benzoxazine-2-carboxylate was formed.

As the result, both enantiomers (*S*)-**2** and (*R*)-**2** obtained by preparative HPLC enantioseparation were used in the next step of coupling with α -amino acids to design new pseudopeptide analogues and to study their conformation behavior.

4. Synthesis of chiral pseudopeptide bearing 1,4-benzoxazine moiety

4.1. Elongation of *N*-terminal extremity (synthesis of pseudodipeptides)

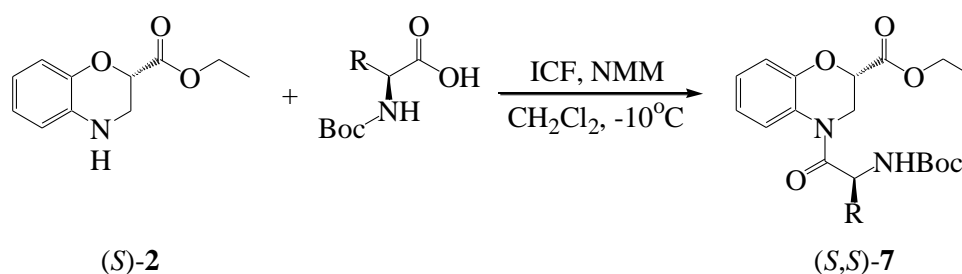
4.1.1. Coupling with Boc-protected α -amino acids

The first attempt to elongate *N*-terminal extremity of enantiomerically pure compounds **2** was coupling with Boc-protected α -amino acid by using anhydride procedure. First, treatment of Boc-protected-*L*-Alanine with *iso*-butyl chloroformate in the presence of *N*-methylmorpholine

(NMM) or *N*-methyl-2-pyrrolidone (NMP) (entry 1, Table 9) gave anhydride as intermediate product. The outcome of that reaction then reacted with amine group of (*S*)-**2** to form pseudopeptide (*S,S*)-**7**. However, instead of having expected compound (*S,S*)-**7**, compound (*S*)-**6** was obtained in 77% of overall yield (Scheme 2.12). Other chloroformates were used but the similar results were obtained.

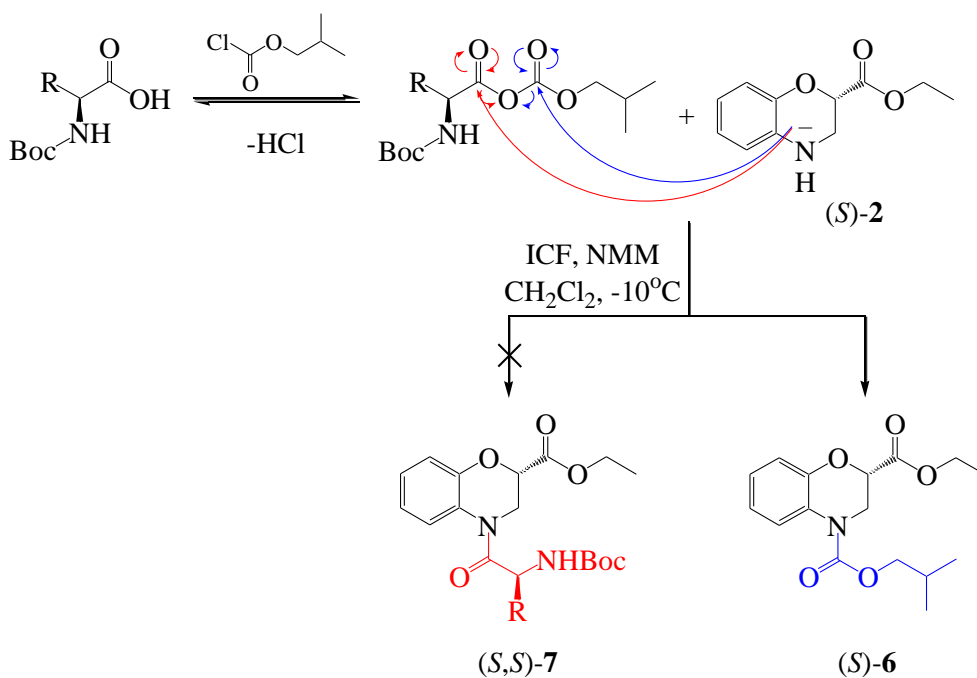
Table 9 Conditions for coupling with Boc-protected α -amino acids

Entry	Conditions	T (°C)	Solvent	Time (hours)
1	<i>iso</i> -butyl chloroformate, NMM or NMP	-10 to 0	THF or CH ₂ Cl ₂	5
2	DCC, HOBT	0 to rt	CH ₂ Cl ₂	24



Scheme 2.12 Coupling reaction of (*S*)-**2** at *N*-terminal extremity with Boc-protected α -amino acids

The failure for obtainment of expected compound might due to the common side-reaction that occurred during the reaction (Scheme 2.13). This limitation was reported in the literature^{38,39}. The different reactivity of the electrophilic centres in anhydride may generate the by-product. One solution was proposed to avoid this side-reaction is reversion of reagents adding order but it gave the same result in our case.

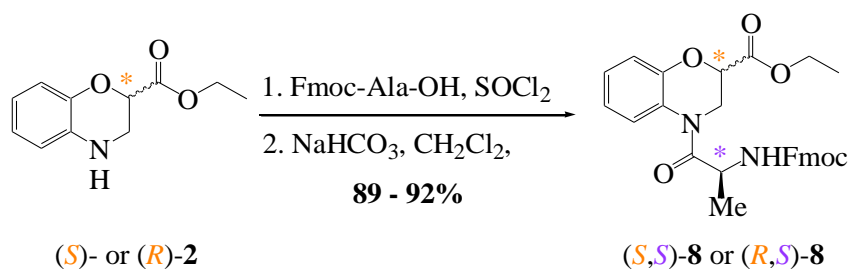


Scheme 2.13 Mechanism explaining the formation of (*S*)-6

This reaction would have been succeeded if it had been used Boc-protected amino acid fluorides which could be obtained from cyanuric fluoride. However, using cyanuric fluoride is toxic and not a cost-effective way to investigate. In addition, changing activating agent to another one like dicyclohexyl carbodiimide (DCC) in the presence of 1-hydroxybenzotriazole HOBt (entry 2, Table 11) did not work. HOBt is known as one of the most effective suppressors to prevent racemization and it does help accelerating the reaction but only starting product was recovered after stirring more than 48 hours. In order to not waste time for this part, Fmoc-protected α -amino acids chloride were used instead.

4.1.2. Coupling with Fmoc-protected α -amino acids

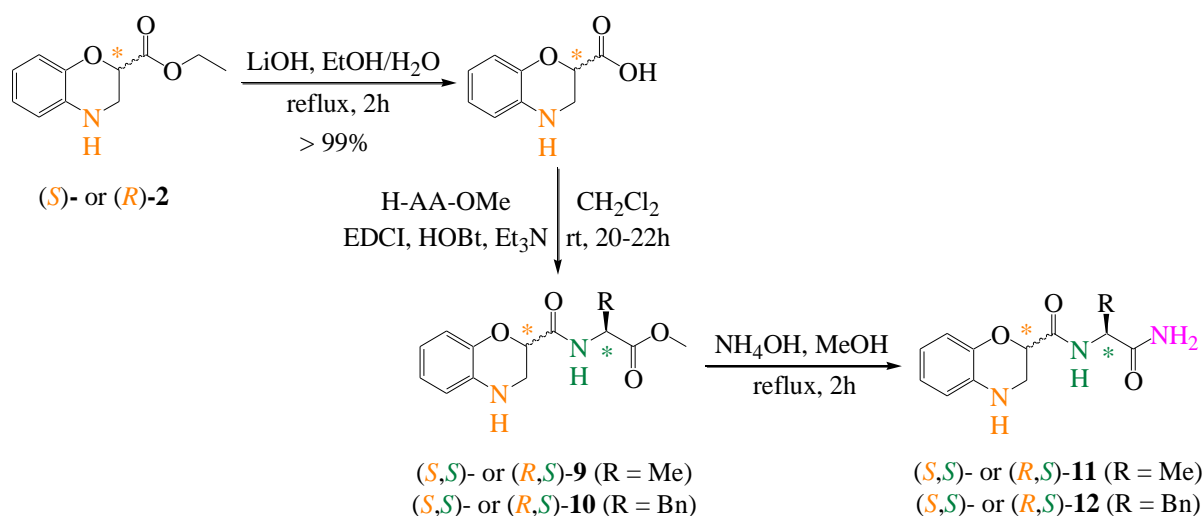
Both enantiomers (*S*)-2 and (*R*)-2 obtained by preparative HPLC enantioseparation were taken and only Fmoc-protection Alanine was chosen for this section. Classically, Fmoc-Ala-OH was treated with thionyl chloride to obtain Fmoc-Ala-Cl which then was coupled with (*S*)-2 or (*R*)-2 to elongate *N*-terminal extremity to form pseudopeptide (*S,S*)-8 and (*R,S*)-8 in excellent yield of 92% and 89%, respectively (Scheme 2.14).



Scheme 2.14 Coupling reaction of (S) -2 and (R) -2 at N -terminal extremity with Fmoc-Ala-OH

4.2. Elongation of C -terminal extremity (synthesis of pseudodipeptides)

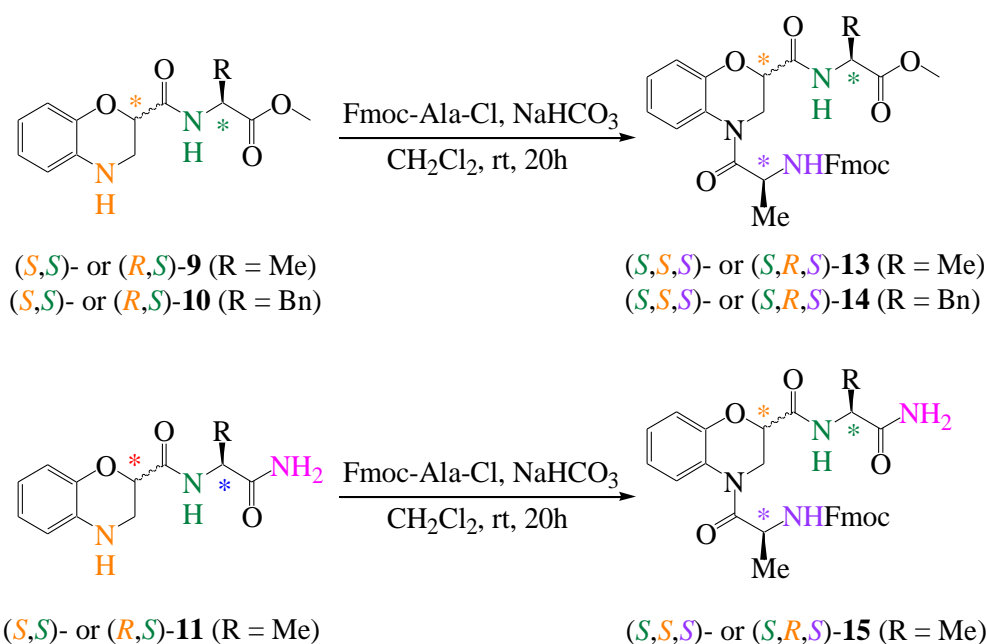
The elongation of C -terminal extremity of enantiomers (S) -2 and (R) -2 started by hydrolysis of each enantiomer with lithium hydroxide (LiOH) in EtOH/H₂O (8/2, v/v) generated the corresponded carboxylic acid. They were then immediately coupled with commercially available methyl ester of α -amino acids in the presence of EDCI, HOBt as activating agents and triethylamine as a base⁴⁰ to generate diastereoisomers (S,S) - and (R,S) -9, 10. HOBt was used to minimize the racemization (Scheme 2.15). Amidation of (S,S) - and (R,S) -9, 10 by ammonia solution in methanol under reflux for 2h gave the corresponded (S,S) - and (R,S) -11, 12 in good yield.



Scheme 2.15 Elongation of C -terminal extremity of (S) -2 and (R) -2

4.3. Elongation of C - and N -terminal extremities (synthesis of pseudotripeptides)

Pseudodipeptides 9, 10 and 11, 12 were coupled with Fmoc-protected Alanine with sodium bicarbonate as a base in CH₂Cl₂ for 20-22 h at room temperature to achieve corresponded pseudotripeptides 13, 14 and 15 (Scheme 2.16) which could be interesting for conformational analysis. The reaction yield was noted in Table 10.



Scheme 2.16 Elongation of C- and N-terminal extremities of (S)-**2** and (R)-**2**

Table 10 Reaction yield

Compounds	Yield (%)	Compounds	Yield (%)
(S,S)- 9	94	(R,S)- 12	73
(R,S)- 9	98	(S,S,S)- 13	82
(S,S)- 10	85	(R,S,S)- 13	65
(R,S)- 10	95	(S,S,S)- 14	60
(S,S)- 11	89	(R,S,S)- 14	72
(R,S)- 11	75	(S,S,S)- 15	42
(S,S)- 12	67	(R,S,S)- 15	25

In conclusion, enantiomers of **1** and **2** had been obtained *via* two different methods: enantioselective synthesis and preparative HPLC enantioseparation of racemate on multigram scale. Unfortunately, enantioselective synthesis of both chiral compounds **1** and **2** had been finished with important racemization issue due to the reaction conditions. However, chiral HPLC enantioseparation of commercially available *rac*-**1** and synthesized *rac*-**2** was successively completed on multigram scale. Both enantiomers of **1** and **2** were obtained in high enantiomeric purity (ee > 99.5%). The two enantiomers (R)-**2** and (S)-**2** then were used to design new small pseudopeptide analogues by elongation of C- and N-terminal extremities with different protected α -amino acids using classical conditions for peptide coupling reaction. The conformational behaviour of obtained pseudopeptides was analyzed in the next chapter.

REFERENCES

- (1) Sharma, S. D.; Kanwar, S.; Rajpoot, S. Aziridines as Templates: A General Strategy for the Stereospecific Synthesis of 2-Azetidinones. *J. Heterocycl. Chem.* **2006**, *43* (1), 11–19.
- (2) Fang, Q. K.; Grover, P.; Han, Z.; McConville, F. X.; Rossi, R. F.; Olsson, D. J.; Kessler, D. W.; Wald, S. A.; Senanayake, C. H. Practical Chemical and Enzymatic Technologies for (S)-1,4-Benzodioxan-2-Carboxypiperazine Intermediate in the Synthesis of (S)-Doxazosin Mesylate. *Tetrahedron: Asymmetry* **2001**, *12* (15), 2169–2174.
- (3) Tsai, C. S.; Shah, U. S.; Bhargava, H. B.; Zaylskie, R. G.; Shelver, W. H. Synthesis of 2-Dialkylaminomethyl-1,4-Benzoxathians. *J. Pharm. Sci.* **1972**, *61* (2), 228–231.
- (4) Butler, R. C. M.; Chapleo, C. B.; Myers, P. L.; Welbourn, A. P. Synthesis of 2-(2-Imidazolynyl) Substituted 2,3-Dihydro-4H-1,4-Benzothiazine and 3,4-Dihydro-2H-1,4-Benzoxazines. *J. Heterocycl. Chem.* **1985**, *22*, 177.
- (5) Bourlot, A.-S.; Guillaumet, G.; Merour, J.-Y. A Straightforward Route 4H-1,4-Benzoxazine-2-Carbaldehydes by Swern Oxidation. *J. Heterocycl. Chem.* **1996**, *33*, 191.
- (6) Tanaka, H.; Shibata, M.; Ohira, K.; Ito, K. Total Synthesis of (±)-Silybin, an Antihepatotoxic Flavonolignan. *Chem. Pharm. Bull.* **1985**, *33* (4), 1419–1423.
- (7) Honda, T.; Terao, T.; Aono, H.; Ban, M. Synthesis of Novel 1,4-Benzoxazin-3-One Derivatives as Inhibitors against Tyrosine Kinases. *Bioorg. Med. Chem* **2009**, *17* (2), 699–708.
- (8) La, D. S.; Belzile, J.; Bready, J. V.; Coxon, A.; DeMelfi, T.; Doerr, N.; Estrada, J.; Flynn, J. C.; Flynn, S. R.; Graceffa, R. F.; Harriman, S. P.; Larrow, J. F.; Long, A. M.; Martin, M. W.; Morrison, M. J.; Patel, V. F.; Roveto, P. M.; Wang, L.; Weiss, M. M.; Whittington, D. A.; Teffera, Y.; Zhao, Z.; Polverino, A. J.; Harmange, J.-C. Novel 2,3-Dihydro-1,4-Benzoxazines as Potent and Orally Bioavailable Inhibitors of Tumor-Driven Angiogenesis [¶]. *J. Med. Chem.* **2008**, *51* (6), 1695–1705.
- (9) Mayer, S.; Arrault, A.; Guillaumet, G.; Mérou, J.-Y. Attempted Synthesis of Ethyl 3,4-Dihydro-2 H -1,4-Benzoxazine-3-Carboxylate and 3-Acetate Derivatives. *J. Heterocycl. Chem.* **2001**, *38* (1), 221–225.
- (10) Touzeau, F.; Arrault, A.; Guillaumet, G.; Scalbert, E.; Pfeiffer, B.; Rettori, M.-C.; Renard, P.; Mérou, J.-Y. Synthesis and Biological Evaluation of New 2-(4,5-Dihydro-1 H -Imidazol-2-Yl)-3,4-Dihydro-2 H -1,4-Benzoxazine Derivatives. *J. Med. Chem.* **2003**, *46* (10), 1962–1979.

- (11) Kumar, V.; Awasthi, A.; Metya, A.; Khan, T. A Metal-Free Domino Process for Regioselective Synthesis of 1,2,4-Trisubstituted Pyrroles: Application toward the Formal Synthesis of Ningalin B. *J. Org. Chem.* **2019**, *84* (18), 11581–11595.
- (12) Rouf, A.; Gupta, P.; Aga, M. A.; Kumar, B.; Chaubey, A.; Parshad, R.; Taneja, S. C. Chemoenzymatic Synthesis of Piperoxan, Prosympal, Dibozane, and Doxazosin. *Tetrahedron: Asymmetry* **2012**, *23* (22–23), 1615–1623.
- (13) Mukaiyama, T.; Shiina, I.; Iwadare, H.; Saitoh, M.; Nishimura, T.; Ohkawa, N.; Sakoh, H.; Nishimura, K.; Tani, Y.; Hasegawa, M.; Yamada, K.; Saitoh, K. Asymmetric Total Synthesis of Taxol. *Chem. Eur. J.* **1999**, *5* (1), 121–161.
- (14) Jervis, P. J.; Cox, L. R. Total Synthesis and Proof of Relative Stereochemistry of (–)-Aureonitol. *J. Org. Chem.* **2008**, *73* (19), 7616–7624.
- (15) Frankland, P. XXXVII-Ethereal Salts of Glyceric Acid, Inactice and Active. *J. Chem. Soc., Trans.* **1893**, *63*, 511–538.
- (16) Brenneman, J. B.; Ginn, J. D.; Hopkins, T. D.; D.Lowe, M.; Sarko, C. R.; A.Westbrook, J.; Yu, M.; Zhang, Z. Heterocyclic Carboxylic Acids as Activators of Soluble Guanylate Cyclase. US 2016/0024059 A1, 2016.
- (17) Udayakumar, V.; Pandurangan, A. A Novel Route for the Synthesis of Alkanes from Glycerol in a Two Step Process Using a Pd/SBA-15 Catalyst. *RSC. Adv.* **2015**, *5* (96), 78719–78727.
- (18) Baughman, T. W.; Sworen, J. C.; Wagener, K. B. The Facile Preparation of Alkenyl Metathesis Synthons. *Tetrahedron* **2004**, *60* (48), 10943–10948.
- (19) Rouf, A.; Aga, M. A.; Kumar, B.; Taneja, S. C. A Facile Approach to Chiral 1,4-Benzodioxane toward the Syntheses of Doxazosin, Prosympal, Piperoxan, and Dibozane. *Tet. Let.* **2013**, *54* (48), 6420–6422.
- (20) Weller, R. L.; Rajski, S. R. Aziridination of γ,δ -Dibromoethyl-2-Pentenoate with Primary Amines: Extension of the Gabriel–Cromwell Reaction. *Tet. Let.* **2004**, *45* (30), 5807–5810.
- (21) Batesky, D. C.; Goldfogel, M. J.; Weix, D. J. Removal of Triphenylphosphine Oxide by Precipitation with Zinc Chloride in Polar Solvents. *J. Org. Chem.* **2017**, *82* (19), 9931–9936.
- (22) Wang, Q.; Sasaki, N. A.; Riche, C.; Potier, P. A Versatile Method for the Facile Synthesis of Enantiopure *Trans*- and *Cis*-2,5-Disubstituted Pyrrolidines. *J. Org. Chem.* **1999**, *64* (23), 8602–8607.

- (23) Mehawed Abdellatif, M.; Acherar, S. Low-Cost and Multi-Gram Scale Synthesis of Chiral N β -Boc Protected α -N α -Hydrazino Diesters. *Tet. Let.* **2017**, *58* (12), 1216–1218.
- (24) Hutchins, Robert. O.; Masilamani, D.; Maryanoff, C. A. A Convenient Synthesis of Labile Optically Active Secondary Alkyl Bromides from Chiral Alcohols. *J. Org. Chem.* **1976**, *41* (6), 1071–1073.
- (25) Canestrari, D.; Cioffi, C.; Biancofiore, I.; Lancianesi, S.; Ghisu, L.; Ruether, M.; O'Brien, J.; Adamo, M. F. A.; Ibrahim, H. Sulphide as a Leaving Group: Highly Stereoselective Bromination of Alkyl Phenyl Sulphides. *Chem. Sci.* **2019**, *10* (39), 9042–9050.
- (26) Martin, A. R.; Caputo, J. F. 1,4-Benzoxathians. 1. Reactions of o-Mercaptophenol with .Alpha.-Halo Michael Acceptors. *J. Org. Chem.* **1974**, *39* (13), 1811–1814.
- (27) Casiraghi, A.; Valoti, E.; Suigo, L.; Artasensi, A.; Sorvillo, E.; Straniero, V. How Reaction Conditions May Influence the Regioselectivity in the Synthesis of 2,3-Dihydro-1,4-Benzoxathiine Derivatives. *J. Org. Chem.* **2018**, *83* (21), 13217–13227.
- (28) Arrault, A.; Mérour, J.-Y.; Léger, J.-M.; Jarry, C.; Guillaumet, G. New Synthetic Approach to Naphtho[1,2-b]Furan and 4'-Oxo-Substituted Spiro[Cyclopropane-1,1'(4'H)-Naphthalene] Derivatives. *Helv. Chim. Acta.* **2001**, *84* (8), 2198–2211.
- (29) Bartsch, H. Studies on the Chemistry of 1,4-Oxazines, XV [1]: Synthesis of Ethyl 3,4-Dihydro-4-Tosyl-2/-/1,4-Benzoxazine-3- Carboxylate. *Monatshefte fur Chemie* **1987**, *118*, 273–276.
- (30) Polavarapu, P. L.; Covington, C. L. Comparison of Experimental and Calculated Chiroptical Spectra for Chiral Molecular Structure Determination: CHIRAL MOLECULAR STRUCTURAL DETERMINATION. *Chirality* **2014**, *26* (9), 539–552.
- (31) Diedrich, C.; Grimme, S. Systematic Investigation of Modern Quantum Chemical Methods to Predict Electronic Circular Dichroism Spectra. *J. Phys. Chem. A* **2003**, *107* (14), 2524–2539.
- (32) Li, X.-C.; Ferreira, D.; Ding, Y. Determination of Absolute Configuration of Natural Products: Theoretical Calculation of Electronic Circular Dichroism as a Tool. *Curr. Org. Chem* **2010**, *14* (16), 1678–1697.
- (33) Berova, N.; Bari, L. D.; Pescitelli, G. Application of Electronic Circular Dichroism in Configurational and Conformational Analysis of Organic Compounds. *Chem. Soc. Rev.* **2007**, *36* (6), 914.
- (34) Maksimenka, K. Absolute Configuration by Circular Dichroism: Quantum Chemical CD Calculations, Julius-Maximilians-Universität, Minsk, Weißrussland, 2010.

- (35) Gaussian 16, Revision A.03, M. J. Frisch, G. W. Trucks, H. B. Schlegel, G. E. Scuseria, M. A. Robb, J. R. Cheeseman, G. Scalmani, V. Barone, G. A. Petersson, H. Nakatsuji, X. Li, M. Caricato, A. V. Marenich, J. Bloino, B. G. Janesko, R. Gomperts, B. Mennucci, H. P. Hratchian, J. V. Ortiz, A. F. Izmaylov, J. L. Sonnenberg, D. Williams-Young, F. Ding, F. Lipparini, F. Egidi, J. Goings, B. Peng, A. Petrone, T. Henderson, D. Ranasinghe, V. G. Zakrzewski, J. Gao, N. Rega, G. Zheng, W. Liang, M. Hada, M. Ehara, K. Toyota, R. Fukuda, J. Hasegawa, M. Ishida, T. Nakajima, Y. Honda, O. Kitao, H. Nakai, T. Vreven, K. Throssell, J. A. Montgomery, Jr., J. E. Peralta, F. Ogliaro, M. J. Bearpark, J. J. Heyd, E. N. Brothers, K. N. Kudin, V. N. Staroverov, T. A. Keith, R. Kobayashi, J. Normand, K. Raghavachari, A. P. Rendell, J. C. Burant, S. S. Iyengar, J. Tomasi, M. Cossi, J. M. Millam, M. Klene, C. Adamo, R. Cammi, J. W. Ochterski, R. L. Martin, K. Morokuma, O. Farkas, J. B. Foresman, and D. J. Fox. Gaussian, Inc., Wallingford CT, 2016.
- (36) Specdis version 1.71. T. Bruhn, A. Schaumlöffel, Y. Hemberger, G. Pescitelli. Berlin, Germany, 2017.
- (37) Littich, R. A. Studies Directed Towards The Total Synthesis Of Cortistatin A, The University of Texas at Austin, 2010.
- (38) Montalbetti, C. A. G. N.; Falque, V. Amide Bond Formation and Peptide Coupling. *Tetrahedron* **2005**, *61* (46), 10827–10852.
- (39) Joullié, M. M.; Lassen, K. M. Evolution of Amide Bond Formation. *Arkivoc* **2010**, *2010* (8), 189–250.
- (40) Devillers, I.; Arrault, A.; Olive, G.; Marchand-Brynaert, J. A Biomimetic Synthesis of Coelenterazine Analogs. *Tet. Let.* **2002**, *43* (17), 3161–3164.

CHAPTER III

CONFORMATIONAL ANALYSIS

The third chapter presents structure analysis of previously obtained 1,4-benzoxazine-based pseudodipeptides and pseudotripeptides. Different physico-chemical tools like spectroscopic methods (*i.e.* infrared (IR) and nuclear magnetic resonance (NMR)) and X-ray diffraction were considered to investigate information about:

- Existence of intra- and/or intermolecular H-bonds
- Solvent dependence of the chemical shift of NH protons
- Spatial arrangement of atoms

1. General introduction

The first method to study structural behaviour is Fourier Transform Infrared (FT-IR). The FT-IR spectroscopy first reveals the presence of different functional groups in a molecule *via* their absorption bands and more thoroughly it can expose the involvement of amide and carbonyl groups to know if they participate to an intramolecular H-bond. In the FT-IR of peptides, the most interesting bands are the stretching vibration region of C=O ($1580 - 1750 \text{ cm}^{-1}$) and N-H functions ($3200 - 3550 \text{ cm}^{-1}$). Those vibration regions give valuable information about potential intramolecular H-bond (C=O----H-N). When carbonyl or amide groups are involved in a H-bond, their absorption bands will shift at low frequencies and their shift values reflect the strength of interaction. It is agreed in the literature¹⁻³ that if NH proton involves in a H-bond, its IR absorption band will shift below 3400 cm^{-1} . However, in the IR spectra, C=O and NH bands can be overlapped so it can be difficult to precisely assign each band. To overcome this problem, deconvolution method is applied to reveal the overlapping bands if necessary. In this work, Levenberg-Marquardt algorithm is used to adjust the positions of deconvoluted bands with root-mean-square (RMS) error below 0.008 for all spectra.

The second method is 1D NMR to study the influence of solvent on the chemical shift of NH protons. This crucial experimental technique is used to (i) check diastereoisomeric purity in a diastereomeric mixture and (ii) analyze effect of solvent on chemical shift of NH protons to show off if that a NH proton is involved in a H-bond or not. Due to the sensitivity towards environment of NH protons, it will be differently behaved in non-polar or polar solvent. Each molecule will be dissolved in non-polar solvent (CDCl_3) and by slowly adding polar solvent ($\text{DMSO-}d_6$), the evolution of the NH chemical shift was followed. If NH proton does not involve in an intramolecular H-bond, its chemical shift will significantly and rapidly change and move towards downfield due to influence of $\text{DMSO-}d_6$ (DMSO contains sulfoxide group that can create H-bond with NH proton). In contrary, if NH proton is involved in an intramolecular H-bond, its chemical shift will not be strongly affected by polar solvent. The

smaller of the two chemical shift values distance is ($\Delta\delta = \delta_{100\% \text{ of DMSO-}d_6} - \delta_{100\% \text{ of CDCl}_3}$), the stronger of the H-bond will be.

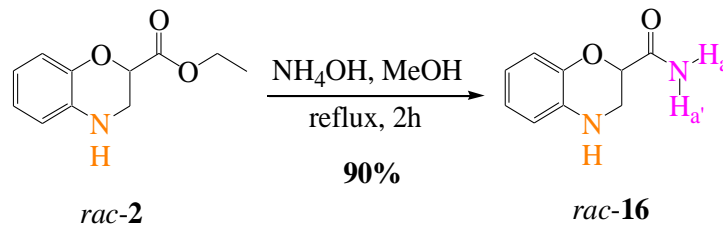
The third method widely used to investigate the structure of a molecule is X-ray diffraction. It provides lot of precise information about its crystallographic structure like bond's length, atoms composition, atoms arrangement or presence of inter and intramolecular H-bond. X-ray method also give detailed information about length of H-bond and torsion angles. However, it requires the formation of a good crystal of the studied molecule to have a good analysis. Unfortunately, not all the compounds can be crystallized, some remains powder or oil.

2. Conformational study of 1,4-benzoxazine-based pseudodipeptides

2.1. Conformational study of (*S*)-2, (*R*)-2 and *rac*-16 as reference models

2.1.1. Solution state analysis of (*S*)-2, (*R*)-2 and *rac*-16

To start the analysis, reference values for free or bonded N-H and C=O participating to an intramolecular H-bond are needed so a small model of 3,4-dihydro-2*H*-1,4-benzoxazine-2-carboxamide *rac*-16 (Scheme 3.1) was obtained by amidation of the ester group of *rac*-2 in 90% yield to be taken as the reference.



Scheme 3.1 Obtainment of racemate 3,4-dihydro-2*H*-1,4-benzoxazine-2-carboxamide *rac*-16

H-bond can be formed within single molecule (intramolecular H-bond) or between several molecules (intermolecular H-bond). The intramolecular H-bond can be observed and characterized *via* NMR and FT-IR spectroscopic studies. The intermolecular H-bond can be revealed *via* NMR and X-ray diffraction studies.

To have a good analysis in solution phase, intermolecular H-bond should be avoided on NMR results. While intramolecular H-bond can be easily observed at low concentration, the intermolecular H-bond changes following the concentration of molecule⁴. Therefore, compound *rac*-16 was checked at different concentrations of 10^{-1} , 10^{-2} and 10^{-3} M in CDCl_3 to verify their nature of inter- or intramolecular H-bond (Figure 3.1). It resulted no considerable difference between chemical shifts (δ) of NH of 1,4-benzoxazine ring and one primary amide

NHa' at variation of concentration between 10^{-1} to 10^{-3} M that meant there was no intermolecular H-bond at concentration of 10^{-2} M for those NHs. One primary amide NHa shifts a bit in upper field at 10^{-1} M ($\delta = 6.83$ ppm at 10^{-1} M) but $\Delta\delta$ ($\delta_{0.1} - \delta_{0.001}$) = 0.29 ppm is consistent. Therefore, all studied compounds would be measured at concentration of 10^{-2} M in CDCl_3 for structural studies in solution state.

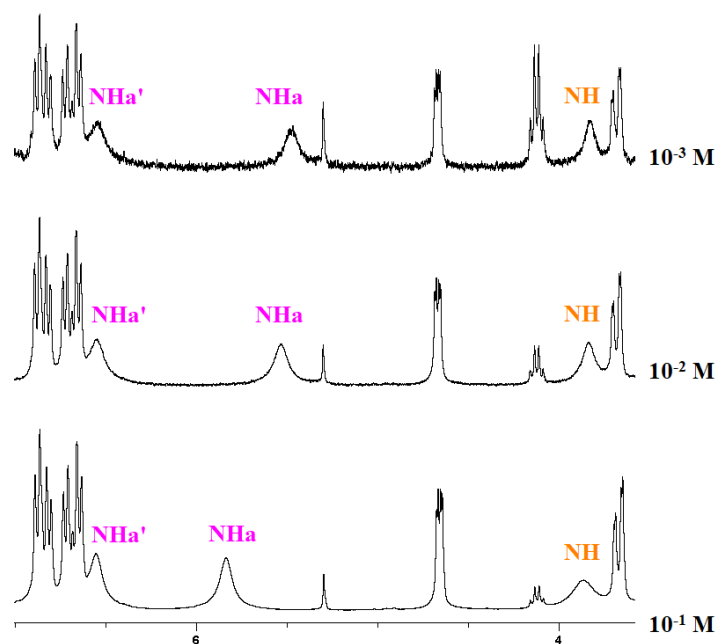


Figure 3.1 ^1H NMR of *rac*-**16** at different concentration (300 MHz, 300K, CDCl_3 , 10^{-2} M)

The ^1H NMR spectrum of compound *rac*-**16** (Figure 3.1) shows two peaks corresponding to displacement of the two primary amidic NH protons which should be assigned as one peak if those two NH protons are similar. Their two peaks on the ^1H NMR spectrum mean that they are not similar and probably one of them is involved in a H-bond and the other is free (non H-bonded). When a NH proton is involved in a H-bond, its chemical shift tends to be deshielded and gives a high value (around 7 ppm)⁴ and in contrary, if it is a free NH proton, its chemical shift will be shifted more upfield (around 5 – 5.5 ppm). The chemical shift free NH of 1,4-benzoxazine is located at 3.84 ppm and the chemical shift of both two primary amidic NH protons (NHa and NHa') are 5.55 ppm (NHa, free) and 6.56 ppm (NHa', H-bonded). The difference of two primary amidic NH protons chemical shifts ($\Delta\delta = \delta_{\text{NHb}} - \delta_{\text{NHa}} = 1.01$ ppm) might suggest a presence of a H-bond within molecule. To strengthen that hypothesis, the solvent-dependence NMR experiments in CDCl_3 and $\text{DMSO-}d_6$ at 10^{-2} M concentration were performed and NH chemical shifts were noted. $\text{DMSO-}d_6$ is a polar solvent used to validate the nature of a NH proton (free or H-bonded). If a NH proton is free, its chemical shift will be strongly affected by $\text{DMSO-}d_6$ to give a significant increase, the $\Delta\delta$ ($\delta_{\text{DMSO-}d_6} - \delta_{\text{CDCl}_3}$) may

bigger than 1.5-2.0 ppm. In reverse, chemical shift of a NH proton involved in H-bond will remain consistent or be slightly adjusted by DMSO- d_6 . In the case of compound *rac-16*, the NH proton which is attached in 1,4-benzoxazine ring boosted from 3.84 ppm at 10^{-2} M in 0% of DMSO- d_6 to 5.83 ppm in 100% of DMSO- d_6 ($\Delta\delta = +1.98$ ppm) and the free primary amidic NH proton (NH_a) rose from 5.55 ppm to 7.37 ppm ($\Delta\delta = +1.82$ ppm) expressing that those two NH protons are free. The chemical shift of the H-bonded primary amidic NH proton (NH_{a'}) inconsiderably increased from 6.56 ppm to 7.43 ppm at 100% of DMSO- d_6 ($\Delta\delta = +0.87$ ppm). The movement of the NH_{a'} chemical shifts is quite complicated to point that it participated in intramolecular H-bond or not. Since only one primary amidic carbonyl group is presented in *rac-16*, and it surely cannot form a H-bond with NH_{a'} proton. Therefore, if the H-bond exists in this molecule, it will be between NH_{a'} and a lone pair of electrons of oxygen atom in 1,4-benzoxazine ring (Figure 3.2) to create a C₅ conformation in CDCl₃ at 10^{-2} M concentration.

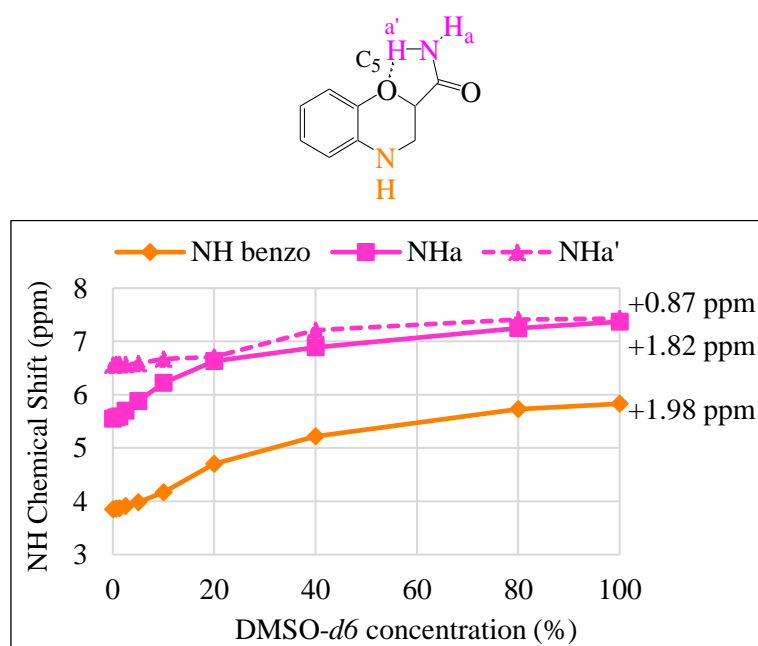


Figure 3.2 Postulated conformation in CDCl₃ solution (up) and effect of solvent (CDCl₃/DMSO- d_6) on NH chemical shifts (down) of *rac-16* (10^{-2} M)

In addition, the FT-IR study (Figure 3.3) is also carried out in CDCl₃ at the same concentration that is used for NMR (*i.e.* 10^{-2} M). The stretching vibration region of N-H and C=O are limited around 3200 cm^{-1} to $3500\text{--}3550\text{ cm}^{-1}$ and 1600 cm^{-1} to 1800 cm^{-1} , respectively. These regions show the most concerned information of H-bonding network. If NH is involved in a H-bond, it will exhibit an absorption band below 3400 cm^{-1} . The FT-IR spectrum of compound *rac-16* depicted three bands in the NH stretching vibration region which are 3523 cm^{-1} (asymmetric primary amidic NH), 3411 cm^{-1} (NH benzo) and 3401 cm^{-1} (symmetric primary amidic NH)⁵.

Normally the two values above 3400 cm^{-1} represented for free NHs but the value 3401 cm^{-1} which is very close to the line border of free and bonded-NH. However, it was reported⁶ that asymmetric and symmetric elongations of a free primary amidic NH in FT-IR analysis were around 3500 cm^{-1} and 3400 cm^{-1} , respectively. Therefore, perhaps no intramolecular H-bond present in *rac*-**16**.

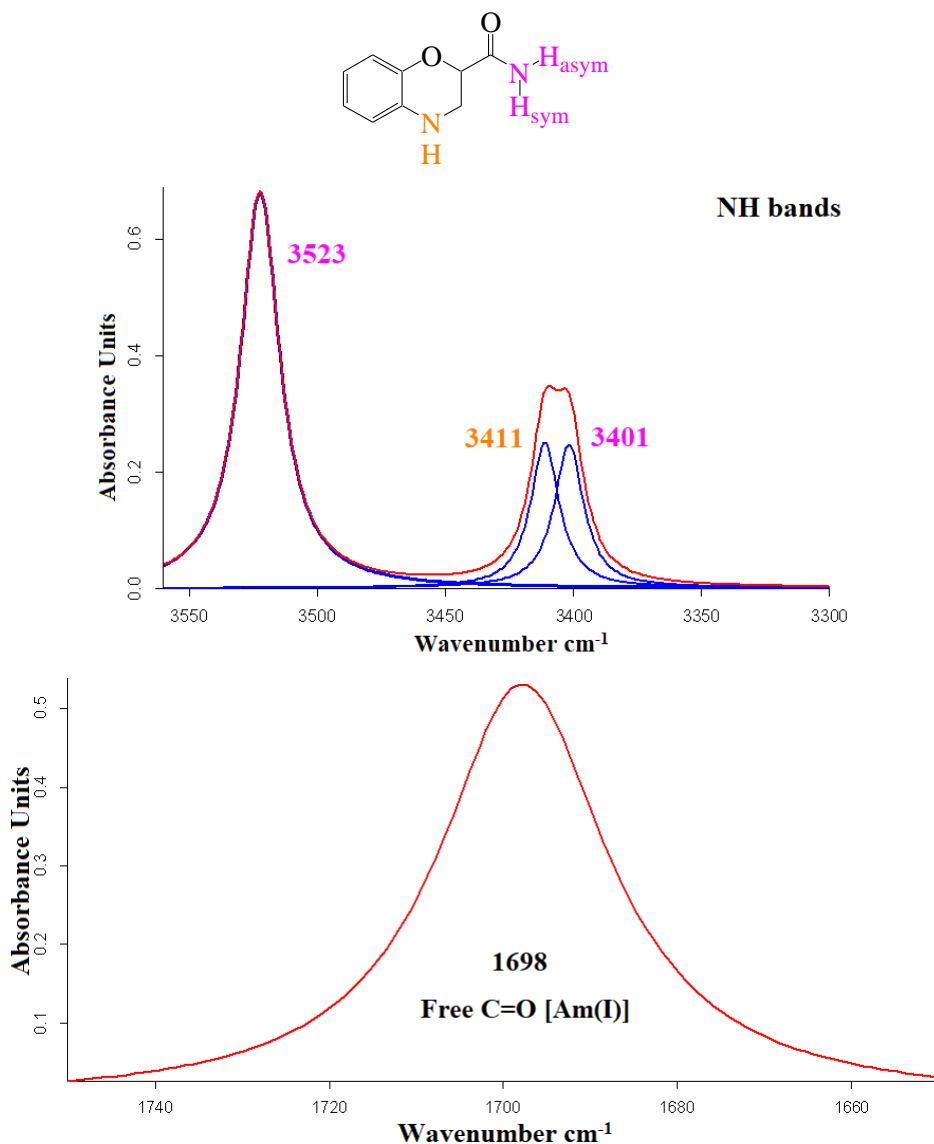


Figure 3.3 IR absorption spectrum (NH and C=O deconvoluted bands) of *rac*-**16** recorded in CDCl_3 at 10^{-2} M

The IR reference values of the small model *rac*-**16** are listed with free NH of 1,4-benzoxazine scaffold in IR absorption spectrum is 3411 cm^{-1} , free primary amidic NH are 3523 cm^{-1} (asymmetric) and 3401 cm^{-1} (symmetric), and a free primary amidic carbonyl group is 1698 cm^{-1} .

Besides compound *rac*-**16**, (*S*)- and (*R*)-**2** also are checked by FTIR to access to the IR reference values of the free NH of 1,4-benzoxazine and ester carbonyl group. The IR absorption band of free NH_{benzo} is 3418 cm⁻¹ for both (*S*)- and (*R*)-**2** which are a bit different to *rac*-**16** (3411 cm⁻¹), perhaps the presence of two primary amidic NHs affect the shift of NH_{benzo}. The free ester carbonyl group is 1746 cm⁻¹ also the same for two enantiomers. The chemical shift of NH_{benzo} of (*S*)-**2** and (*R*)-**2** placed at 3.77 ppm. Once all reference values are noted, several pseudodipeptides containing 1,4-benzoxazine scaffold start being analyzed.

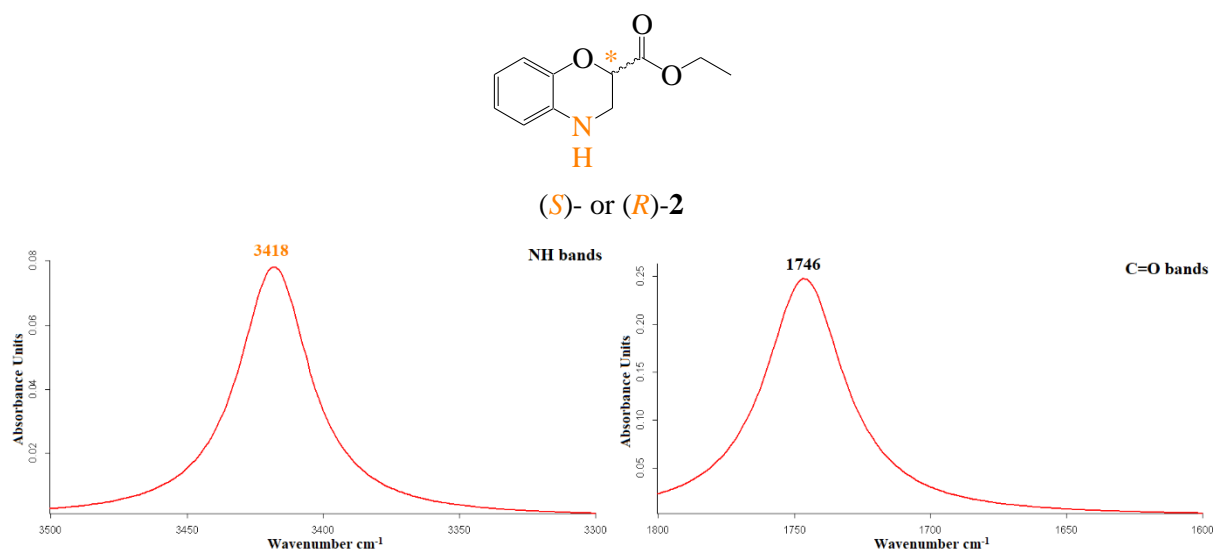


Figure 3.4 IR spectrum of (*S*)-**2** and (*R*)-**2** recorded in CDCl₃ at 10⁻² M

2.1.2. Solid state analysis of *rac*-**16**

After several attempts, crystal of *rac*-**16** was obtained by dissolving a little quantity of compound in chloroform then let the solvent slowly evaporated at room temperature. After analyzing this crystal by X-ray diffraction (Figure 3.5), it was shown that compound *rac*-**16** was crystallized in the space group P2₁/c. The X-ray diffraction exhibits a C₅ pseudocycle that is formed *via* an intramolecular H-bond between a lone pair of electrons of oxygen atom and one primary amidic NH proton. The measured distance of this bond is 2.15 Å. This result conflicts to solution state analysis of *rac*-**16**. The analyzed result above did not indicate that a primary amidic proton is involved in H-bond. However, by X-ray diffraction picture, the H-bond does exist. This result is in agreement with NMR analysis in solution phase of *rac*-**16** that the asymmetric primary amide NH proton was involved in H-bond ($\Delta\delta_{\text{NH}_{\text{asym}}} = +0.87$ ppm; $\delta_{\text{NH}_{\text{asym}}} = 6.56$ ppm).

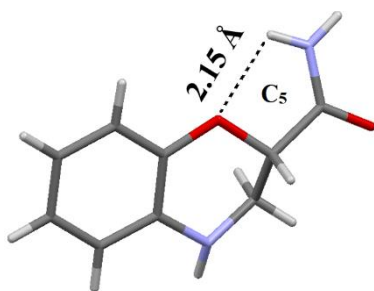
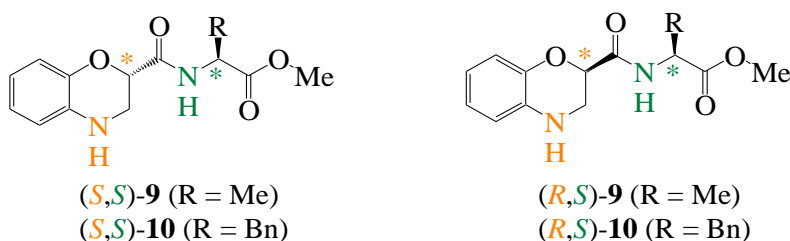


Figure 3.5 X-ray diffraction structure of compound *rac*-**16** crystallized in chloroform

2.2. Solution state analysis of compounds (*S,S*)- and (*R,S*)-**9**, -**10**

Conformational study of four pseudodipeptides (*S,S*)-**9**, -**10** and (*R,S*)-**9**, -**10** at a concentration of 10^{-2} M had been initiated by examining firstly the solvent-dependence of NH protons chemical shifts by ^1H NMR in mixture of $\text{DMSO-}d_6$ in CDCl_3 (0-100%, v/v) and secondly by FTIR absorption spectroscopy in CDCl_3 .



As we concern about the racemization problem and HOBt is used to prevent it occurs, ^1H NMR studies of (*S,S*)-**9**, -**10** and (*R,S*)-**9**, -**10** are taken to compare with NMR values of their diastereoisomeric mixture to be sure they were not racemized (Figure 3.6). Two single diastereoisomers are different in physical properties so they can be separated by normal column chromatography. Even in this work, 1,4-benzoxazine enantiomer as starting compound is taken from chiral HPLC, we tried to separate them from their diastereoisomer mixture and used for examining conditions of coupling reaction.

The overlay of the ^1H NMR spectra of single diastereoisomer (*S,S*)-**9** or (*R,S*)-**9** and their diastereoisomeric mixture in CDCl_3 at 10^{-2} M are presented in the Figure 3.6A. The ^1H NMR spectrum of diastereoisomeric mixture of (*S,S*)-**9** and (*R,S*)-**9** shows two singlets of each methoxy group (OCH_3 , at 3.73 ppm and OCH_3 at 3.79 ppm) and two doublets for each methyl lateral chain of alanine (CH_3 at 1.43 ppm and CH_3 , at 1.49 ppm). The ^1H NMR spectrum of single (*S,S*)-**9** or (*R,S*)-**9** reveals only one signal for each group. Similarly, two compounds (*S,S*)-**10** and (*R,S*)-**10** is also compared with their diastereoisomeric mixture. As shown in the Figure 3.6B, the CH_2 of phenylalanine of (*S,S*)-**10** shifted upfield while CH_2 , of (*R,S*)-**10** shifts

a bit downfield. The O-CH_a of (*S,S*)-**10**, however, is deshielded comparing to CH_a' of (*R,S*)-**10**. The methoxy group of (*S,S*)-**10** (OCH₃) shifted around 3.74 ppm while in (*R,S*)-**10** is 3.67 ppm (OCH₃'). All those signals appeared together in the ¹H NMR spectrum of diastereoisomeric mixture. Based on these two figures, it can be confirmed that there is no racemization occurs during coupling step.

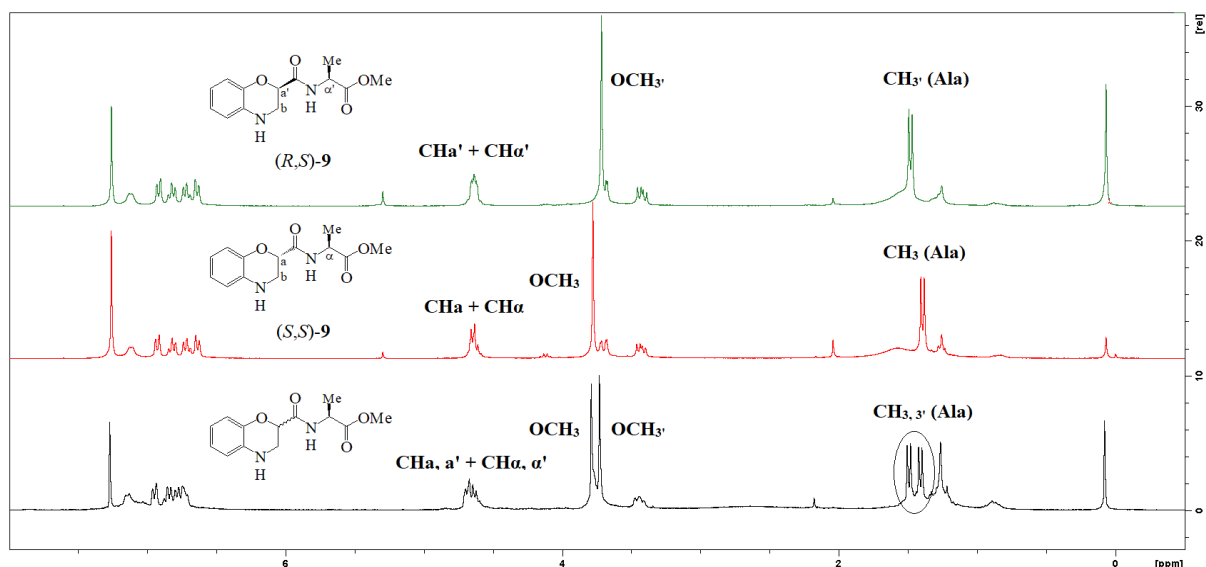


Figure 3.6A Comparison of ¹H NMR spectra of (*S,S*)-**9** and (*R,S*)-**9** with its diastereoisomeric mixture (300 MHz, 300K, CDCl₃, 10⁻² M)

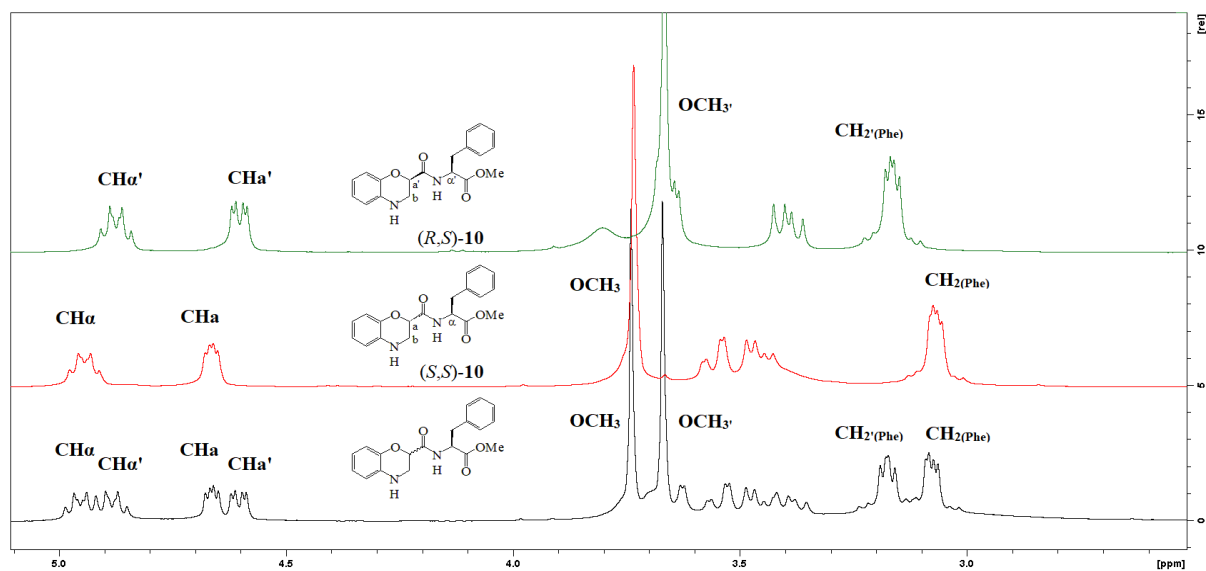


Figure 3.6B Comparison of ¹H NMR spectra of (*S,S*)-**10** and (*R,S*)-**10** with its diastereoisomeric mixture (300 MHz, 300K, CDCl₃, 10⁻² M)

The NMR solvent-dependence experiments are studied to evaluate the solvent sensitivity of the NH protons. The chemical shifts of NH_{benzo} of (*S,S*)- and (*R,S*)-**9**, **10** are significantly increased ($\Delta\delta = +2.18$, $+2.27$ ppm and $+2.13$ ppm, $+2.05$ ppm, respectively) that means NH of

1,4-benzoxazine scaffold remains non-intramolecularly H-bonded. The secondary amide NH α , however, gradually rises ($\Delta\delta = +1.35$ ppm, +1.36 ppm for compound **9** and +1.2 ppm, +1.32 ppm for compound **10**). The $\Delta\delta$ of secondary amidic NH of both compounds is moderately different. Even they do not express a strong effect of DMSO- d_6 but also its affect does not too weak ($\Delta\delta \approx 1.2$ ppm). Therefore, probably both pseudopeptides **9** and **10** do not have an intramolecular H-bond.

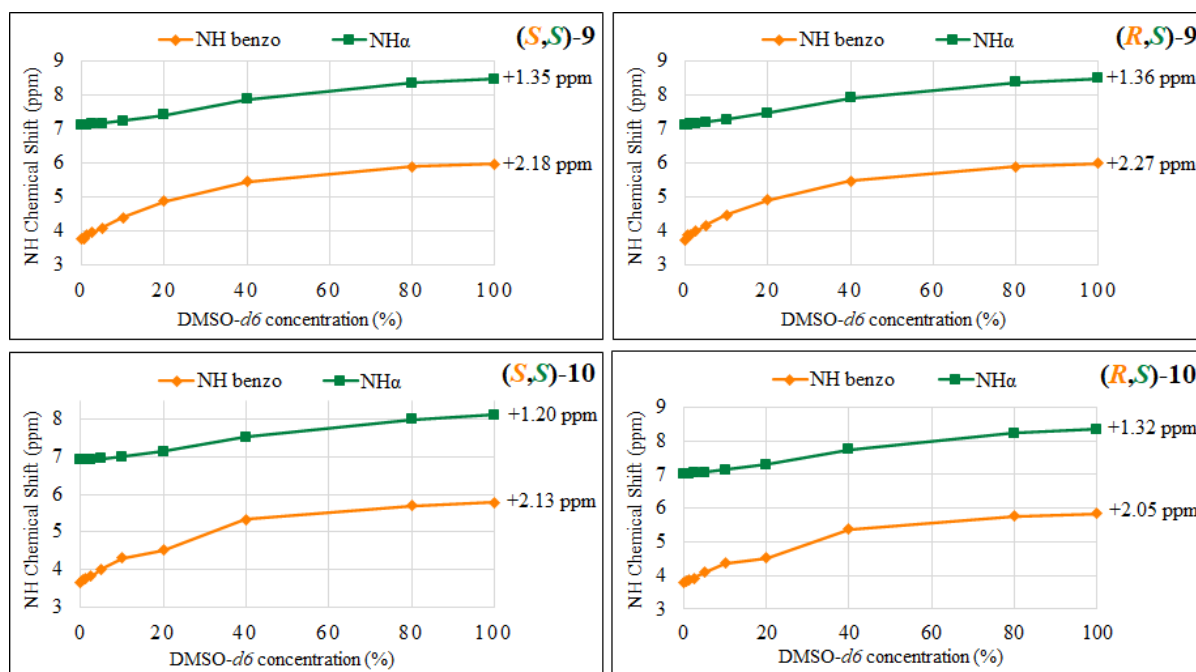
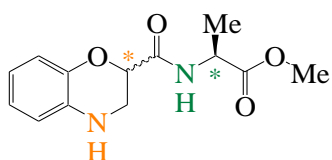


Figure 3.7 Solvent-dependence in mixed CDCl₃/DMSO- d_6 at 10^{-2} M of NH chemical shift of compound **9** (up) and **10** (down)

FTIR spectroscopy in solution was performed on four compounds. The IR absorption spectra of the two diastereoisomers (*S,S*)-**9** and (*R,S*)-**9** (Figure 3.8) are presented below. Compound (*S,S*)-**9** exhibits two NH bands at 3413 cm^{-1} (NH α) and 3427 cm^{-1} (NH_{benzo}) and its diastereoisomer (*R,S*)-**9** had exactly the same values. The presence of those bands above 3400 cm^{-1} indicates that there is no N-H involved in the intramolecular H-bonding network of two compounds. In the carbonyl absorption region, the band of ester carbonyl group is observed at 1743 cm^{-1} ; each amide carbonyl group absorbed at 1678 cm^{-1} for both (*S,S*)- and (*R,S*)-**9**.



(*S,S*)- and (*R,S*)-**9**

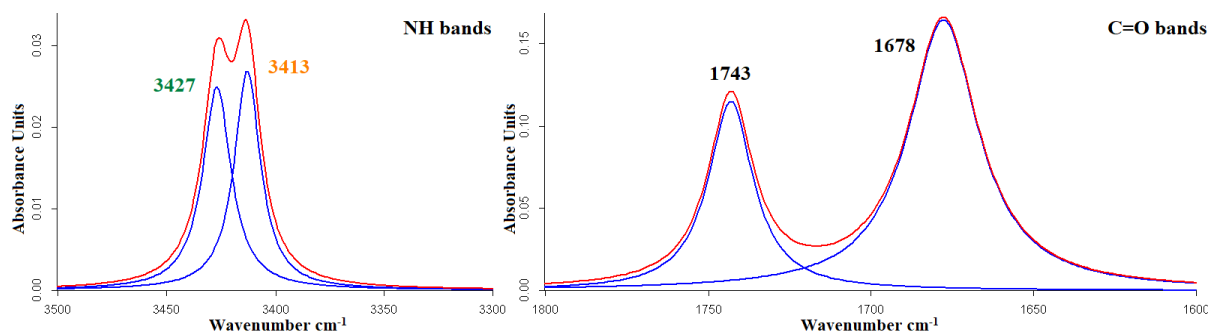
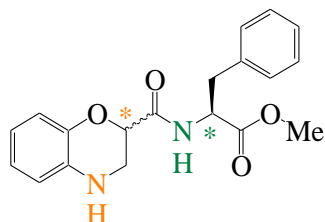


Figure 3.8 FTIR absorption spectra (in red) and N-H and C=O deconvoluted bands (in blue) of (*S,S*)- and (*R,S*)-**9** (CDCl_3 , 10^{-2} M)

IR absorption spectra of the two pseudodipeptides (*S,S*)-**10** and (*R,S*)-**10** contain two bands in the stretching vibration region of NH which are 3422 cm^{-1} ($\text{NH}\alpha$), $3410/3408\text{ cm}^{-1}$ (NH benzo) (Figure 3.9). Because those values are above 3400 cm^{-1} , they probably imply the absence of intramolecular H-bond. Moreover, the C=O stretching region demonstrate two bands at 1743 cm^{-1} and 1680 cm^{-1} which correspond to free secondary amidic and ester carbonyl groups for both compounds (*S,S*)-**10** and (*R,S*)-**10**.



(*S,S*)- and (*R,S*)-**10**

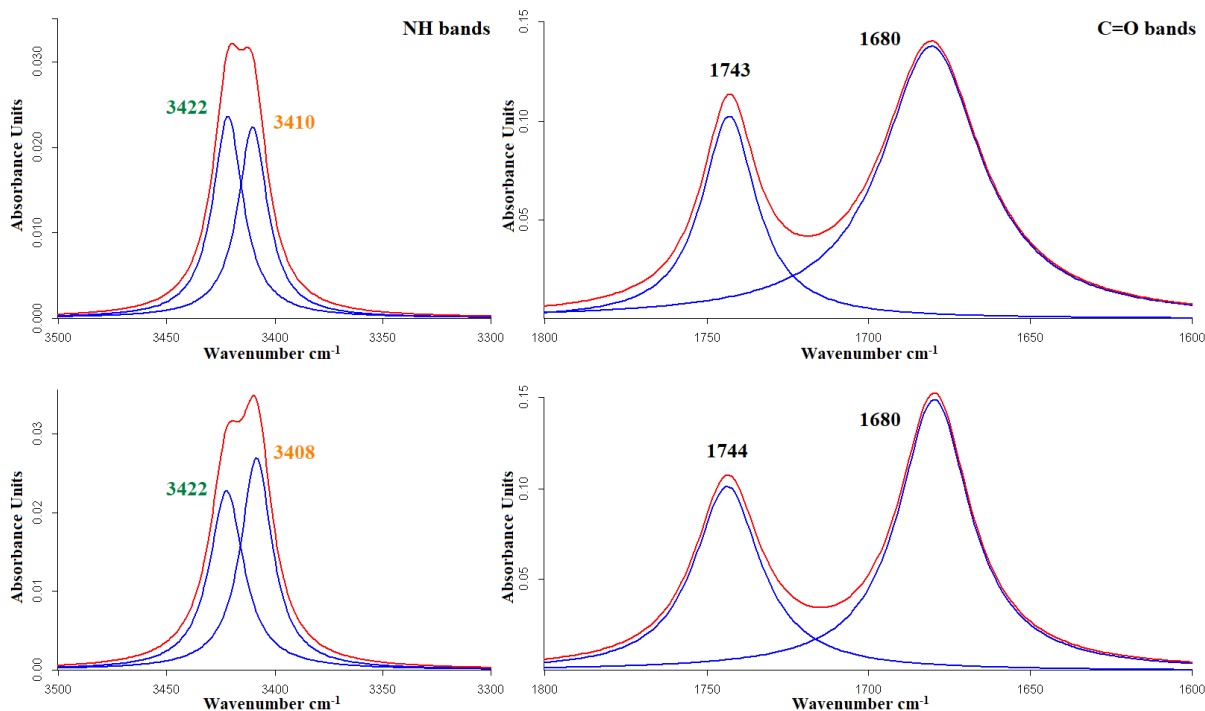


Figure 3.9 IR absorption spectra (in red) and N-H and C=O deconvoluted bands (in blue) of (*S,S*)-**10** (up) and (*R,S*)-**10** (down) (CDCl_3 , 10^{-2} M)

Based on data above, it may conclude that elongation of *C*-terminal extremity by methyl ester α -amino acid does not create intramolecular H-bond within molecule. The Table 13 and 14 summarize the chemical shifts of NH and IR absorption bands in the stretching region of NH and C=O for *rac*-**16**, (*S,S*)-**9**, -**10** and (*R,S*)-**9**, -**10**. These values can be used as reference for free primary and secondary amidic NHs, free C=O of primary and secondary amides and ester.

Table 13 ^1H NMR chemical shifts (δ_{NH}) of different NH protons of *rac*-**16**, (*S*)-**2**, (*R*)-**2**, (*S,S*)-**9**, -**10** and (*R,S*)-**9**, -**10** (300 MHz, 300K, CDCl_3 , 10^{-2} M)

Type of NH*	δ_{NH} (ppm)						
	<i>rac</i> - 16	(<i>S</i>)- 2	(<i>R</i>)- 2	(<i>S,S</i>)- 9	(<i>R,S</i>)- 9	(<i>S,S</i>)- 10	(<i>R,S</i>)- 10
Benzo	3.84	3.77	3.77	3.78	3.71	3.65	3.80
Am (I)	5.55 (free) 6.56 (H-bonded)	-	-	-	-	-	-
Am (II)	-	-	-	7.11	7.12	6.92	7.02

*Benzoxazine (Benzo), primary amide [Am (I)], secondary amide [Am (II)]

Table 14 IR absorption bands in the stretching region of NH and C=O of *rac*-**16**, (*S*)-**2**, (*R*)-**2**, (*S,S*)-**9**, -**10** and (*R,S*)-**9**, -**10** (CDCl_3 , 10^{-2} M)

Type of NH*	NH stretching (cm ⁻¹)						
	<i>rac-16</i>	(<i>S</i>)- 2	(<i>R</i>)- 2	(<i>S,S</i>)- 9	(<i>R,S</i>)- 9	(<i>S,S</i>)- 10	(<i>R,S</i>)- 10
Benzo	3411	3418	3419	3413	3413	3410	3408
Am (I)	3523 (asym.) 3402 (sym.)	-	-	-	-	-	-
Am (II)	-	-	-	3427	3427	3422	3422

Type of C=O*	C=O stretching (cm ⁻¹)						
	<i>rac-16</i>	(<i>S</i>)- 2	(<i>R</i>)- 2	(<i>S,S</i>)- 9	(<i>R,S</i>)- 9	(<i>S,S</i>)- 10	(<i>R,S</i>)- 10
Am (I)	1698	-	-	-	-	-	-
Am (II)	-	-	-	1678	1678	1680	1680
Ester	-	1746	1746	1743	1743	1743	1744

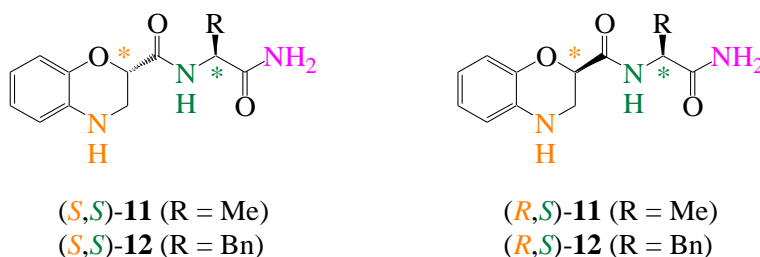
*Benzoxazine (Benzo), primary amide [Am (I)], secondary amide [Am (II)]

The four molecules (*S,S*)-**9**, -**10** and (*R,S*)-**9**, -**10** are all small models and do not allow H-bonds to form in the molecule. For this reason, we did amidation reaction of compounds **9** and **10** for changing methyl ester group to NH₂ (compounds **11** and **12**) to increase probabilities of H-bond formation.

2.3. Conformational study of compounds (*S,S*)- and (*R,S*)-**11**, -**12**

2.3.1. Solution state analysis of compounds (*S,S*)- and (*R,S*)-**11**, -**12**

Firstly, the conformational analysis of compound (*S,S*)-**11**, -**12** and (*R,S*)-**11**, -**12** are reported by studying the effect of varying ratios of solvent in the mixture of CDCl₃/DMSO-*d*₆ (at concentration of 10⁻² M) of the NH chemical shifts.



¹H NMR data of four diastereoisomers (*S,S*)-**11**, -**12** and (*R,S*)-**11**, -**12** have been analyzed (Figure 3.10). Comparing to NH value of reference model *rac-16*, the free (NH_a, 5.39 ppm) and H-bonded (NH_a', 6.09 ppm) primary amidic protons NH protons of compound **11** and **12** shift more upfield than ones in *rac-16*. Besides, the (*S*)-configuration seems always give the chemical shifts of all NH shift at low field comparing to the (*R*)-configuration.

Solvent-dependence of (*S,S*)-**11** (Figure 3.10) presents the chemical shift of the secondary amidic NH proton (NH α) slightly increases from 7.08 ppm at 10⁻² M in 100% of CDCl₃ to 7.87 ppm in 100% DMSO-*d*₆ ($\Delta\delta = \delta_{\text{DMSO-}d_6} - \delta_{\text{CDCl}_3}$). This $\Delta\delta$ value of NH α (+0.79 ppm) is quite close to $\Delta\delta$ of the H-bonded primary amidic NH α' of *rac*-**16** (+0.87 ppm) which was confirmed involving in a H-bond so probably, the NH α of (*S,S*)-**11** is H-bonded. One of the primary amidic proton NH α' of (*S,S*)-**11** is moderately affected by polar solvent ($\Delta\delta = +1.42$ ppm) so it should be free. Two NH protons are highly affected by increasing volume of polar solvent and correspond to one primary amidic NH α and NH_{benzo} with $\Delta\delta = +1.78$ ppm and +2.05 ppm, respectively. It is obviously seen that those two are also non H-bonded (free) because they are strongly affected by the addition of DMSO-*d*₆. Similarly, secondary amidic NH α and one primary amidic NH α' protons of (*R,S*)-**11** are poorly influenced in polar environment ($\Delta\delta = +1.03$ ppm, +1.58 ppm, respectively). The NH α and NH_{benzo} move ≈ 2 ppm while increasing DMSO-*d*₆ ratio in the solvent mixture (Figure 3.10). These results from study of solvent-dependence probably displayed that NH α protons of both diastereoisomers are involved in a weak H-bond because their chemical shifts do not give a big $\Delta\delta$ while the others are highly influenced in polar environment so they should be free.

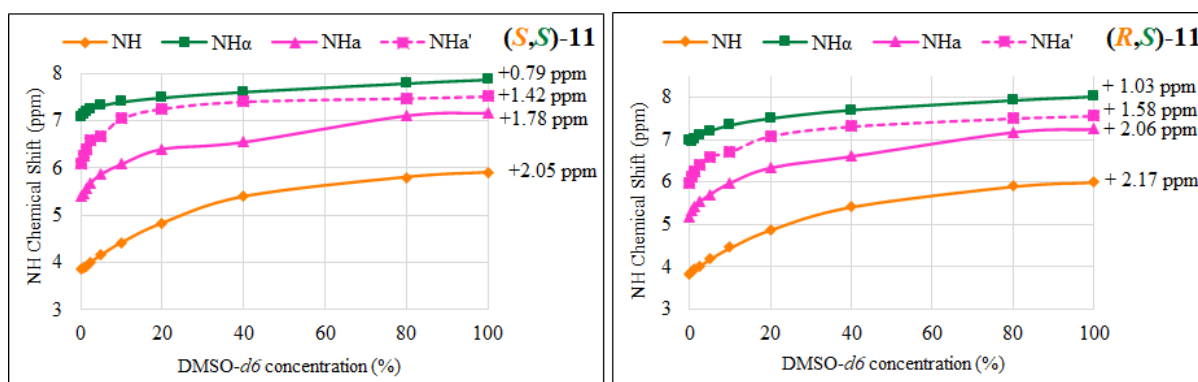


Figure 3.10 Solvent-dependence in mixed CDCl₃/DMSO-*d*₆ at 10⁻² M of NH chemical shift of compounds **11**

The result obtained after ¹H NMR study of solvent-dependence of two diastereoisomers (*S,S*)-**12** and (*R,S*)-**12** are also comparable to those for compound **11** (Figure 3.11). It seems that there is not any crucial affection to structural behavior when changing the side chain of amino acid between alanine and phenyl-alanine. The NH α proton of secondary amide of (*S,S*)-**12** shifts at 7.11 ppm in 100% of CDCl₃ and is poorly affected when adding more DMSO-*d*₆ ($\Delta\delta = +0.59$ ppm) then probably it participates in H-bond. The two NH α and NH α' protons and also the NH_{benzo} proton boost approximately 2 ppm from 100% of non-polar solvent CDCl₃ to polar

solvent (DMSO- d_6). Also in molecule (*R,S*)-**12**, the secondary amidic NH α proton shifted a bit upfield (6.89 ppm) comparing to NH α of (*S,S*)-**12** and it slowly moves from 0% to 100% of DMSO- d_6 in CDCl $_3$ ($\Delta\delta = +1.00$ ppm) so perhaps it is involved in H-bond. The chemical shift of two primary amidic NH α , NH α' protons and NH $_{benzo}$ move 1.75 ppm, 1.92 ppm and 2.21 ppm, respectively which indicate that they are highly influenced by DMSO- d_6 so all are free NH.

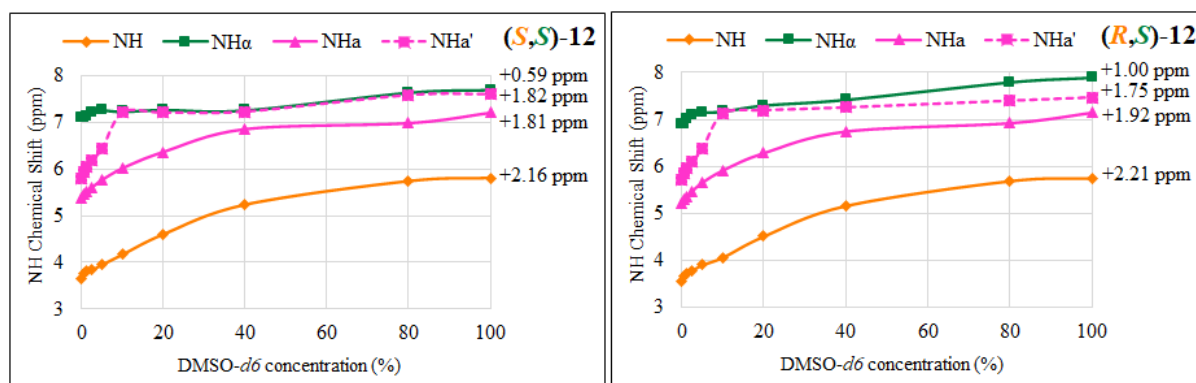


Figure 3.11 Solvent-dependence in mixed CDCl $_3$ /DMSO- d_6 at 10^{-2} M of NH chemical shift of compounds **12**

Based on the chemical shift of the NH α proton ($\delta \approx 7$ ppm) in four structures and its evolution in polar environment, it can be uncertainly indicated that they are H-bonded. Because the NMR study of NH evolution in different environment polarity of pseudodipeptides **11** and **12** shows no convinced proof of H-bond, the FT-IR spectroscopic may help to confirm.

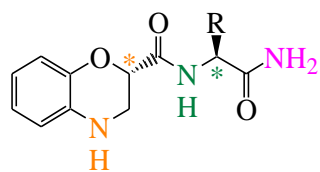
Secondly, in order to validate the presence of H-bond with more evidence, FT-IR of four diastereoisomers (*S,S*)-**11**, -**12** and (*R,S*)-**11**, -**12** are studied (Figure 3.12).

The NH stretching vibration region ($3200 - 3550$ cm $^{-1}$) of (*S,S*)-**11** contained four bands at 3417 (NH $_{benzo}$), 3492 (NH α), 3407 and 3524 cm $^{-1}$ (symmetric and asymmetric bands of free primary amide, NH α , α') and of (*R,S*)-**11** at 3418 , 3500 , 3406 and 3524 cm $^{-1}$, respectively for same type of NH (Figure 3.12A). The bands for NH $_{benzo}$, symmetric and asymmetric primary amide and NH α are consistent with the absence of H-bonds. In the solution state, the NH stretching vibration of secondary amide (NH α) occurs in the region around $3420 - 3460$ cm $^{-1}$ for free NH and $3270 - 3370$ cm $^{-1}$ for H-bonded NH. Theoretically, it should be no NH participating to H-bond network for these two molecules. It was reported before that two free symmetric and asymmetric primary amidic NH protons will show absorption bands at approximately 3500 cm $^{-1}$ and 3400 cm $^{-1}$ that similar to our molecule⁷. IR absorption

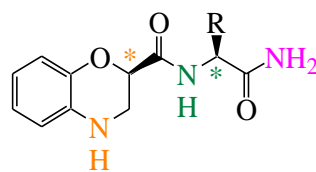
spectroscopic spectra in the NH stretching region of (*S,S*)- and (*R,S*)-**12** (Figure 3.12B) also exposes four bands which all locate above 3400 cm⁻¹. Two bands are close in proximity to 3400 cm⁻¹ correspond to symmetric primary amidic NH proton (3403 cm⁻¹ for (*S,S*)-**12** and 3409 for (*R,S*)-**12**). The solution state analysis including NMR study for solvent-dependence and FTIR analysis of pseudodipeptides **11** and **12** are in agreement that probably secondary amide NH α proton is involved in a H-bond.

In the C=O stretching vibration region (1600 – 1800 cm⁻¹), (*S,S*)- and (*R,S*)-**11** demonstrate two bands at 1698/1664 cm⁻¹ and 1698/1678 cm⁻¹ which correspond to primary and secondary amide carbonyl groups, respectively (Figure 3.12A). Two diastereoisomers (*S,S*)- and (*R,S*)-**12** exhibit quite similar values with two bands at 1688/1661 cm⁻¹ and 1693/1679 cm⁻¹, respectively (Figure 3.12B). As observed, primary amide C=O of both (*S,S*)- and (*R,S*)-**11** are free due to the same absorption value (1698 cm⁻¹) comparing to *rac*-**16**. The secondary amide C=O in (*R,S*)-**11** have similar value (1678 cm⁻¹) as free one in compounds **9** and **10** (Table 14), and this value decreases a bit to 1664 cm⁻¹ in (*R,S*)-**11**. However, the absorption band of primary amidic C=O of **12** decreases a bit to 1688 cm⁻¹ for (*S,S*)-**12** and 1693 cm⁻¹ for (*R,S*)-**12**. Even they are proximate values but probably, changing side chain of amino acid creates this difference. Furthermore, the absorption band of secondary amide C=O in (*S,S*)-**12** is lower than in (*R,S*)-**12** and are similar with those obtained with (*S,S*)-**11** is lower than in (*R,S*)-**11**, respectively. The chirality at C2 position of 1,4-benzoxazine seems have a minor influence on structural behavior because it does not generate considerable difference between absorption values or chemical shifts between two diastereoisomers.

To conclude, the solution state analysis including NMR study for solvent-dependence and FTIR analysis of pseudodipeptides **11** and **12** are done. The resulted analysis by ¹H NMR for influence of solvent indicates that probably secondary amidic NH α proton is involved in a H-bond with a lone pair of electrons of oxygen atom in 1,4-benzoxazine ring but not with a carbonyl group. This H-bond does not been affected by either absolute configuration of 1,4-benzoxazine scaffold (at C2 position) or side chain of amino acid. This H-bond can be recognized by evolution of NH α proton chemical shift in solvent-dependence study but not by FTIR analysis. The IR spectra show NH absorbance bands are below 3400 cm⁻¹ which mean all NHs are free and this is conflict to NMR study of solvent-dependence. The reason can be due to the H-bond which is not formed between NH and C=O as usual.



(*S,S*)-**11** (R = Me)



(*R,S*)-**11** (R = Me)

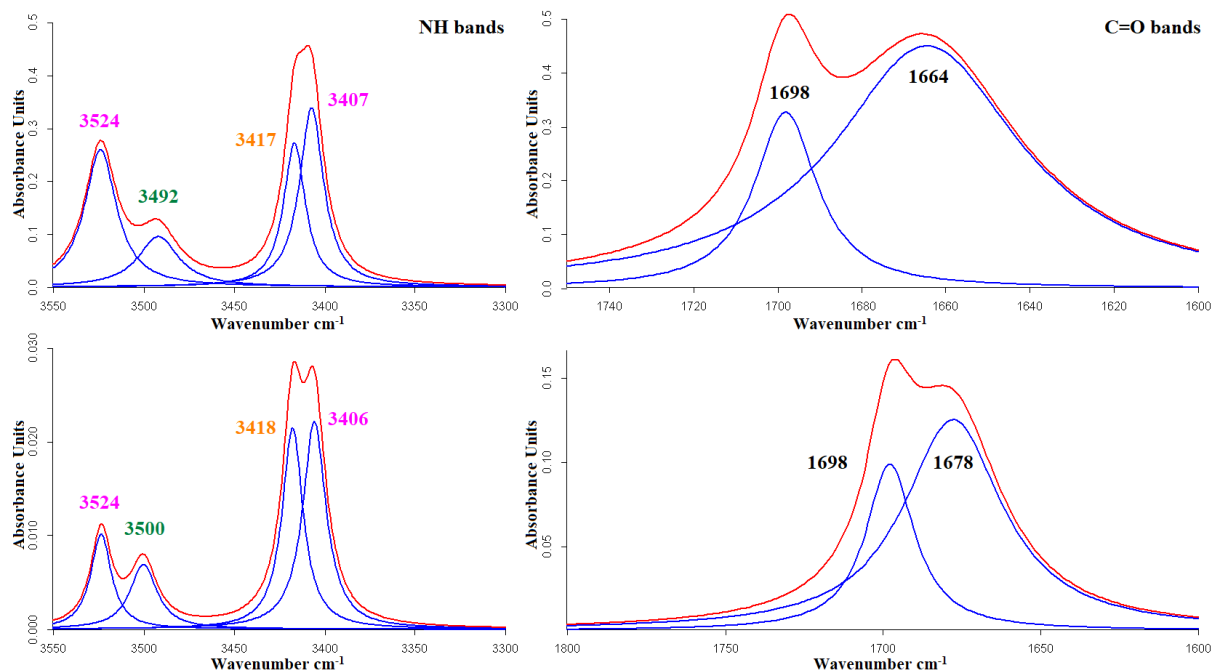


Figure 3.12A IR absorption spectra (in red) and N-H and C=O deconvoluted bands (in blue) of (*S,S*)-**11** (up) and (*R,S*)-**11** (down) (CDCl_3 , 10^{-2} M)

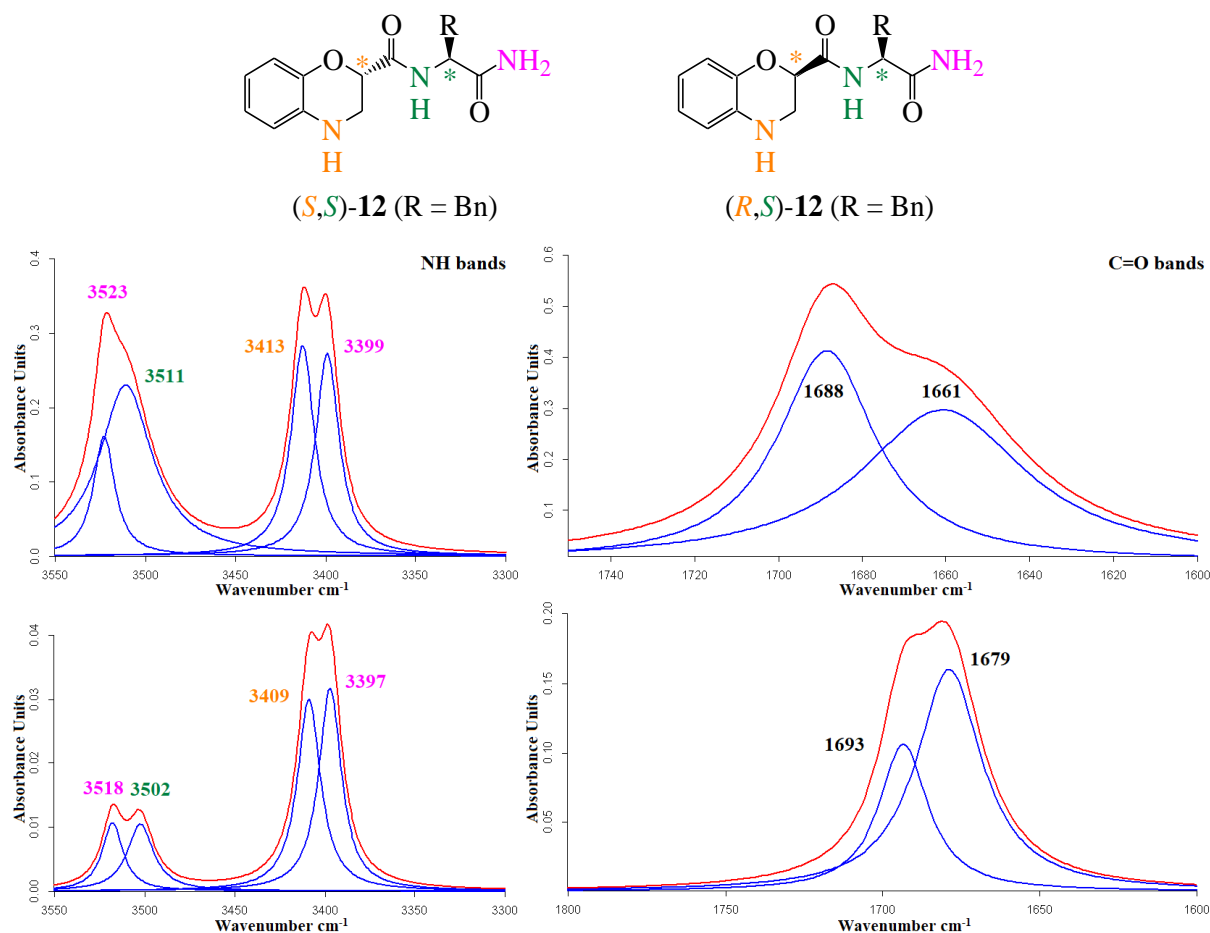


Figure 3.12B IR absorption spectra (in red) and N-H and C=O deconvoluted bands (in blue) of (*S,S*)-**12** (up) and (*R,S*)-**12** (down) (CDCl₃, 10⁻² M)

The Tables 15 and 16 below summarize the ¹H NMR chemical shifts of NH protons and IR absorption bands in the stretching region of NH and C=O for (*S,S*)-**11**, -**12** and (*R,S*)-**11**, -**12**.

Table 15 ¹H NMR chemical shifts (δ_{NH}) of different NH protons of (*S,S*)-**11**, -**12** and (*R,S*)-**11**, -**12** (300 MHz, 300K, CDCl₃, 10⁻² M)

Type of NH*	δ_{NH} (ppm)			
	(<i>S,S</i>)- 11	(<i>R,S</i>)- 11	(<i>S,S</i>)- 12	(<i>R,S</i>)- 12
Benzo	3.85	3.83	3.65	3.62
Am (I)	5.39	5.19	5.39	5.22
Am (II)	6.09	5.98	5.79	5.71
Am (II)	7.08	6.99	7.11	6.89

*Benzoxazine (Benzo), primary amide [Am (I)], secondary amide [Am (II)]

Table 16 IR absorption bands in the stretching region of NH and C=O of (*S,S*)-**11**, -**12** and (*R,S*)-**11**, -**12** (CDCl₃, 10⁻² M)

NH stretching (cm⁻¹)				
Type of NH*	<i>(S,S)</i> - 11	<i>(R,S)</i> - 11	<i>(S,S)</i> - 12	<i>(R,S)</i> - 12
Benzo	3417	3418	3413	3409
Am (I)	3524	3524	3523	3518
	3407	3406	3399	3397
Am (II)	3492	3500	3511	3502

C=O stretching (cm⁻¹)				
Type of C=O*	<i>(S,S)</i> - 11	<i>(R,S)</i> - 11	<i>(S,S)</i> - 12	<i>(R,S)</i> - 12
Am (I)	1698	1698	1688	1693
Am (II)	1664	1678	1661	1679

*Benzoxazine (Benzo), primary amide [Am (I)], secondary amide [Am (II)]

2.3.2. Solid state analysis of compounds *(S,S)*-**11**, *(R,S)*-**11** and *(S,S)*-**12**

Crystallization of three pseudodipeptides *(S,S)*-**11**, *(R,S)*-**11** and *(S,S)*-**12** are done by searching and trying to dissolve each molecule and to crystallize after their slowly evaporation at room temperature. The crystallization of each of the three pseudodipeptide *(S,S)*-**11**, *(R,S)*-**11** and *(S,S)*-**12** is done by trying to find the right mixture of solvents capable of dissolving the molecule and crystallizing the molecule after the slow evaporation at room temperature. *(S,S)*-**11** crystal was obtained in a mixture of ethyl acetate/*n*-hexane, *(R,S)*-**11** in a mixture of CH₂Cl₂/heptane and *(S,S)*-**12** in methanol/hexane. Their solid state was analyzed by X-Ray diffraction. Three crystallographic data of molecules *(S,S)*-**11**, *(R,S)*-**11** and *(S,S)*-**12** appear in the space group C2. Their structures confirm the presence of an intramolecular H-bond (*i.e.* C₅ pseudocycle) between secondary amidic NH α proton and a lone pair of electron of oxygen atom attached on 1,4-benzoxazine ring (Figure 3.13). The H-bond which is presented in two diastereoisomers *(S,S)*-**11** and *(R,S)*-**11** has similar length (2.19 Å and 2.20 Å, respectively). Therefore, it showed that the absolute configuration at C2 position of 1,4-benzoxazine scaffold does not affect the formation of the C₅ pseudocycle. The H-bond's length in *(S,S)*-**12** is 2.08 Å. Except the C₅ pseudocycle, there is no other intramolecular folds within those molecules.

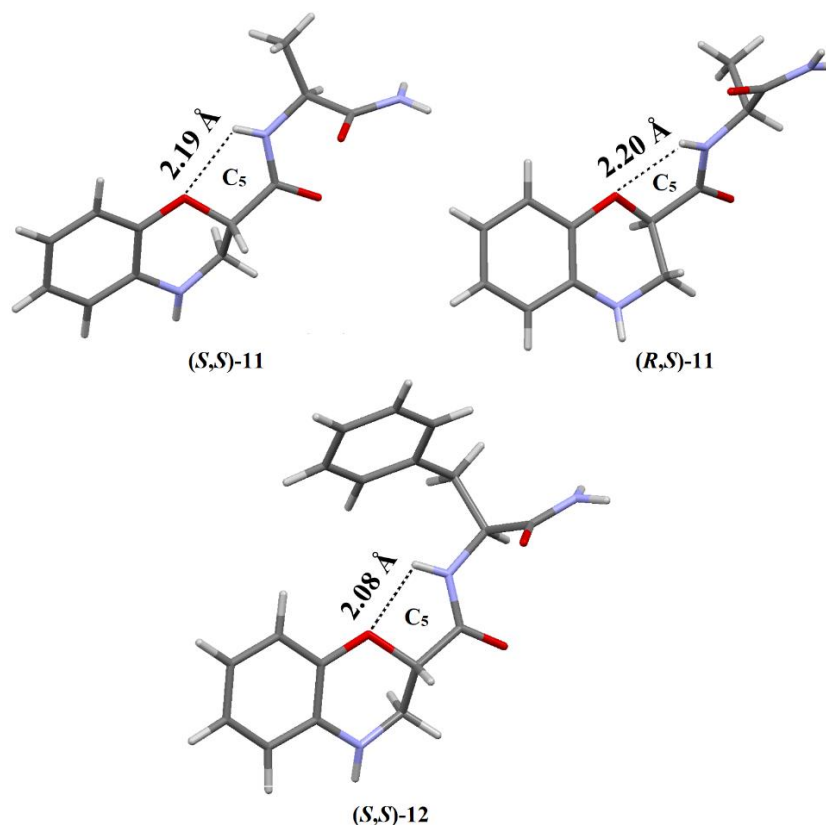
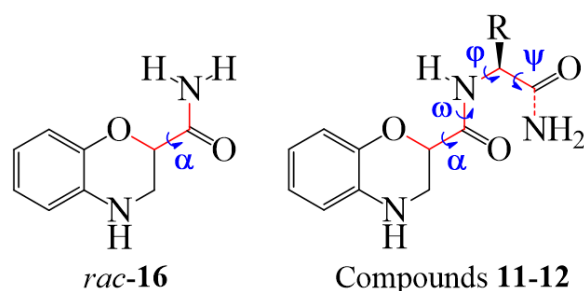


Figure 3.13 X-ray diffraction structure of compound (S,S)-11, (R,S)-11 and (S,S)-12

Besides the distance measurement of intramolecular H-bond, the torsional angles (ω , ϕ , ψ) of each compounds are also calculated (Table 17). An additional torsion angle arbitrarily named α was measured between oxygen atom of 1,4-benzoxazine scaffold, carbon atom at C2 position of 1,4-benzoxazine scaffold, C α of secondary amide and NH α of secondary amide to prove the good orientation of the oxygen atom in the 1,4-benzoxazine ring and NH to induce the C₅ conformation. The obtainment of α value closed to 0° is in agreement with the formation of C₅ conformation (Table 17). The comparison of compounds **11** and (S,S)-**12** with the reference mode *rac*-**16** confirmed that either the side chain of amino acid or the absolute configuration of 1,4-benzoxazine ring at C2 position do not have a big effect on the establishing of the C₅ pseudocycle. There is only a slight difference between the (S,S)- and (R,S)-configuration due to the α value. The length of the H-bond in (S,S)-**12** is a little bit closer than in (S,S)-**11**.

The appearance of the C₅ conformation totally conflicts to solution state analysis of the three pseudodipeptides in FTIR spectroscopic analyses which showed no intramolecular H-bonds. The secondary amide NH α is absorbed at high wavelength ($\approx 3500 \text{ cm}^{-1}$), which is not compatible with the establishing of H-bond interaction. These data suppose that the conformational behaviour of compounds **11**, (S,S)-**12** in solution and solid states is different.

Table 17 Torsional angles of compounds **11**, (*S,S*)-**12** and *rac*-**16**

Torsional angles (deg)					
	ω	ϕ	ψ	α	Conformation
(<i>S,S</i>)- 11	171.6	-58.8	146.9	8.3	C ₅
(<i>R,S</i>)- 11	-175.7	-149.6	169.9	12.7	C ₅
(<i>S,S</i>)- 12	173.4	72.8	160.6	7.4	C ₅
<i>rac</i> - 16	-	-	-	5.1	C ₅

Not only distance measurement of intramolecular H-bond, the X-ray diffraction analysis reveals all intermolecular H-bonds if they exist. Structure of (*S,S*)-**11** (Figure 3.14A) presents the intermolecular H-bond network within molecule. The primary amidic C=O interacts to one primary amidic NH proton of the other molecule in the tube to create H-bond with a length of 2.03 Å (Figure 3.14A). The other primary amidic NH proton reaches to secondary amide C=O of another molecule which a H-bond distance of 2.13 Å (Figure 3.14A). In addition, the presence of 1,4-benzoxazine ring in each molecule can raise π - π stacking interaction between two molecules, this interaction is not affected by the side chain of the amino acid but it is strongly affected by absolute configuration at C2 position of 1,4-benzoxazine ring (Figure 3.14A, B). The distance between two planar parts of (*S,S*)-**11** is 4.92 Å while in (*R,S*)-**11** is double in length (10.01 Å). The arrangement of different molecules in the tube is different between two diastereoisomers (Figure 3.14A, B) which lead to the different shape while presenting them in intermolecular H-bond network. While compound (*S,S*)-**11** arranges in vertical direction along the *c* axis, compound (*R,S*)-**11** is presented in horizontal direction. In order to reveal all intermolecular H-bonds that NH₂ of primary amide and C=O of secondary amide are involved, compound (*R,S*)-**11** is presented along the *b* axis. The intramolecular H-bond is drawn in black dot line, the intermolecular H-bond is drawn in blue dot line. All proton atoms (except those of NH groups) are omitted for the clarity.

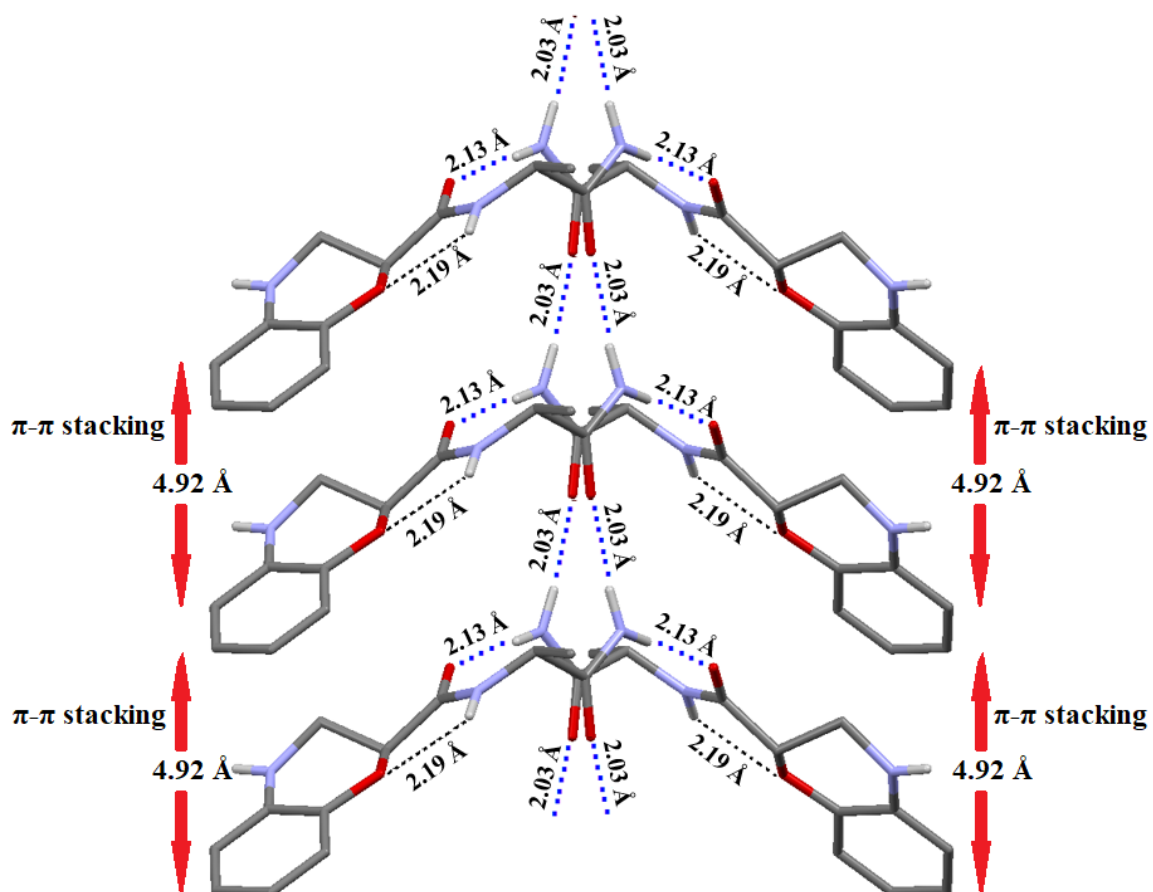


Figure 3.14A Intermolecular network in the solid state along the *c* axis of (*S,S*)-11

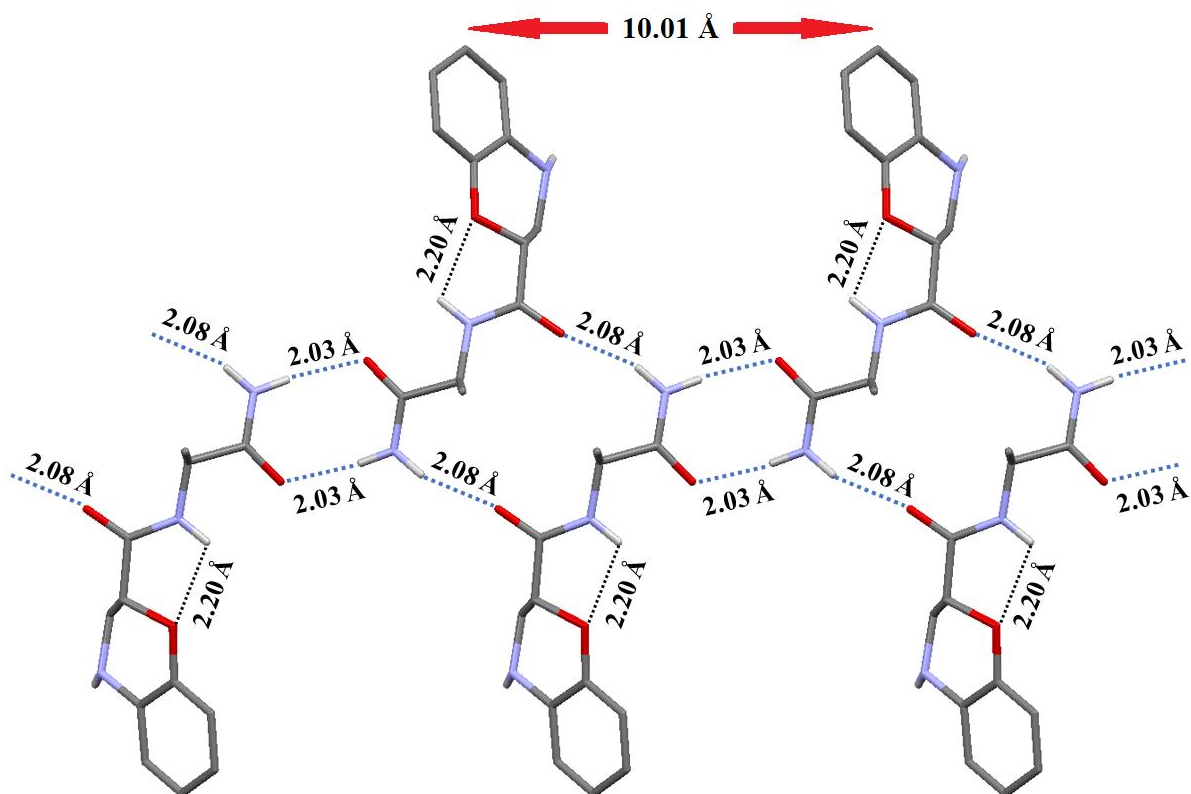


Figure 3.14B Intermolecular network in the solid state along the *b* axis of (*R,S*)-11

Figure 3.15A displays intermolecular H-bond network of diastereoisomer (*S,S*)-**12** in vertical orientation along the *a* axis but unfortunately we did not succeed in obtainment of crystal of (*R,S*)-**12** to compare. For instance, (*R,S*)-**11** shows unlikely arrangement of different molecules in its crystal comparing to (*S,S*)-**11** and -**12** so probably it will be the same to (*R,S*)-**12**. Compound (*S,S*)-**12** contained two planar parts which are benzoxazine ring and benzyl group of phenylalanine that can create the π - π stacking interaction. The distance between two benzoxazine ring is 4.08 Å as well as between two benzyl rings. So (*S,S*)-**12** presented two π - π stacking interactions. Therefore, it is clearly seen that the π - π stacking interaction is not affected by the side chain of amino acid but by the absolute configuration at C2 position of 1,4-benzoxazine scaffold.

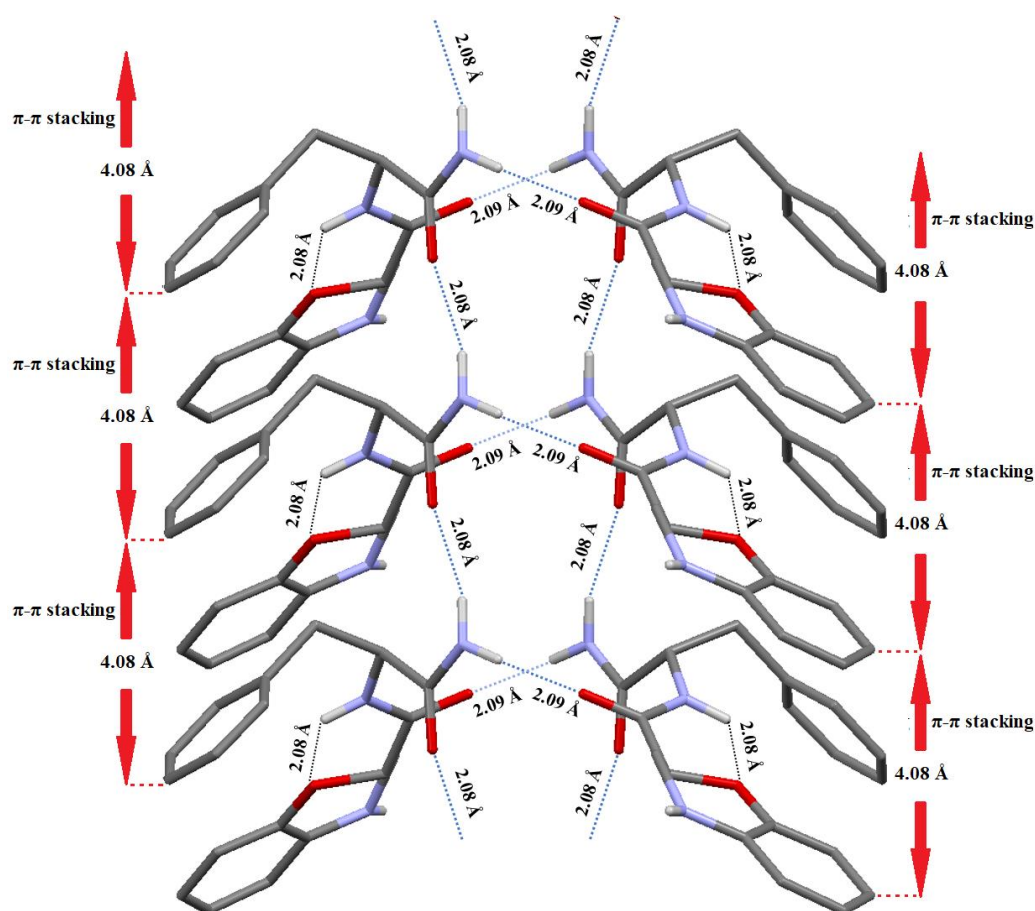


Figure 3.15A Intermolecular network in the solid state along the *a* axis of (*S,S*)-**12**

In addition, this pseudodipeptide (*S,S*)-**12** had one distinct point that it shows intermolecular H-bond of NH_{benzo} in the crystal (Figure 3.15B) while the others does not. The secondary carbonyl group of compounds **11** only bonds to primary amidic NH proton of other molecule in its solid state but secondary C=O group of (*S,S*)-**12** contains two intermolecular bonds: (i)

with the NH of primary amide (2.08 Å) and (ii) with the NH of 1,4-benzoxazine ring (2.14 Å). Perhaps the presence of the benzyl group influences the conformation of (*S,S*)-**12**.

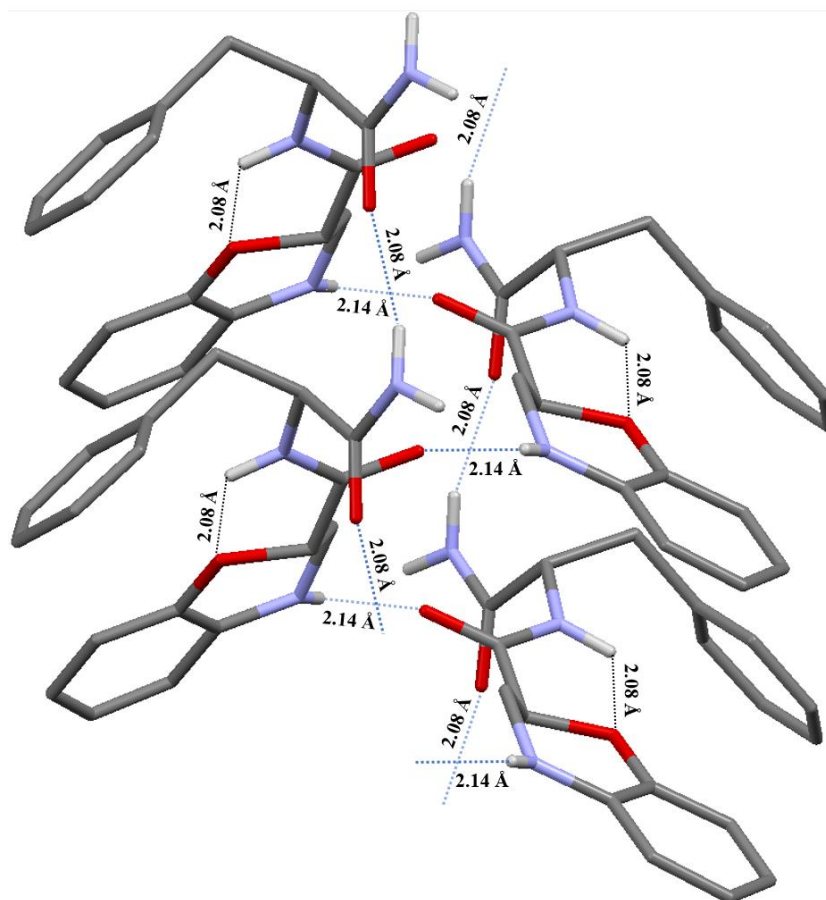


Figure 3.15B Intermolecular H-bond between secondary carbonyl group and NH of 1,4-benzoxazine ring in (*S,S*)-**12**

Based on the conformational analysis of compounds **11** and **12**, we could conclude that there is always one intramolecular H-bond formed between secondary amidic NH proton and oxygen of 1,4-benzoxazine to establish the C₅ conformation. X-ray diffraction indicates intermolecular H-bond network created between (i) both primary amide NH protons and primary amide C=O of other molecule; (ii) one primary amide NH proton with C=O of secondary amide of the other molecule in its crystal. One exception in the case of compound (*S,S*)-**12**, the N-H of 1,4-benzoxazine ring forms intermolecular H-bond with C=O of secondary amide of other molecule. The π - π stacking interaction can be generated between planar parts of molecule which are benzoxazine ring and benzyl group of phenylalanine. However, the π - π stacking interaction is strongly affected by absolute configuration of 1,4-benzoxazine but not by side chain at C-extremity terminal.

3. Conformational study of 1,4-benzoxazine-based pseudotriptides

3.1. Conformational study of (*S,S*)- and (*R,S*)-**8** as reference models

Two molecules (*S,S*)- and (*R,S*)-**8** were synthesized (Scheme 2.14) by coupling *N*-terminal with Fmoc-Ala-OH to be used as reference models for analyzing 1,4-benzoxazine-based pseudotriptide compounds **13-15**. Two molecules (*S,S*)- and (*R,S*)-**8** are analyzed by IR absorption spectra (Figure 3.16); it is predicted that there would have no intramolecular H-bond. The carbamidic NH (in purple color, Figure 3.16) shows one band at 3431/3432 cm^{-1} in (*S,S*)- and (*R,S*)-**8**, respectively, which means it is definitely free. The three carbonyl bands in the region from 1600-1800 cm^{-1} are 1750/1751 cm^{-1} (ester), 1720/1715 cm^{-1} (carbamide) and 1664/1662 cm^{-1} (tertiary amide) in (*S,S*)- and (*R,S*)-**8**, respectively. Those values can also be considered as reference for free carbamidic NH, free carbamidic C=O and free ester C=O for the conformational analysis of compounds **13-15**.

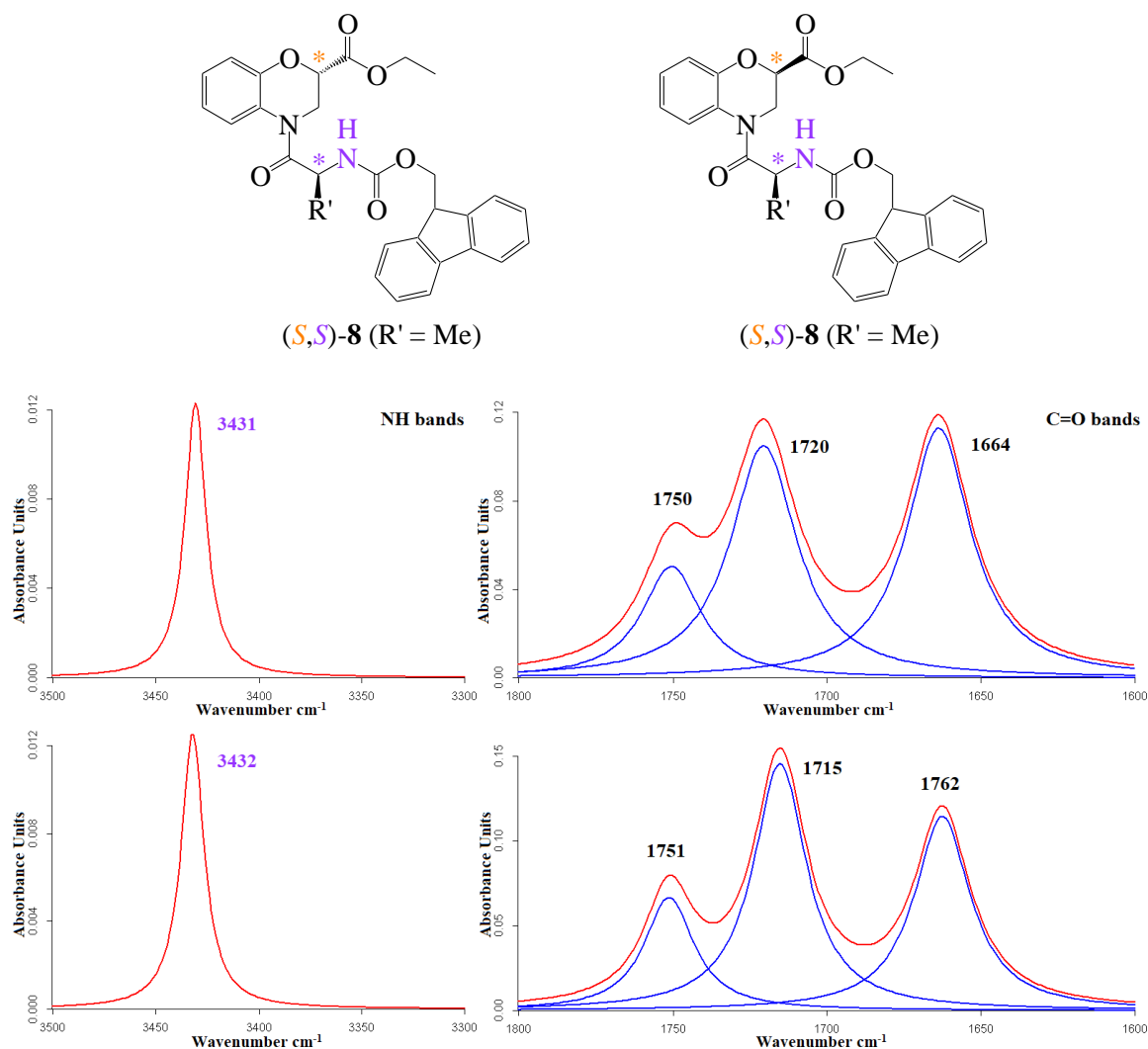


Figure 3.16 IR absorption spectra (in red) and N-H and C=O deconvoluted bands (in blue) of (*S,S*)-**8** (up) and (*R,S*)-**8** (down) (CDCl_3 , 10^{-2} M)

3.2. Conformational study of (*S,S,S*)-**13**, -**14** and (*S,R,S*)-**13**, -**14**

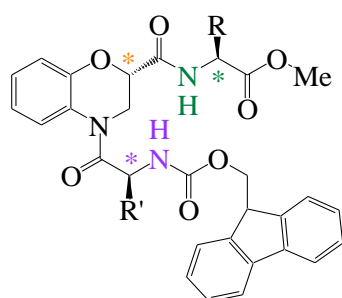
3.2.1. Solution state analysis of (*S,S,S*)-**13**, -**14** and (*S,R,S*)-**13**, -**14**

Pseudotripeptides (*S,S,S*)- and (*S,R,S*)-**13**, -**14** are analyzed to study their conformational behavior in solution state (CDCl₃). Only crystal of (*S,R,S*)-**13** is obtained and analyzed in solid state. After several attempts, the other compounds are not succeeded in obtainment of crystal.

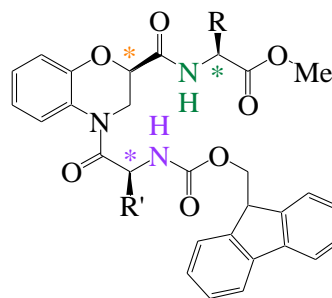
The study of solvent-dependence of pseudotripeptides **13** is performed at the concentration of 10⁻² M and starts from 100% CDCl₃ in DMSO-*d*₆ then reduces to 0%. As showed in Figure 3.16, both secondary amide NH (NH_α) and carbamide NH (NH_{cb}) protons are affected while increasing percentage of polar solvent (DMSO-*d*₆). The Δδ +1.59/+1.77 ppm for NH_α proton and +1.66/+2.19 ppm for NH_{cb} proton in (*S,S,S*)- and (*S,R,S*)-**13**, respectively (Figure 3.17). This adjustment promotes an assumption that both NH protons in this case are free. To confirm this assumption, FTIR spectroscopic analysis in solution state (CDCl₃, 10⁻² M) is performed for pseudotripeptides **13**.

The FTIR absorption spectra of both pseudotripeptides **13** (Figure 3.18) are similar with two bands in the NH stretching vibration region (3200 – 3500 cm⁻¹) and four bands in the C=O stretching vibration region (1600 – 1800 cm⁻¹). The secondary amidic NH_α proton is located at 3415/3416 cm⁻¹, carbamidic NH_{cb} at 3432/3431 cm⁻¹, ester C=O at 1741/1742 cm⁻¹, carbamide C=O at 1719/1719 cm⁻¹, secondary amide C=O at 1686/1685 cm⁻¹ and tertiary amide C=O at 1672/1670 cm⁻¹ for (*S,S,S*)- and (*S,R,S*)-**13**, respectively. The IR absorption bands of two NH above 3400 cm⁻¹ can confirm that they are free but the band at 3415/3416 cm⁻¹ which are quite close to 3400 cm⁻¹ of primary amide made confusion. Those bands perhaps indicate that secondary amide NH proton is involved in H-bond as the analysis of pseudodipeptides above.

The NH_α chemical shift in (*S,S,S*)-**13** is 7.15 ppm and 6.91 ppm in (*S,R,S*)-**13**. If a NH proton is involved in a H-bond, its chemical shift will be deshielded in the ¹H NMR spectrum (δ ≈ 7 ppm) so in this case, both NH_α proton of two molecules seem encourage the assumption that they are H-bonded. In addition, because the C₅ conformation seems predominant in pseudodipeptides and be confirmed by X-ray diffraction, it does not be disturbed by either absolute configuration or side chain of amino acid so probably, for pseudotripeptide molecules, the same C₅ conformation can be existed.



(S,S,S)-13 (R, R' = Me)



(S,R,S)-13 (R, R' = Me)

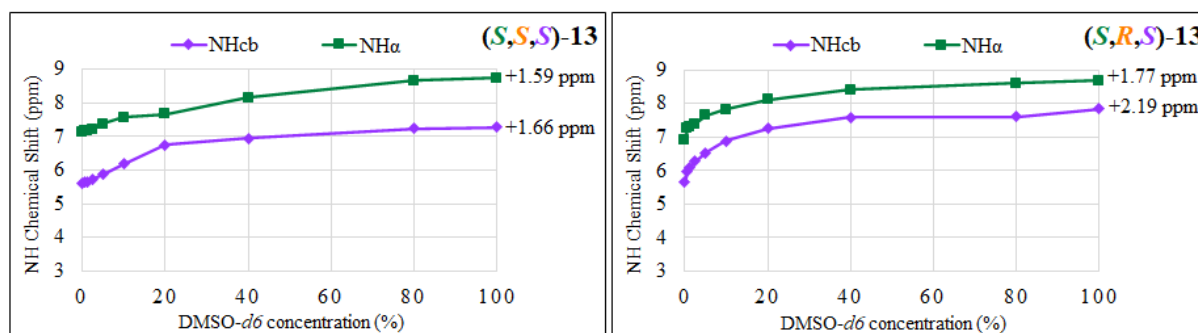


Figure 3.17 Solvent-dependence in mixed $\text{CDCl}_3/\text{DMSO-}d_6$ at 10^{-2} M of NH chemical shift of compound *(S,S,S)*- and *(S,R,S)*-13

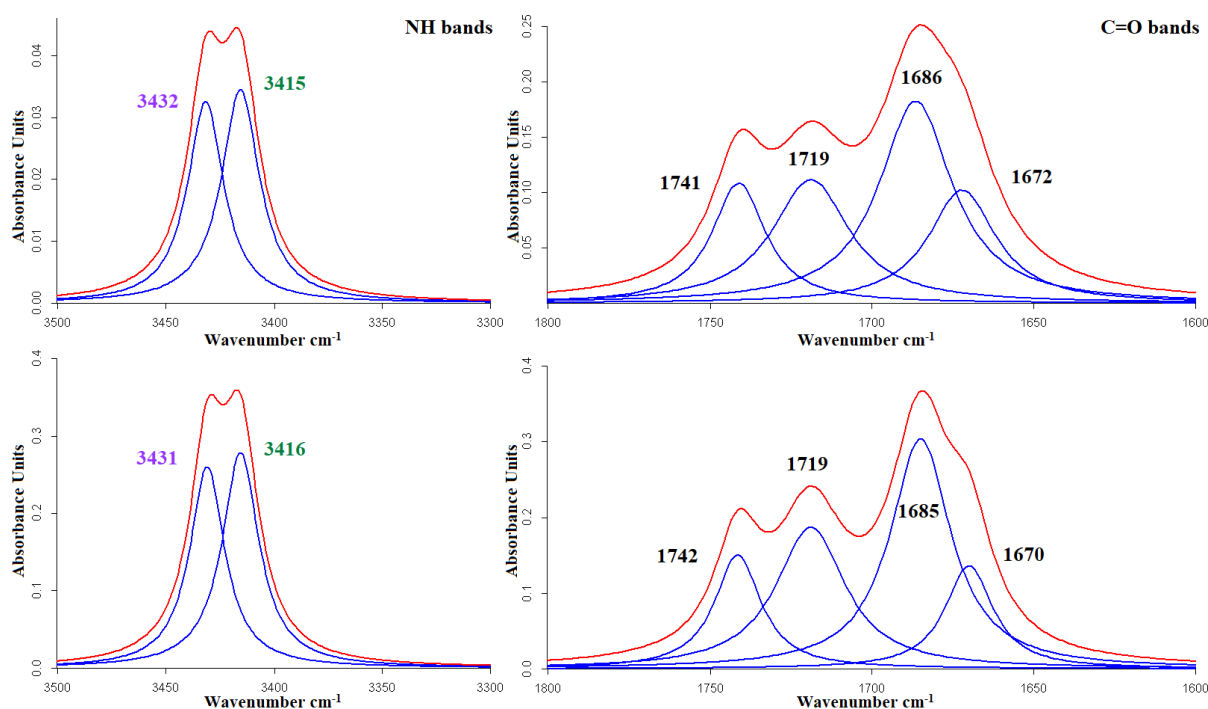


Figure 3.18 IR absorption spectra (in red) and N-H and C=O deconvoluted bands (in blue) of *(S,S,S)*-13 (up) and *(S,R,S)*-13 (down) (CDCl_3 , 10^{-2} M)

Pseudotriptide *(S,S,S)*- and *(S,R,S)*-14 are also studied by ^1H NMR for solvent sensitivity of the NH chemical shifts (Figure 3.19) and FTIR spectroscopy (Figure 3.20). As mentioned

before, the side chain of amino acid does not have strong influence on the conformational behavior of molecule structure, so these results are similar as reported above.

The secondary amidic NH_α and carbamidic NH_{cb} protons of (*S,S,S*)- and (*S,R,S*)-**14** shifted from 7.27/5.61 ppm and 7.29/5.65 ppm in 100% of CDCl_3 to 8.47/7.14 ppm and 8.55/7.62 ppm in 100% of $\text{DMSO-}d_6$, respectively. The $\Delta\delta$ for NH_α proton is +1.20/+1.26 ppm and +1.53/+1.97 ppm for NH_{cb} proton. It seems that $\Delta\delta$ of NH_α proton of both molecules **14** are slightly affected when increasing polar solvent in CDCl_3 and may suggest a presence of weak H-bond. The chemical shift of NH_{cb} are moderately changed in polar environment so they should be free. Comparison of $\Delta\delta$ values of all NHs between (*S,S,S*)-**13** and (*S,S,S*)-**14** shows no considerable change.

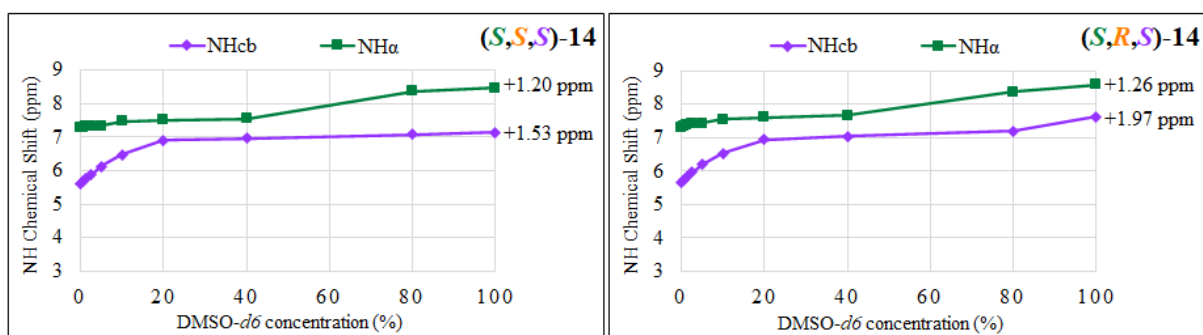
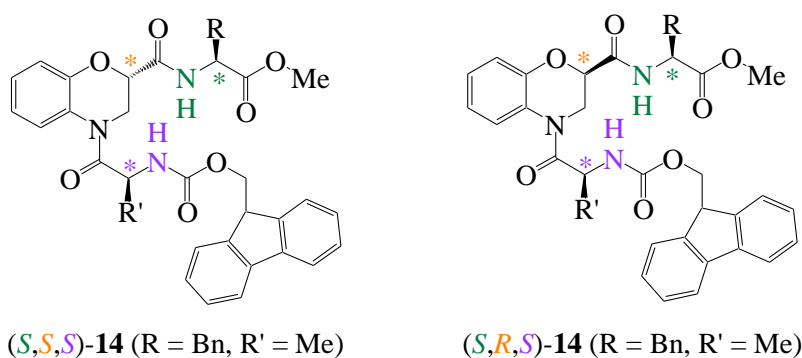


Figure 3.19 Solvent-dependence in mixed $\text{CDCl}_3/\text{DMSO-}d_6$ at 10^{-2} M of NH chemical shift of compound (*S,S,S*)- and (*S,R,S*)-**14** (right)

Pseudotriptide (*S,S,S*)-**14** demonstrates two bands at 3416 cm^{-1} (secondary amidic NH_α) and 3430 cm^{-1} (carbamide NH_{cb}) in the IR absorption spectra (Figure 3.20). Four free $\text{C}=\text{O}$ bands are located at 1743 , 1719 , 1686 and 1670 cm^{-1} and corresponded to $\text{C}=\text{O}$ of ester, carbamide, secondary amide and tertiary amide, respectively. For (*S,R,S*)-**14**, NH stretching region reveals similar bands for NH_α (3413 cm^{-1}) and NH_{cb} (3428 cm^{-1}) as (*S,S,S*)-**14**, while the CO vibration region shows some difference for the four absorption bands (Figure 3.20). The four $\text{C}=\text{O}$ bands are located at 1742 cm^{-1} (ester), 1716 cm^{-1} (carbamide), 1681 cm^{-1} (secondary amide) and 1708

cm⁻¹ (tertiary amide). Even if the tertiary amide C=O is absorbed in higher wavelength compared to (*S,S,S*)-**14**, but this variation does not express that the conformational behavior of (*S,R,S*)-**14** is divergent.

Analyzed data of four molecules above are compared together to see if there is any critical contrast between pseudotripeptides **13** and **14**. The results note that either side chain of amino acid or absolute configuration of C2 position of benzoxazine ring do not induce particular adjustment of molecule structure in solution state. The solution state analysis of (*S,S,S*)-**13**, **14** and (*S,R,S*)-**13**, **14** may demonstrate an involvement of intramolecular H-bond between NH α and aromatic oxygen atom. Fortunately, even if the study of FTIR and solvent sensitivity of NH protons by NMR are not very clear, X-Ray diffraction of (*S,R,S*)-**13** again concedes a different outcome.

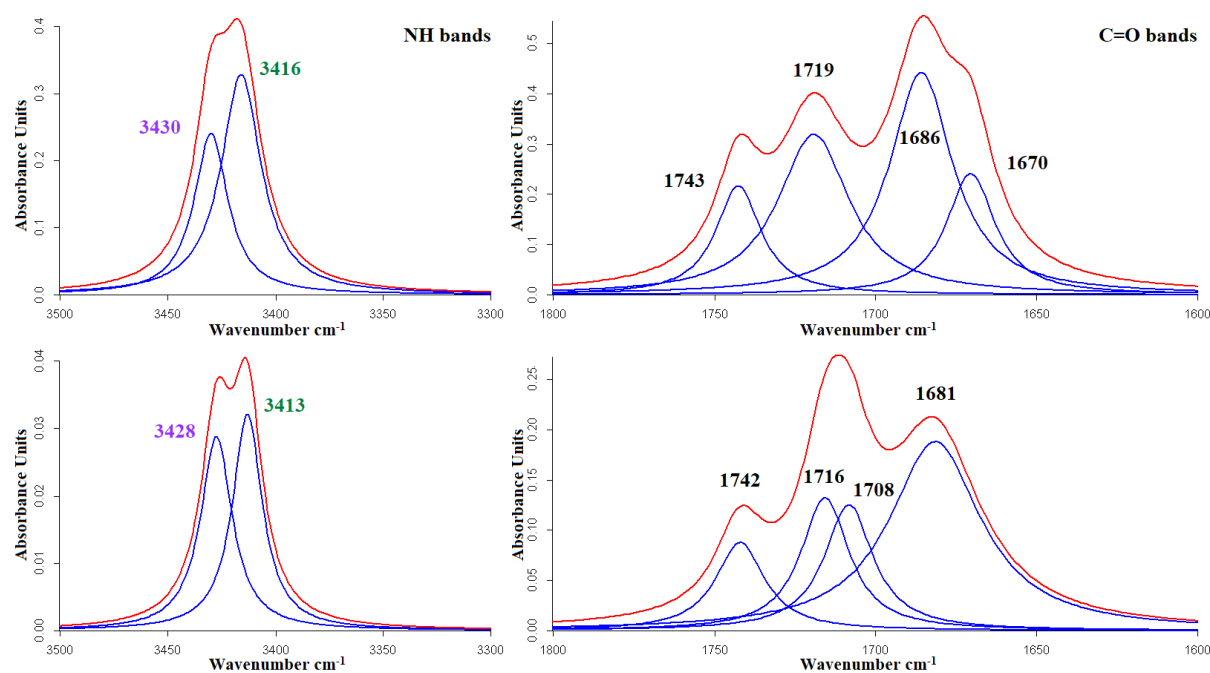


Figure 3.20 IR absorption spectra (in red) and N-H and C=O deconvoluted bands (in blue) of (*S,S,S*)-**14** (up) and (*S,R,S*)-**14** (down) (CDCl₃, 10⁻² M)

Table 17 and 18 summarize the chemical shifts of NH and absorption bands in the stretching region of NH and C=O for (*S,S*)-**13**, **14** and (*R,S*)-**13**, **14**.

Table 17 ^1H NMR chemical shifts (δ_{NH}) of different NH protons of (*S,S*)-**8**, (*R,S*)-**8**, (*S,S,S*)-**13**, **14** and (*S,R,S*)-**13**, **14** (300 MHz, 300K, CDCl_3 , 10^{-2} M)

Type of NH*	δ_{NH} (ppm)					
	(<i>S,S</i>)- 8	(<i>R,S</i>)- 8	(<i>S,S,S</i>)- 13	(<i>S,R,S</i>)- 13	(<i>S,S,S</i>)- 14	(<i>S,R,S</i>)- 14
Am (II)	-	-	7.15	6.91	7.27	7.32
Cb	5.60	5.50	5.62	5.66	5.61	5.65

*Secondary amide [Am (II)], carbamide (Cb)

Table 18 IR absorption bands in the stretching region of NH and C=O of (*S,S*)-**8**, (*R,S*)-**8**, (*S,S,S*)-**13**, **14** and (*S,R,S*)-**13**, **14** (CDCl_3 , 10^{-2} M)

Type of NH*	NH stretching (cm^{-1})					
	(<i>S,S</i>)- 8	(<i>R,S</i>)- 8	(<i>S,S,S</i>)- 13	(<i>S,R,S</i>)- 13	(<i>S,S,S</i>)- 14	(<i>S,R,S</i>)- 14
Am (II)	-	-	3415	3416	3416	3413
Cb	3431	3432	3432	3431	3430	3428

Type of C=O*	C=O stretching (cm^{-1})					
	(<i>S,S</i>)- 8	(<i>R,S</i>)- 8	(<i>S,S,S</i>)- 13	(<i>S,R,S</i>)- 13	(<i>S,S,S</i>)- 14	(<i>S,R,S</i>)- 14
Am (II)	-	-	1686	1685	1686	1681
Am (III)	1664	1662	1672	1670	1670	1708
Cb	1720	1715	1719	1719	1719	1716
Ester	1750	1751	1741	1742	1743	1742

*Secondary amide [Am (II)], tertiary amide [Am (III)], carbamide (Cb)

3.2.2. Solid state analysis of compound (*S,R,S*)-**13**

The crystal of pseudotriptide (*S,R,S*)-**13** (Figure 3.21) is obtained by dissolving molecule in mixture of ethyl acetate and heptane then let it at room temperature for slow evaporation. The molecule (*S,R,S*)-**13** crystallized in the space group $P2_12_12_1$. As we predicted, the C_5 pseudocycle is formed by intramolecular H-bond between secondary amidic $\text{NH}\alpha$ proton and a lone pair of electrons of oxygen atom in 1,4-benzoxazine. The length of the H-bond is 2.22 Å but no other intramolecular H-bond is found. This result is a bit disappointed. In addition, the intermolecular H-bond network of (*S,R,S*)-**13** reveals two H-bonds between: (i) secondary amidic NH proton and tertiary amide C=O ($d = 1.89$ Å); (ii) carbamidic NH proton and ester C=O ($d = 2.04$ Å) from one molecule to the other within its crystal. Because this

pseudotriptide contains both 1,4-benzoxazine rings and Fmoc-protected group which are planar so they can raise the π - π stacking interaction. The π - π stacking interaction's length between two benzoxazine rings is 6.48 Å as same as two fluorene parts of Fmoc-protected group. This distance is between those measured for (*S,S*)-**11** (4.92 Å), (*S,S*)-**12** (4.01 Å) and (*R,S*)-**12** (10.01 Å). The torsion angles are -172.8° , -143.8° , 177.1° and 6.6° correspond to ω , φ , ψ and α angles. The value $\alpha = 6.6^\circ$ which is smallest and closes to 0° proves a presence of C_5 conformation between secondary amide NH and a lone pair of electrons of oxygen atom in 1,4-benzoxazine.

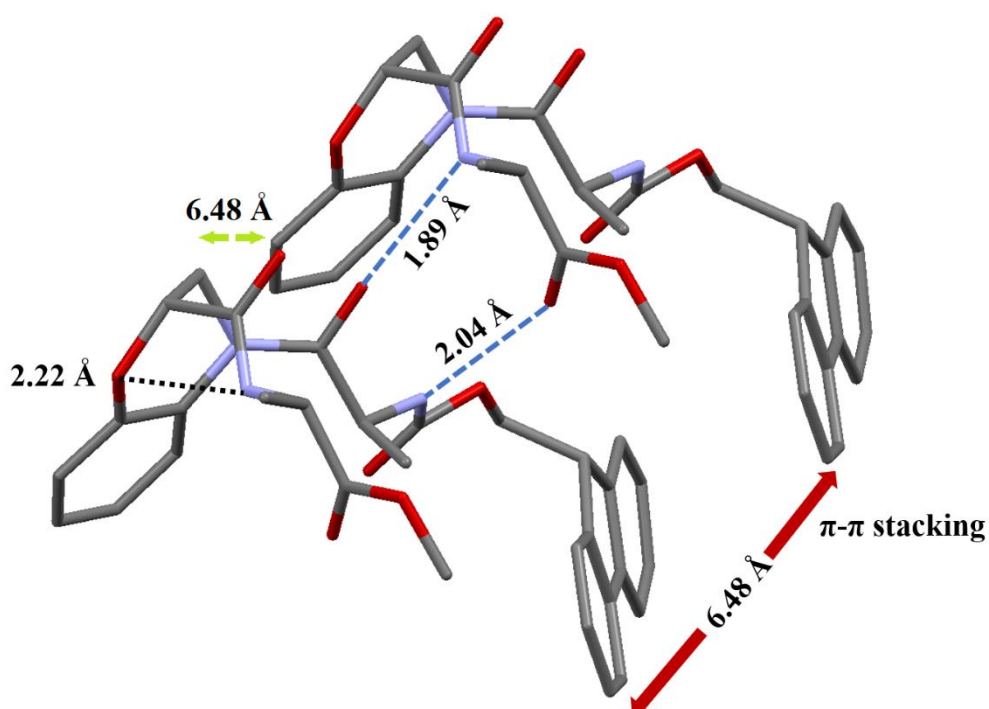


Figure 3.21 Intermolecular H-bond network in the solid state of (*S,R,S*)-**13**

Thanks to reported data above, it is emphasized that the C_5 pseudocycle, which is created by intramolecular H-bond between a lone pair of electrons of oxygen atom in 1,4-benzoxazine and secondary amidic NH proton, is predominant. It is not affected by the side chain of amino acid, the number of attached amino acids either on *C*- or *N*-terminal extremities or the absolute configuration at C2 position of 1,4-benzoxazine. No matter the NMR study of solvent-dependence influence demonstrates small or moderate change of NH chemical shift, the C_5 conformation will be absolutely occurred. Even the secondary amidic NH proton is absorbed at high frequency in FT-IR analysis but based on its behavior in NMR study of solvent-dependence ($\Delta\delta \leq 1.30$ ppm) and chemical shift in ^1H NMR ($\delta \approx 7.00$ ppm), it can be recognized if it involves in H-bond or not. However, in this work, the chosen amino acids do not create

steric hindrance effect like leucine or valine amino acid so that the information does not support if steric hindrance effect may influence structural behavior or not. It can be interesting to further study this part.

3.3. Conformational study of (*S,S,S*)- and (*S,R,S*)-**15**

As the study of 1,4-benzoxazine-based pseudodipeptides, amidation of (*S,S,S*)- and (*S,R,S*)-**13** are done to achieve corresponded products (*S,S,S*)- and (*S,R,S*)-**15**. By changing methyl ester group to NH₂, we expected that it could build other pseudocycle than the existed C₅.

Interestingly, it seemed that our expectation came true. The study of solvent influence shows that maybe other potential H-bond is formed. Figure 3.22 described the effect of solvent on NH chemical shifts when increasing volume of DMSO-*d*₆ in CDCl₃. Because these two pseudotripeptides contain four NH groups, they are too polar to solubilize in 100% of CDCl₃. Thus, they are dissolved in CDCl₃ containing 1% of DMSO-*d*₆ at concentration of 10⁻² M to study. The chemical shift of NH can be affected by the engagement of DMSO. The $\Delta\delta$ of the secondary amidic NH proton ($\delta = 7.12/7.16$ ppm) are +0.80/+0.95 ppm for (*S,S,S*)- and (*S,R,S*)-**15**, respectively and as usual, this NH will be involved in H-bond to create the C₅ with a lone pair of electrons of oxygen atom in 1,4-benzoxazine scaffold. The carbamidic NH proton remains free ($\delta = 5.75$ ppm) with its chemical shift values are highly affected by polar solvent ($\Delta\delta = +1.98/+2.02$ ppm). Compound (*S,S,S*)- and (*S,R,S*)-**15** demonstrate one primary amidic NH proton shifts at 5.57/5.42 ppm and the other primary NH shifts at 6.39/6.33 ppm, respectively. For pseudodipeptides (*S,S*)- and (*R,S*)-**11**, two free primary NH (free and H-bonded) protons have $\Delta\delta = +1.42/+1.58$ ppm and +1.78/+2.06 ppm. For the two primary amidic protons of (*S,S,S*)- and (*S,R,S*)-**15**, the symmetric one is moderately affected ($\Delta\delta = +1.47/+1.62$ ppm) but asymmetric primary amidic NH is poorly influenced by polar solvent DMSO-*d*₆ ($\Delta\delta = +0.79/+1.04$ ppm). Based on this data, it can be said that one primary amide NH proton is involved in an intramolecular H-bond.

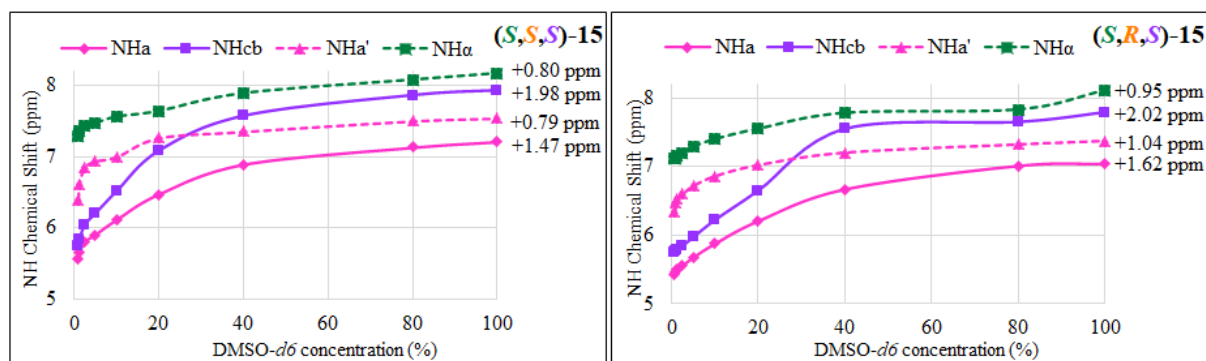


Figure 3.22 Solvent-dependence in mixed CDCl₃/DMSO-*d*₆ at 10⁻² M of NH chemical shift of compound (S,S,S)-15 (left) and (S,R,S)-15 (right)

In order to precise which group involves in intramolecular H-bond with H-bonded primary amidic NH_α' and secondary amidic NH_α, FTIR analysis of two pseudotriptides (S,S,S)- and (S,R,S)-15 were checked (Figure 3.23).

For pseudotriptide (S,S,S)-15, there are four IR absorption bands in the stretching vibration region of NH and C=O. The carbamidic NH_{cb} located at 3429 cm⁻¹, the secondary amidic NH is 3416 cm⁻¹, symmetric and asymmetric bands for primary amidic NH₂ are 3405 cm⁻¹ and 3523 cm⁻¹. In addition, all NH in pseudotriptide (S,R,S)-15 are absorbed at a bit lower area comparing to (S,S,S)-15, the symmetric primary amide NH_α is absorbed at 3396 cm⁻¹ which is very close to the border between free and H-bonded NH. This value may say that this primary amidic NH proton participates in an intramolecular H-bond. Even the other values are higher than 3400 cm⁻¹ but based on analyzed data described above, the secondary amide NH_α of both molecules will be involved in H-bond with a lone pair of electrons of oxygen atom in 1,4-benzoxazine scaffold. Since there are two NH protons are involved in H-bond, it is necessary there will be one carbonyl group joins them to form another pseudocycle but C₅.

In the stretching vibration region of C=O of pseudotriptide (S,S,S)-15, four bands are found. They are compared to reported values of studied compounds above to be assigned. Four bands of C=O are located at 1717 cm⁻¹ (carbamide), 1699 cm⁻¹ (primary amide), 1667 cm⁻¹ (secondary amide) and 1679 cm⁻¹ (tertiary amide). It can be certainly recognized that no carbonyl is unusually changed. In comparison with (S,S)-11, both secondary amidic C=O are around 1665 cm⁻¹. Pseudodipeptide (S,S)-11 was confirmed that it contained no other H-bond except the C₅ conformation of NH_α and a lone pair of electrons of oxygen atom in 1,4-benzoxazine scaffold so the value around 1665 cm⁻¹ that is absolutely assigned for free secondary amidic carbonyl. The tertiary amidic C=O is even absorbed at higher frequency than (S,S)-8 so it is also indicated

as free one. However, comparison between secondary amide C=O values in IR spectra of diastereoisomers **15** and **13** suggests that this carbonyl group is involved in H-bond because they are absorbed at lower frequency from 1686 cm^{-1} of (*S,S,S*)-**13** to 1667 cm^{-1} of (*S,S,S*)-**15** and from 1685 cm^{-1} of (*S,R,S*)-**13** to 1648 cm^{-1} of (*S,R,S*)-**15**. Therefore, in this case, the most reasonable conformation can be generated within diastereoisomers **15** contains two intramolecular H-bonds which are formed between (i) secondary amidic NH α proton and a lone pair of electrons of oxygen atom in 1,4-benzoxazine (C₅) and (ii) H-bonded primary amidic NH α' proton and secondary carbonyl (C₇) (Figure 3.22).

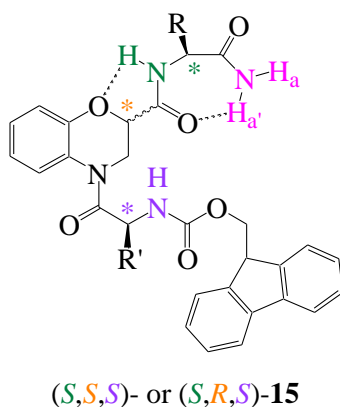


Figure 3.22 Postulated conformation based on solution state data analysis of pseudotripeptides **15**

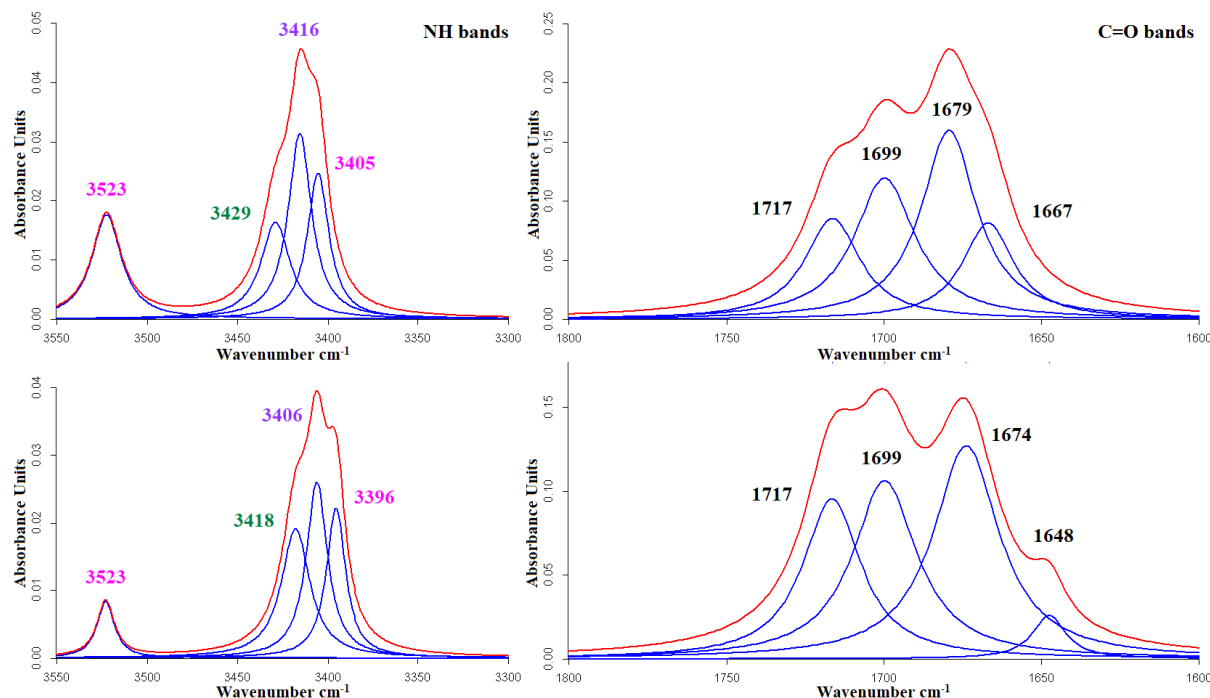


Figure 3.23 IR absorption spectra (in red) and N-H and C=O deconvoluted bands (in blue) of (*S,S,S*)-**15** (up) and (*S,R,S*)-**15** (down) (CDCl_3 , 10^{-2} M)

The signal of NH on ^1H NMR and absorption values of NH and C=O of pseudotripeptides (*S,S,S*)-**15** and (*S,R,S*)-**15** on IR absorption spectra are summarized in the Tables 18 and 19 below.

Table 18 ^1H NMR chemical shifts (δ_{NH}) of different NH protons of (*S,S,S*)-**15** and (*S,R,S*)-**15** [300 MHz, 300K, $\text{CDCl}_3/\text{DMSO}-d_6$ (99/1, v/v), 10^{-2} M]

Type of NH*	δ_{NH} (ppm)	
	(<i>S,S,S</i>)- 15	(<i>S,R,S</i>)- 15
Am (I)	5.57	5.42
	6.39	6.33
Am (II)	7.29	7.16
Cb	5.75	5.77

*Primary amide [Am (I)], secondary amide [Am (II)], carbamide (Cb)

Table 19 IR absorption bands in the stretching region of NH and C=O of (*S,S,S*)-**15** and (*S,R,S*)-**15** [300 MHz, $\text{CDCl}_3/\text{DMSO}-d_6$ (99/1, v/v), 10^{-2} M]

Type of NH*	NH stretching (cm^{-1})	
	(<i>S,S,S</i>)- 15	(<i>S,R,S</i>)- 15
Am (I)	3523	3523
	3405	3396
Am (II)	3416	3418
Cb	3429	3406

Type of C=O*	C=O stretching (cm^{-1})	
	(<i>S,S,S</i>)- 15	(<i>S,R,S</i>)- 15
Am (I)	1699	1699
Am (II)	1667	1648
Am (III)	1679	1674
Cb	1717	1717

*Primary amide [Am (I)], secondary amide [Am (II)], tertiary amide [Am (III)], carbamide (Cb)

4. Conclusion

All obtained pseudodipeptides **9-12** and pseudotripeptides **13-15** are studied for the conformational behavior in solution state by NMR of solvent-dependence and FT-IR spectroscopic analysis. Crystals of compounds (*S,S*)-**11**, (*R,S*)-**11**, (*S,S*)-**12** and (*S,R,S*)-**13** are

successfully obtained to be analyzed by X-ray diffraction. The results show that in solution state, according to solvent-dependence study by ^1H NMR, the secondary amide $\text{NH}\alpha$ proton is always participated in intramolecular H-bond with a lone pair of electrons of oxygen atom in 1,4-benzoxazine scaffold. However, all absorption bands in stretching vibration region of NH and C=O in FT-IR spectra show no values which are in agreement with the presence of intramolecular H-bond.

Thanks to X-ray diffraction analysis, it confirmed that the C_5 conformation between $\text{NH}\alpha$ and a lone pair of electrons of oxygen atom in 1,4-benzoxazine is predominant. This C_5 conformation does not been affected by either absolute configuration at C_2 position of 1,4-benzoxazine scaffold, side chain of amino acid or number of amino acids that attached to C- and N-terminal extremities. The X-ray diffraction analysis also reveals the intermolecular H-bond network of compounds (*S,S*)-**11**, (*R,S*)-**11**, (*S,S*)-**12** and (*S,R,S*)-**13**. It demonstrates that two primary amidic $\text{NH}\alpha, \alpha'$ of one molecule can create a H-bond with (i) primary amide C=O and (i) secondary amide C=O of the other within its crystal. In addition, the secondary amidic carbonyl of (*S,S*)-**12** can create H-bond with NH of aromatic ring. The π - π stacking interaction is raised between the planar part of molecule but it is strongly affected by chirality of C_2 position of 1,4-benzoxazine but not side chain of amino acid. The structural behavior of pseudotriptides **15** can be postulated that it consists of two pseudocycles which are created *via* intramolecular H-bond between (i) secondary amide $\text{NH}\alpha$ and a lone pair of electrons of oxygen atom in 1,4-benzoxazine (C_5) and (ii) asymmetric amide $\text{NH}\alpha'$ and secondary carbonyl (C_7). Prolongation of N-terminal extremity establishes an affection to conformational behavior of 1,4-benzoxazine-based pseudopeptide analogues. Without attachment of amino acid at N-terminal extremity, two primary amide $\text{NH}\alpha, \alpha'$ are free. Figure 3.24 summarizes obtained and studied molecules in this work.

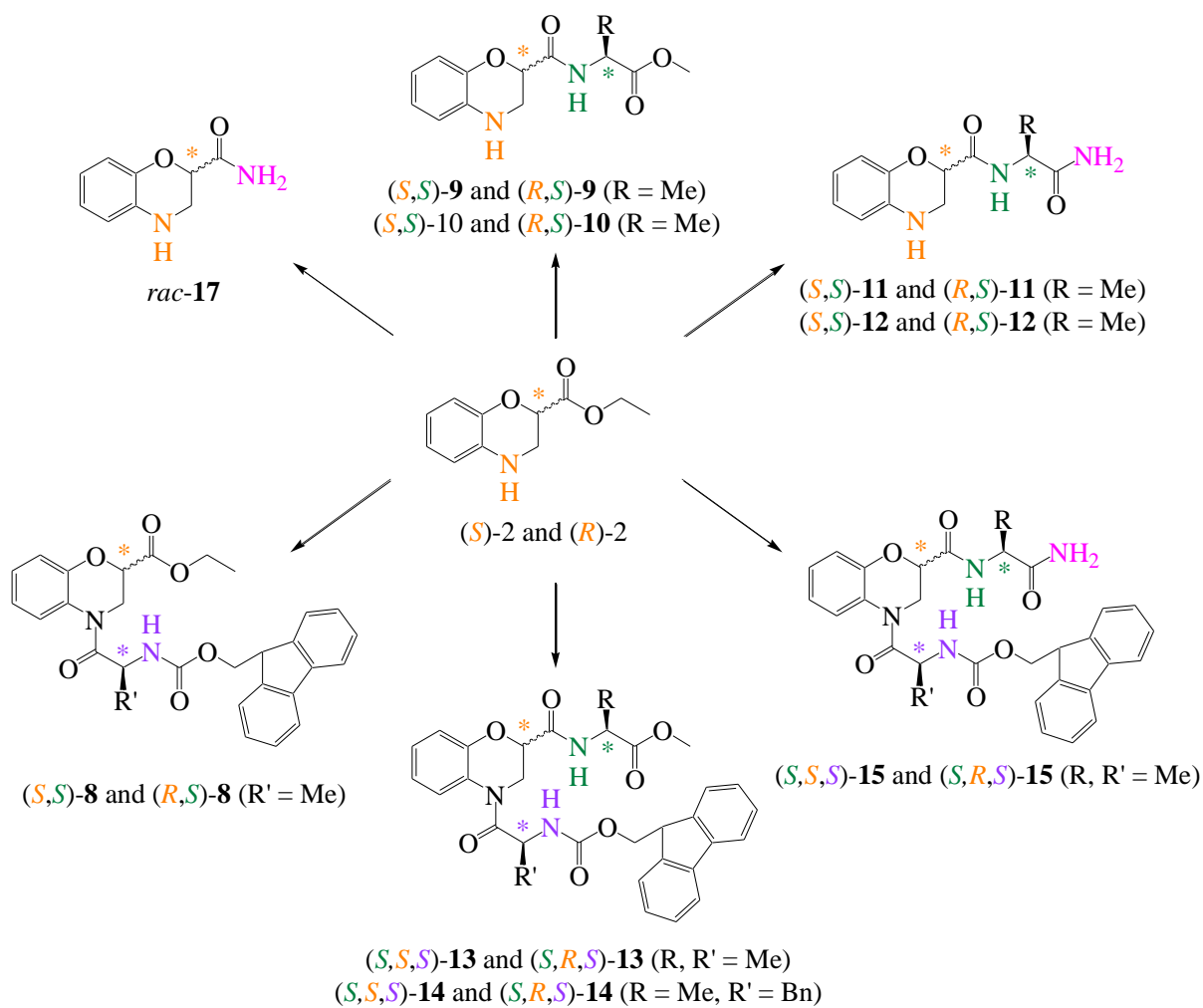


Figure 3.24 Summarized studied 1,4-benzoxazine-based pseudodipeptides and pseudotripeptides

REFERENCE

- (1) Jiménez, A. I.; Cativiela, C.; Gómez-Catalán, J.; Pérez, J. J.; Aubry, A.; París, M.; Marraud, M. Influence of Side Chain Restriction and NH \cdots π Interaction on the β -Turn Folding Modes of Dipeptides Incorporating Phenylalanine Cyclohexane Derivatives. *J. Am. Chem. Soc.* **2000**, *122* (24), 5811–5821.
- (2) Chang, X.-W.; Han, Q.-C.; Jiao, Z.-G.; Weng, L.-H.; Zhang, D.-W. 1-Aminoxymethylcyclopropanecarboxylic Acid as Building Block of β N–O Turn and Helix: Synthesis and Conformational Analysis in Solution and in the Solid State. *Tetrahedron* **2010**, *66* (51), 9733–9737.
- (3) Zhou, Z.; Deng, C.; Abbas, C.; Didierjean, C.; Averlant-Petit, M.-C.; Bodiguel, J.; Vanderesse, R.; Jamart-Grégoire, B. Synthesis and Structural Characterization of 2:1 [α /Aza]-Oligomers: Synthesis and Characterization of 2:1 [α /Aza]-Oligomers. *Eur. J. Org. Chem.* **2014**, *2014* (34), 7643–7650.
- (4) Grzesiek, S.; Becker, E. D. Hydrogen Bonding. In *Encyclopedia of Magnetic Resonance*; Harris, R. K., Ed.; John Wiley & Sons, Ltd: Chichester, UK, 2011.
- (5) Moritz, A. G. N–H Stretching Frequencies of Amines and Amides. *Nature* **1962**, *195* (4843), 800–800.
- (6) Krueger, P. J.; Smith, D. W. Amino Group Stretching Vibrations in Primary Acid Amides. *Can. J. Chem.* **1967**, *45* (14), 1611–1618.
- (7) Moussodia, R.-O.; Romero, E.; Wenger, E.; Jamart-Grégoire, B.; Acherar, S. Self-Organization Ability of Chiral N^{α} -Substituted, N^{β} -Boc Protected α -Hydrazinoacetamides in the Crystal and Solution States. *J. Org. Chem.* **2017**, *82* (19), 9937–9945.

GENERAL CONCLUSIONS AND PERSPECTIVES

1. General conclusions

3,4-dihydro-2*H*-1,4-benzoxazine and its derivatives were reported as potential candidates that contain many pharmacological activities such as antibacterial, anti-hypertensive or anti-angiogenesis. Due to those potential effects, this benzoheterocyclic compound became an attractive target to develop as a favorable core for medicinal chemistry.

Our targeted molecule ethyl 3,4-dihydro-2*H*-1,4-benzoxazine-2-carboxylate contains carboxylic group attaches to α -carbon and amine group attaches to β -carbon, its structure simulates β -amino acid that makes this heterocyclic molecule mimics the β -amino acid analogue and more inquisitive to study.

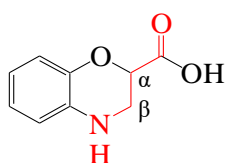


Figure 4.1 3,4-dihydro-2*H*-1,4-benzoxazine-2-carboxylic simulates β -amino acid structure

Due to receptor selectivity and differences in biological and pharmacological activities, enantioselective synthesis now becomes a top subject in chemistry. Many chiral compounds have been reported with one of its enantiomers exhibiting better pharmacological activities than the other such as levofloxacin or thalidomide. Therefore, in this thesis, we targeted to synthesize new enantiopure 3,4-dihydro-2*H*-1,4-benzoxazine analogues as pseudodipeptides and pseudotripeptides. These new pseudopeptides that may mimic the β -turn starting from enantiomers of 1,4-benzoxazine as scaffold and their conformational behaviours would be studied.

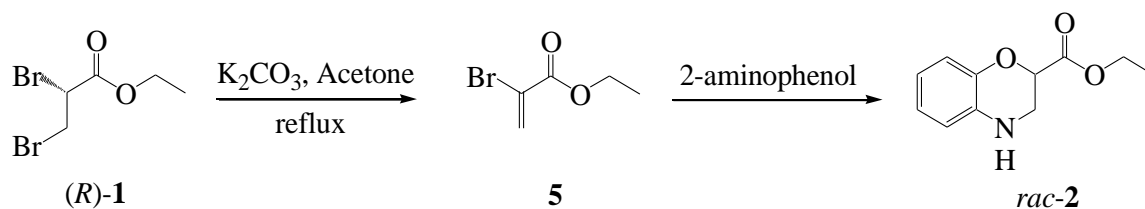
Firstly, in order to obtain enantiopure ethyl 3,4-dihydro-2*H*-1,4-benzoxazine-2-carboxylate **2** to use as scaffold for pseudopeptide analogues synthesis, both enantiomers of ethyl 2,3-dibromopropionate **1** were investigated by two strategies: *via* enantioselective synthesis and *via* preparative HPLC enantioseparation of the commercially available racemate.

At the beginning, the enantioselective synthesis of (*S*)-**1** met difficulties for obtainment of enantiopure product due to the rapidly degradation of (*S*)-**1** in purification step by flash silica gel chromatography leading to very low yield. After many attempts to avoid the degradation, (*S*)-**1** was afforded in 3 steps (59% overall yield) from (*S*)-serine after quick purification with a very low height of silica gel in the column. However, equipments and devices in our laboratory did not allow us for checking the enantiomeric purity of chiral compounds so we had to search

for a collaboration with another laboratory having an expertise in this field. We contacted to a colleague working at “Plateforme de chromatographie chirale” in Aix-Marseille University to collaborate for examining the enantiomeric purity of (*S*)-**1**.

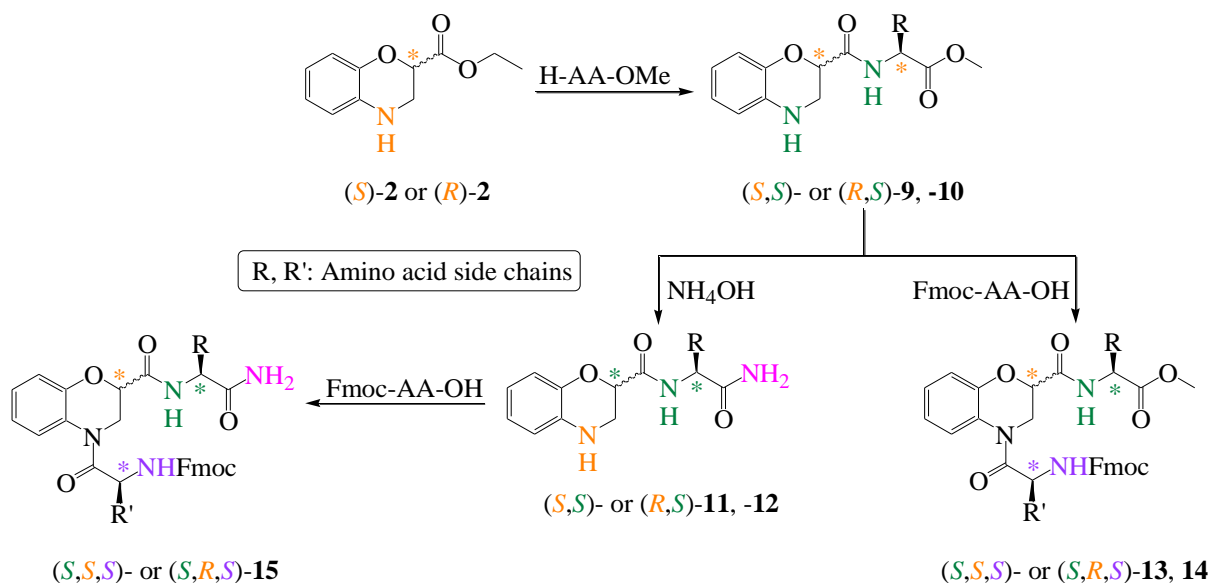
To determine the best conditions for enantioseparation of racemate **1** (*rac*-**1**), various chiral stationary phases (CSP) were screened. Preparative Chiralpak AD-H was found to be the best CSP for separation of both enantiomers with high enantiopurity ($ee \geq 99.5\%$) on multigram scale. Based on the recorded data, ee of the synthesized (*S*)-**1** was examined. The result was dissatisfied because the ee of (*S*)-**1** only reached 17-36% which meant (*S*)-**1** was racemized during the enantioselective synthesis. After several attempts searching for the cause, it showed that the racemization process occurred during the bromination of (*S*)-ethyl glycerate intermediate with CBr_4 and PPh_3 as reagents. The quantification of racemization process (influence of reaction time and reagent's equivalent) gave $ee \approx 9\text{-}50\%$ and concluded that a longer reaction time induced higher yield of synthesized (*S*)-**1** but with a less measured ee . In contrary, the use of the less reagent quantity was profitable for the ee of the product but with a lower yield. Tf_2O was applied to replace bromide by triflate which is a good leaving group but once again, the β -elimination happened. Therefore, both enantiomers **1** obtained by preparative HPLC enantioseparation on multigram scale (5 g) were used to synthesize corresponding enantiopure compound **2** *via* a double $\text{S}_{\text{N}}2$ reaction with 2-aminophenol.

As both enantiomers (*S*)- and (*R*)-ethyl 3,4-dihydro-2*H*-1,4-benzoxazine-2-carboxylate **2** were not described in the literature, they were separated *via* preparative HPLC enantioseparation of synthesized racemate **2** (*rac*-**2**) on multigram scale (12 g) using Lux-Cellulose-2[®] CSP then the ee of the synthesized (*R*)-**2** was checked. Unfortunately, during the double $\text{S}_{\text{N}}2$ step yet performed in mild conditions, the synthesized (*R*)-**2** was also partial racemized ($ee \approx 55\%$ or 66%). The reason in this case was predicted based on a postulated mechanism was reported in the literature involved dehydrobromination of dibromo compound **1**. The inevitable formation of eliminated ethyl 2-bromoacrylate **5** was proved as the cause of racemization of **2** in this case (Scheme 4.1). The formation of **5** from (*R*)-**1** in the presence of K_2CO_3 under refluxed acetone was investigated (Scheme 4.1, first step) and the reaction progress was monitored by analytical achiral HPLC. The result showed that 57% of **5** was quickly formed after 2 h followed by a slower increase of **5** during the rest of the reaction (reaching a maximum of 93% within 16 h).



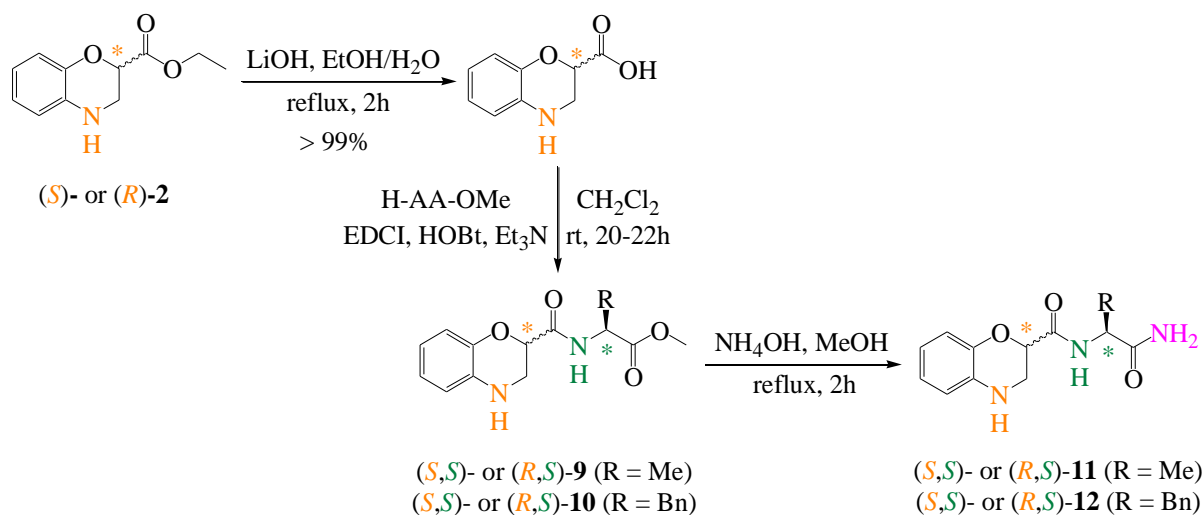
Scheme 4.1 Obtainment of racemized compound **2**

Due to this result, both enantiomers of **2** were isolated *via* preparative HPLC enantioseparation (*ee* \geq 99.5%) of *rac*\text{-2} on multigram scale (12 g) and then used in the next step as scaffold to design new 1,4-benzoxazine-based pseudopeptide analogues (Scheme 4.2).



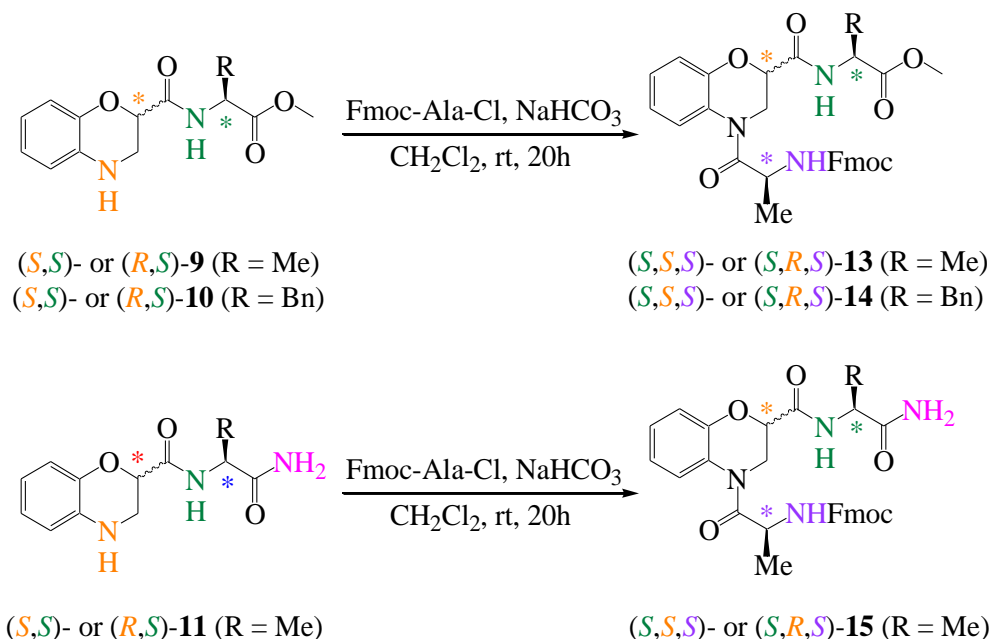
Scheme 4.2 Obtainment of 1,4-benzoxazine-based pseudopeptide analogues

Secondly, the *C*- and *N*-terminal extremities of *(S)*\text{-2} and *(R)*\text{-2} were modified by peptide coupling reactions with alanine and/or phenylalanine in order to achieve novel enantiopure 3,4-dihydro-2*H*-1,4-benzoxazine analogues as pseudopeptides. Introduction of 1,4-benzoxazine scaffold in pseudodipeptides started by saponification of ethyl ester group with lithium hydroxide in EtOH/H₂O (8/2, v/v) to afford carboxylic acid group then coupling with hydrochloride methyl ester of alanine or phenylalanine using HOBt, TEA and EDCI as coupling reagents. Due to the low reactivity of NH proton on the 1,4-benzoxazine scaffold, the insertion of α -amino acid at *C*-terminus did not require a Boc- or Fmoc-protection of NH group. Four molecules *(S,S)*\text{-} and *(R,S)*\text{-}9, -10 were obtained as pure diastereoisomer thanks to presence of HOBt. Next, in order to increase the possibility of intramolecular H-bond formation, amidation of the methyl ester group of *(S,S)*\text{-} and *(R,S)*\text{-}9, -10 was performed by ammonium solution 35% to generate *(S,S)*\text{-} and *(R,S)*\text{-}11, -12 pseudodipeptides (Scheme 4.3).



Scheme 4.3 Elongation of C-terminal extremity of (*S*)-2 and (*R*)-2

In order to obtain pseudotripeptides, elongation of *N*-terminal extremity is realised by coupling highly reactive Fmoc amino acid chlorides. Fmoc-Ala-OH was chlorinated by thionyl chloride to afford Fmoc-Ala-Cl. The reaction of obtained pseudodipeptides and Fmoc-Ala-Cl in the presence of NaHCO₃ as base generated corresponded pseudotripeptides (*S,S,S*)- and (*S,R,S*)-13, -14, -15 (Scheme 4.4).



Scheme 4.4 Elongation of *N*-terminal extremities of (*S,S*)- and (*R,S*)- 9, -10, -11

Finally, the conformational behaviour of the previously obtained compounds were meticulously studied by NMR and FT-IR spectroscopies. Furthermore, crystals of compounds (*S,S*)-11, (*R,S*)-11, (*S,S*)-12 and (*S,R,S*)-13 are successfully obtained in different mixture of solvents and their crystals are analyzed by X-Ray diffraction. For compounds 11-14, the results

showed that in solution state, only one intramolecular H-bond is formed between the secondary amide NH proton and a lone pair of electrons of the oxygen atom in 1,4-benzoxazine scaffold to create a C₅ pseudocycle. The X-Ray diffraction analysis of (*S,S*)-**11**, (*R,S*)-**11**, (*S,S*)-**12** and (*S,R,S*)-**13** were in agreement with their analyzed data in solution state. Moreover, (*S,S,S*)-**15** and (*S,R,S*)-**15** revealed probably except C₅, it might contain a C₇ pseudocycle created between primary amide NH proton and C=O of secondary amide (Figure 4.2). However, the C₅ conformation seems predominant in all 1,4-benzoxazine-based pseudopeptide analogues.

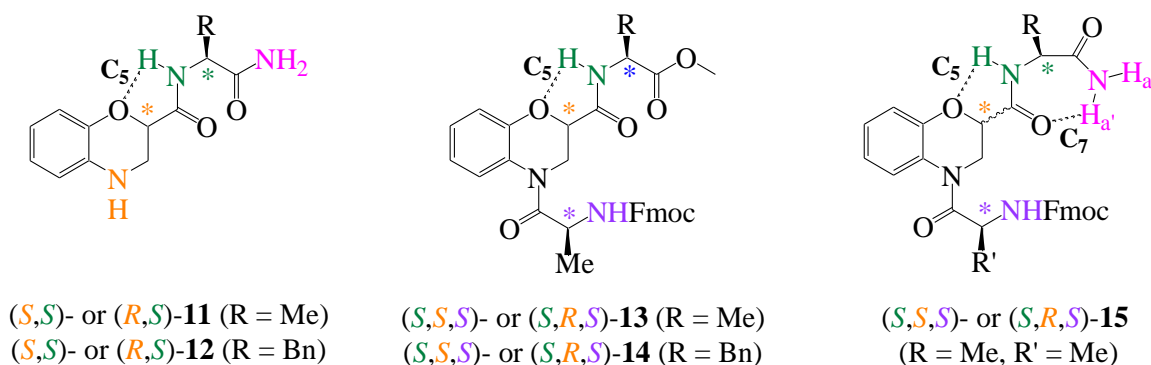


Figure 4.2 The predominant C₅ pseudocycle in pseudo-dipeptides and -tripeptides

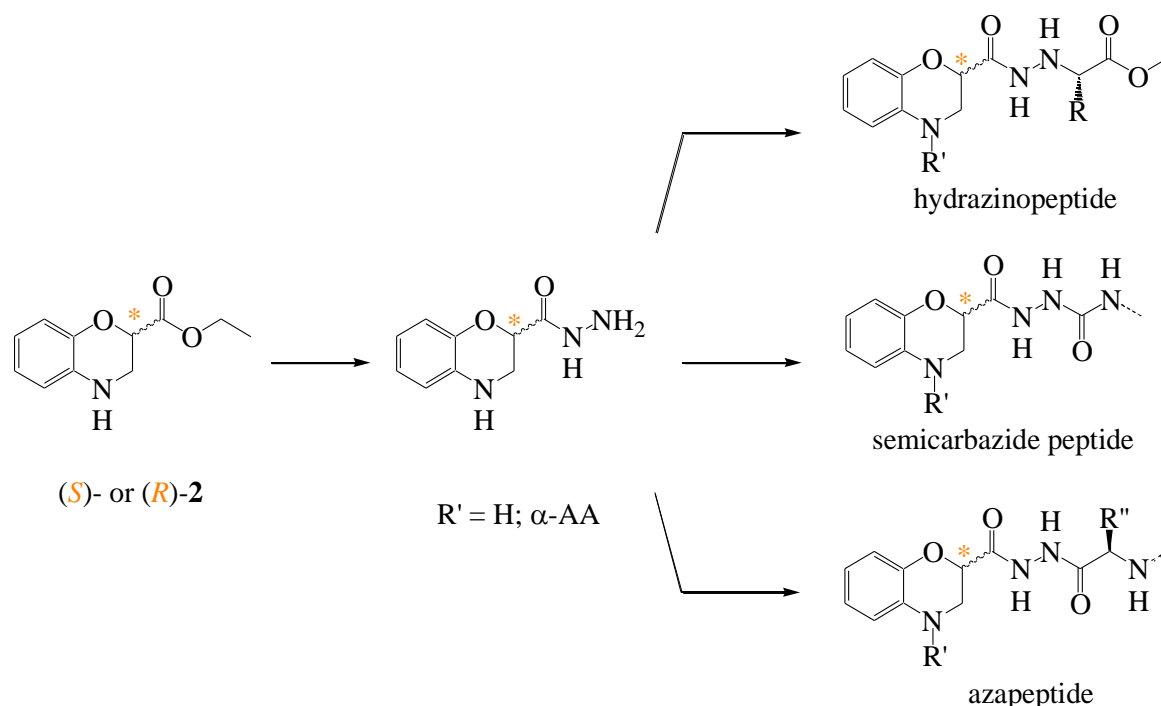
2. Perspectives

It was reported in this work that the absolute configuration at C2 position of the 1,4-benzoxazine scaffold and the side chain of α -amino acid do not have strong influence to the structural behavior of synthesized 1,4-benzoxazine-based pseudopeptides. However, the chosen α -amino acids in this work for coupling are alanine and/or phenylalanine which do not create a big steric hindrance effect. Thus, it can be interesting to study the effect of other different α -amino acids with sterically congested side chains such as leucine, valine, *etc.* on structuration.

Moreover, one of our purpose is to deprotect the Fmoc-protected group in order to obtain the second amine group -NH₂. Increasing the number of NH can raise more possibility to generate intramolecular H-bond. Classically, the deprotection of Fmoc was done by several attempts using different bases (10-20%) like morpholine, DIEA, piperidine or triethylamine in different solvents such as acetone, DMF or CH₂Cl₂ for 15-30 min, monitoring by TLC using CH₂Cl₂/MeOH (95/5, v/v) as eluent. Reaction solution was concentrated under *vacuo*. The resulted oil was treated by several ways. Unfortunately, it was not possible to obtain the pure desired product after deprotection certainly due to the high polarity of resulted molecule. The first trial was purification by reverse phase preparative HPLC. Achiral preparative HPLC using

CH₃CN/H₂O containing 0.1% of TFA as eluent was applied to purify deprotected-compound but 97% of product was lost and only 2 mg of expected compound was recovered after injection and elution of 60 mg of crude. The second effort was precipitation of deprotected-product in cold Et₂O or *n*-hexane did not work also. The third attempt was treating the resulted residue after solvent evaporation with water and extracted with CH₂Cl₂. Our expected compound should preferable to solubilize in aqueous phase. The collected aqueous phases were freezed in nitrogen liquid and dried by lyophilisation overnight. However, as same as preparative HPLC, less than 1 mg was recovered from 60 mg of departure product. This was really shame because it would have been very interesting to study the structural behavior of this deprotected compound. In perspective, if the Fmoc-protected group can be successfully deprotected for all 1,4-benzoxazine-based analogues as pseudotripeptides, it will be interesting to analyze them.

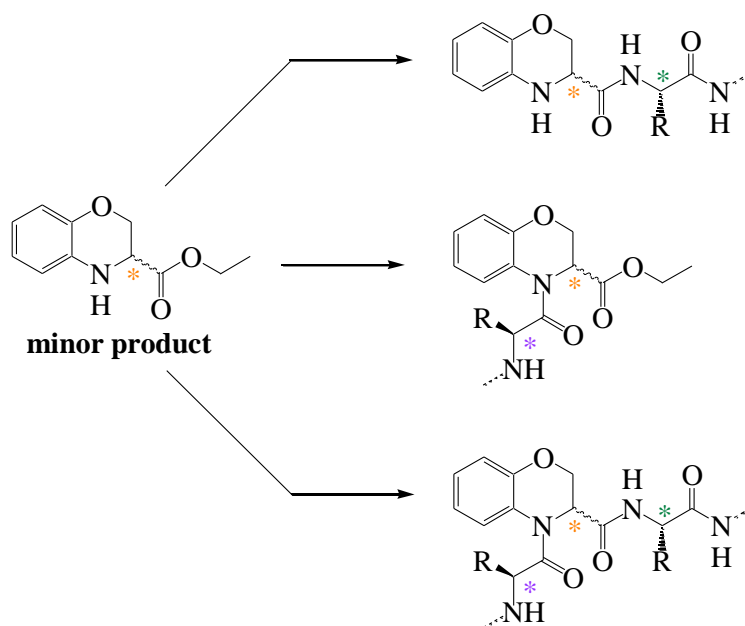
Another perspective for this enchanting scaffold is to install at C2 position of 1,4-benzoxazine ring an hydrazino group by hydrazidation of ethyl ester group of (*S*)- and (*R*)-**2** (Scheme 4.5). The resulting compound then can be used to design hydrazinopeptides, semicarbazide peptides or azapeptides.



Scheme 4.5 Insertion of hydrazide to C-terminal extremity for increasing possibility of H-bond

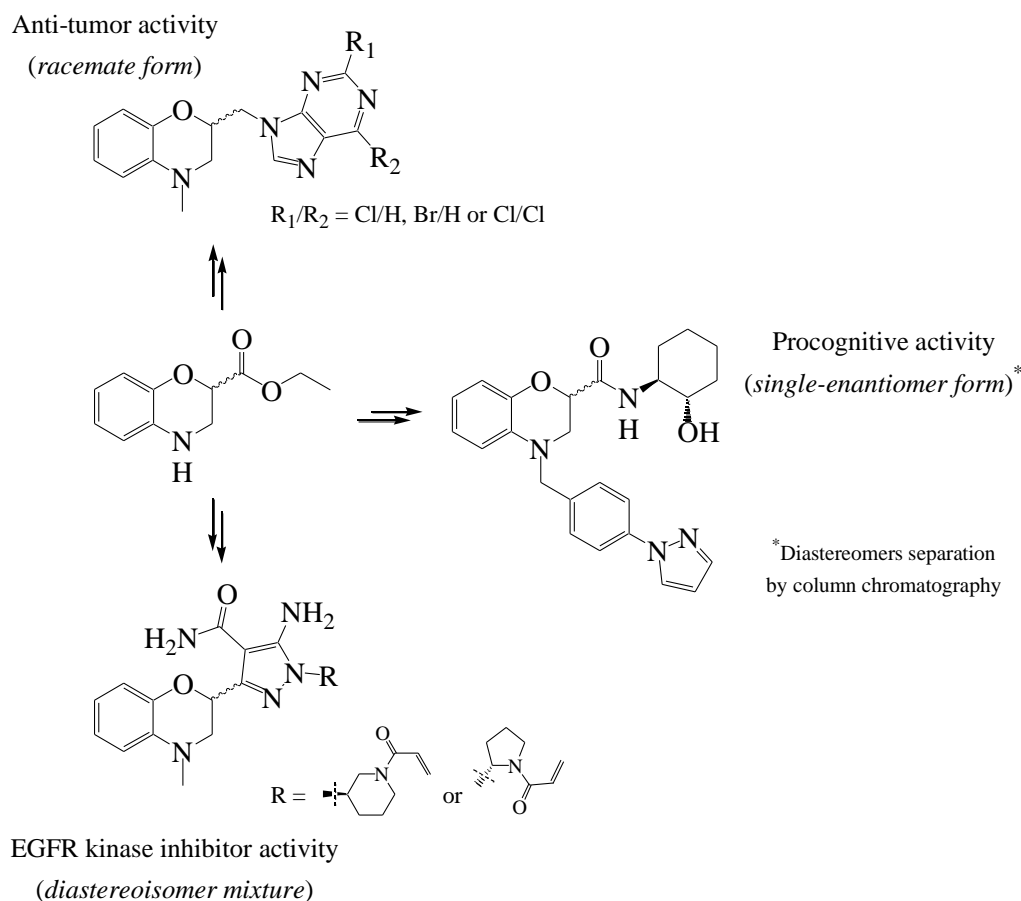
The synthesis of ethyl ester 3,4-dihydro-2*H*-1,4-benzoxazine always gives major product with ethyl ester group attaches at C2 position and minor product where it attaches at C3 position. The minor product ethyl 3,4-dihydro-2*H*-1,4-benzoxazine-3-carboxylate mimics the structure of α -amino acid (Scheme 4.6). Therefore, it can be attractive to study its conformation if we

elongate the *N*-terminal extremity by insertion of different amino acids. By that the predominant of C₅ pseudocycle can be avoided.



Scheme 4.6 Elongation of *N*-terminal extremity on minor product 1,4-benzoxazine

For further research on 1,4-benzoxazine scaffold, enantiomers (*S*)- and (*R*)-**2** can be used as starting materials to design new potential therapeutic drugs based on the literature (Scheme 4.7).



Scheme 4.7 Some examples of 1,4-benzoxazine-based therapeutic drug¹⁻³

REFERENCE

- (1) Campos Rosa, J. M.; Garcia Rubino, M. E.; Marchal Corrales, J. A.; Morata Tarifa, C.; Ramirez Rivera, A.; Paz Rojas, A. Preparation of Six-Membered Benzo-Heterocycles Having Oxygen and Nitrogen Atoms with Anti-Tumor Activity. WO 2017064350 A1, **2017**.
- (2) Rook, J. M.; Bertron, J. L.; Cho, H. P.; Garcia-Barrantes, P. M.; Moran, S. P.; Maksymetz, J. T.; Nance, K. D.; Dickerson, J. W.; Remke, D. H.; Chang, S.; Harp, J. M.; Blobaum, A. L.; Niswender, C. M.; Jones, C. K.; Stauffer, S. R.; Conn, P. J.; Lindsley, C. W. A Novel M₁ PAM VU0486846 Exerts Efficacy in Cognition Models without Displaying Agonist Activity or Cholinergic Toxicity. *ACS Chem. Neurosci.* **2018**, 9 (9), 2274–2285.
- (3) Zhang, G.; Ren, B.; Wang, H.; Zhao, H.; Guo, Y.; Wang, Z.; Zhou, C. 5-Amino-4-Carbamoyl-Pyrazole Compounds as Selective and Irreversible T790M over WT-EGFR Kinase Inhibitors and Their Preparation. WO 2016/008411 A1, **2016**.

EXPERIMENTAL PART

Unless otherwise stated, all chemicals were purchased from Sigma-Aldrich as the highest purity commercially available and were used without further purification. Dry solvents were obtained by distillation over P₂O₅ under an argon atmosphere and other reagent-grade solvents were used as received.

Reactions were monitored by thin-layer chromatography (TLC) using aluminium-backed silica gel plates (Macherey–Nagel ALUGRAM® SIL G/UV254). TLC spots were viewed under ultraviolet light or/and by heating the plate after treatment with a staining solution of phosphomolybdic acid or using iodine vapour. Product purifications were performed using Geduran 60 H Silica Gel (63-200 mesh). NMR spectra (¹H, ¹³C, 2D COSY, 2D HSQC, 2D HMBC) were recorded on a Bruker Advance 300 spectrophotometer in CDCl₃ at 300 K. Chemical shift (δ) are reported in parts per million (ppm) and are referenced to the signal of tetramethylsilane (TMS, δ = 0 ppm) as internal standard for ¹H NMR, and CDCl₃ was used as an internal standard (δ = 77.0 ppm) for ¹³C NMR. Coupling constants (*J*) are given in hertz (Hz) and the multiplicity is defined as s for singlet, d for doublet, t for triplet, q for quadruplet, m for multiplet, br for broad or combinations thereof. H_{Ar} represent the aromatic protons.

Electrospray mass spectroscopy (ESI-MS) was performed on a Bruker MicroToF-QHR spectrometer at Faculté des Sciences et Techniques in Vandœuvre-lès-Nancy.

LC-MS analysis was performed on UFLC Shimadzu and LCMS-2020 Shimadzu mass detector. The analytical column (250 x 4.6 mm) is packed with Nucléodur silica gel C18 (10 μm), CH₃CN/H₂O containing 0.1% of formic acid was used as the mobile phase. The flow rate was 1 mL/min and the injection volume was 20 μL. The peaks were detected by UV at 214 and 254 nm. The positive ions ionization ESI mode was applied.

Achiral analytical HPLC spectra were performed on a Shimadzu High Performance Liquid Chromatography apparatus. The analytical column (250 x 4 mm) is packed with Nucleosil silica gel C4 (5 μm), CH₃CN/H₂O containing 0.1% of TFA was used as the mobile phase. The flow rate was 1 mL/min and the volume of injected sample was 20 μL. The peaks were detected by UV at 254 nm.

Analytical and preparative chiral HPLC experiments were performed on an Agilent 1260 Infinity unit (pump G1311B, autosampler G1329B, DAD G1315D), with Jasco CD-1595 circular dichroism detector. The analytical (250 x 4.6 mm) and preparative column were purchased from Chiral Technologies Europe (Illkirch, France), Phenomenex (Le Pecq, France)

or Regis Technologies (Morton Grove, USA). HPLC grade heptane, hexane and ethanol were degassed and filtered on a 45 μm Millopore membrane before use. Retention time R_t in minutes, retention factors $k_i = (R_{t_i} - R_{t_0})/R_{t_0}$ and enantioselectivity factor $\alpha = k_2/k_1$ and resolution $R_s = 1.18 (R_{t_2} - R_{t_1}) / (w_1 + w_2)$ are given. R_{t_0} was determined by injection of tri-tertio-butyl benzene and w_i was the peak width at half-height.

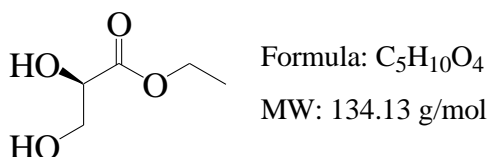
FTIR spectra were recorded with a Bruker Alpha Platinum ATR Spectrometer. FT-IR spectra (128 scans) were obtained at 2 cm^{-1} resolution using a $50\text{ }\mu\text{m}$ CaF_2 solution cell and a dry air purged Bruker Tensor 27 equipped with liquid nitrogen cooled MCT-detector. All samples were dissolved at concentration of 10^{-2} M in spectrophotometric grade solvent (CDCl_3 or $\text{DMSO-}d_6$).

Melting points were measured with a Buchi M-560 melting-point apparatus.

The purity of all synthesized molecules was checked by HPLC or LC-MS. All compounds have high purity ($\geq 97\%$).

EXPERIMENTAL PROCEDURES

(S)-Ethyl glycerate, (S)-3



To a solution of *L*-Serine (10 g, 95.1 mmol) in water (20 mL) at 0°C were added aqueous sulfuric acid (3M, 51 mL) and aqueous sodium nitrite (3M, 17 mL). The mixture was stirred for 5 h at room temperature then aqueous sodium nitrite (3M, 17 mL) was added at 0°C. The reaction was stirred for 3 days at room temperature then aqueous sulfuric acid (3M, 25 mL) and aqueous sodium nitrite (3M, 17 mL) were added at 0°C. After the reaction was stirred for 2 days at room temperature, water was removed under vacuum and a solution of sodium hydroxide (4.2 g) in water (10 mL) was added to the resulting residue at 0°C. A mixture of EtOH (30 mL) and acetone (10 mL) was added to the stirring mixture and the salt was filtered through celite. After evaporation of solvent, a mixture of EtOH (30 mL) and acetone (10 mL) was added again. This operation was repeated until no white salt formed after adding solvent mixture. The residue was dissolved in EtOH (72.6 mL) and acidified by concentrated sulfuric acid (4-5 drops). Triethyl orthoformate (0.08 mmol, 13.6 mL) was added to the mixture. The reaction was stirred for 30 minutes at 80°C then it was neutralized by sodium ethoxide 21% w/w in EtOH to pH 7 at 0°C. Solvent was evaporated and the crude was purified by flash column chromatography (PE/EtOAc, 3/7, v/v) to afford (S)-3 as yellow oil.

Yield 72%

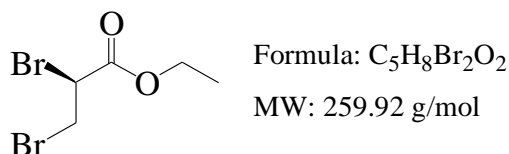
$[\alpha]_{\text{D}}^{28} = -11.2^{\circ}$ (CHCl₃, $c = 0.05$) [Lit. $[\alpha]_{\text{D}}^{23} = -11.6^{\circ}$ (CHCl₃, $c = 1.00$)]

¹H NMR (10⁻² M, CDCl₃, 300 MHz): $\delta = 1.30$ (t, 3H, $J = 7.2$ Hz, CH₃), 2.58 (br s, 1H, OH), 3.43 (br s, 1H, OH), 3.83 (dd, 1H, $J = 11.7$ and 3.6 Hz, CH₂-OH), 3.90 (dd, 1H, $J = 11.7$ and 3.3 Hz, CH₂-OH), 4.24-4.31 (m, 3H, CH-OH, O-CH₂)

¹³C NMR (CDCl₃, 75 MHz): $\delta = 14.8$ (CH₃), 62.8 (CH₂-OH), 64.7 (O-CH₂), 72.3 (CH-OH), 173.7 (C=O)

HRMS (ESI) calculated for C₅H₁₀O₄ [M+Na]⁺ m/z 157.0483, found 157.0471

Enantioselective synthesis of (*S*)-ethyl 2,3-dibromopropionate, (*S*)-1



Method A:

N-bromosuccinimide (1 or 3 equiv.) and PPh₃ (1 or 3 equiv.) were added successively to a solution of (*S*)-**3** (200 mg, 1.5 mmol, 1 equiv.) in CH₂Cl₂ or Et₂O (10 mL) by portions at 0°C. The mixture was stirred for 3 h at 0°C and then for 3 to 9 h at room temperature. The reaction mixture was concentrated *in vacuo*, and the resulting crude material was purified by flash chromatography (hexane/EtOAc, 3/7, v/v). Only the starting material (*S*)-**3** (80%) was recovered without racemization.

Method B:

Pyridine (1.1 equiv.) was added to a solution of (*S*)-**3** (200 mg, 1.5 mmol, 1 equiv.) in CH₂Cl₂ or Et₂O (10 mL) at -10°C. After 15 min of stirring, PBr₃ (1, 3 or 5 equiv.) was added dropwise at -10°C and the resulting mixture was stirred at room temperature for 2 to 24 h. The reaction mixture was poured over ice and extracted with CH₂Cl₂ or Et₂O (3 × 20 mL). The organic phases were combined and washed with saturated NaHCO₃ (10 mL) and brine (10 mL), dried over MgSO₄, and concentrated. The reaction mixture was concentrated *in vacuo*, and the resulting crude material was purified by flash chromatography (hexane/EtOAc, 3/7, v/v). Only the starting material (*S*)-**3** (70%) was recovered without racemization.

Method C:

PPh₃ (2 or 3 equiv.) was added to a solution of (*S*)-**1** (200 mg, 1.5 mmol, 1 equiv.) in CH₂Cl₂ (10 mL) at 0°C. After 20 to 30 minutes of stirring, CBr₄ (2 or 3 equiv.) was added in small portion at 0°C and the resulting mixture was stirred at room temperature for either 8, 11, 14, 17, or 20 hours. The reaction mixture was concentrated *in vacuo*, and the resulting crude material was purified by flash chromatography (PE/EtOAc, 9/1, v/v) to afford the dibromo compound (*S*)-**1** as yellow oil (ee ≈ 9-50%) (See Table 5, Page 56).

Yield 24 - 82%

^1H NMR (10^{-2} M, CDCl_3 , 300 MHz): $\delta = 1.33$ (t, 3H, $J = 6.9$ Hz, CH_3), 3.67 (dd, 1H, $J = 9.9$ and 4.2 Hz, $\text{CH}_2\text{-Br}$), 3.85 (dd, 1H, $J = 11.1$ and 9.9 Hz, $\text{CH}_2\text{-Br}$), 4.29 (m, 2H, O- CH_2), 4.42 (dd, 1H, $J = 11.4$ and 4.5 Hz, CH-Br)

^{13}C NMR (CDCl_3 , 75 MHz): $\delta = 14.6$ (CH_3), 30.4 ($\text{CH}_2\text{-Br}$), 41.8 (CH-Br), 63.2 (O- CH_2), 168.2 (C=O)

HRMS (ESI) calculated for $\text{C}_5\text{H}_8\text{Br}_2\text{O}_2$ [$\text{M}+\text{Na}$] $^+$ m/z 280.8788, found 280.8783

Analytical and preparative HPLC enantioseparation of (*S*)-1** and (*R*)-**1****

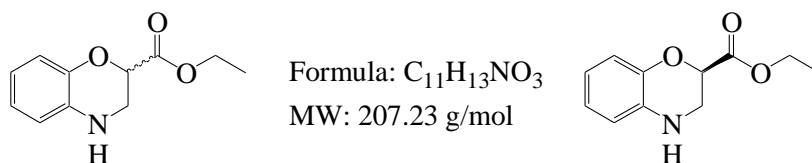
1. Analytical HPLC

20 μL of a 3 mg/mL solution of commercially available *rac*-**1** in EtOH was injected on the chiral column and detected with an UV and circular dichroism detectors at 254 nm. A mixture of heptan/EtOH (98/2 or 95/5, v/v) as mobile phase with a flow-rate of 1 mL/min was used (See Table 2, Page 51).

2. Preparative HPLC

About 5 g of *rac*-**1** was dissolved in 60 mL of a mixture hexane/EtOH (95/5, v/v) and put on CSP Chiralpak AD-H (250 x 10 mm). Hexane/EtOH (95/5, v/v) was used as the mobile phase with flow rate of 5 mL/min under UV detection at 254nm. Two eluted fractions were obtained at 4.73 min for (*S*)-**1** (2.3 g) and 5.18 min for (*R*)-**2** (2.3 g) with high enantiopurity (ee > 99.5%).

Synthesis of racemic and (*R*)-ethyl 3,4-dihydro-2*H*-1,4-benzoxazine-2-carboxylate, *rac*-2 and (*R*)-2



To a stirring solution of 2-aminophenol (1 equiv.) and anhydrous K₂CO₃ (2.2 equiv.) in dry acetone, was added *rac*-1 or (*R*)-1 (1.1 equiv.). The reaction was refluxed at 60°C and allowed to stir for 16 h. The resulting mixture was concentrated *in vacuo*, diluted in CH₂Cl₂ and washed with water. The organic layer was dried over MgSO₄ and concentrated *in vacuo*. The resulting crude material was purified by flash chromatography (PE/EtOAc, 3/7, v/v) to afford *rac*-2 or (*R*)-2 as dark orange oil.

Yield 83-85%

(*R*)-2: ee ≈ 55% and 66% (See Figure 2.5, Page 60)

¹H NMR (10⁻² M, CDCl₃, 300Hz): δ = 1.27 (t, 3H, *J* = 7.2 Hz, CH₃), 3.52-3.63 (m, 2H, N-CH₂), 3.75 (br s, 1H, NH), 4.20-4.30 (m, 2H, O-CH₂), 4.79 (dd, 1H, *J* = 4.7 and 3.6 Hz, O-CH), 6.60 (dd, 1H, *J* = 7.8 and 1.8 Hz, H_{Af}), 6.68- 6.81 (m, 2H, H_{Af}), 6.93 (dd, 1H, *J* = 7.8 and 1.5 Hz, H_{Af}). These data are in agreement with those described in the literature (Ref. 75, Page 41)

Analytical and preparative HPLC enantioseparation of (*S*)-2 and (*R*)-2

1. Analytical HPLC

20 μL of a 3 mg/mL solution of synthesized *rac*-2 in EtOH was injected on the chiral column and detected with an UV and circular dichroism detectors at 254 nm. A mixture of heptane/EtOH (7/3, v/v) as mobile phase with a flow-rate of 1 mL/min was used (See Table 6, Page 59).

2. Preparative HPLC

About 12 g of *rac*-2 was dissolved in 180 mL of mixture heptane/EtOH (5/5, v/v) and put on CSP Lux-Cellulose-2[®] (250 x 10 mm). Heptane/EtOH (7/3, v/v) was used as the mobile phase with flow rate of 5 mL/min under UV detection at 254 nm. Two eluted fractions were obtained at 5.59 min for (*S*)-2 (5.7 g) and 8.53 min for (*R*)-2 (5.6 g) with high enantiopurity (ee > 99.5%).

(S)-Ethyl-3,4-dihydro-2H-1,4-benzoxazine-2-carboxylate, (S)-2

Mp = 131°C (yellow solid)

ee > 99.5 %; $[\alpha]_D^{25} = -37^\circ$ (CH₂Cl₂, c = 0.2)

¹H NMR (10⁻² M, CDCl₃, 300 MHz): $\delta = 1.27$ (t, 3H, *J* = 7.2 Hz, CH₃), 3.52-3.64 (m, 2H, N-CH₂), 3.77 (br s, 1H, NH), 4.21-4.29 (m, 2H, O-CH₂), 4.80 (dd, 1H, *J* = 5.1 and 3.3 Hz, O-CH), 6.63 (dd, 1H, *J* = 7.8 and 1.8 Hz, H_{Ar}), 6.69-6.79 (m, 2H, H_{Ar}), 6.93 (dd, 1H, *J* = 7.8 and 1.5 Hz, H_{Ar})

¹³C NMR (CDCl₃, 75 MHz): $\delta = 14.8$ (CH₃), 43.3 (N-CH₂), 62.3 (O-CH₂), 73.4 (CH), 116.7 (CH_{Ar}), 117.7 (CH_{Ar}), 120.6 (CH_{Ar}), 122.3 (CH_{Ar}), 132.8 (C), 143.8 (C), 170.0 (C=O)

IR (10⁻² M, CDCl₃): 3418, 1746 cm⁻¹

(R)-Ethyl-3,4-dihydro-2H-1,4-benzoxazine-2-carboxylate, (R)-2

Mp = 131°C (orange solid)

ee > 99.5%; $[\alpha]_D^{25} = +37^\circ$ (CH₂Cl₂, c = 0.19)

¹H NMR (10⁻² M, CDCl₃, 300 MHz): $\delta = 1.27$ (t, 3H, *J* = 7.2 Hz, CH₃), 3.53-3.63 (m, 2H, N-CH₂), 3.77 (br s, 1H, NH), 4.20 - 4.31 (m, 2H, O-CH₂), 4.79 (dd, 1H, *J* = 4.8 and 3.6 Hz, O-CH), 6.60 (dd, 1H, *J* = 7.8 and 1.5 Hz, H_{Ar}), 6.69 - 6.81 (m, 2H, H_{Ar}), 6.93 (dd, 1H, *J* = 7.8 and 1.5 Hz, H_{Ar})

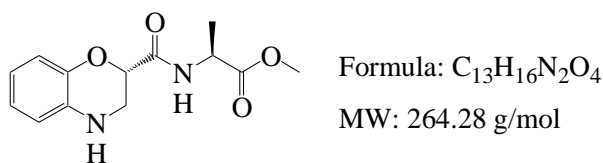
¹³C NMR (CDCl₃, 75 MHz): $\delta = 14.8$ (CH₃), 43.3 (N-CH₂), 62.3 (O-CH₂), 73.5 (O-CH), 116.7 (CH_{Ar}), 117.7 (CH_{Ar}), 120.6 (CH_{Ar}), 122.3 (CH_{Ar}), 133.3 (C), 143.7 (C), 170.1 (C=O)

IR (10⁻² M, CDCl₃): 3419, 1746 cm⁻¹

**General procedure for coupling at C-terminal extremity: synthesis of (S,S)- and (R,S)-9,
-10**

1. To a solution of enantiopure (*S*)-**2** or (*R*)-**2** (207 mg, 1 mmol) in EtOH/H₂O (8/2, v/v, 10 mL) was added lithium hydroxide (47.9 mg, 2 mmol). The reaction mixture was stirred under reflux for 2 h. After cooling, the solution was acidified by HCl 3N to pH 2 then extracted with EtOAc (3×10 mL). The organic layer was dried over MgSO₄ and solvent was evaporated under *vacuo* to obtain 3,4-dihydro-2*H*-1,4-benzoxazine-2-carboxylic acid in excellent yield (≥ 95%). The reaction product was used for next step without additional purification.
2. To a suspension of 3,4-dihydro-2*H*-1,4-benzoxazine-2-carboxylic acid (170 mg, 0.95 mmol) in dry CH₂Cl₂ (10 mL) were added corresponding hydrochloride methyl ester of α -amino acid (1.04 mmol), HOBt (141 mg, 1.04 mmol) and TEA (192 mg, 1.89 mmol, 263 μ L). The mixture was stirred at 0°C and coupling reagent EDCI (184 mg, 0.96 mmol) was added at one portion. After stirring at room temperature after 8-10 h (monitoring by TLC), the precipitate was filtered and the filtrate was washed with a solution of HCl 0.1N (2×15 mL), saturated solution of NaHCO₃ (2×15 mL) and brine (1×15 mL). The organic layer was collected and dried over MgSO₄. After evaporate solvent, the crude was purified by silica flash column chromatography (hexane/EtOAc, 1/1, v/v) to afford desired product.

(S)-methyl 2-[(S)-3,4-dihydro-2H-1,4-benzoxazine-2-carboxamido]propanoate, (S,S)-9



Yield 94 %

Mp = 96°C (Yellow solid)

$[\alpha]_{\text{D}}^{22} = -25^{\circ}$ (CH₂Cl₂, *c* = 0.1)

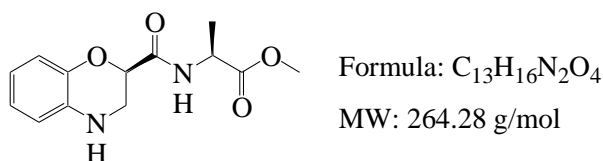
¹H NMR (10⁻² M, CDCl₃, 300 MHz): δ = 1.39 (d, 3H, *J* = 7.2 Hz, βCH₃ Ala), 3.43 (dd, 1H, *J* = 11.7 and 7.2 Hz, N-CH₂), 3.70 (dd, 1H, *J* = 11.7 and 2.7 Hz, N-CH₂), 3.77 (s, 3H, O-CH₃), 3.78 (br s, 1H, NH), 4.58-4.67 (m, 2H, αCH Ala, O-CH), 6.62-6.74 (m, 2H, H_{Ar}), 6.79-6.84 (m, 1H, H_{Ar}), 6.92 (d, 1H, *J* = 7.8 Hz, H_{Ar}), 7.11 (d, 1H, *J* = 6.6 Hz, NH)

¹³C NMR (CDCl₃, 75 MHz): δ = 19.0 (βCH₃ Ala), 43.3 (N-CH₂), 48.4 (αCH Ala), 53.2 (O-CH₃), 74.6 (O-CH), 116.7 (CH_{Ar}), 117.5 (CH_{Ar}), 120.1 (CH_{Ar}), 122.9 (CH_{Ar}), 133.6 (C), 142.8 (C), 169.3 (C=O), 173.6 (C=O)

IR (10⁻² M, CDCl₃): 3413, 3427, 1678, 1743 cm⁻¹

LC-MS (ESI) calculated for C₁₃H₁₆N₂O₄ [M+H]⁺ *m/z* 265, found 265

(S)-methyl 2-[(R)-3,4-dihydro-2H-1,4-benzoxazine-2-carboxamido]propanoate, (R,S)-9



Yield 98 %

Mp = 96°C (Yellow solid)

$[\alpha]_{\text{D}}^{22} = +27^\circ$ (CH₂Cl₂, *c* = 0.1)

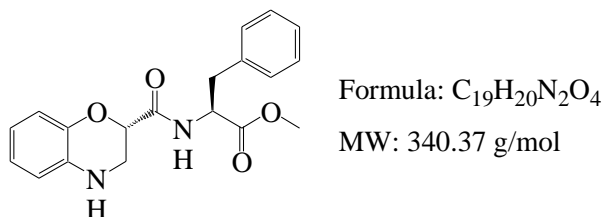
¹H NMR (10⁻² M, CDCl₃, 300 MHz): δ = 1.48 (d, 3H, *J* = 7.2 Hz, βCH₃ Ala), 3.42 (dd, 1H, *J* = 12.0 and 7.8 Hz, N-CH₂), 3.68 (d, 1H, *J* = 2.7 Hz, N-CH₂), 3.70 (s, 3H, O-CH₃), 3.71 (br s, 1H, NH), 4.62-4.66 (m, 2H, αCH Ala, O-CH), 6.63-6.74 (m, 2H, H_{Ar}), 6.80-6.85 (m, 1H, H_{Ar}), 6.92 (d, 1H, *J* = 7.8 Hz, H_{Ar}), 7.12 (d, 1H, *J* = 5.4 Hz, NH)

¹³C NMR (CDCl₃, 75 MHz): δ = 19.0 (βCH₃ Ala), 43.4 (N-CH₂), 48.5 (αCH Ala), 53.2 (O-CH₃), 74.7 (O-CH), 116.7 (CH_{Ar}), 117.6 (CH_{Ar}), 120.0 (CH_{Ar}), 122.9 (CH_{Ar}), 133.7 (C), 142.9 (C), 169.3 (C=O), 173.5 (C=O)

IR (10⁻² M, CDCl₃): 3413, 3427, 1678, 1743 cm⁻¹

LC-MS (ESI) calculated for C₁₃H₁₆N₂O₄ [M+H]⁺ *m/z* 265, found 265

(S)-methyl 2-[(S)-3,4-dihydro-2H-1,4-benzoxazine-2-carboxamido]-3-phenylpropanoate, (S,S)-10



Yield 85 % (Brown oil)

$[\alpha]_D^{22} = -23^\circ$ (CH₂Cl₂, *c* = 0.1)

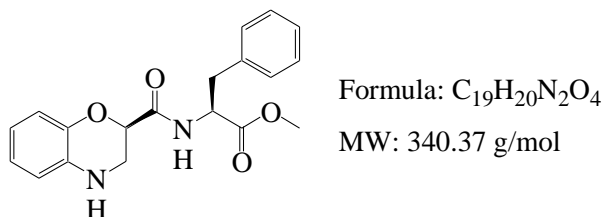
¹H NMR (10⁻² M, CDCl₃, 300 MHz): δ = 3.06 (t, 2H, *J* = 2.4 Hz, βCH₂ Phe), 3.43-3.58 (m, 2H, N-CH₂), 3.65 (br s, 1H, NH), 3.74 (s, 3H, O-CH₃), 4.66 (dd, 1H, *J* = 5.1 and 3.0 Hz, O-CH), 4.94 (dd, 1H, *J* = 13.8 and 5.7 Hz, αCH Phe), 6.64-6.75 (m, 2H, H_{Ar}), 6.83-6.91 (m, 4H, H_{Ar}), 6.92 (d, 1H, *J* = 7.2 Hz, NH), 7.15 (d, 3H, *J* = 5.1 Hz, H_{Ar})

¹³C NMR (CDCl₃, 75 MHz): δ = 38.7 (βCH₂ Phe), 42.8 (N-CH₂), 53.1 (O-CH₃), 53.4 (αCH Phe), 74.9 (O-CH), 116.8 (CH_{Ar}), 117.6 (CH_{Ar}), 120.2 (CH_{Ar}), 122.9 (CH_{Ar}), 127.7 (CH_{Ar}), 129.2 (CH_{Ar}), 129.9 (CH_{Ar}), 133.9 (C), 136.1 (C), 142.9 (C), 169.6 (C=O), 172.1 (C=O)

IR (10⁻² M, CDCl₃): 3410, 3422, 1680, 1743 cm⁻¹

LC-MS (ESI) calculated for C₁₉H₂₀N₂O₄ [M+H]⁺ *m/z* 341, found 341

(S)-methyl 2-[(R)-3,4-dihydro-2H-1,4-benzoxazine-2-carboxamido]-3-phenylpropanoate, (R,S)-10



Yield 95 % (Orange oil)

$[\alpha]_D^{22} = +24^\circ$ (CH₂Cl₂, *c* = 0.1)

¹H NMR (10⁻² M, CDCl₃, 300 MHz): δ = 3.16 (m, 2H, β CH₂ Phe), 3.39 (dd, 1H, *J* = 11.7 and 7.5 Hz, N-CH₂), 3.64 (d, 1H, *J* = 3.0 Hz, N-CH₂), 3.67 (s, 3H, O-CH₃), 3.80 (br s, 1H, NH), 4.60 (dd, 1H, *J* = 7.5 and 2.7 Hz, O-CH), 4.84 - 4.91 (m, 1H, α CH Ala), 6.61-6.83 (m, 4H, H_{Ar}), 7.02 (d, 1H, *J* = 7.8 Hz, NH), 7.14-7.34 (m, 5H, H_{Ar}).

¹³C NMR (CDCl₃, 75 MHz): δ = 38.6 (β CH₂ Phe), 42.3 (N-CH₂), 53.0 (O-CH₃), 53.5 (α CH Phe), 74.7 (O-CH), 116.7 (CH_{Ar}), 117.5 (CH_{Ar}), 119.9 (CH_{Ar}), 122.9 (CH_{Ar}), 127.9 (CH_{Ar}), 129.4 (CH_{Ar}), 129.9 (CH_{Ar}), 133.7 (C), 136.3 (C), 142.8 (C), 169.4 (C=O), 171.9 (C=O).

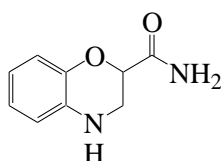
IR (10⁻² M, CDCl₃): 3408, 3422, 1680, 1744 cm⁻¹

LC-MS (ESI) calculated for C₁₉H₂₀N₂O₄ [M+H]⁺ *m/z* 341, found 341

General procedure for amidation of (S,S)- and (R,S)-9, 10: synthesis of (S,S)- and (R,S)-11, -12

To a stirring mixture of *rac*-2, (S,S)- or (R,S)-9, -10 (1 mmol) in dry CH₂Cl₂ (10 mL) was added ammonia solution (35%) (2 mL). The reaction solution was placed under reflux for 3-4 h (monitoring by TLC) then evaporate to dryness. The crude then was purified by silica flash column chromatography using pure EtOAc as eluent to obtain *rac*-16, (S,S)- or (R,S)-11, -12 in good yield.

Racemate 3,4-dihydro-2H-1,4-benzoxazine-2-carboxamide, *rac*-16



Formula: C₉H₁₀N₂O₂

MW: 178.19 g/mol

Yield 90 %

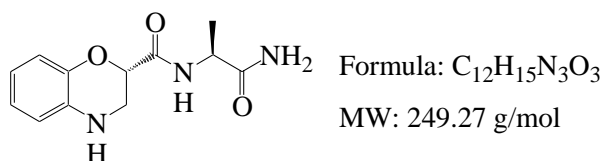
Mp = 145°C (Brown solid)

¹H NMR (CDCl₃, 300Hz): δ = 3.49 (dd, 1H, *J* = 11.7 and 6.9 Hz, N-CH₂), 3.68 (dd, 1H, *J* = 12 and 2.7 Hz, N-CH₂), 3.84 (br s, 1H, NH), 4.67 (dd, 1H, *J* = 6.9 and 3 Hz, O-CH), 5.55 (br s, 1H, NH), 6.55 (br s, 1H, NH), 6.63-6.73 (m, 2H, H_{Ar}), 6.80-6.89 (m, 2H, H_{Ar})

¹³C NMR (CDCl₃, 300Hz): δ = 43.1 (N-CH₂), 74.9 (CH), 116.7 (CH_{Ar}), 117.4 (CH_{Ar}), 120.0 (CH_{Ar}), 122.9 (CH_{Ar}), 133.8 (C), 142.8 (C), 172.5 (C=O)

IR (CDCl₃): 3411, 3523, 3401, 1698 cm⁻¹.

(S)-N-[(S)-1-amino-1-oxopropan-2-yl]-3,4-dihydro-2H-1,4-benzoxazine-2-carboxamide, (S,S)-11



Yield 89 %

Mp = 130°C (Yellow solid)

$[\alpha]_D^{22} = -7.4^\circ$ (CH₂Cl₂, *c* = 0.1)

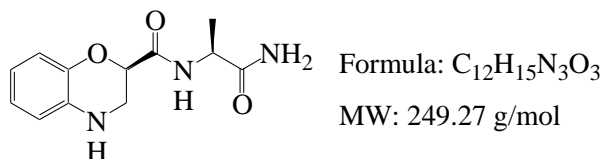
¹H NMR (10⁻² M, CDCl₃, 300 MHz): δ = 1.38 (d, 3H, *J* = 7.2 Hz, βCH₃ Ala), 3.43 (dd, 1H, *J* = 11.7 and 7.2 Hz, N-CH₂), 3.69 (dd, 1H, *J* = 11.7 and 2.7 Hz, N-CH₂), 3.85 (br s, 1H, NH), 4.56 - 4.47 (m, 1H, αCH Ala), 4.65 (dd, 1H, *J* = 7.2 and 2.7 Hz, O-CH), 5.39 (br s, 1H, NH), 6.09 (br s, 1H, NH), 6.63 (dd, 1H, *J* = 7.8 and 1.5 Hz, H_{Ar}), 6.68 - 6.74 (m, 1H, H_{Ar}), 6.79-6.85 (m, 1H, H_{Ar}), 6.91 (d, 1H, *J* = 7.8 Hz, H_{Ar}), 7.08 (d, 1H, *J* = 5.7 Hz, NH)

¹³C NMR (CDCl₃, 75 MHz): δ = 18.3 (βCH₃ Ala), 43.3 (N-CH₂), 48.8 (αCH Ala), 74.7 (O-CH), 116.5 (CH_{Ar}), 117.5 (CH_{Ar}), 120.4 (CH_{Ar}), 123.1 (CH_{Ar}), 133.7 (C), 142.7 (C), 170.0 (C=O), 174.2 (C=O)

IR (10⁻² M, CDCl₃): 3407, 3417, 3500, 3524, 1664, 1698 cm⁻¹

LC-MS (ESI) calculated for C₁₂H₁₅N₃O₄ [M+H]⁺ *m/z* 250, found 250

(S)-N-[(R)-1-amino-1-oxopropan-2-yl]-3,4-dihydro-2H-1,4-benzoxazine-2-carboxamide, (R,S)-11



Yield 75 %

Mp = 141°C (Yellow powder)

$[\alpha]_D^{22} = +12^\circ$ (CH₂Cl₂, *c* = 0.1)

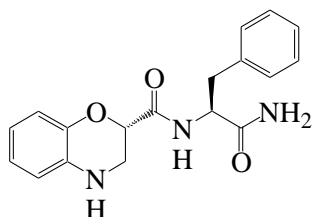
¹H NMR (10⁻² M, CDCl₃, 300 MHz): δ = 1.45 (d, 3H, *J* = 6.9 Hz, βCH₃ Ala), 3.54 (dd, 1H, *J* = 11.7 and 5.7 Hz, N-CH₂), 3.63 (dd, 1H, *J* = 11.7 and 2.7 Hz, N-CH₂), 3.83 (br s, 1H, NH), 4.50-4.60 (m, 1H, αCH Ala), 4.73 (dd, 1H, *J* = 5.7 and 3 Hz, O-CH), 5.19 (br s, 1H, NH), 5.98 (br s, 1H, NH), 6.62-6.91 (m, 4H, H_{Ar}), 6.99 (br s, 1H, NH)

¹³C NMR (CDCl₃, 75 MHz): δ = 18.3 (βCH₃ Ala), 43.3 (N-CH₂), 48.9 (αCH Ala), 75.1 (O-CH), 116.7 (CH_{Ar}), 117.6 (CH_{Ar}), 120.5 (CH_{Ar}), 123.1 (CH_{Ar}), 133.8 (C), 142.7 (C), 170.1 (C=O), 174.3 (C=O)

IR (10⁻² M, CDCl₃): 3405, 3418, 3500, 3524, 1678, 1698 cm⁻¹

LC-MS (ESI) calculated for C₁₂H₁₅N₃O₃ [M+H]⁺ *m/z* 250, found 250

(S)-N-[(S)-1-amino-1-oxo-3-phenylpropan-2-yl]-3,4-dihydro-2H-1,4-benzoxazine-2-carboxamide, (S,S)-12



Formula: C₁₈H₁₉N₃O₃

MW: 325.36 g/mol

Yield 67 %

Mp = 168°C (Yellow solid)

$[\alpha]_D^{22} = -5.8^\circ$ (CH₂Cl₂, *c* = 0.1)

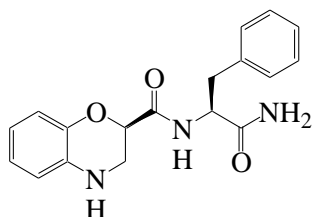
¹H NMR (10⁻² M, CDCl₃, 300 MHz): δ = 3.05 (dd, 2H, *J* = 6.3 and 6.6 Hz, βCH₂ Phe), 3.35 (dd, 1H, *J* = 11.7 and 6.3 Hz, N-CH₂), 3.59 (dd, 1H, *J* = 11.7 and 2.4 Hz, N-CH₂), 3.65 (br s, 1H, NH), 4.66 (dd, 2H, *J* = 6.3 and 2.7 Hz, O-CH), 4.72 (dd, 2H, *J* = 14.7 and 7.2 Hz, αCH Phe), 5.39 (br s, 1H, NH), 5.79 (br s, 1H, NH), 6.64 (d, 1H, *J* = 7.5 Hz, H_{Ar}), 6.73-6.90 (m, 3H, H_{Ar}), 7.11 (d, 1H, NH), 7.23-7.35 (m, 5H, H_{Ar}).

¹³C NMR (CDCl₃, 75 MHz): δ = 38.6 (βCH₂ Phe), 43.0 (N-CH₂), 54.3 (αCH Phe), 74.9 (O-CH), 116.8 (CH_{Ar}), 117.6 (CH_{Ar}), 120.2 (CH_{Ar}), 122.9 (CH_{Ar}), 127.7 (CH_{Ar}), 129.4 (CH_{Ar}), 129.9 (CH_{Ar}), 133.8 (C), 137.0 (C), 142.7 (C), 170.1 (C=O), 172.9 (C=O).

IR (10⁻² M, CDCl₃): 3399, 3413, 3511, 3523, 1661, 1688 cm⁻¹

LC-MS (ESI) calculated for C₁₈H₁₉N₃O₃ [M+H]⁺ *m/z* 326, found 326

(S)-N-[(R)-1-amino-1-oxo-3-phenylpropan-2-yl]-3,4-dihydro-2H-1,4-benzoxazine-2-carboxamide, (R,S)-12



Formula: C₁₈H₁₉N₃O₃

MW: 325.36 g/mol

Yield 73 %

Mp = 168°C (Yellow solid)

$[\alpha]_D^{22} = +6^\circ$ (CH₂Cl₂, *c* = 0.1)

¹H NMR (10⁻² M, CDCl₃, 300 MHz): δ = 3.05 (dd, 1H, *J* = 14.1 and 6.3 Hz, βCH₂ Phe), 3.19 (dd, 1H, *J* = 14.1 and 6.3 Hz, βCH₂ Phe), 3.51 (d, 2H, *J* = 3.9 Hz, N-CH₂), 3.62 (br s, 1H, NH), 4.65-4.71 (m, 2H, O-CH, αCH Phe), 5.22 (br s, 1H, NH), 5.71 (br s, 1H, NH), 6.56-6.79 (m, 4H, H_{Ar}), 6.89 (d, 1H, *J* = 7.5 Hz, NH), 7.24-7.32 (m, 5H, H_{Ar}).

¹³C NMR (CDCl₃, 75 MHz): δ = 38.0 (βCH₂ Phe), 43.1 (N-CH₂), 54.2 (αCH Phe), 74.9 (O-CH), 116.6 (CH_{Ar}), 117.5 (CH_{Ar}), 120.5 (CH_{Ar}), 123.0 (CH_{Ar}), 127.9 (CH_{Ar}), 129.5 (CH_{Ar}), 129.9 (CH_{Ar}), 133.7 (C), 136.6 (C), 142.5 (C), 170.2 (C=O), 173.4 (C=O).

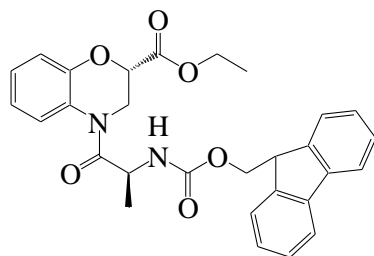
IR (10⁻² M, CDCl₃): 3397, 3409, 3502, 3518, 1679, 1693 cm⁻¹

LC-MS (ESI) calculated for C₁₈H₁₉N₃O₃ [M+H]⁺ *m/z* 326, found 326

General procedure for coupling at *N*-terminal extremity: synthesis of (*S,S*)- and (*R,S*)-8, (*S,S,S*)- and (*S,R,S*)-13, -14, -15

1. To a solution of Fmoc-Ala-OH (1 g, 3.2 mmol) at 0°C in dry CH₂Cl₂ (17 mL) was added thionyl chloride (3.8 g, 32 mmol). The reaction mixture was heated to reflux under nitrogen for 2 h. Thionyl chloride and solvent was evaporated under *vacuo*. A yellow mixture was obtained and extracted first with dry CH₂Cl₂ (4 mL) and hexane (34 mL). White solid (Fmoc-Ala-Cl) was filtered and dried to use in the next step without additional purification.
2. At -10°C, to a solution of Fmoc-Ala-Cl (330 mg, 1.5 mmol) in CH₂Cl₂ (5 mL) was added dropwise to a stirred suspension of corresponding 3,4-dihydro-2*H*-1,4-benzoxazine derivative (1 mmol) and NaHCO₃ (185 mg, 2.2 mmol) in dry CH₂Cl₂ (5 mL) and H₂O (10 mL). The reaction mixture was maintained at 0°C for 1 h then 8-10 h at room temperature. The organic layer was separated and washed with water, dried over MgSO₄ and solvent was evaporated to dryness. The crude was purified by silica flash column chromatography using hexane/EtOAc (1/1, v/v) as eluent to afford desired product.

(S)-Ethyl 4-[(S)-2-(((9H-fluoren-9-yl)methoxy)carbonyl)amino]propanoyl]-3,4-dihydro-2H-1,4-benzoxazine-2-carboxylate, (S,S)-8



Formula: C₂₉H₂₈N₂O₆

MW: 500.54 g/mol

Yield 89 %

Mp = 168°C (Yellow solid)

$[\alpha]_D^{22} = +37^\circ$ (CH₂Cl₂, *c* = 0.05)

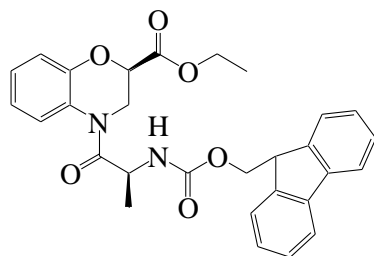
¹H NMR (10⁻² M, CDCl₃, 300 MHz): δ = 1.22-1.29 (m, 6H, β CH₃ Ala, CH₃), 3.47 (br s, 1H, N-CH₂), 4.11-4.25 (m, 4H, N-CH₂, O-CH₂, CH Fmoc), 4.39 (d, 2H, *J* = 6.9 Hz, CH₂ Fmoc), 4.98 (br s, 1H, O-CH), 5.25 (br s, 1H, α CH Ala), 5.60 (d, 1H, *J* = 8.7 Hz, NH), 6.95-7.16 (m, 3H, H_{Ar}), 7.26-7.42 (m, 5H, H_{Ar}), 7.59 (d, 2H, *J* = 7.5 Hz, H_{Ar}), 7.76 (d, 2H, *J* = 7.5 Hz, H_{Ar})

¹³C NMR (CDCl₃, 75 MHz): δ = 14.7 (CH₃), 19.9 (β CH₃ Ala), 42.8 (N-CH₂), 47.8 (CH Fmoc), 48.1 (α CH Ala), 54.1 (O-CH₂), 67.7 (CH₂ Fmoc), 74.7 (O-CH), 118.4 (CH_{Ar}), 120.6 (CH_{Ar}), 122.0 (CH_{Ar}), 124.4 (CH_{Ar}), 125.8 (CH_{Ar}), 127.7 (CH_{Ar}), 128.4 (CH_{Ar}), 141.9 (C), 144.5 (C), 144.6 (C), 156.2 (C=O), 168.9 (C=O)

IR (10⁻² M, CDCl₃): 3431, 1664, 1720, 1750 cm⁻¹

LC-MS (ESI) calculated for C₂₉H₂₈N₂O₆ [M+Na]⁺ *m/z* 523, found 523

(R)-Ethyl 4-[(S)-2-(((9H-fluoren-9-yl)methoxy)carbonyl)amino]propanoyl]-3,4-dihydro-2H-1,4-benzoxazine-2-carboxylate, (R,S)-8



Formula: C₂₉H₂₈N₂O₆

MW: 500.54 g/mol

Yield 73 %

Mp = 168°C (Yellow solid)

$[\alpha]^{22}_{\text{D}} = +20^{\circ}$ (CH₂Cl₂, *c* = 0.05)

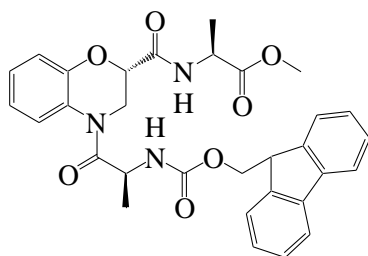
¹H NMR (10⁻² M, CDCl₃, 300 MHz): δ = 1.23-1.28 (m, 6H, β CH₃ Ala, CH₃), 3.48 (br s, 1H, N-CH₂), 4.11-4.25 (m, 4H, N-CH₂, O-CH₂, CH Fmoc), 4.39 (d, 2H, *J* = 6.9 Hz, CH₂ Fmoc), 4.98 (br s, 1H, O-CH), 5.25 (br s, 1H, α CH Ala), 5.50 (d, 1H, *J* = 7.8 Hz, NH), 6.98-7.17 (m, 3H, H_{Ar}), 7.29-7.42 (m, 4H, H_{Ar}), 7.60 (d, 3H, *J* = 6.6 Hz, H_{Ar}), 7.76 (d, 2H, *J* = 7.2 Hz, H_{Ar})

¹³C NMR (CDCl₃, 75 MHz): δ = 14.8 (CH₃), 19.7 (β CH₃ Ala), 41.8 (N-CH₂), 47.8 (CH Fmoc), 48.1 (α CH Ala), 62.6 (O-CH₂), 67.7 (CH₂ Fmoc), 74.5 (O-CH), 118.3 (CH_{Ar}), 120.6 (CH_{Ar}), 121.9 (CH_{Ar}), 124.6 (CH_{Ar}), 125.8 (CH_{Ar}), 127.7 (CH_{Ar}), 128.4 (CH_{Ar}), 141.9 (C), 144.5 (C), 144.6 (C), 156.4 (C=O), 169.5 (C=O)

IR (10⁻² M, CDCl₃): 3432, 1663, 1715, 1751 cm⁻¹

LC-MS (ESI) calculated for C₂₉H₂₈N₂O₆ [M+Na]⁺ *m/z* 523, found 523

(S)-Methyl 2-[(S)-4-((S)-2-(((9H-fluoren-9-yl)methoxy)carbonyl)amino)propanoyl]-3,4-dihydro-2H-1,4-benzoxazine-2-carboxamido)propanoate, (S,S,S)-13



Formula: C₃₁H₃₁N₃O₇

MW: 557.59 g/mol

Yield 82 %

Mp = 183°C (Dark green solid)

$[\alpha]_D^{22} = +31^\circ$ (CH₂Cl₂, *c* = 0.05)

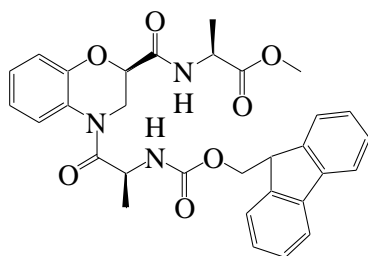
¹H NMR (10⁻² M, CDCl₃, 300 MHz): δ = 1.28 (s, 3H, β CH₃ Ala), 1.40 (d, 3H, *J* = 6.9 Hz, β CH₃ Ala), 3.78 (s, 3H, O-CH₃), 4.23 (t, 1H, *J* = 6.6 Hz, CH Fmoc), 4.40 (d, 2H, *J* = 6.9 Hz, CH₂ Fmoc), 4.63 (dd, 1H, *J* = 14.1 and 6.9 Hz, α CH Ala), 4.74 (br s, 1H, O-CH), 5.12 (br s, 1H, α CH Ala), 5.62 (d, 1H, *J* = 7.8 Hz, NH), 7.03-7.11 (m, 4H, CH_{Ar}), 7.15 (d, 1H, *J* = 3.9 Hz, NH), 7.28 - 7.43 (m, 4H, H_{Ar}), 7.61 (d, 2H, *J* = 4.5 Hz, H_{Ar}), 7.77 (d, 2H, *J* = 7.2 Hz, H_{Ar})

¹³C NMR (CDCl₃, 75 MHz): δ = 19.0 (β CH₃ Ala), 19.4 (β CH₃ Ala), 43.3 (N-CH₂), 47.8 (CH Fmoc), 48.1 (α CH Ala), 48.5 (α CH Ala), 53.3 (O-CH₃), 67.7 (CH₂ Fmoc), 76.0 (O-CH), 118.1 (CH_{Ar}), 120.7 (CH_{Ar}), 122.5 (CH_{Ar}), 125.0 (CH_{Ar}), 125.8 (C), 126.1 (CH_{Ar}), 127.8 (CH_{Ar}), 128.4 (CH_{Ar}), 141.9 (C), 144.4 (C), 144.5 (C), 156.4 (C=O), 167.7 (C=O), 172.7 (C=O), 173.5 (C=O)

IR (10⁻² M, CDCl₃): 3416, 3432, 1672, 1686, 1719, 1742 cm⁻¹

LC-MS (ESI) calculated for C₃₁H₃₁N₃O₇ [M+Na]⁺ *m/z* 580, found 580

(S)-Methyl 2-[(R)-4-((S)-2-(((9H-fluoren-9-yl)methoxy)carbonyl)amino)propanoyl]-3,4-dihydro-2H-1,4-benzoxazine-2-carboxamido)propanoate, (S,R,S)-13



Formula: C₃₁H₃₁N₃O₇

MW: 557.59 g/mol

Yield 65 %

Yield 65 %; mp = 182°C

$[\alpha]_D^{22} = -23^\circ$ (CH₂Cl₂, *c* = 0.05)

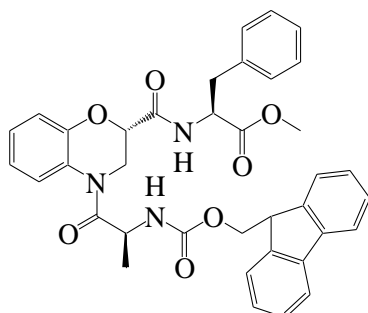
¹H NMR (10⁻² M, CDCl₃, 300 MHz): δ = 1.28 (s, 3H, β CH₃ Ala), 1.46 (d, 3H, *J* = 7.2 Hz, β CH₃ Ala), 3.69 (s, 3H, O-CH₃), 4.23 (t, 1H, *J* = 6.9 Hz, CH Fmoc), 4.36 (d, 2H, *J* = 6.6 Hz, CH₂ Fmoc), 4.59 (dd, 1H, *J* = 21.6 and 6.9 Hz, α CH Ala), 4.81 (br s, 1H, O-CH), 5.01 (br s, 1H, α CH Ala), 5.66 (br s, 1H, NH), 6.99-7.17 (m, 4H, CH_{Ar}), 6.91 (br s, 1H, NH), 7.26-7.42 (m, 4H, H_{Ar}), 7.60 (d, 2H, *J* = 5.1 Hz, H_{Ar}), 7.76 (d, 2H, *J* = 7.5 Hz, H_{Ar})

¹³C NMR (CDCl₃, 75 MHz): δ = 18.9 (β CH₃ Ala), 19.7 (β CH₃ Ala), 47.8 (CH Fmoc), 48.2 (α CH Ala), 48.6 (α CH Ala), 53.2 (O-CH₃), 67.7 (CH₂ Fmoc), 76.2 (O-CH), 118.2 (CH_{Ar}), 120.6 (CH_{Ar}), 122.4 (CH_{Ar}), 124.7 (CH_{Ar}), 125.8 (CH_{Ar}), 127.7 (CH_{Ar}), 128.3 (CH_{Ar}), 141.9 (C), 144.5 (C), 144.6 (C), 146.2 (C=O), 156.2 (C=O), 167.8 (C=O), 173.3 (C=O)

IR (10⁻² M, CDCl₃): 3416, 3431, 1670, 1685, 1719, 1741 cm⁻¹

LC-MS (ESI) calculated for C₃₁H₃₁N₃O₇ [M+Na]⁺ *m/z* 580, found 580

(S)-Methyl 2-[(S)-4-((S)-2-(((9H-fluoren-9-yl)methoxy)carbonyl)amino)propanoyl]-3,4-dihydro-2H-1,4-benzoxazine-2-carboxamido]-3-phenylpropanoate, (S,S,S)-14



Formula: C₃₇H₃₅N₃O₇

MW: 633.69 g/mol

Yield 60 %

Mp = 163°C (Light brown solid)

$[\alpha]^{22}_{\text{D}} = +6^{\circ}$ (CH₂Cl₂, *c* = 0.02)

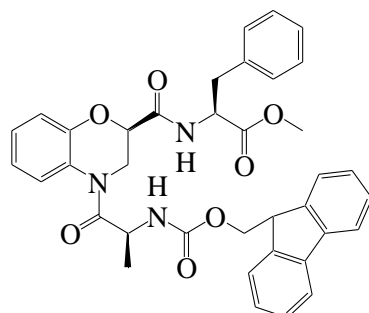
¹H NMR (10⁻² M, CDCl₃, 300 MHz): δ = 1.26 (br s, 3H, β CH₃ Ala), 3.07 (d, 2H, *J* = 3.9 Hz, β CH₂ Phe), 3.76 (s, 3H, O-CH₃), 4.22 (t, 1H, *J* = 6.6 Hz, CH Fmoc), 4.38 (d, 2H, *J* = 6.9 Hz, CH₂ Fmoc), 4.71 (br s, 1H, O-CH), 4.91 (d, 1H, *J* = 7.8 Hz, α CH Phe), 5.09 (br s, 1H, α CH Ala), 5.61 (d, 1H, *J* = 7.5 Hz, NH), 6.96-7.42 (m, 13H, H_{Ar}), 7.27 (br s, 1H, NH), 7.59 (br s, 2H, H_{Ar}), 7.76 (d, 2H, *J* = 7.2 Hz, H_{Ar})

¹³C NMR (CDCl₃, 75 MHz): δ = 19.4 (β CH₃ Ala), 38.6 (β CH₂ Phe), 47.9 (CH Fmoc), 48.1 (α CH Ala), 53.2 (O-CH₃), 53.3 (α CH Phe), 67.8 (CH₂ Fmoc), 76.0 (O-CH), 118.0 (CH_{Ar}), 120.7 (CH_{Ar}), 122.5 (CH_{Ar}), 125.0 (CH_{Ar}), 125.8 (CH_{Ar}), 126.2 (C), 127.8 (CH_{Ar}), 127.9 (CH_{Ar}), 128.4 (CH_{Ar}), 129.3 (CH_{Ar}), 129.9 (CH_{Ar}), 135.8 (C), 142.0 (C), 144.5 (C), 144.6 (C), 156.4 (C=O), 167.8 (C=O), 171.9 (C=O)

IR (10⁻² M, CDCl₃): 3416, 3430, 1670, 1686, 1719, 1743 cm⁻¹

LC-MS (ESI) calculated for C₃₇H₃₅N₃O₇ [M+H]⁺ *m/z* 635, found 635

(S)-Methyl 2-[(R)-4-((S)-2-(((9H-fluoren-9-yl)methoxy)carbonyl)amino)propanoyl]-3,4-dihydro-2H-1,4-benzoxazine-2-carboxamido]-3-phenylpropanoate, (S,R,S)-14



Formula: C₃₇H₃₅N₃O₇

MW: 633.69 g/mol

Yield 72 %

Mp = 163°C (Light brown solid)

$[\alpha]^{22}_{\text{D}} = -4^{\circ}$ (CH₂Cl₂, *c* = 0.02)

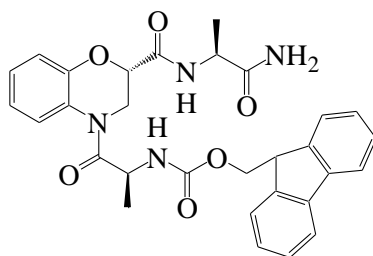
¹H NMR (10⁻² M, CDCl₃, 300 MHz): δ = 1.37 (br s, 3H, β CH₃ Ala), 3.17 (t, 2H, *J* = 6.6 Hz, β CH₂ Phe), 3.67 (s, 3H, O-CH₃), 4.24 (d, 1H, *J* = 6.6 Hz, CH Fmoc), 4.38 (d, 1H, *J* = 6.9 Hz, CH₂ Fmoc), 4.79 (br s, 1H, O-CH), 4.83-4.89 (q, 1H, α CH Phe), 5.02 (br s, 1H, α CH Ala), 5.65 (br s, 1H, NH), 6.98-7.03 (m, 3H, H_{Ar}), 7.14 (d, 3H, *J* = 6.6 Hz, H_{Ar}), 7.28-7.44 (m, 7H, H_{Ar}), 7.61 (br s, 2H, H_{Ar}), 7.78 (d, 2H, *J* = 7.5 Hz, H_{Ar}), 7.32 (br s, 1H, NH)

¹³C NMR (CDCl₃, 75 MHz): δ = 19.7 (β CH₃ Ala), 38.5 (β CH₂ Phe), 47.8 (CH Fmoc), 48.2 (α CH Ala), 53.1 (O-CH₃), 53.6 (α CH Phe), 67.7 (CH₂ Fmoc), 76.1 (O-CH), 118.2 (CH_{Ar}), 120.6 (CH_{Ar}), 122.4 (CH_{Ar}), 124.5 (CH_{Ar}), 125.9 (CH_{Ar}), 127.8 (CH_{Ar}), 128.0 (CH_{Ar}), 128.4 (CH_{Ar}), 129.4 (CH_{Ar}), 129.9 (CH_{Ar}), 136.1 (C), 141.9 (C), 144.5 (C), 144.6 (C), 156.0 (C=O), 167.9 (C=O), 171.9 (C=O)

IR (10⁻² M, CDCl₃): 3413, 3428, 1681, 1708, 1716, 1742 cm⁻¹

LC-MS (ESI) calculated for C₃₇H₃₅N₃O₇ [M+H]⁺ *m/z* 635, found 635

(9H-fluoren-9-yl)methyl [(S)-1-((S)-2-(((S)-1-amino-1-oxopropan-2-yl)carbamoyl)-2H-1,4-benzoxazine-4(3H)-yl)-1-oxopropan-2-yl]carbamate, (S,S,S)-15



Formula: C₃₀H₃₀N₄O₆

MW: 542.58 g/mol

Yield 42 %

Mp = 203°C (White solid)

$[\alpha]_D^{22} = +36^\circ$ (DMSO-*d*₆, *c* = 0.01)

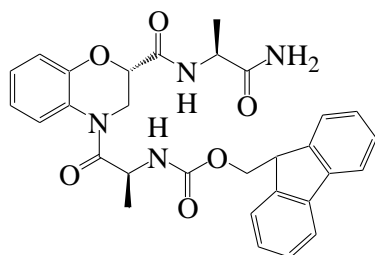
¹H NMR (10⁻² M, 1% DMSO-*d*₆ in CDCl₃, 300 MHz): δ = 1.23 (s, 3H, βCH₃ Ala), 1.35 (d, 3H, *J* = 6.9 Hz, βCH₃ Ala), 4.19 (t, 1H, *J* = 6.9 Hz, CH Fmoc), 4.35 (d, 2H, *J* = 6.9 Hz, CH₂ Fmoc), 4.50 (t, 1H, *J* = 7.2 Hz, αCH Ala), 4.68 (br s, 1H, O-CH), 5.05 (br s, 1H, αCH Ala), 5.57 (br s, 1H, NH), 5.75 (d, 1H, *J* = 7.8 Hz, NH), 6.39 (d, 1H, *J* = 7.8 Hz, NH), 7.05-7.39 (m, 8H, H_{Ar}), 7.29 (br s, 1H, NH), 7.58 (d, 2H, *J* = 7.2 Hz, H_{Ar}), 7.73 (d, 2H, *J* = 7.5 Hz, H_{Ar}).

¹³C NMR (1% DMSO-*d*₆ in CDCl₃, 75 MHz): δ = 19.2 (βCH₃ Ala), 19.3 (βCH₃ Ala), 47.8 (CH Fmoc), 48.0 (αCH Ala), 48.7 (αCH Ala), 67.6 (CH₂ Fmoc), 74.6 (O-CH), 116.5 (CH_{Ar}), 117.5 (CH_{Ar}), 118.2 (CH_{Ar}), 119.9 (CH_{Ar}), 120.6 (CH_{Ar}), 122.3 (CH_{Ar}), 122.8 (CH_{Ar}), 124.8 (CH_{Ar}), 125.7 (CH_{Ar}), 127.7 (CH_{Ar}), 128.3 (CH_{Ar}), 141.9 (C), 144.4 (C), 156.4 (C=O), 167.8 (C=O), 174.2 (C=O)

IR (10⁻² M, 1% DMSO-*d*₆ in CDCl₃): 3416, 3429, 1667, 1679, 1699, 1717 cm⁻¹

LC-MS (ESI) calculated for C₃₀H₃₀N₄O₆ [M+Na]⁺ *m/z* 565, found 565

(9H-fluoren-9-yl)methyl [(S)-1-((R)-2-(((S)-1-amino-1-oxopropan-2-yl)carbamoyl)-2H-1,4-benzoxazine-4(3H)-yl)-1-oxopropan-2-yl]carbamate (S,R,S)-15



Formula: C₃₀H₃₀N₄O₆

MW: 542.58 g/mol

Yield 25 %

Mp = 203°C (White solid)

$[\alpha]_D^{22} = +22^\circ$ (DMSO-*d*₆, *c* = 0.01)

¹H NMR (10⁻² M, 1% DMSO-*d*₆ in CDCl₃, 300 MHz): δ = 1.21 (s, 3H, βCH₃ Ala), 1.38 (d, 3H, *J* = 6.9 Hz, βCH₃ Ala), 4.20 (d, 1H, *J* = 6.6 Hz, CH Fmoc), 4.33 (d, 2H, *J* = 7.2 Hz, CH₂ Fmoc), 4.50 (t, 1H, *J* = 7.2 Hz, αCH Ala), 4.83 (br s, 1H, O-CH), 4.99 (br s, 1H, αCH Ala), 5.42 (br s, 1H, NH), 5.77 (d, 1H, *J* = 7.8 Hz, NH), 6.33 (br s, 1H, NH), 6.92-7.13 (m, 3H, H_{Ar}), 7.16 (br s, 1H, NH), 7.24-7.37 (m, 5H, H_{Ar}), 7.56 (d, 2H, *J* = 6.9 Hz, H_{Ar}), 7.71 (d, 2H, *J* = 7.5 Hz, H_{Ar})

¹³C NMR (1% DMSO-*d*₆ in CDCl₃, 75 MHz): δ = 18.9 (βCH₃ Ala), 19.3 (βCH₃ Ala), 47.7 (CH Fmoc), 48.1 (αCH Ala), 48.8 (αCH Ala), 67.5 (CH₂ Fmoc), 75.0 (O-CH), 118.2 (CH_{Ar}), 120.5 (CH_{Ar}), 122.2 (CH_{Ar}), 124.6 (CH_{Ar}), 125.7 (CH_{Ar}), 127.6 (CH_{Ar}), 128.3 (CH_{Ar}), 141.8 (C), 144.4 (C), 156.3 (C=O), 168.2 (C=O), 174.1 (C=O).

IR (10⁻² M, 1% DMSO-*d*₆ in CDCl₃): 3396, 3418, 1647, 1674, 1699, 1717 cm⁻¹

LC-MS (ESI) calculated for C₃₀H₃₀N₄O₆ [M+Na]⁺ *m/z* 565, found 565

APPENDIX 1

Absolute configuration determination by comparison of calculated and experimental ECD spectra

1. Re-optimization of the conformers, frequency calculations at SMD(CH₃CN)/B3LYP-D3/6-311+g(d,p) level and TD-DFT calculations at SMD(CH₃CN)/CAMB3LYP-D3/6-311+g(d,p) level: 100 excited states were computed for each conformation.

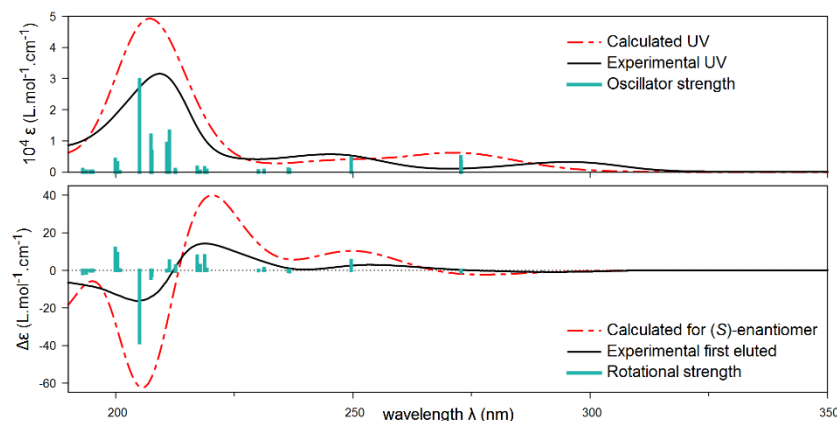


Figure 2. Comparison of UV (top) and ECD (bottom) experimental spectra in acetonitrile ($c = 0.6$ mM) for the first eluted enantiomer of **2** on Lux-Cellulose-2 and TD-DFT calculated spectra (Boltzmann averages of two conformers, = 0.29 eV, shifted by 9 nm). Vertical bars are oscillator and rotational strengths calculated for the two conformers with arbitrary unit.

2. Re-optimization of the conformers, frequency and TD-DFT calculations at SMD(CH₃CN)/M06-2X-D3/Def2SVP level: 100 excited states were computed for each conformation.

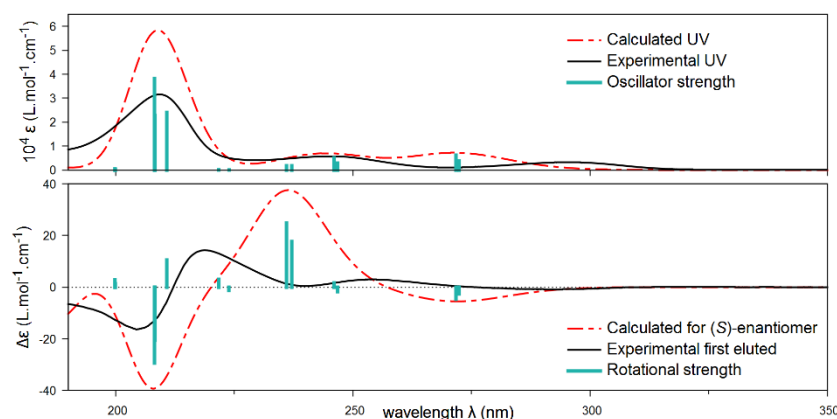


Figure 3. Comparison of UV (top) and ECD (bottom) experimental spectra in acetonitrile ($c = 0.6$ mM) for the first eluted enantiomer of **2** on Lux-Cellulose-2 and TD-DFT calculated spectra (Boltzmann

averages of two conformers, = 0.29 eV, shifted by 20 nm). Vertical bars are oscillator and rotational strengths calculated for the two conformers with arbitrary unit.

3. Re-optimization of the conformers, frequency and TD-DFT calculations at SMD(CH₃CN)/ ω B97X-D/Def2SVP level: 100 excited states were computed for each conformation.

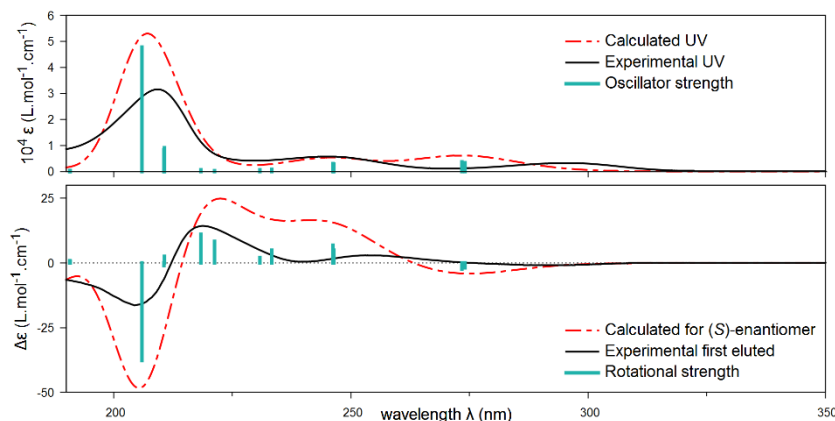


Figure 4. Comparison of UV (top) and ECD (bottom) experimental spectra in acetonitrile ($c = 0.6$ mM) for the first eluted enantiomer of **2** on Lux-Cellulose-2 and TD-DFT calculated spectra (Boltzmann averages of two conformers, = 0.29 eV, shifted by 17 nm). Vertical bars are oscillator and rotational strengths calculated for the two conformers with arbitrary unit.

4. Re-optimization of the conformers, frequency and TD-DFT calculations at SMD(CH₃CN)/PBE0-D3/Def2SVP level: 100 excited states were computed for each conformation.

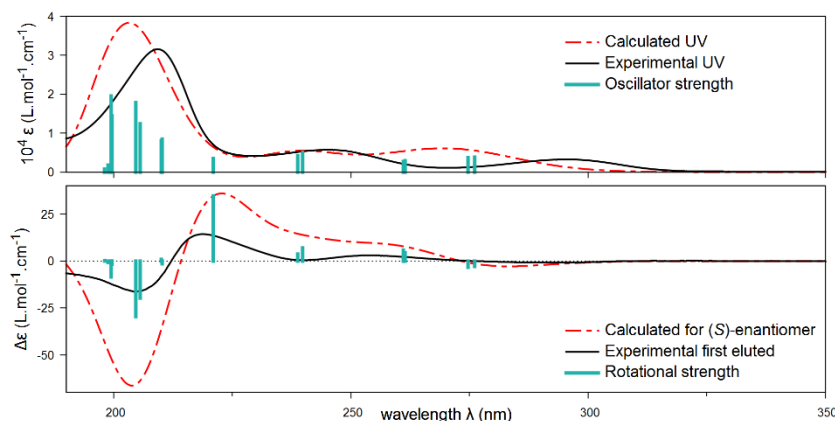
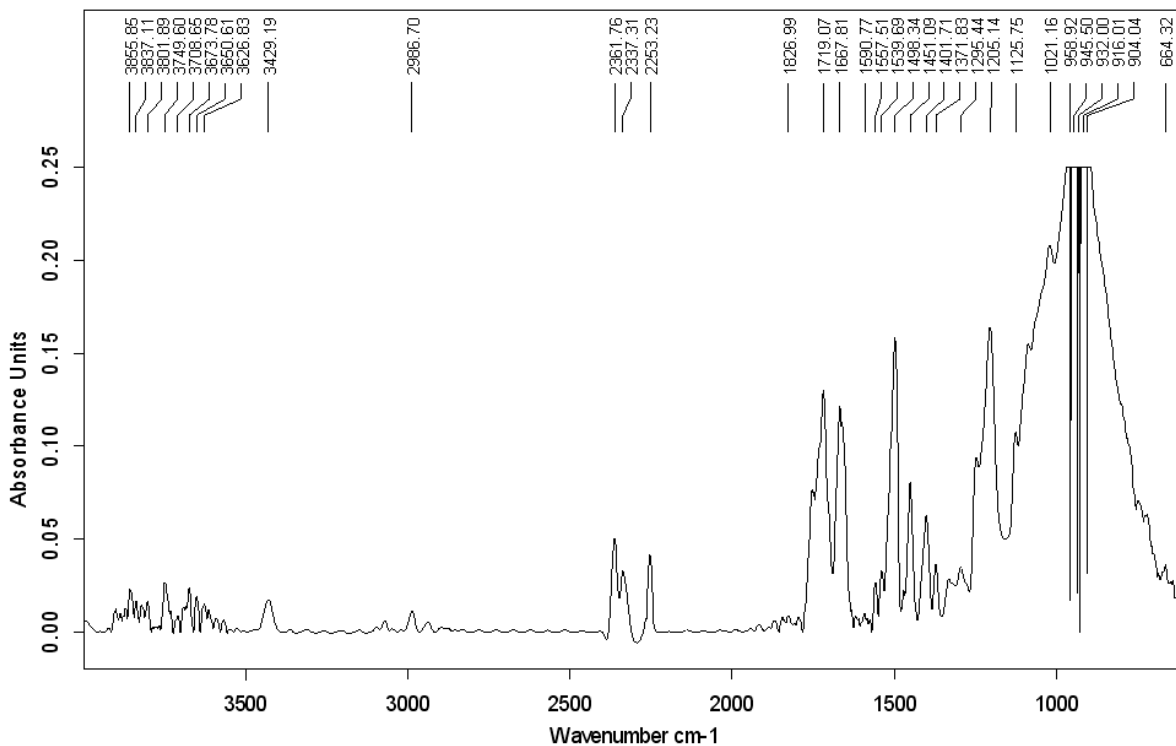


Figure 5. Comparison of UV (top) and ECD (bottom) experimental spectra in acetonitrile ($c = 0.6$ mM) for the first eluted enantiomer of **2** on Lux-Cellulose-2 and TD-DFT calculated spectra (Boltzmann averages of two conformers, = 0.29 eV, shifted by 9 nm). Vertical bars are oscillator and rotational strengths calculated for the two conformers with arbitrary unit.

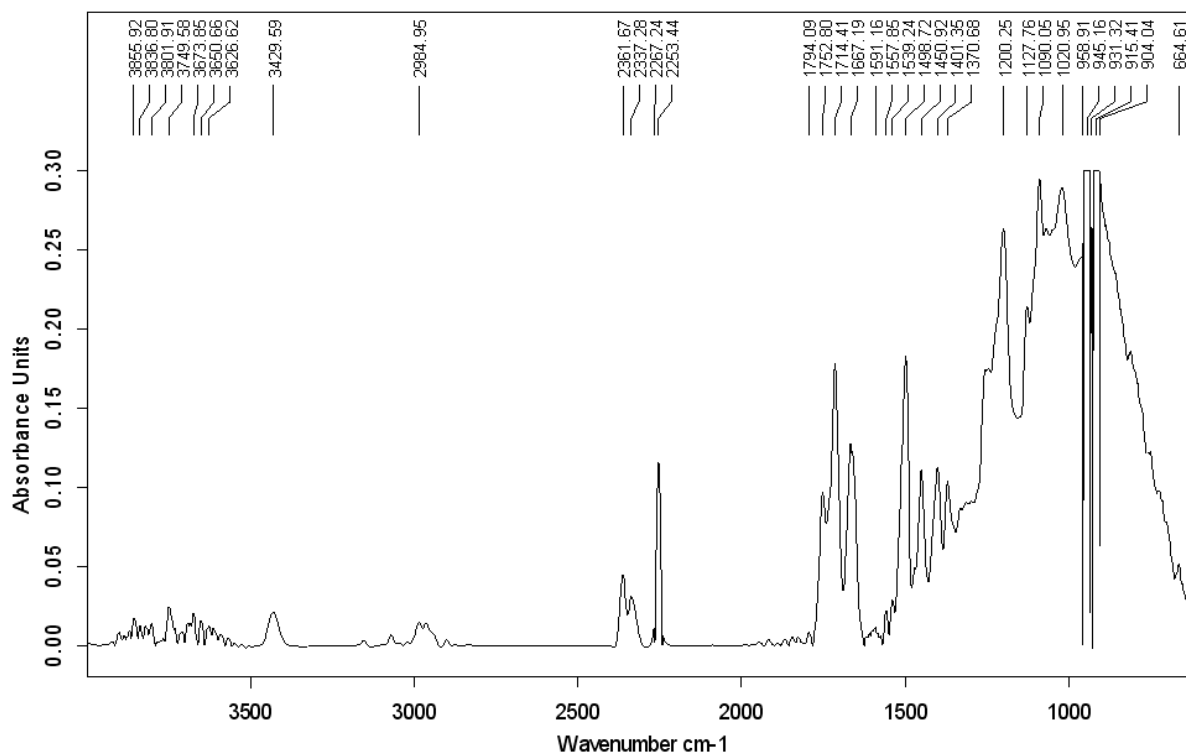
APPENDIX 2

INFRARED SPECTRA

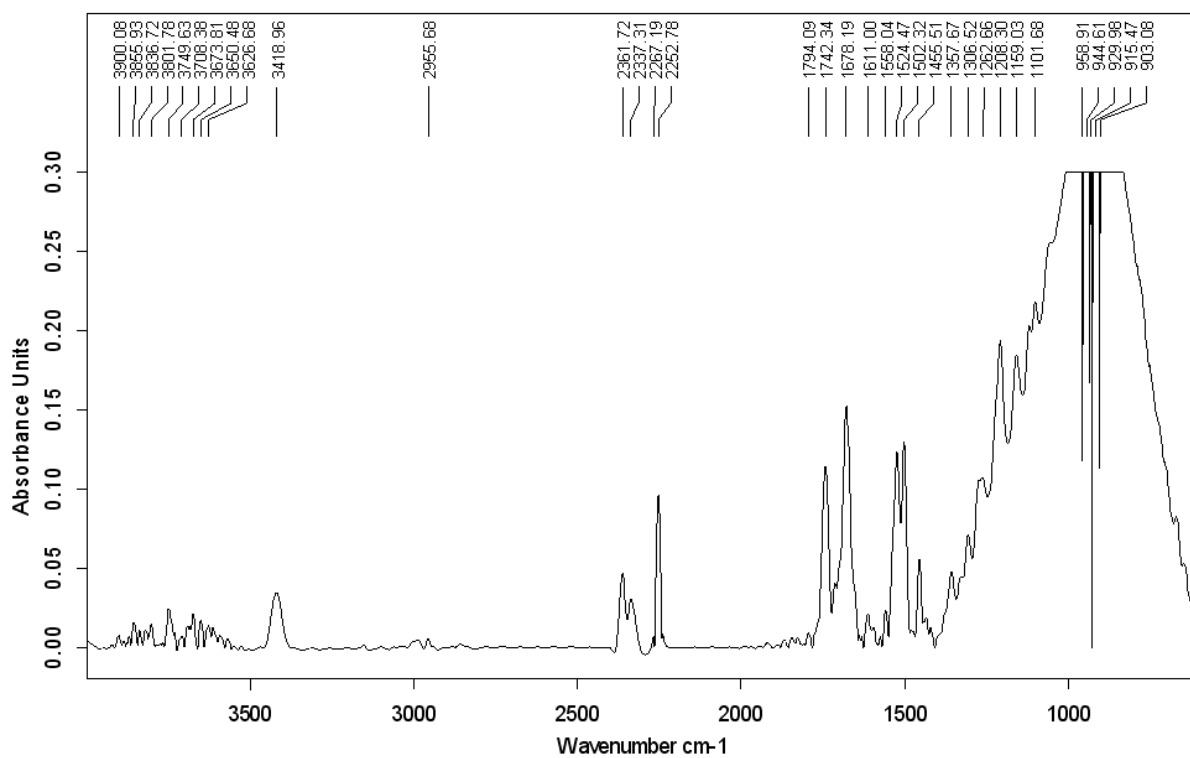
1. (S,S)-8



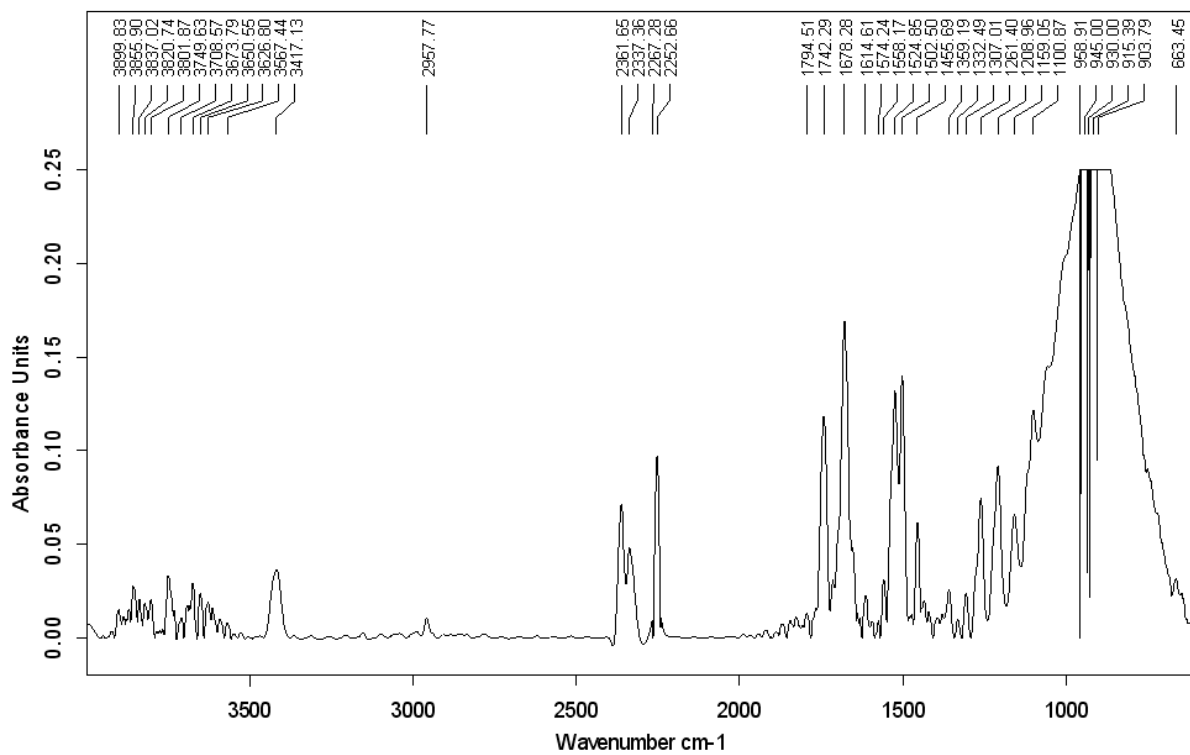
2. (R,S)-8



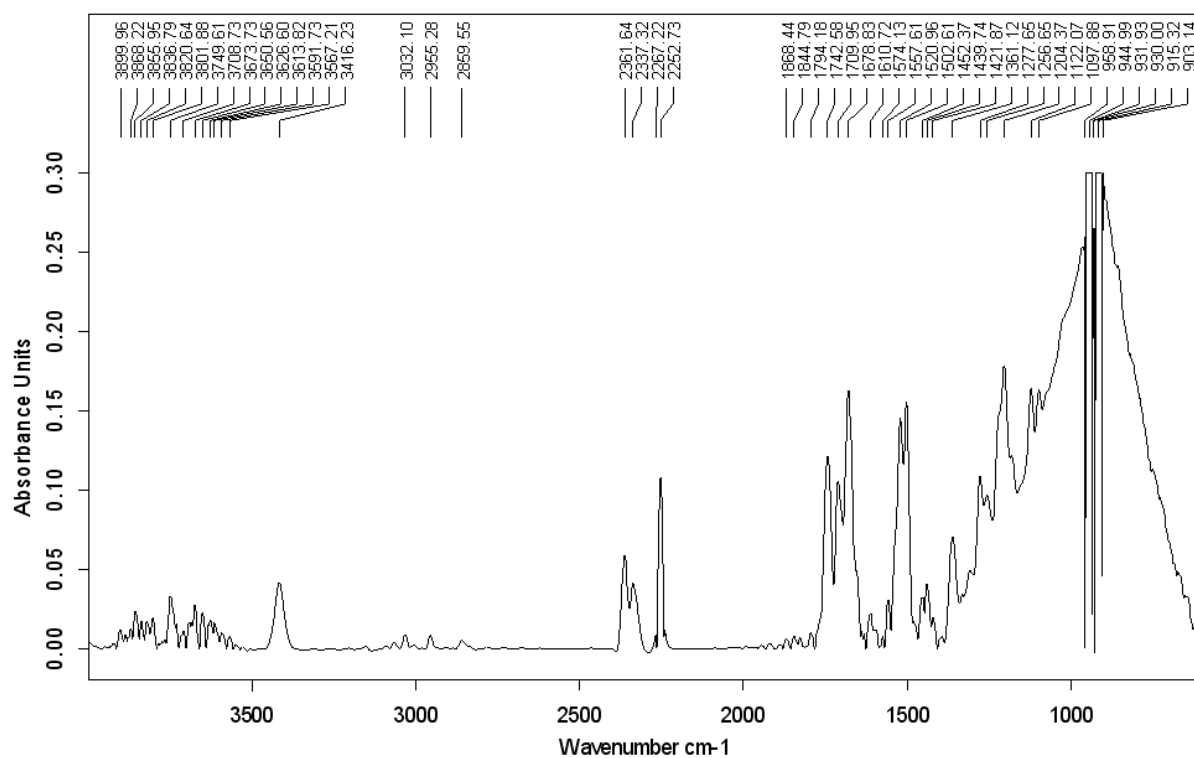
3. (S,S)-9



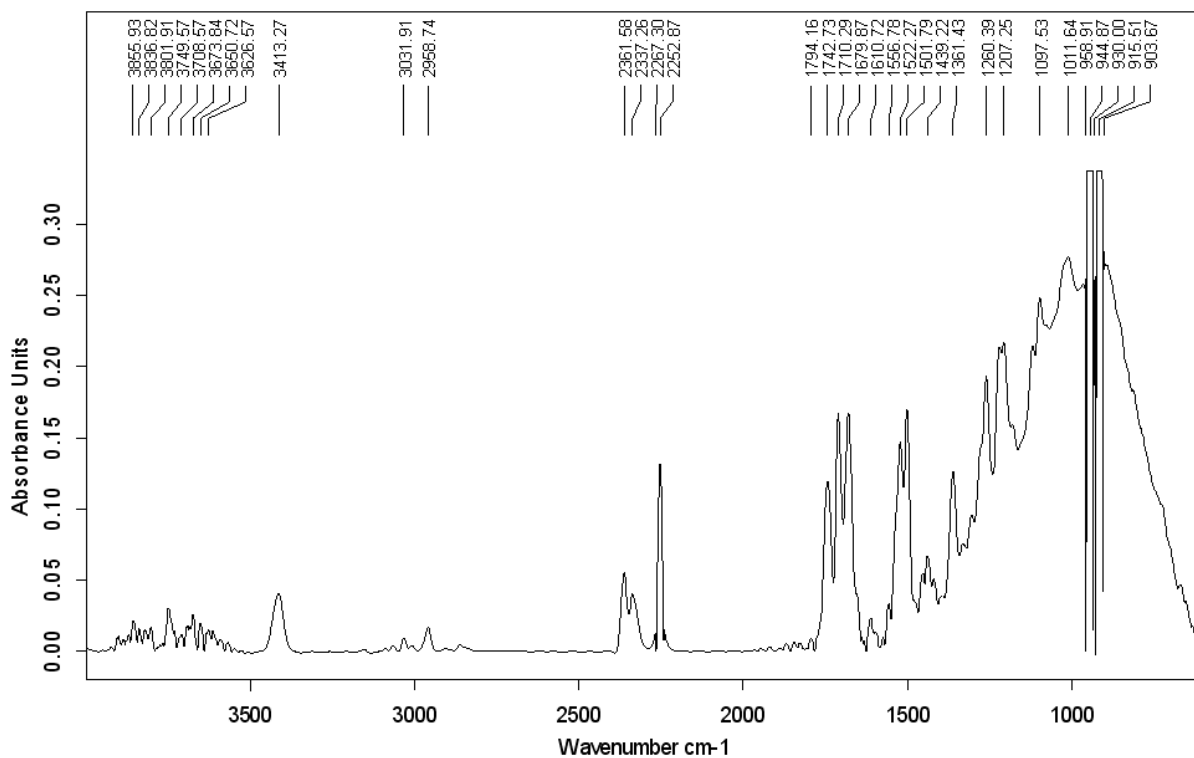
4. (R,S)-9



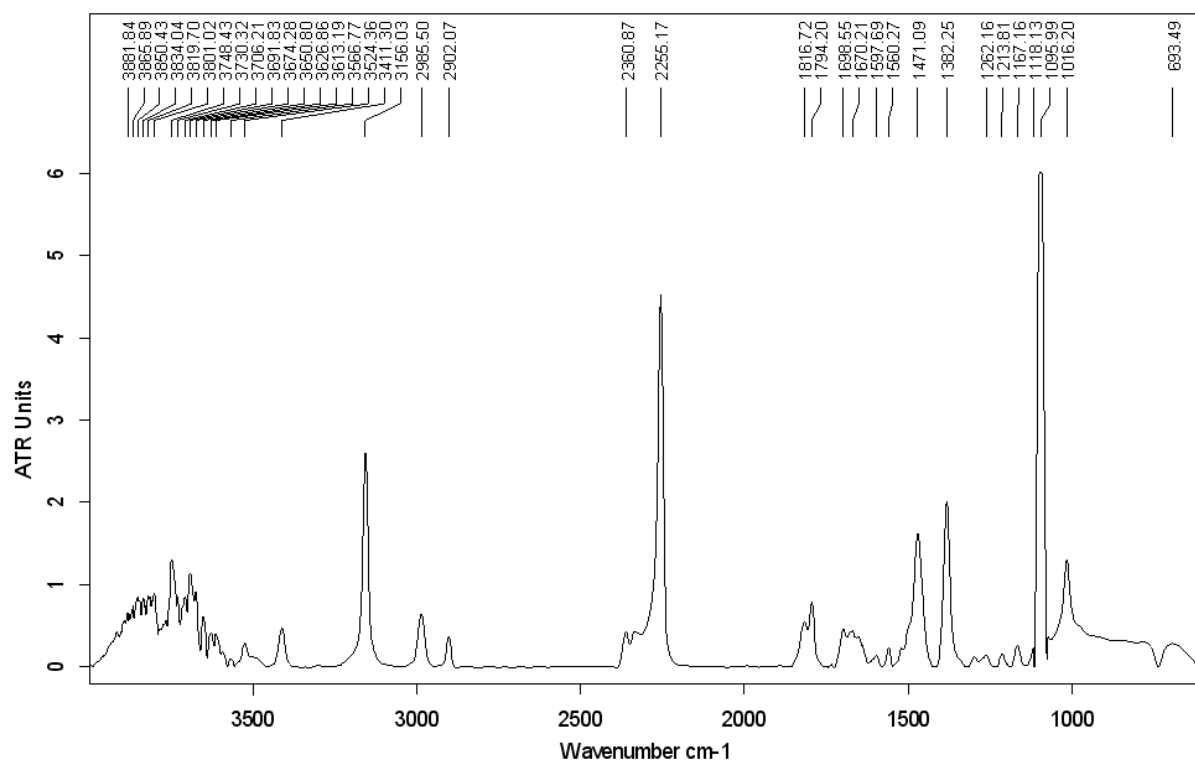
5. (S,S)-10



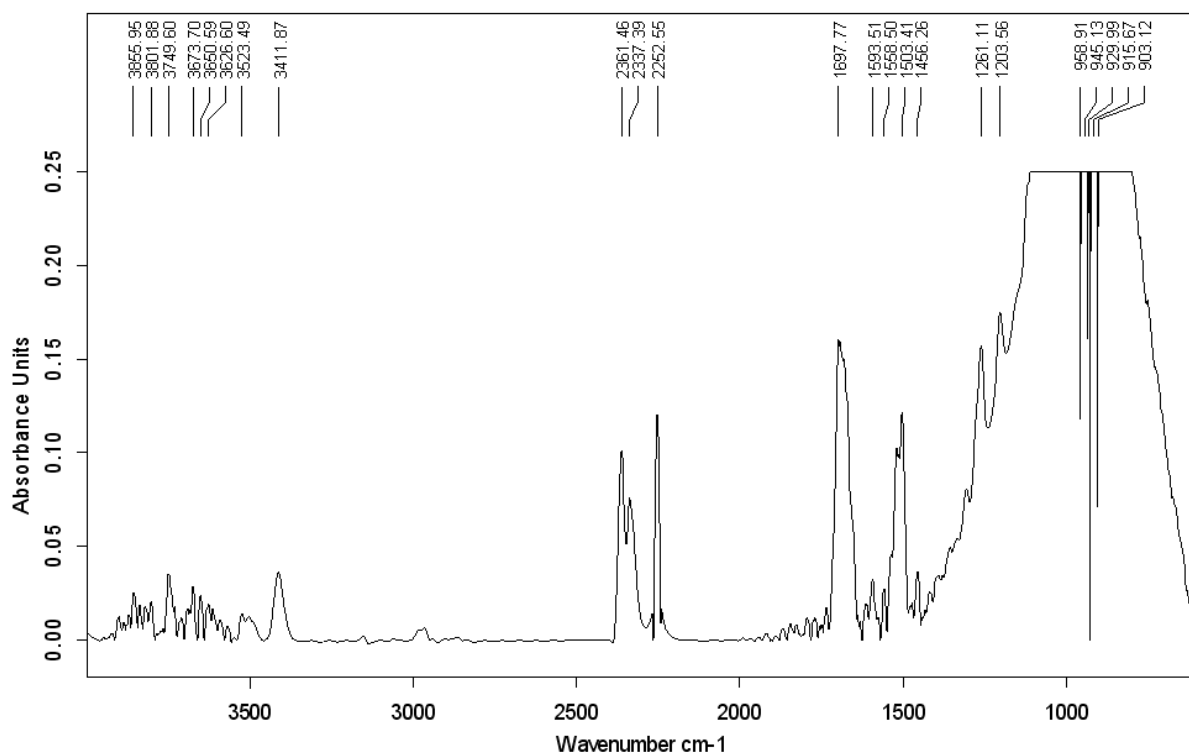
6. (R,S)-10



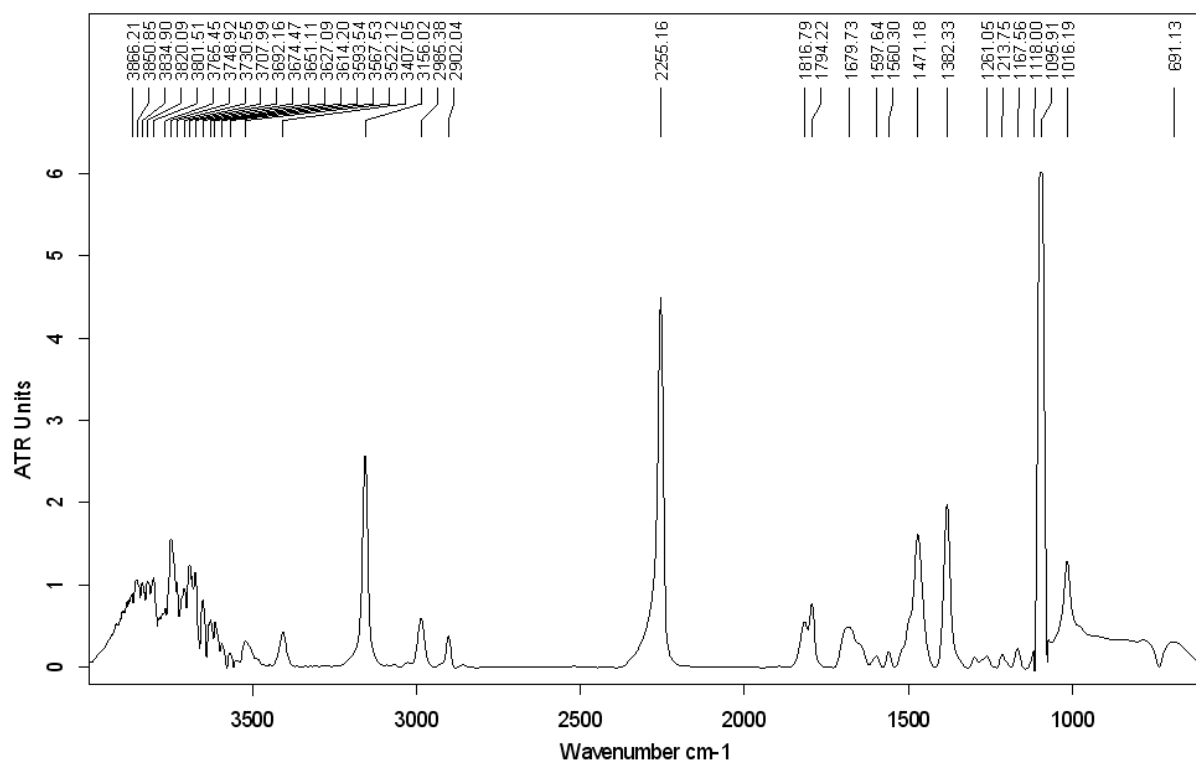
7. (S,S)-11



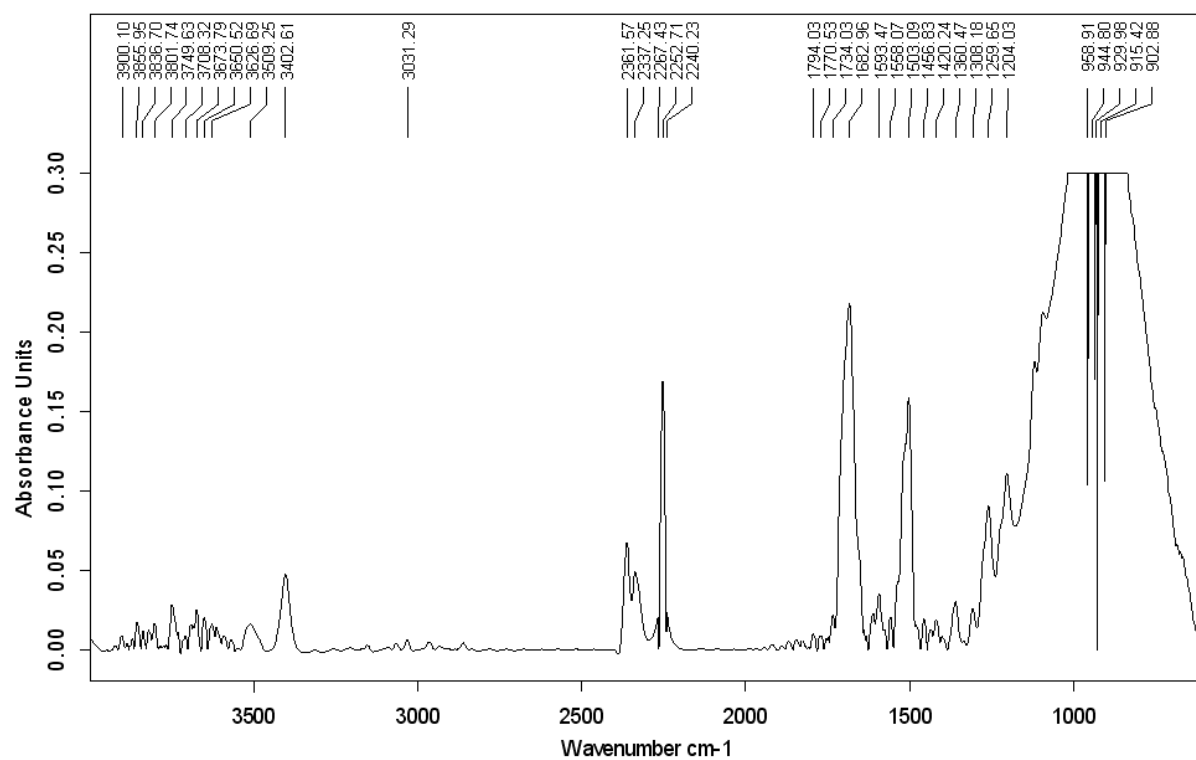
8. (R,S)-11



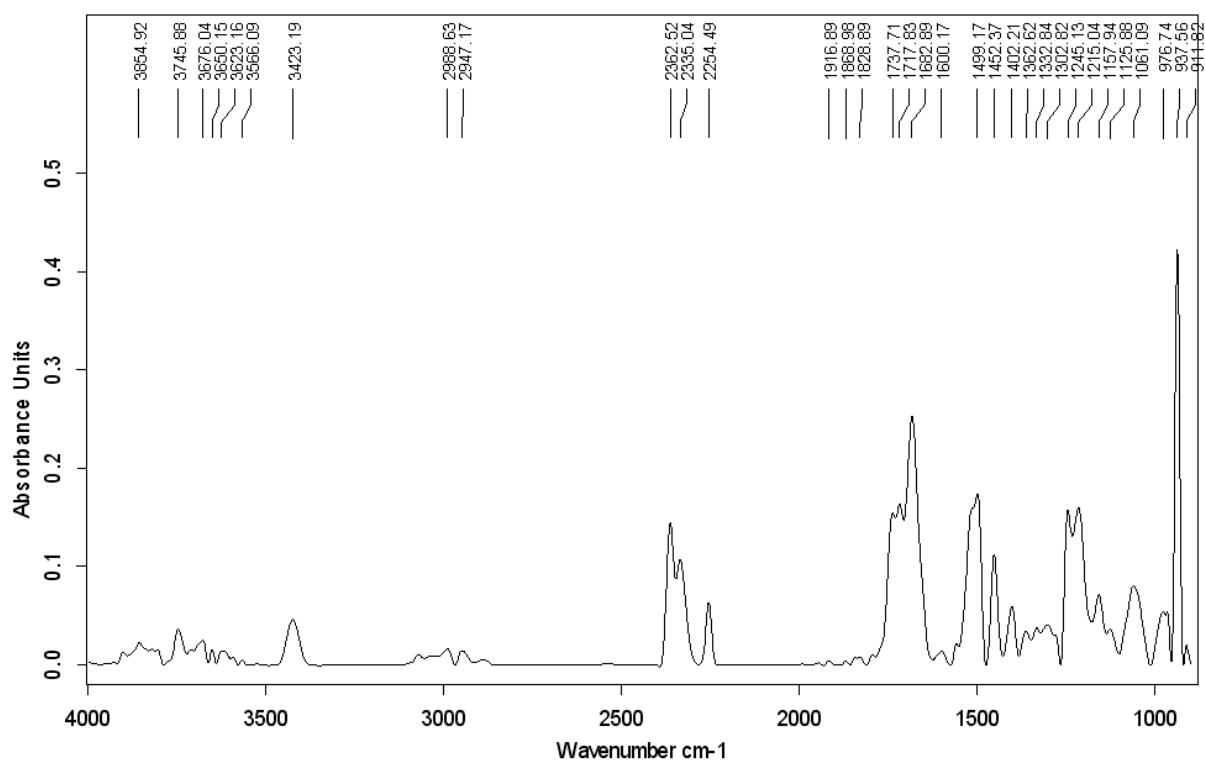
9. (S,S)-12



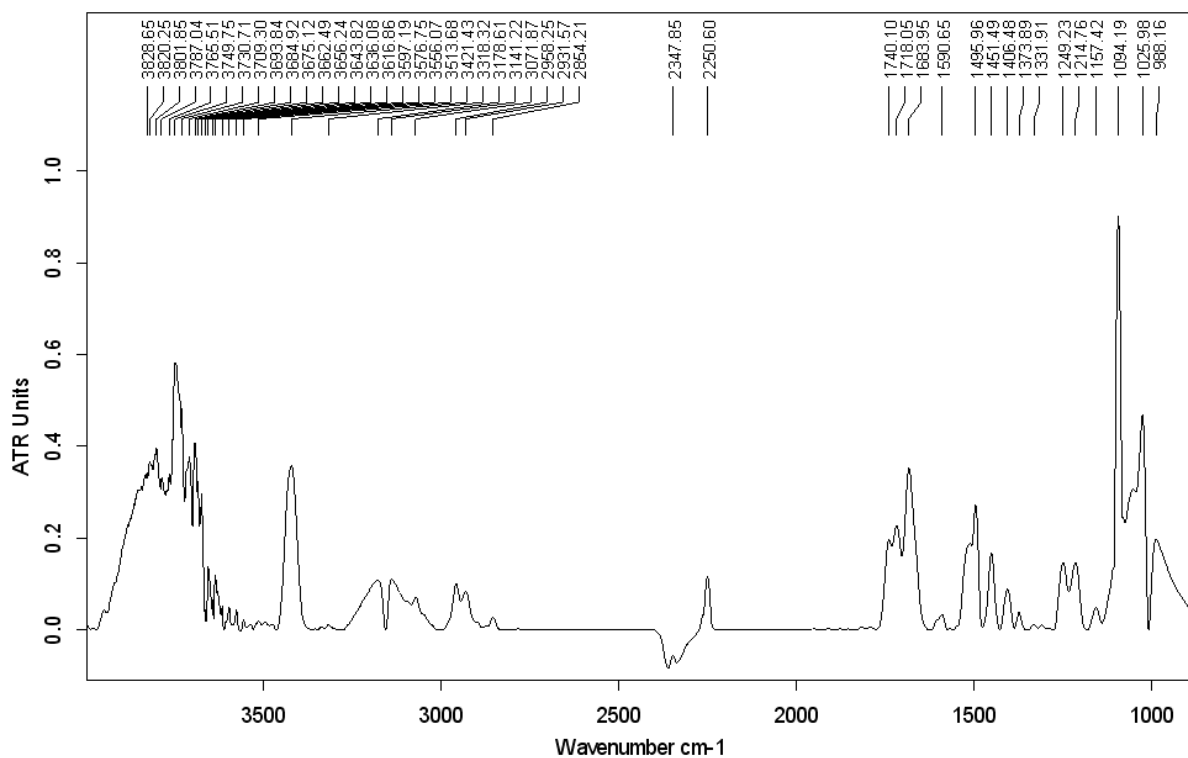
10. (R,S)-12



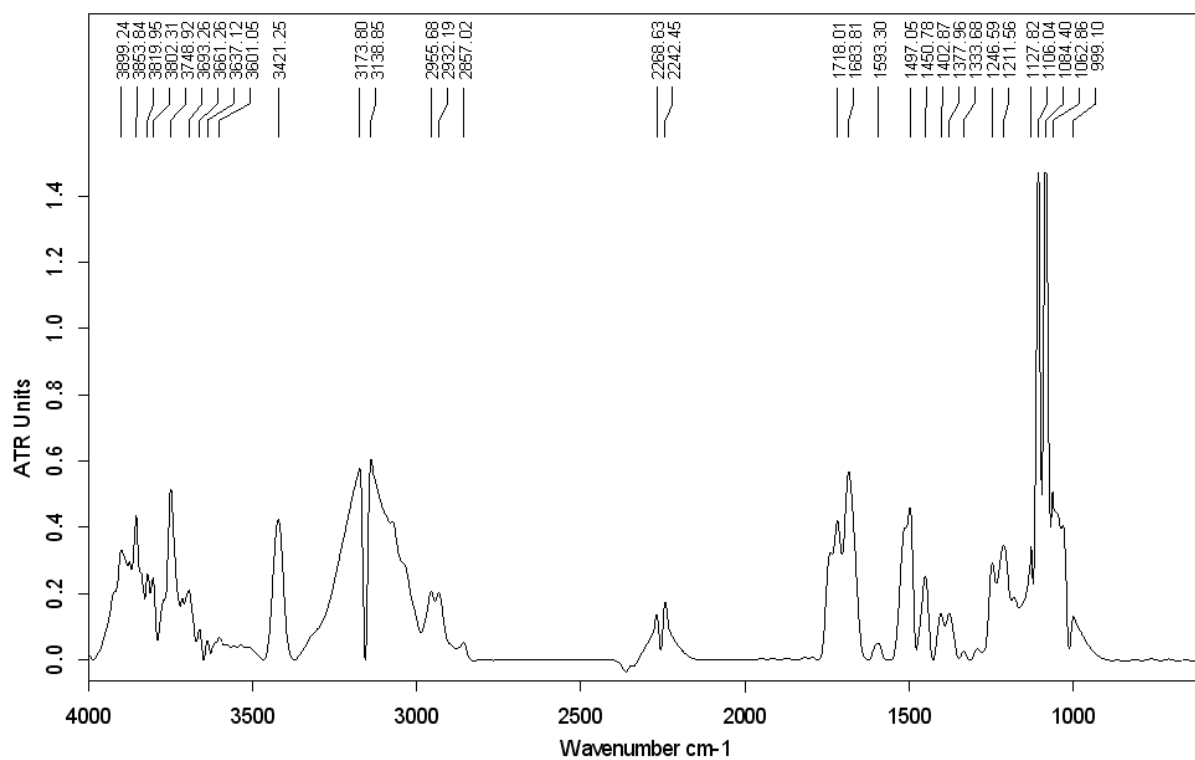
11. (S,S,S)-13



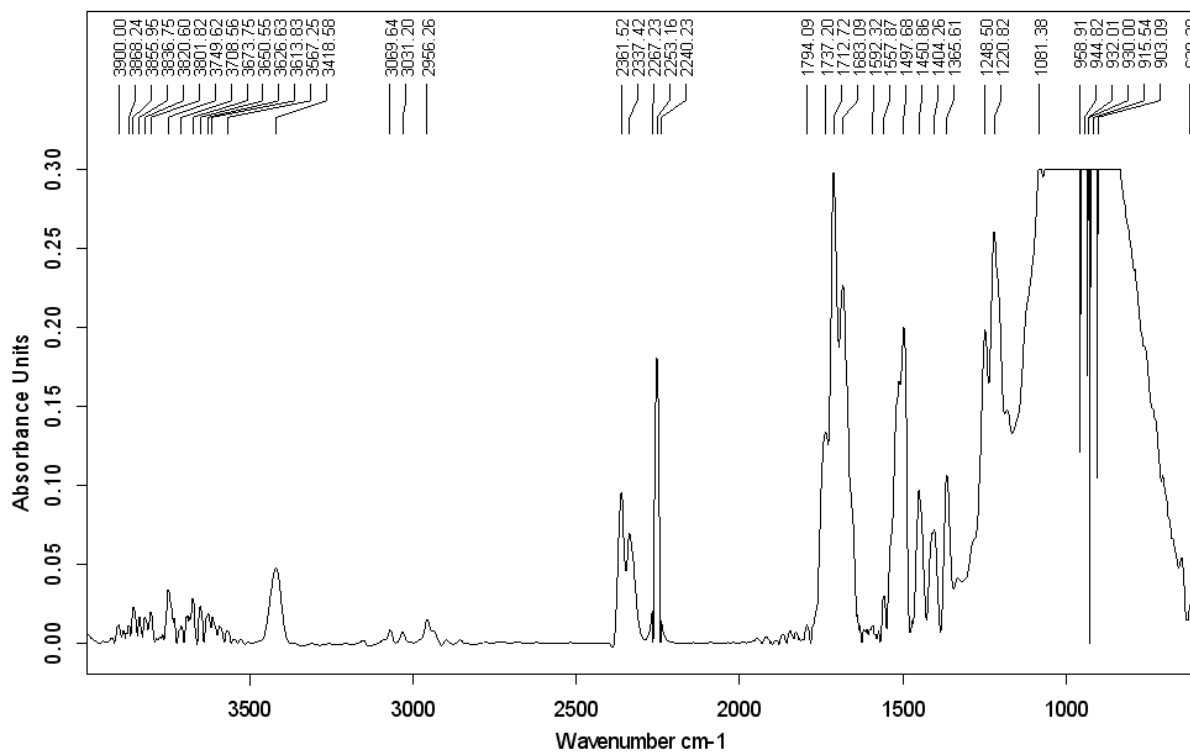
12. (S,R,S)-13



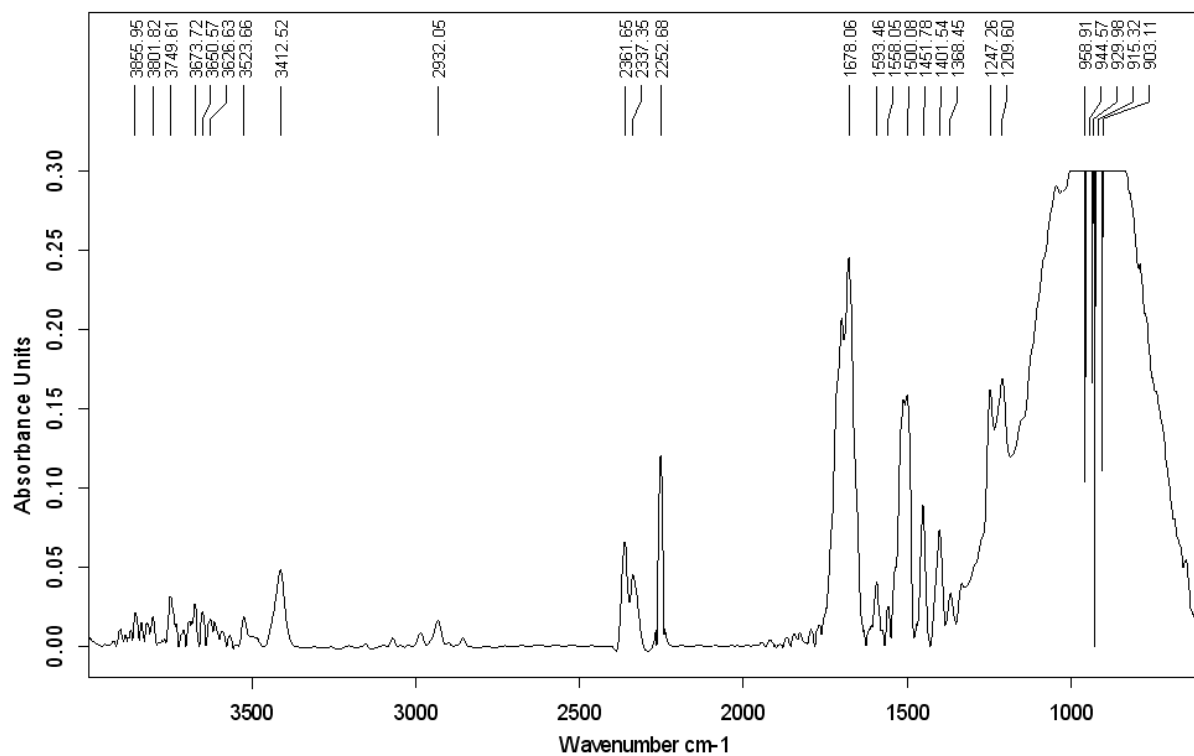
13. (S,S,S)-14



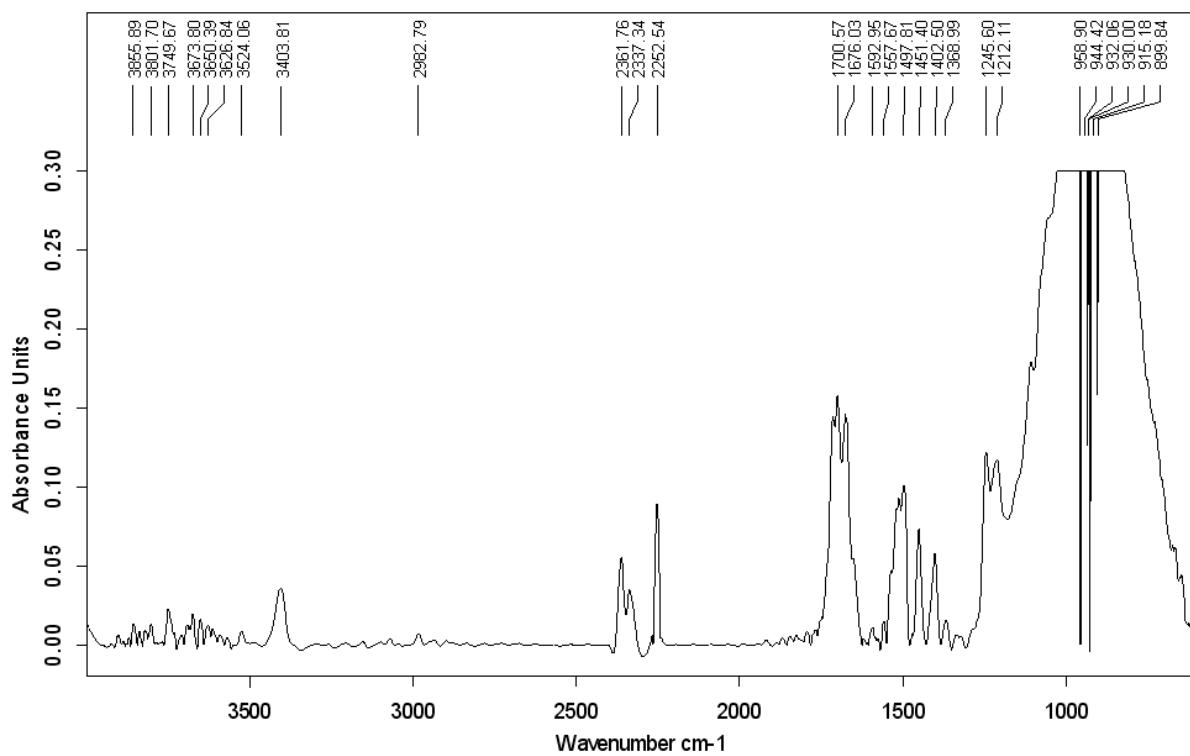
14. (S,R,S)-14



15. (S,S,S)-15



16. (S,R,S)-15

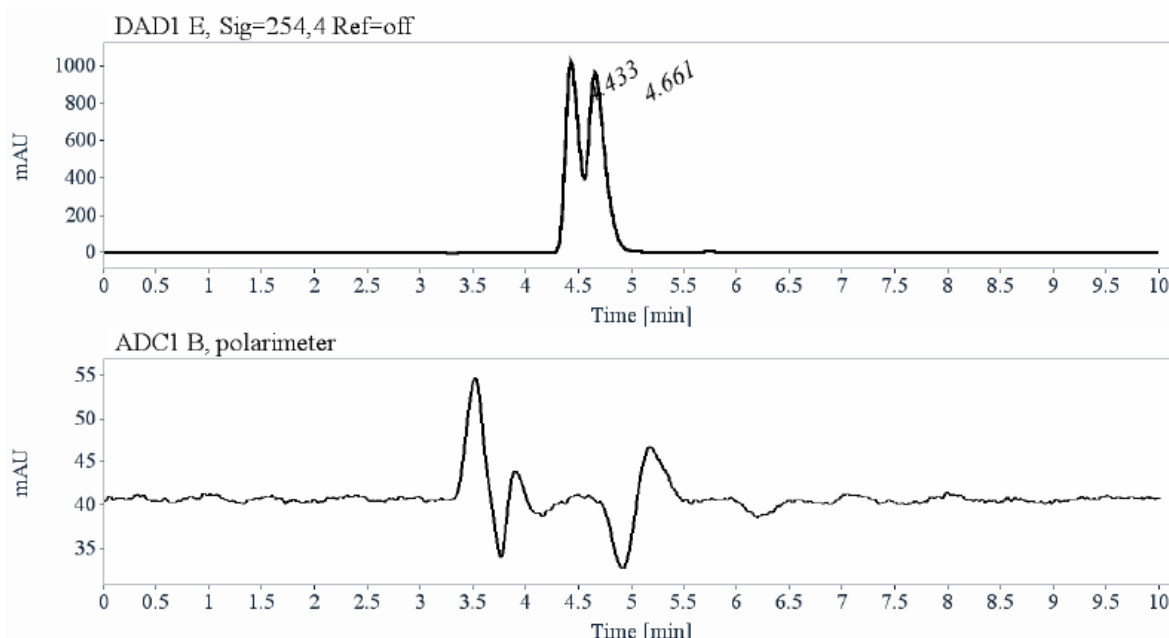


APPENDIX 3

SCREENING OF CHIRAL STATIONARY PHASES FOR HPLC ENANTIOSEPRATION OF ENANTIOPURE ETHYL 3,4-DIHYDRO-2*H*-1,4-BENZOXAZINE (SA1) AND ETHYL 2,3-DIBROMOPROPIONATE (SA2)

Chiral HPLC report

Sample name: SA1-rac
Column: Chiralpak ASH
Temperature:
Mobile phase: Heptane/Ethanol (70/30), 1 mL/min



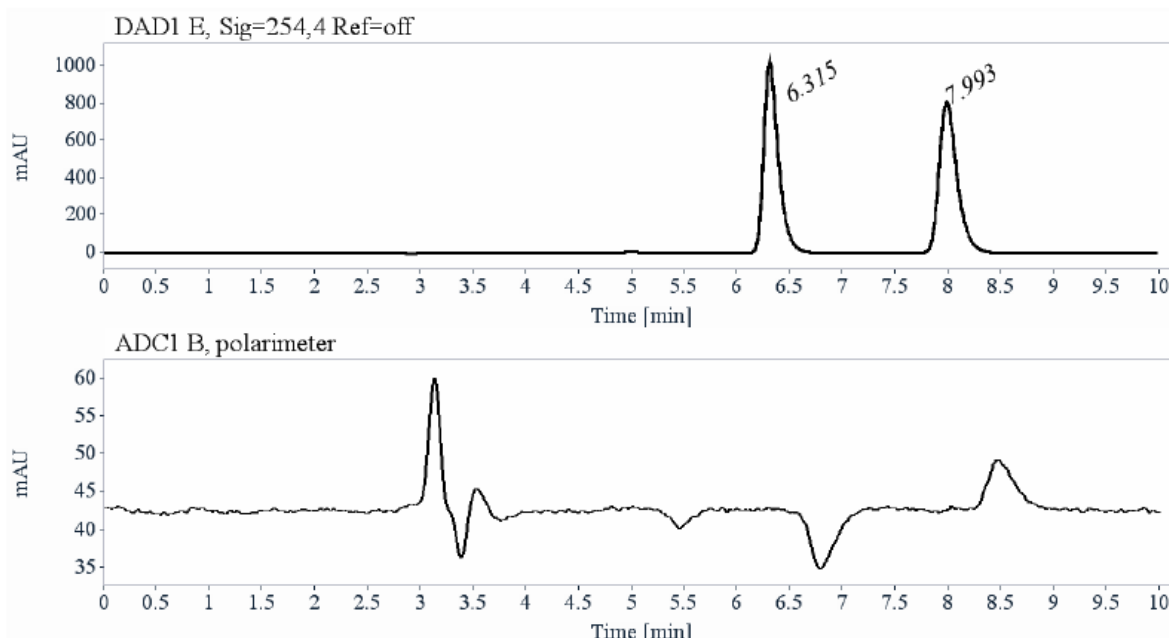
Signal: DAD1 E, Sig=254,4 Ref=off

RT [min]	Area	Area%	Capacity Factor	Enantioselectivity	Resolution (USP)
4.43	9028	45.94	0.50		
4.66	10622	54.06	0.58	1.15	0.82
Sum	19649	100.00			

Data file: C:\CHEM32\1\DATA\28-01-2019\SA1-RAC_ASH_4.D
Injection date: 1/28/2019 8:43:12 PM **Injection volume:** 20.000
Acq. method: E-30-CD254NM.M **Analysis method:** E-30-CD254NM-RAPSA1-B.M
Last changed: 1/29/2019 9:34:43 AM **Location:** Vial 83
Column void time (min): 2.950

Chiral HPLC report

Sample name: SA1-rac
Column: Chiralcel OD-3
Temperature:
Mobile phase: Heptane/Ethanol (70/30), 1 mL/min



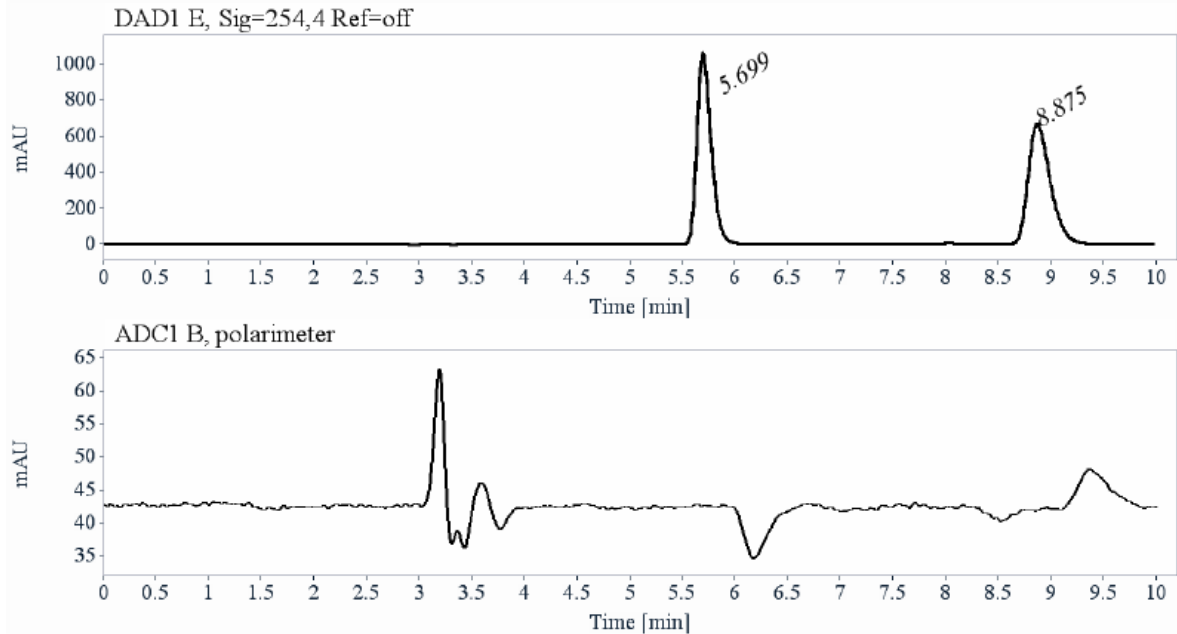
Signal: DAD1 E, Sig=254,4 Ref=off

RT [min]	Area	Area%	Capacity Factor	Enantioselectivity	Resolution (USP)
6.32	9968	50.65	1.14		
7.99	9710	49.35	1.71	1.50	6.08
Sum	19678	100.00			

Data file: C:\CHEM32\1\DATA\28-01-2019\SA1-RAC_OD3_4.D
Injection date: 1/28/2019 6:03:12 PM **Injection volume:** 20.000
Acq. method: E-30-CD254NM.M **Analysis method:** E-30-CD254NM-RAPSA1-B.M
Last changed: 1/29/2019 9:32:18 AM **Location:** Vial 83
Column void time (min) 2.950

Chiral HPLC report

Sample name: SA1-rac
Column: Lux-Cellulose-2
Temperature:
Mobile phase: Heptane/Ethanol (70/30), 1 mL/min



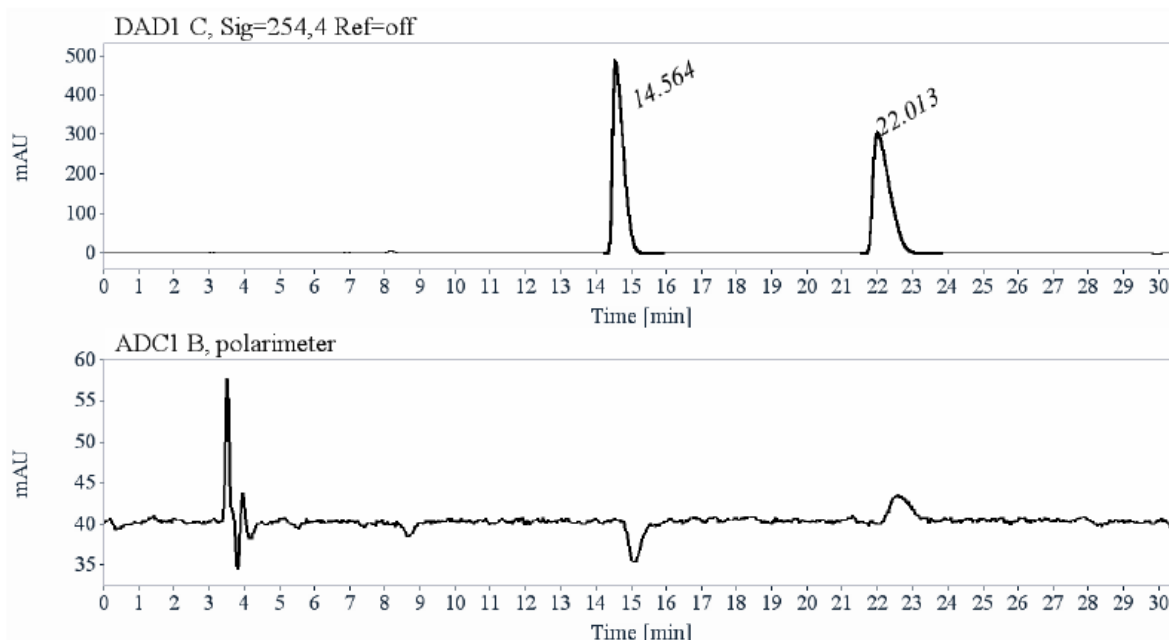
Signal: DAD1 E, Sig=254,4 Ref=off

RT [min]	Area	Area%	Capacity Factor	Enantioselectivity	Resolution (USP)
5.70	9982	50.63	0.93		
8.87	9734	49.37	2.01	2.16	10.09
Sum	19716	100.00			

Data file: C:\CHEM32\1\DATA\28-01-2019\SA1-RAC_LC2_4.D
Injection date: 1/28/2019 6:28:13 PM **Injection volume:** 20.000
Acq. method: E-30-CD254NM.M **Analysis method:** E-30-CD254NM-RAPSA1-B.M
Last changed: 1/29/2019 9:33:00 AM **Location:** Vial 83
Column void time (min) 2.950

Chiral HPLC report

Sample name: SA1-rac
Column: Lux-Cellulose-3
Temperature:
Mobile phase: Heptane/Ethanol (70/30), 1 mL/min



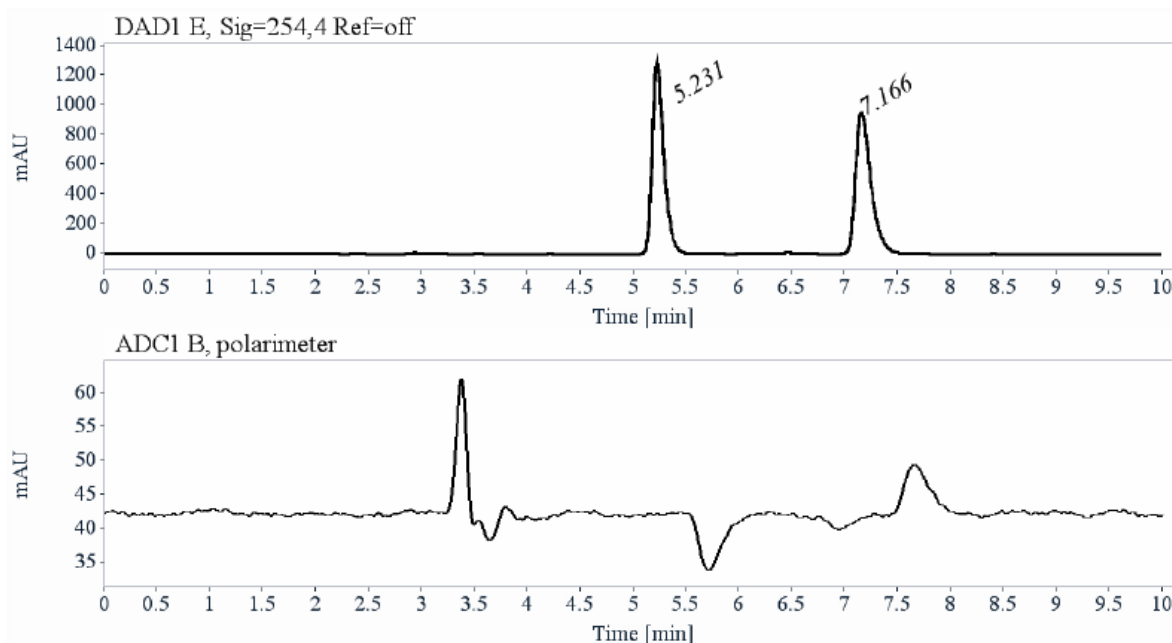
Signal: DAD1 C, Sig=254,4 Ref=off

RT [min]	Area	Area%	Capacity Factor	Enantioselectivity	Resolution (USP)
14.56	10267	50.69	3.94		
22.01	9989	49.31	6.46	1.64	10.06
Sum	20256	100.00			

Data file: C:\CHEM32\1\DATA\28-01-2019\SA1-RAC_LC3_4.D
Injection date: 1/29/2019 1:48:34 AM **Injection volume:** 20.000
Acq. method: E-30-CD254NM-45MIN.M **Analysis method:** E-30-CD254NM-RAPSA1-B.M
Last changed: 1/29/2019 9:40:33 AM **Location:** Vial 83
Column void time (min) 2.950

Chiral HPLC report

Sample name: SA1-rac
Column: Lux-Cellulose-4
Temperature:
Mobile phase: Heptane/Ethanol (70/30), 1 mL/min



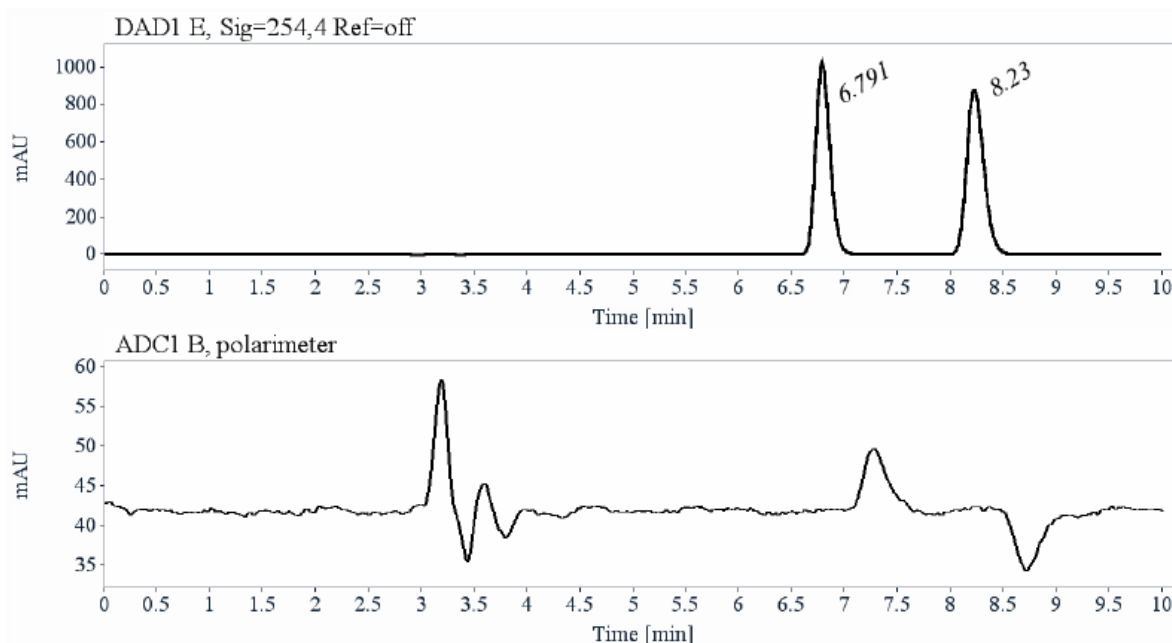
Signal: DAD1 E, Sig=254,4 Ref=off

RT [min]	Area	Area%	Capacity Factor	Enantioselectivity	Resolution (USP)
5.23	9960	50.57	0.77		
7.17	9734	49.43	1.43	1.85	8.43
Sum	19694	100.00			

Data file: C:\CHEM32\1\DATA\28-01-2019\SA1-RAC_LC4_4.D
Injection date: 1/28/2019 6:53:13 PM **Injection volume:** 20.000
Acq. method: E-30-CD254NM.M **Analysis method:** E-30-CD254NM-RAPSA1-B.M
Last changed: 1/29/2019 9:33:00 AM **Location:** Vial 83
Column void time (min) 2.950

Chiral HPLC report

Sample name: SA1-rac
Column: Lux-Amylose-1
Temperature:
Mobile phase: Heptane/Ethanol (70/30), 1 mL/min



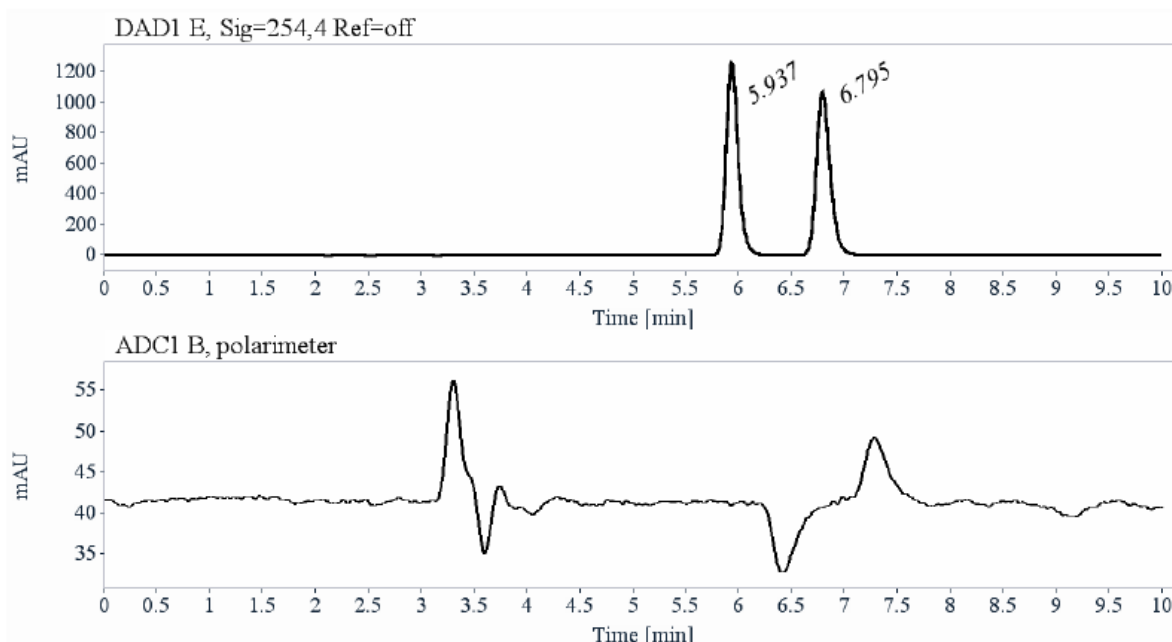
Signal: DAD1 E, Sig=254,4 Ref=off

RT [min]	Area	Area%	Capacity Factor	Enantioselectivity	Resolution (USP)
6.79	9676	49.16	1.30		
8.23	10008	50.84	1.79	1.37	5.23
Sum	19685	100.00			

Data file: C:\CHEM32\1\DATA\28-01-2019\SA1-RAC_LUXA1_4.D
Injection date: 1/28/2019 7:18:14 PM **Injection volume:** 20.000
Acq. method: E-30-CD254NM.M **Analysis method:** E-30-CD254NM-RAPSA1-B.M
Last changed: 1/29/2019 9:33:00 AM **Location:** Vial 83
Column void time (min): 2.950

Chiral HPLC report

Sample name: SA1-rac
Column: Lux-Amylose-2
Temperature:
Mobile phase: Heptane/Ethanol (70/30), 1 mL/min



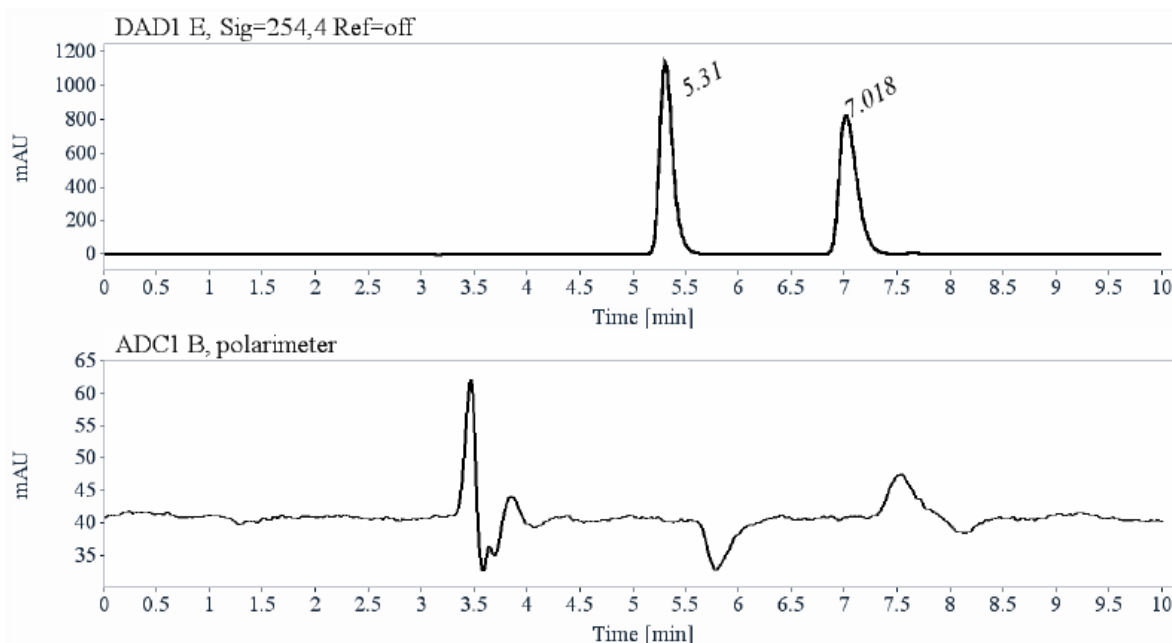
Signal: DAD1 E, Sig=254,4 Ref=off

RT [min]	Area	Area%	Capacity Factor	Enantioselectivity	Resolution (USP)
5.94	9958	50.68	1.01		
6.79	9689	49.32	1.30	1.29	3.89
Sum	19647	100.00			

Data file: C:\CHEM32\1\DATA\28-01-2019\SA1-RAC_LA2_4.D
Injection date: 1/28/2019 7:43:12 PM **Injection volume:** 20.000
Acq. method: E-30-CD254NM.M **Analysis method:** E-30-CD254NM-RAPSA1-B.M
Last changed: 1/29/2019 9:33:00 AM **Location:** Vial 83
Column void time (min) 2.950

Chiral HPLC report

Sample name: SA1-rac
Column: Chiralpak AZ-H
Temperature:
Mobile phase: Heptane/Ethanol (70/30), 1 mL/min



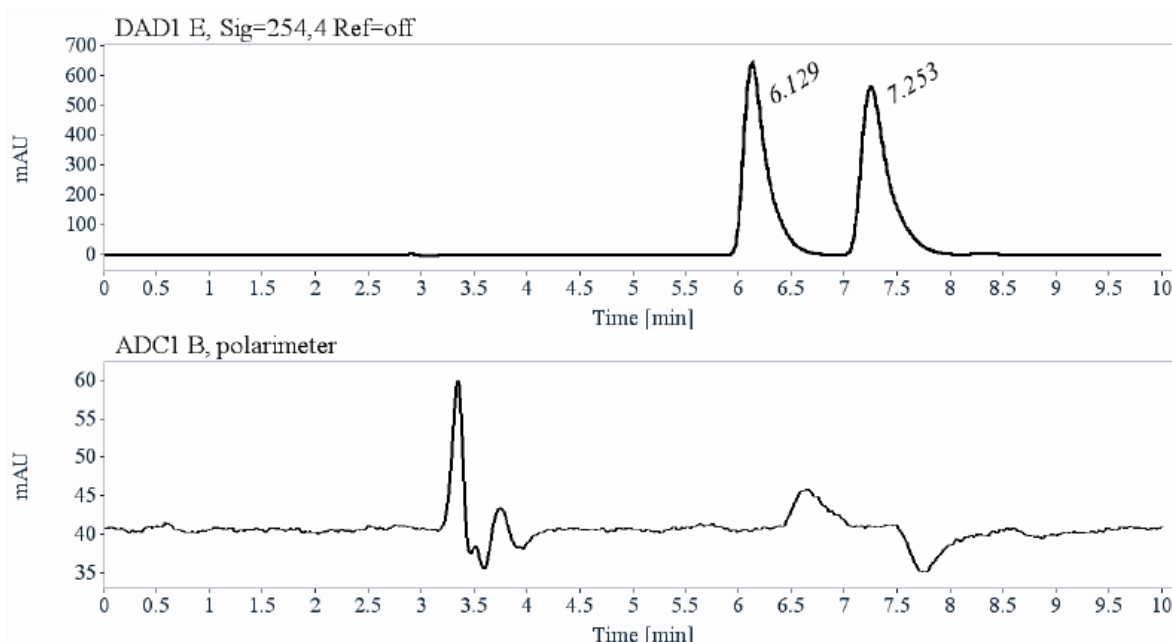
Signal: DAD1 E, Sig=254,4 Ref=off

RT [min]	Area	Area%	Capacity Factor	Enantioselectivity	Resolution (USP)
5.31	9951	50.77	0.80		
7.02	9648	49.23	1.38	1.72	6.38
Sum	19599	100.00			

Data file: C:\CHEM32\1\DATA\28-01-2019\SA1-RAC_AZH_4.D
Injection date: 1/28/2019 8:08:12 PM **Injection volume:** 20.000
Acq. method: E-30-CD254NM.M **Analysis method:** E-30-CD254NM-RAPSA1-B.M
Last changed: 1/29/2019 9:34:43 AM **Location:** Vial 83
Column void time (min) 2.950

Chiral HPLC report

Sample name: SA1-rac
Column: Chiralpak IA
Temperature:
Mobile phase: Heptane/Ethanol (70/30), 1 mL/min



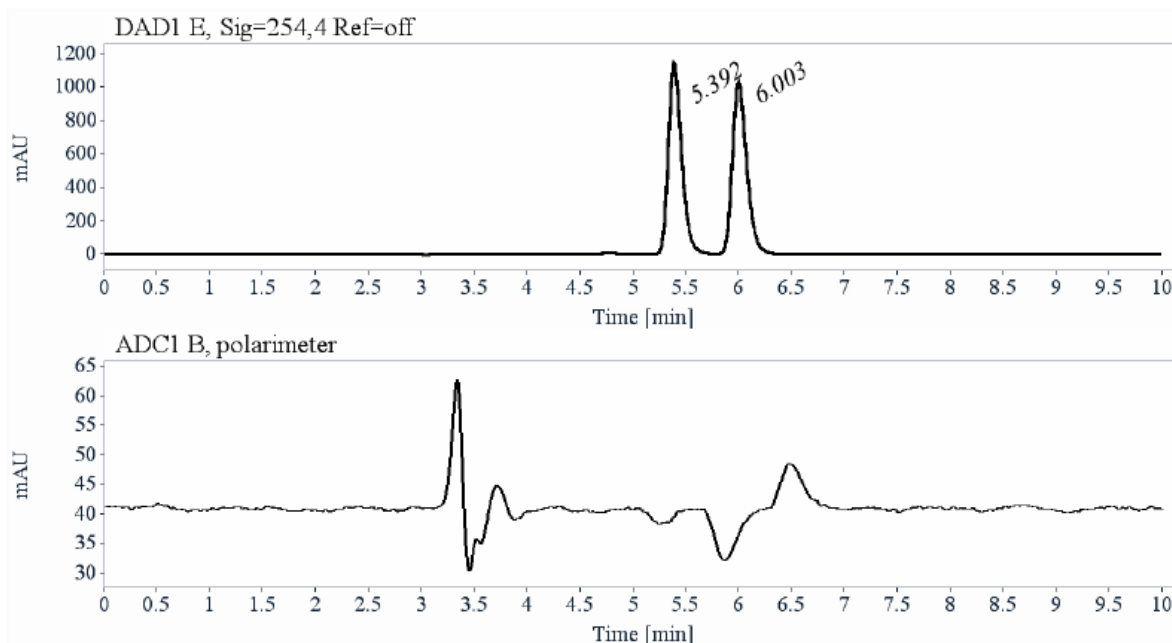
Signal: DAD1 E, Sig=254,4 Ref=off

RT [min]	Area	Area%	Capacity Factor	Enantioselectivity	Resolution (USP)
6.13	9732	49.29	1.08		
7.25	10014	50.71	1.46	1.35	2.85
Sum	19745	100.00			

Data file: C:\CHEM32\1\DATA\28-01-2019\SA1-RAC_IA_4.D
Injection date: 1/28/2019 9:18:17 PM **Injection volume:** 20.000
Acq. method: E-30-CD254NM.M **Analysis method:** E-30-CD254NM-RAPSA1-B.M
Last changed: 1/29/2019 9:34:43 AM **Location:** Vial 83
Column void time (min): 2.950

Chiral HPLC report

Sample name: SA1-rac
Column: Chiralpak IB
Temperature:
Mobile phase: Heptane/Ethanol (70/30), 1 mL/min



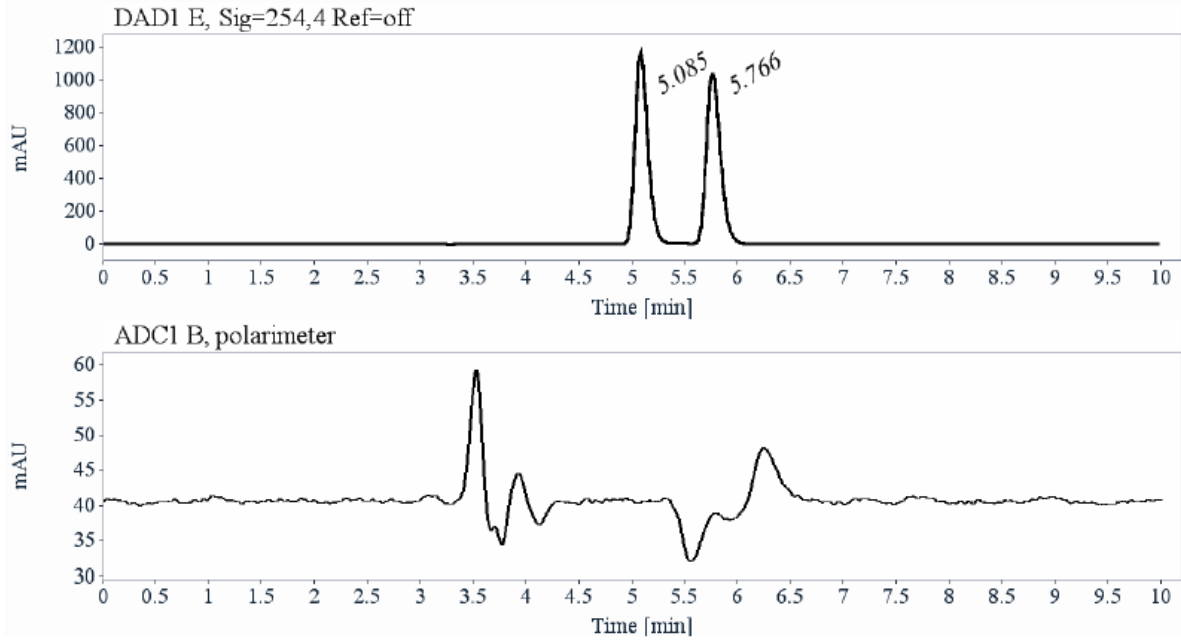
Signal: DAD1 E, Sig=254,4 Ref=off

RT [min]	Area	Area%	Capacity Factor	Enantioselectivity	Resolution (USP)
5.39	9985	50.80	0.83		
6.00	9671	49.20	1.03	1.25	2.60
Sum	19656	100.00			

Data file: C:\CHEM32\1\DATA\28-01-2019\SA1-RAC_IB_4.D
Injection date: 1/28/2019 9:53:19 PM **Injection volume:** 20.000
Acq. method: E-30-CD254NM.M **Analysis method:** E-30-CD254NM-RAPSA1-B.M
Last changed: 1/29/2019 9:34:43 AM **Location:** Vial 83
Column void time (min): 2.950

Chiral HPLC report

Sample name: SA1-rac
Column: Chiralpak IC
Temperature:
Mobile phase: Heptane/Ethanol (70/30), 1 mL/min



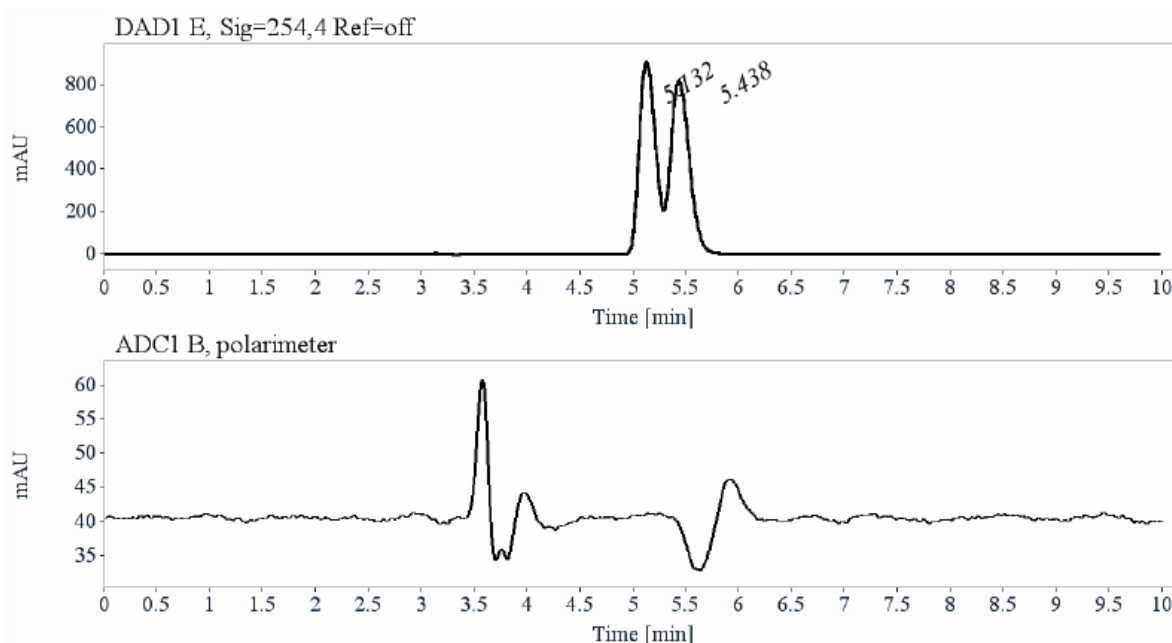
Signal: DAD1 E, Sig=254,4 Ref=off

RT [min]	Area	Area%	Capacity Factor	Enantioselectivity	Resolution (USP)
5.09	9905	50.67	0.72		
5.77	9642	49.33	0.95	1.32	2.90
Sum	19547	100.00			

Data file: C:\CHEM32\1\DATA\28-01-2019\SA1-RAC_IC_4.D
Injection date: 1/28/2019 10:28:18 PM **Injection volume:** 20.000
Acq. method: E-30-CD254NM.M **Analysis method:** E-30-CD254NM-RAPSA1-B.M
Last changed: 1/29/2019 9:34:43 AM **Location:** Vial 83
Column void time (min) 2.950

Chiral HPLC report

Sample name: SA1-rac
Column: Chiralpak ID
Temperature:
Mobile phase: Heptane/Ethanol (70/30), 1 mL/min



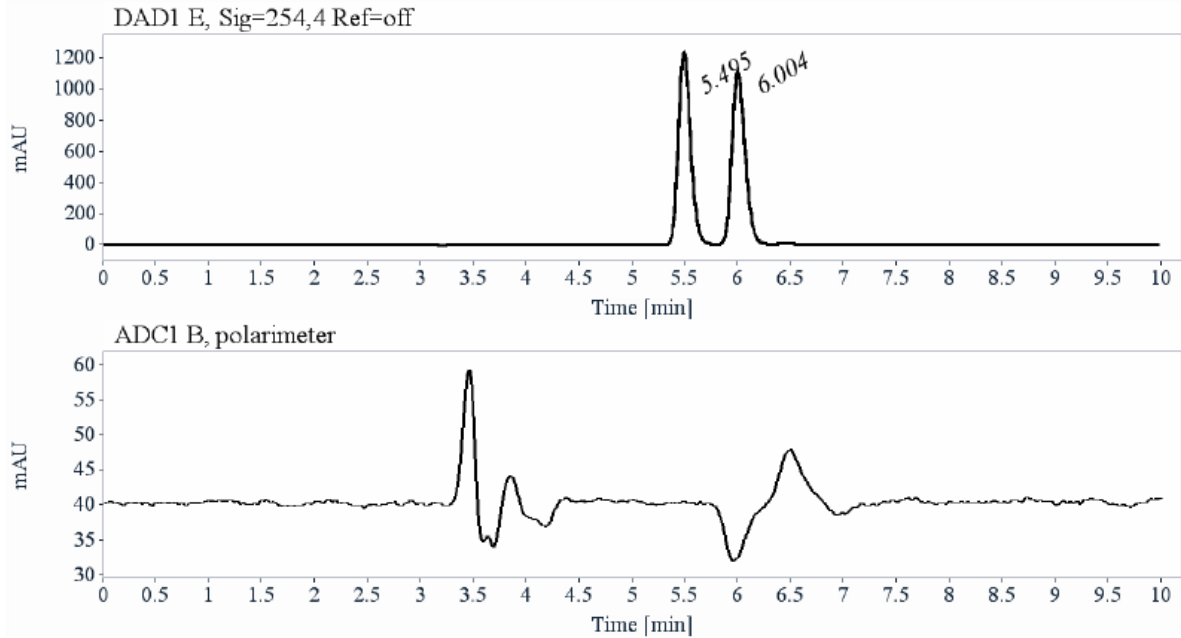
Signal: DAD1 E, Sig=254,4 Ref=off

RT [min]	Area	Area%	Capacity Factor	Enantioselectivity	Resolution (USP)
5.13	9730	48.96	0.74		
5.44	10143	51.04	0.84	1.14	0.98
Sum	19872	100.00			

Data file: C:\CHEM32\1\DATA\28-01-2019\SA1-RAC_ID_4.D
Injection date: 1/28/2019 11:03:20 PM **Injection volume:** 20.000
Acq. method: E-30-CD254NM.M **Analysis method:** E-30-CD254NM-RAPSA1-B.M
Last changed: 1/29/2019 9:34:43 AM **Location:** Vial 83
Column void time (min) 2.950

Chiral HPLC report

Sample name: SA1-rac
Column: Chiralpak IE
Temperature:
Mobile phase: Heptane/Ethanol (70/30), 1 mL/min



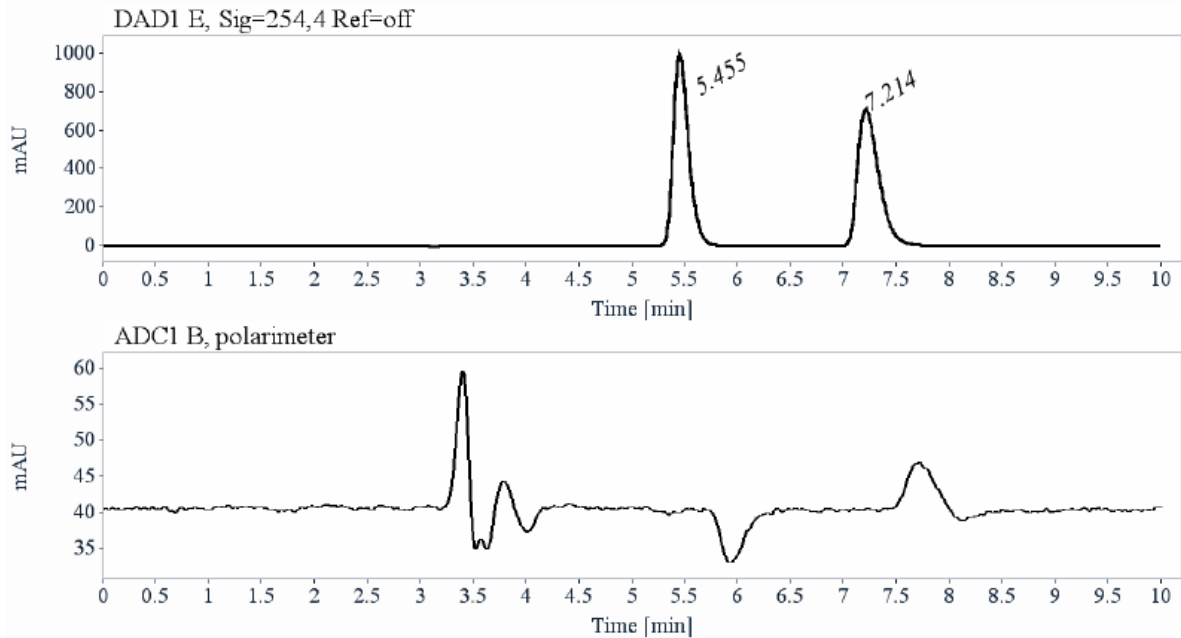
Signal: DAD1 E, Sig=254,4 Ref=off

RT [min]	Area	Area%	Capacity Factor	Enantioselectivity	Resolution (USP)
5.49	9970	50.78	0.86		
6.00	9664	49.22	1.04	1.20	2.30
Sum	19634	100.00			

Data file: C:\CHEM32\1\DATA\28-01-2019\SA1-RAC_IE_4.D
Injection date: 1/28/2019 11:38:21 PM **Injection volume:** 20.000
Acq. method: E-30-CD254NM.M **Analysis method:** E-30-CD254NM-RAPSA1-B.M
Last changed: 1/29/2019 9:34:43 AM **Location:** Vial 83
Column void time (min) 2.950

Chiral HPLC report

Sample name: SA1-rac
Column: Chiralpak IF
Temperature:
Mobile phase: Heptane/Ethanol (70/30), 1 mL/min



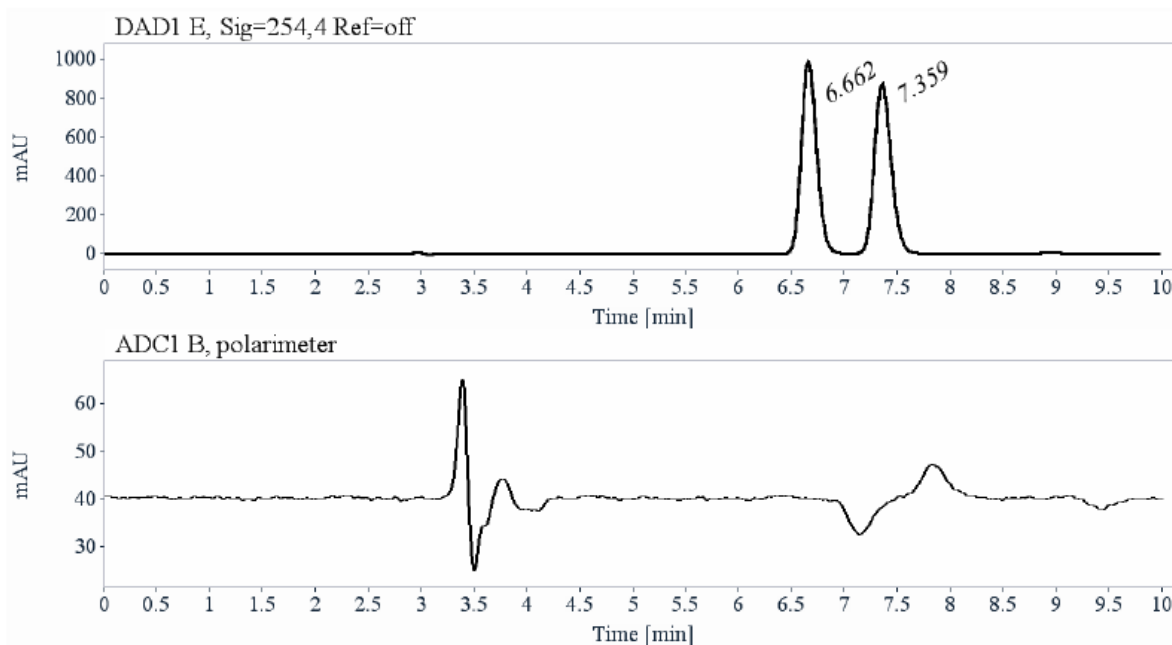
Signal: DAD1 E, Sig=254,4 Ref=off

RT [min]	Area	Area%	Capacity Factor	Enantioselectivity	Resolution (USP)
5.45	10057	50.48	0.85		
7.21	9865	49.52	1.45	1.70	5.60
Sum	19922	100.00			

Data file: C:\CHEM32\1\DATA\28-01-2019\SA1-RAC_IF_4.D
Injection date: 1/29/2019 12:13:23 AM **Injection volume:** 20.000
Acq. method: E-30-CD254NM.M **Analysis method:** E-30-CD254NM-RAPSA1-B.M
Last changed: 1/29/2019 9:34:43 AM **Location:** Vial 83
Column void time (min) 2.950

Chiral HPLC report

Sample name: SA1-rac
Column: Chiralpak IG
Temperature:
Mobile phase: Heptane/Ethanol (70/30), 1 mL/min



Signal: DAD1 E, Sig=254,4 Ref=off

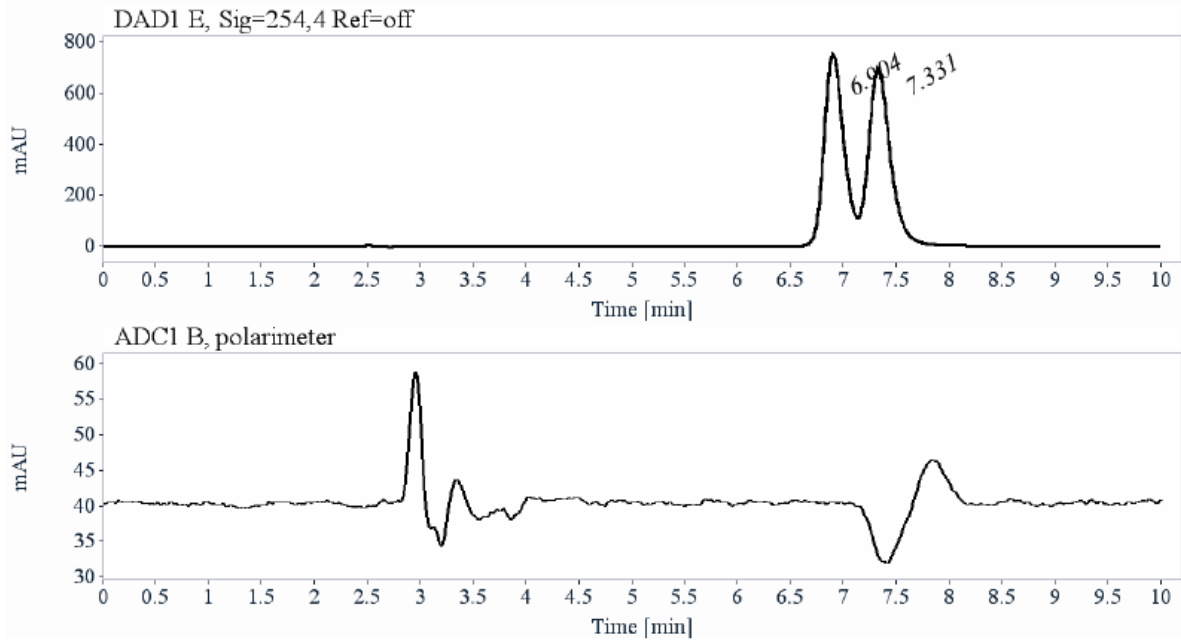
RT [min]	Area	Area%	Capacity Factor	Enantioselectivity	Resolution (USP)
6.66	10068	50.73	1.26		
7.36	9777	49.27	1.49	1.19	2.46
Sum	19845	100.00			

Data file: C:\CHEM32\1\DATA\28-01-2019\SA1-RAC_IG_4.D
Injection date: 1/29/2019 12:48:24 AM
Acq. method: E-30-CD254NM.M
Last changed: 1/29/2019 9:34:43 AM
Column void time (min): 2.950

Injection volume: 20.000
Analysis method: E-30-CD254NM-RAPSA1-B.M
Location: Vial 83

Chiral HPLC report

Sample name: SA1-rac
Column: (S,S)-Whelk-O1
Temperature:
Mobile phase: Heptane/Ethanol (70/30), 1 mL/min



Signal: DAD1 E, Sig=254,4 Ref=off

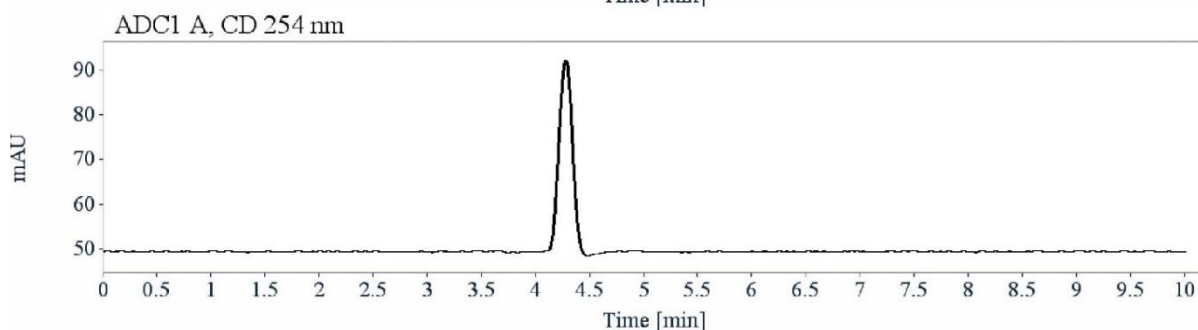
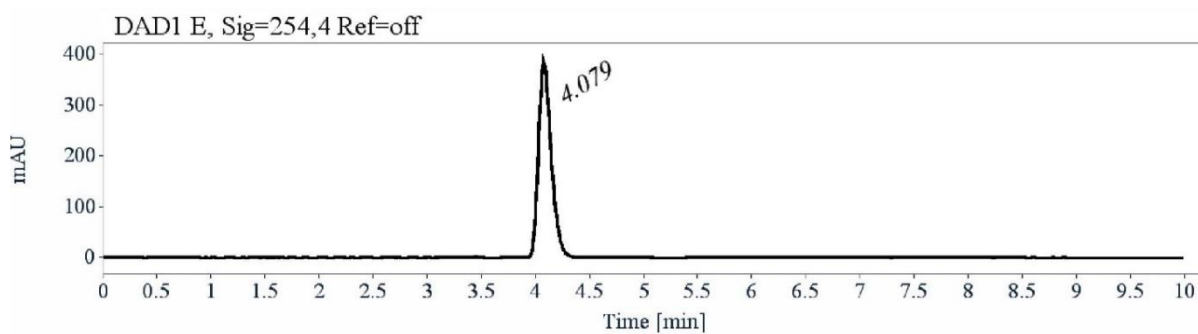
RT [min]	Area	Area%	Capacity Factor	Enantioselectivity	Resolution (USP)
6.90	9774	49.30	1.34		
7.33	10052	50.70	1.49	1.11	1.20
Sum	19826	100.00			

Data file: C:\CHEM32\1\DATA\28-01-2019\SA1-RAC_WHELK_4.D
Injection date: 1/29/2019 1:23:25 AM
Acq. method: E-30-CD254NM.M
Last changed: 1/29/2019 9:34:43 AM
Column void time (min): 2.950

Injection volume: 20.000
Analysis method: E-30-CD254NM-RAPSA1-B.M
Location: Vial 83

Chiral HPLC report

Sample name: SA2
Column: Chiralpak ASH
Temperature:
Mobile phase: Heptane/ethanol (98/2), 1 mL/min



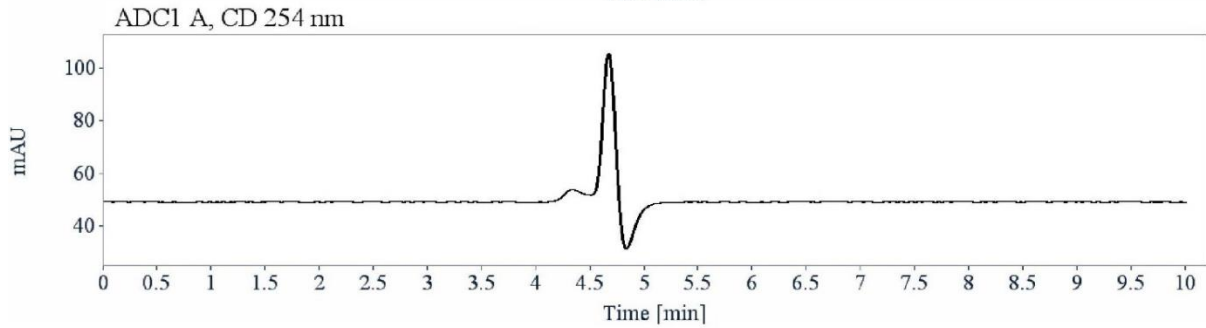
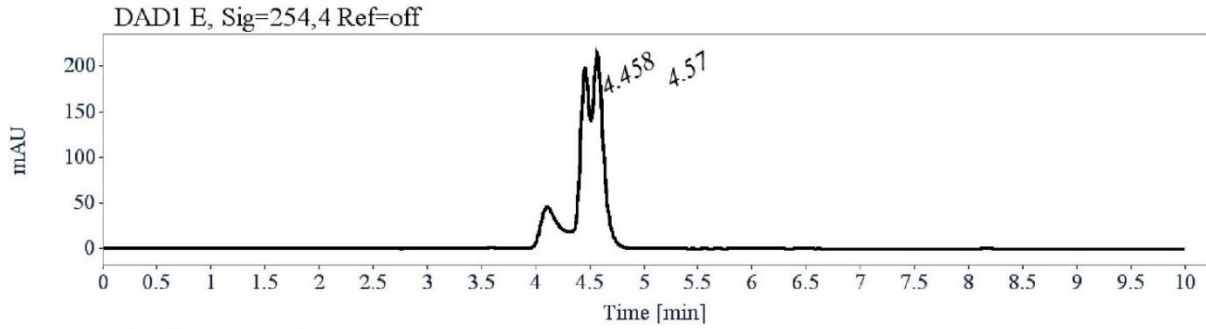
Signal: DAD1 E, Sig=254,4 Ref=off

RT [min]	Area	Area%	Capacity Factor	Enantioselectivity	Resolution (USP)
4.08	3202	100.00	0.38		
Sum	3202	100.00			

Data file: C:\CHEM32\1\DATA\ACHERAR\SA2\SA2_ASH_8.D
Injection date: 10/19/2018 7:28:54 PM
Acq. method: E-2-CD254NM.M
Last changed: 1/28/2019 10:13:40 AM
Column void time (min): 2.950
Injection volume: 20.000
Analysis method: E-2-CD254NM.M
Location: Vial 20

Chiral HPLC report

Sample name: SA2
Column: Chiralcel OD-3
Temperature:
Mobile phase: Heptane/ethanol (98/2), 1 mL/min



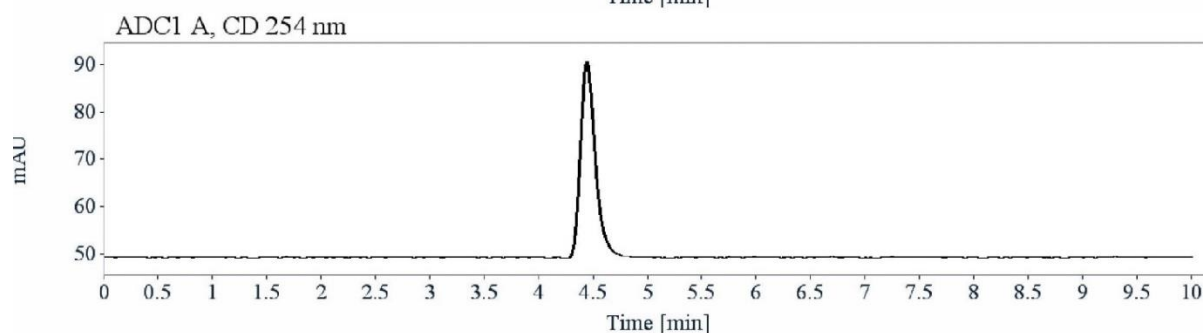
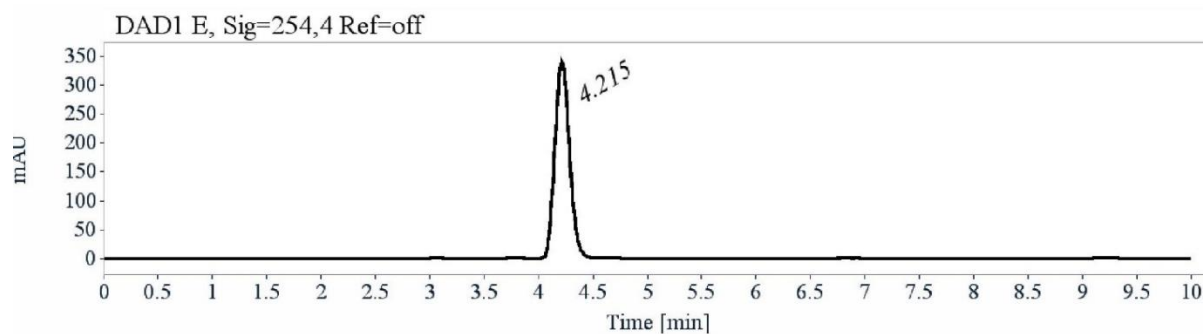
Signal: DAD1 E, Sig=254,4 Ref=off

RT [min]	Area	Area%	Capacity Factor	Enantioselectivity	Resolution (USP)
4.46	1192	44.13	0.51		
4.57	1509	55.87	0.55	1.07	0.52
Sum	2701	100.00			

Data file: C:\CHEM32\1\DATA\ACHERAR\SA2\SA2_OD3_7.D
Injection date: 10/19/2018 3:36:39 PM **Injection volume:** 20.000
Acq. method: E-2-CD254NM.M **Analysis method:** E-2-CD254NM.M
Last changed: 1/28/2019 10:13:40 AM **Location:** Vial 20
Column void time (min): 2.950

Chiral HPLC report

Sample name: SA2
Column: Lux-Cellulose-2
Temperature:
Mobile phase: Heptane/ethanol (98/2), 1 mL/min



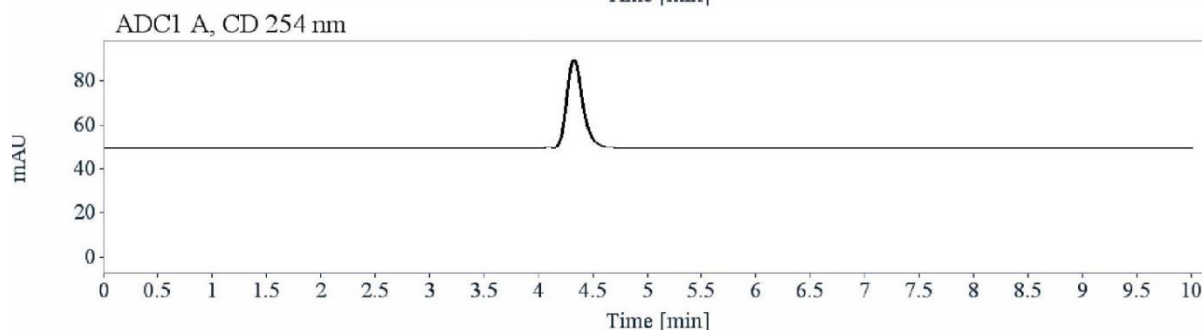
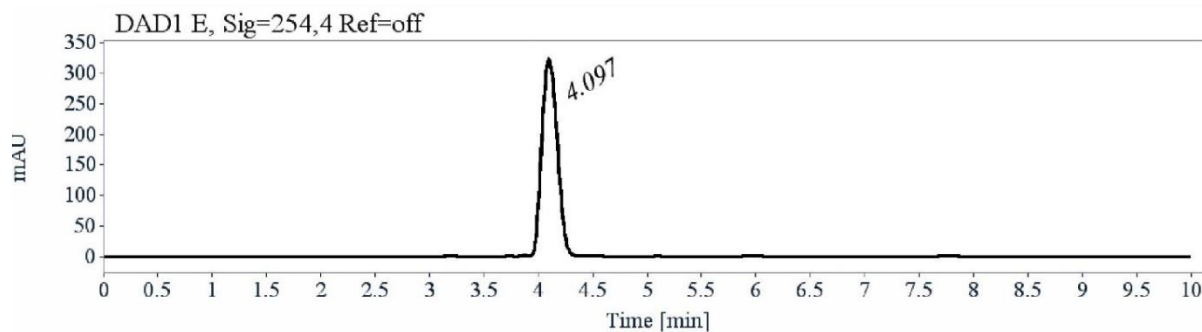
Signal: DAD1 E, Sig=254,4 Ref=off

RT [min]	Area	Area%	Capacity Factor	Enantioselectivity	Resolution (USP)
4.22	3213	100.00	0.43		
Sum	3213	100.00			

Data file: C:\CHEM32\1\DATA\ACHERAR\SA2\SA2_LC2_7.D
Injection date: 10/19/2018 4:00:10 PM
Acq. method: E-2-CD254NM.M
Last changed: 1/28/2019 10:13:40 AM
Column void time (min): 2.950
Injection volume: 20.000
Analysis method: E-2-CD254NM.M
Location: Vial 20

Chiral HPLC report

Sample name: SA2
Column: Lux-Cellulose-4
Temperature:
Mobile phase: Heptane/ethanol (98/2), 1 mL/min



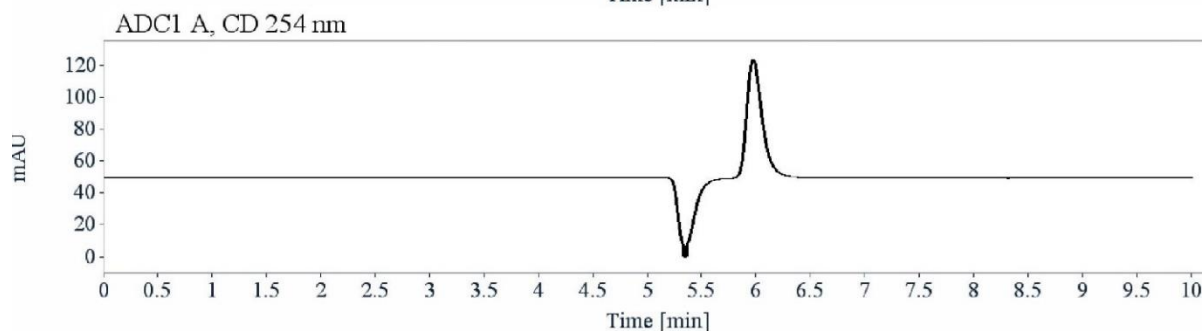
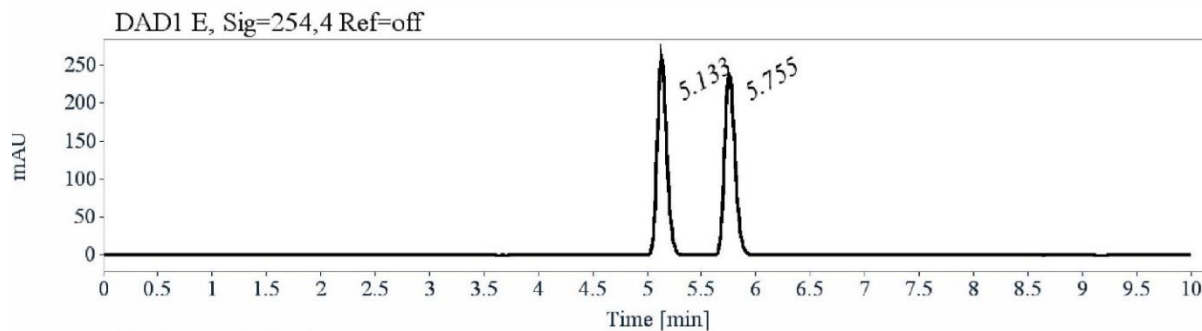
Signal: DAD1 E, Sig=254,4 Ref=off

RT [min]	Area	Area%	Capacity Factor	Enantioselectivity	Resolution (USP)
4.10	3210	100.00	0.39		
Sum	3210	100.00			

Data file: C:\CHEM32\1\DATA\ACHERAR\SA2\SA2_LC4_8.D
Injection date: 10/19/2018 5:55:00 PM
Acq. method: E-2-CD254NM.M
Last changed: 1/28/2019 10:13:40 AM
Column void time (min): 2.950
Injection volume: 20.000
Analysis method: E-2-CD254NM.M
Location: Vial 20

Chiral HPLC report

Sample name: SA2
Column: Lux-Amylose-1
Temperature:
Mobile phase: Heptane/ethanol (98/2), 1 mL/min



Signal: DAD1 E, Sig=254,4 Ref=off

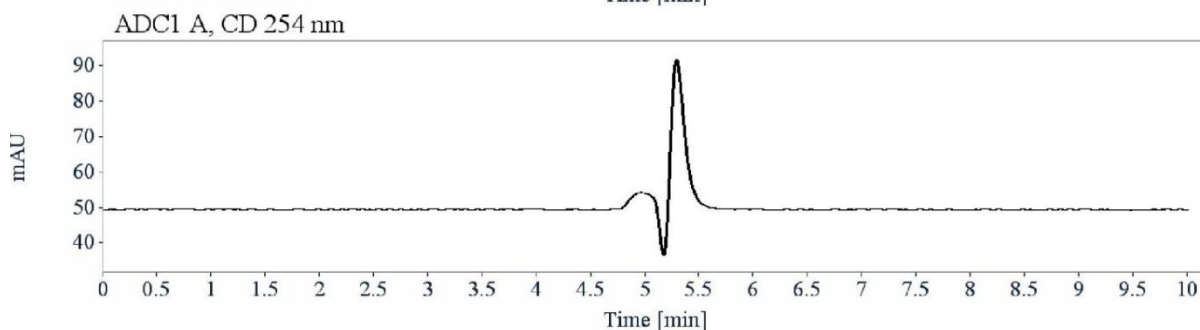
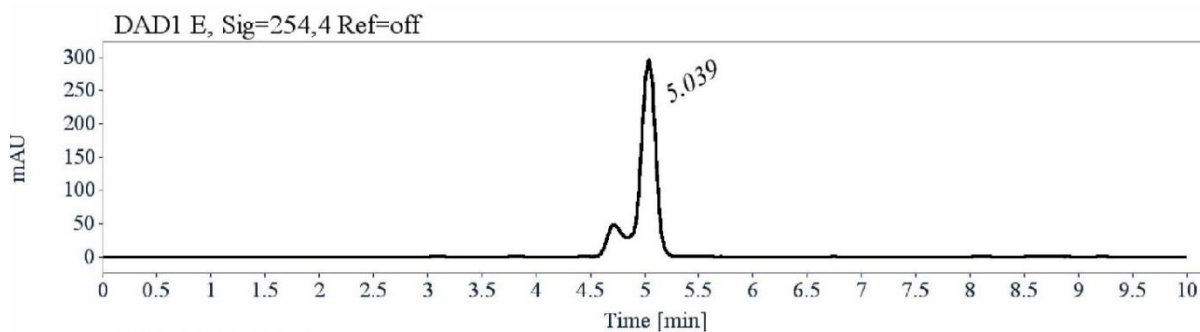
RT [min]	Area	Area%	Capacity Factor	Enantioselectivity	Resolution (USP)
5.13	1589	49.94	0.74		
5.76	1593	50.06	0.95	1.29	3.68
Sum	3182	100.00			

Data file: C:\CHEM32\1\DATA\ACHERAR\SA2\SA2_LUXA1_8.D
Injection date: 10/19/2018 6:18:29 PM
Acq. method: E-2-CD254NM.M
Last changed: 1/28/2019 10:13:40 AM
Column void time (min): 2.950

Injection volume: 20.000
Analysis method: E-2-CD254NM.M
Location: Vial 20

Chiral HPLC report

Sample name: SA2
Column: Lux-Amylose-2
Temperature:
Mobile phase: Heptane/ethanol (98/2), 1 mL/min



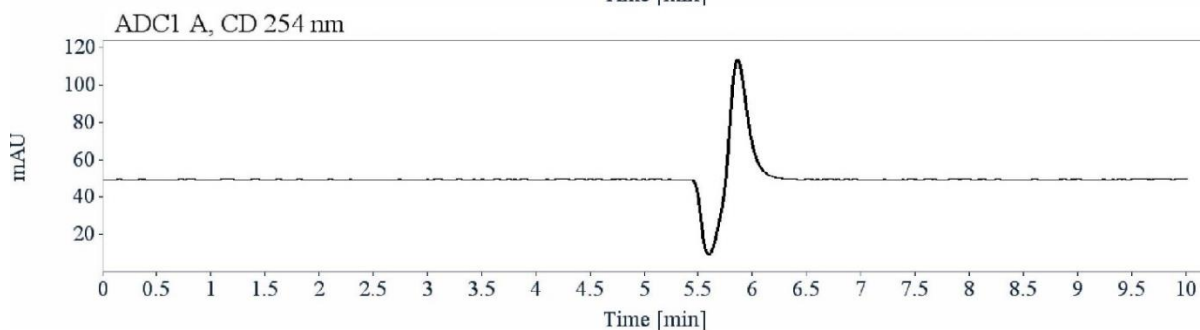
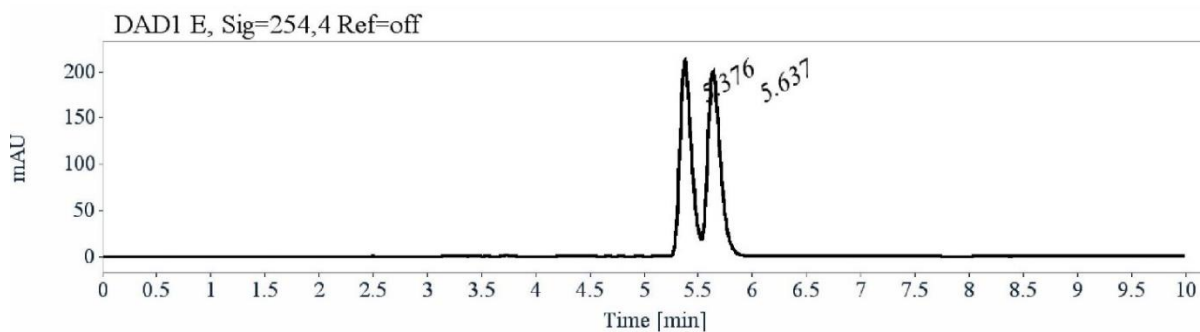
Signal: DAD1 E, Sig=254,4 Ref=off

RT [min]	Area	Area%	Capacity Factor	Enantioselectivity	Resolution (USP)
5.04	2393	100.00	0.71		
Sum	2393	100.00			

Data file: C:\CHEM32\1\DATA\ACHERAR\SA2\SA2_LA2_8.D
Injection date: 10/19/2018 6:41:57 PM **Injection volume:** 20.000
Acq. method: E-2-CD254NM.M **Analysis method:** E-2-CD254NM.M
Last changed: 1/28/2019 10:13:40 AM **Location:** Vial 20
Column void time (min) 2.950

Chiral HPLC report

Sample name: SA2
Column: Chiralpak AZ-H
Temperature:
Mobile phase: Heptane/ethanol (98/2), 1 mL/min



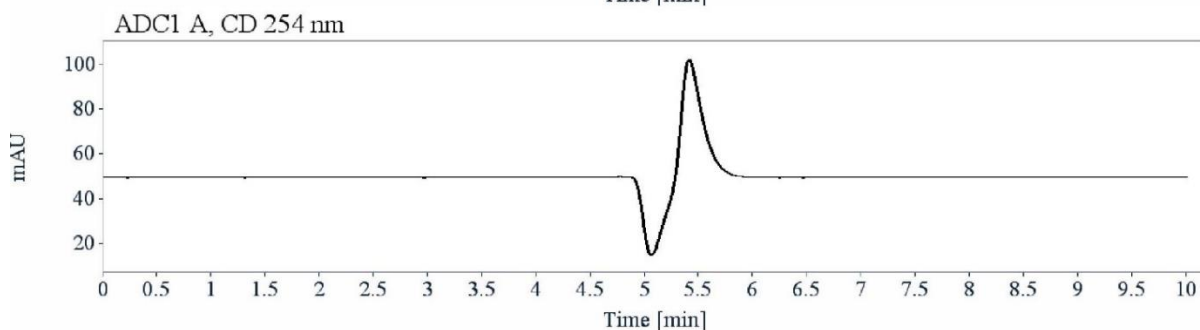
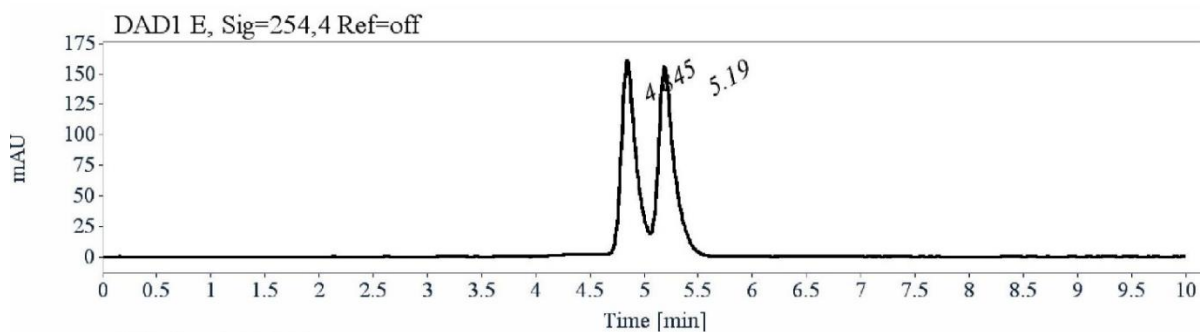
Signal: DAD1 E, Sig=254,4 Ref=off

RT [min]	Area	Area%	Capacity Factor	Enantioselectivity	Resolution (USP)
5.38	1563	48.80	0.82		
5.64	1641	51.20	0.91	1.11	1.28
Sum	3204	100.00			

Data file: C:\CHEM32\1\DATA\ACHERAR\SA2\SA2_AZH_8.D
Injection date: 10/19/2018 7:05:26 PM **Injection volume:** 20.000
Acq. method: E-2-CD254NM.M **Analysis method:** E-2-CD254NM.M
Last changed: 1/28/2019 10:13:40 AM **Location:** Vial 20
Column void time (min): 2.950

Chiral HPLC report

Sample name: SA2
Column: Chiralpak IA
Temperature:
Mobile phase: Heptane/ethanol (98/2), 1 mL/min



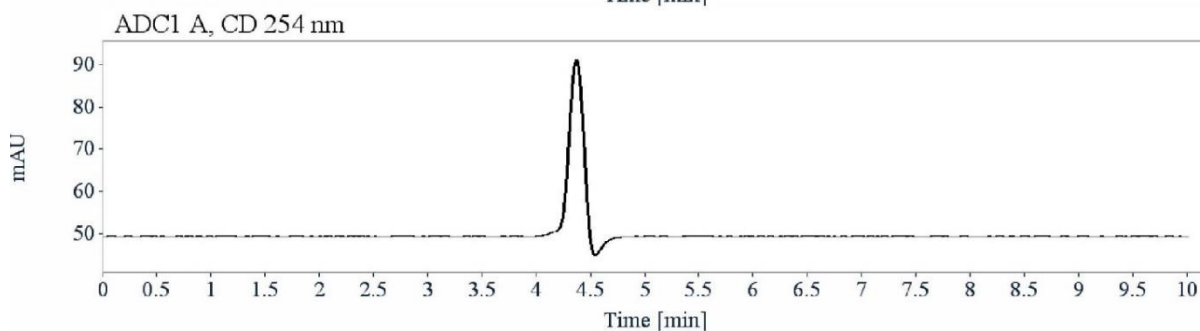
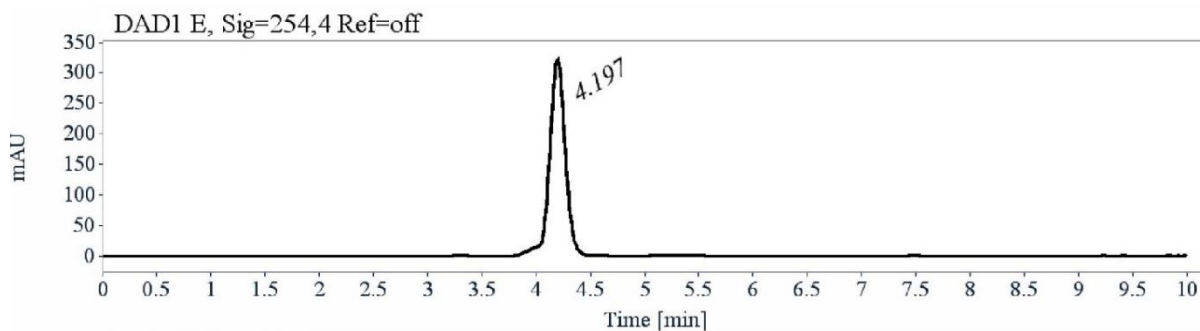
Signal: DAD1 E, Sig=254,4 Ref=off

RT [min]	Area	Area%	Capacity Factor	Enantioselectivity	Resolution (USP)
4.84	1608	49.74	0.64		
5.19	1624	50.26	0.76	1.18	1.40
Sum	3232	100.00			

Data file: C:\CHEM32\1\DATA\ACHERAR\SA2\SA2_IA_8.D
Injection date: 10/19/2018 7:52:27 PM **Injection volume:** 20.000
Acq. method: E-2-CD254NM.M **Analysis method:** E-2-CD254NM.M
Last changed: 1/28/2019 10:13:40 AM **Location:** Vial 20
Column void time (min): 2.950

Chiral HPLC report

Sample name: SA2
Column: Chiralpak IB
Temperature:
Mobile phase: Heptane/ethanol (98/2), 1 mL/min



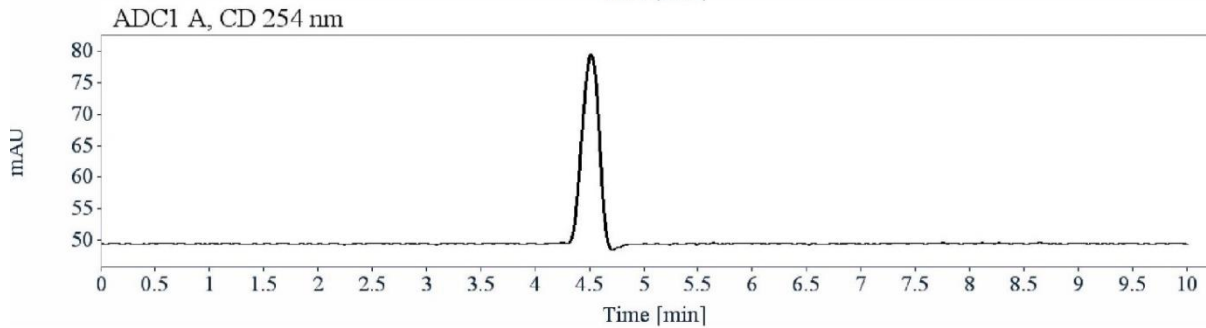
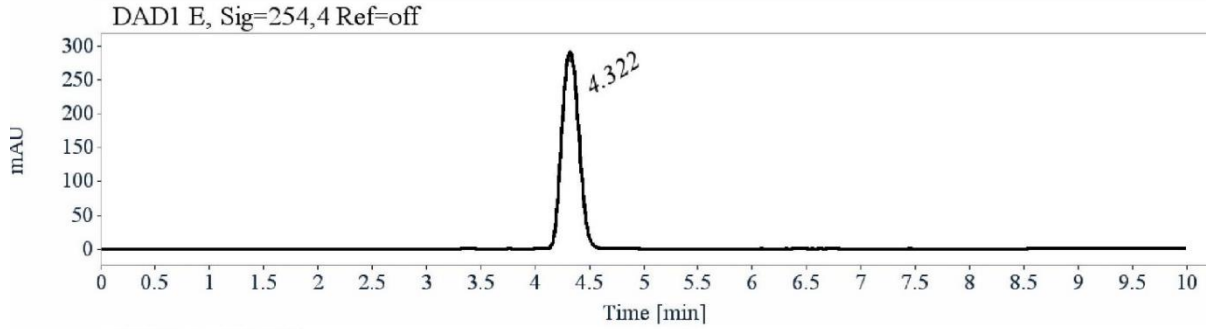
Signal: DAD1 E, Sig=254,4 Ref=off

RT [min]	Area	Area%	Capacity Factor	Enantioselectivity	Resolution (USP)
4.20	3254	100.00	0.42		
Sum	3254	100.00			

Data file: C:\CHEM32\1\DATA\ACHERAR\SA2\SA2_IB_8.D
Injection date: 10/19/2018 8:15:59 PM **Injection volume:** 20.000
Acq. method: E-2-CD254NM.M **Analysis method:** E-2-CD254NM.M
Last changed: 1/28/2019 10:13:40 AM **Location:** Vial 20
Column void time (min): 2.950

Chiral HPLC report

Sample name: SA2
Column: Chiralpak IC
Temperature:
Mobile phase: Heptane/ethanol (98/2), 1 mL/min



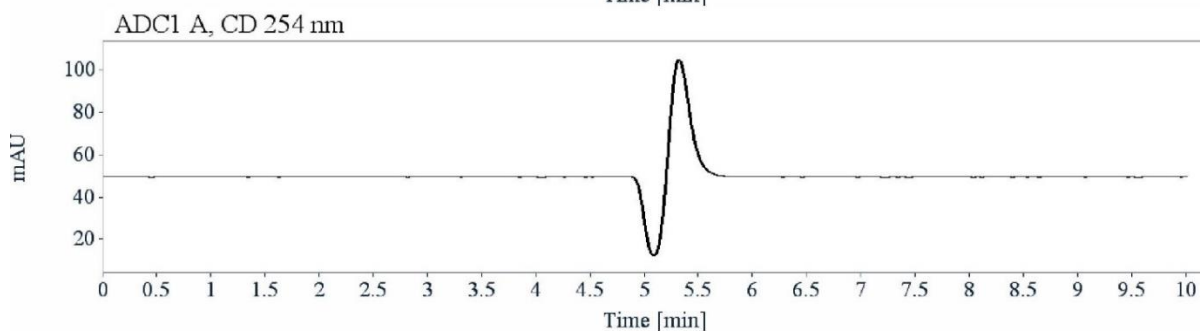
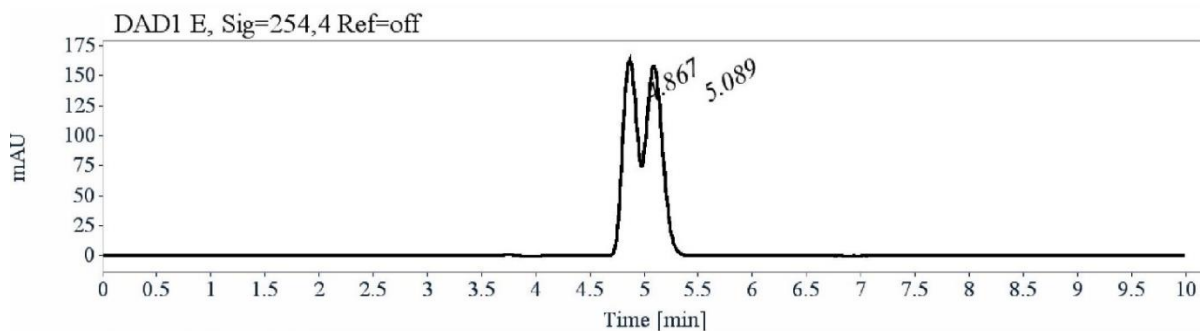
Signal: DAD1 E, Sig=254,4 Ref=off

RT [min]	Area	Area%	Capacity Factor	Enantioselectivity	Resolution (USP)
4.32	3227	100.00	0.46		
Sum	3227	100.00			

Data file: C:\CHEM32\1\DATA\ACHERAR\SA2\SA2_IC_8.D
Injection date: 10/19/2018 8:39:27 PM
Acq. method: E-2-CD254NM.M
Last changed: 1/28/2019 10:13:40 AM
Column void time (min): 2.950
Injection volume: 20.000
Analysis method: E-2-CD254NM.M
Location: Vial 20

Chiral HPLC report

Sample name: SA2
Column: Chiralpak ID
Temperature:
Mobile phase: Heptane/ethanol (98/2), 1 mL/min



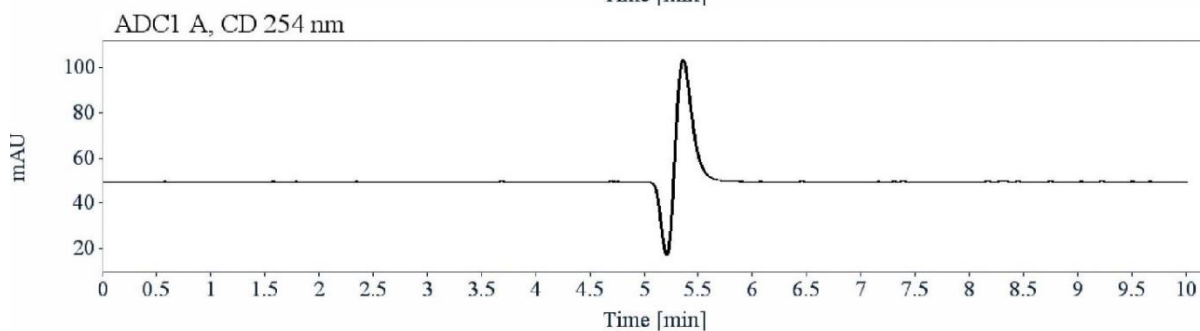
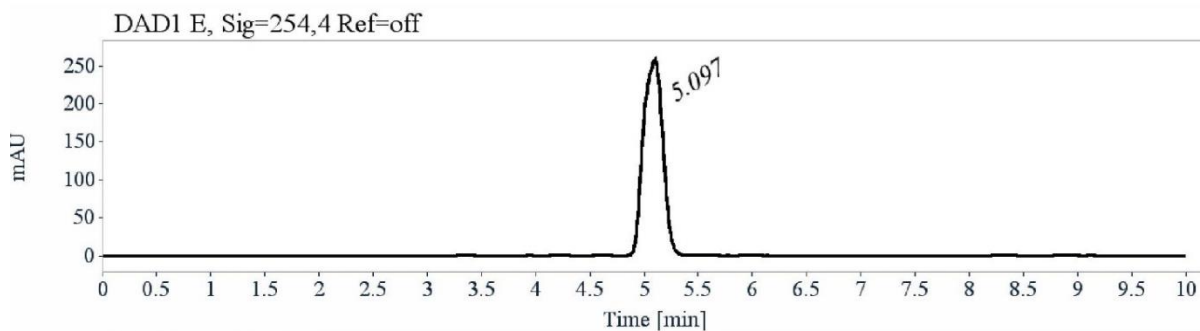
Signal: DAD1 E, Sig=254,4 Ref=off

RT [min]	Area	Area%	Capacity Factor	Enantioselectivity	Resolution (USP)
4.87	1526	46.98	0.65		
5.09	1722	53.02	0.73	1.12	0.76
Sum	3248	100.00			

Data file: C:\CHEM32\1\DATA\ACHERAR\SA2\SA2_ID_8.D
Injection date: 10/19/2018 9:02:57 PM **Injection volume:** 20.000
Acq. method: E-2-CD254NM.M **Analysis method:** E-2-CD254NM.M
Last changed: 1/28/2019 10:13:40 AM **Location:** Vial 20
Column void time (min) 2.950

Chiral HPLC report

Sample name: SA2
Column: Chiralpak IE
Temperature:
Mobile phase: Heptane/ethanol (98/2), 1 mL/min



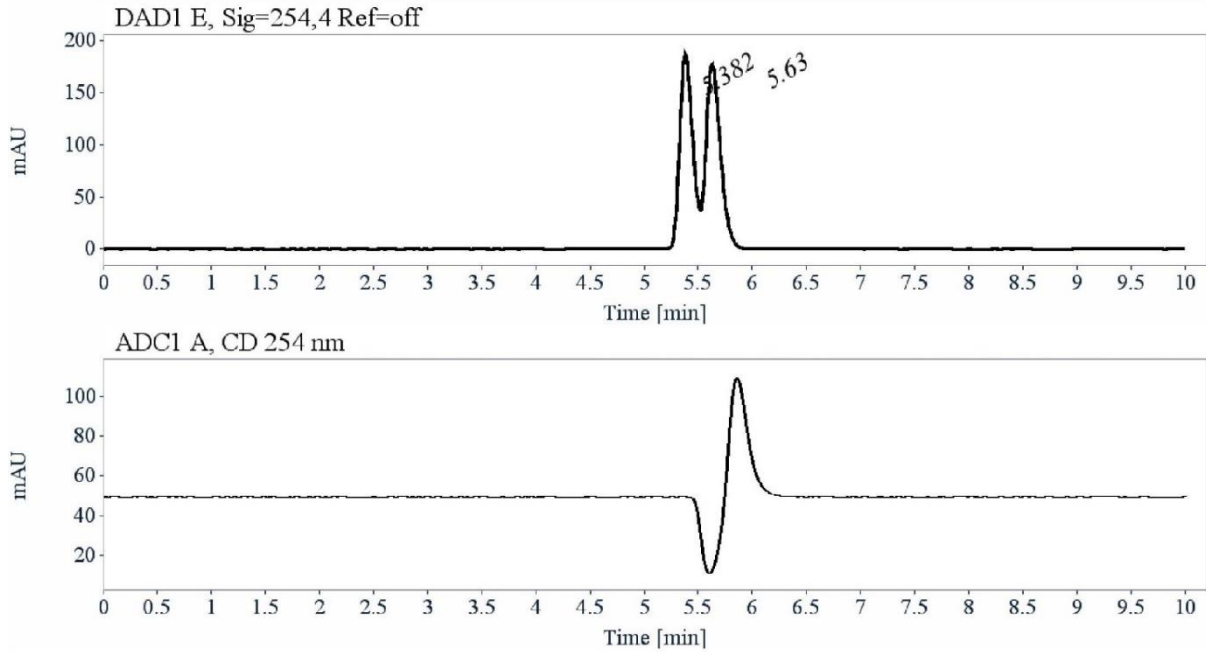
Signal: DAD1 E, Sig=254,4 Ref=off

RT [min]	Area	Area%	Capacity Factor	Enantioselectivity	Resolution (USP)
5.10	3248	100.00	0.73		
Sum	3248	100.00			

Data file: C:\CHEM32\1\DATA\ACHERAR\SA2\SA2_IE_8.D
Injection date: 10/19/2018 9:26:27 PM
Acq. method: E-2-CD254NM.M
Last changed: 1/28/2019 10:13:40 AM
Column void time (min): 2.950
Injection volume: 20.000
Analysis method: E-2-CD254NM.M
Location: Vial 20

Chiral HPLC report

Sample name: SA2
Column: Chiralpak IF
Temperature:
Mobile phase: Heptane/ethanol (98/2), 1 mL/min



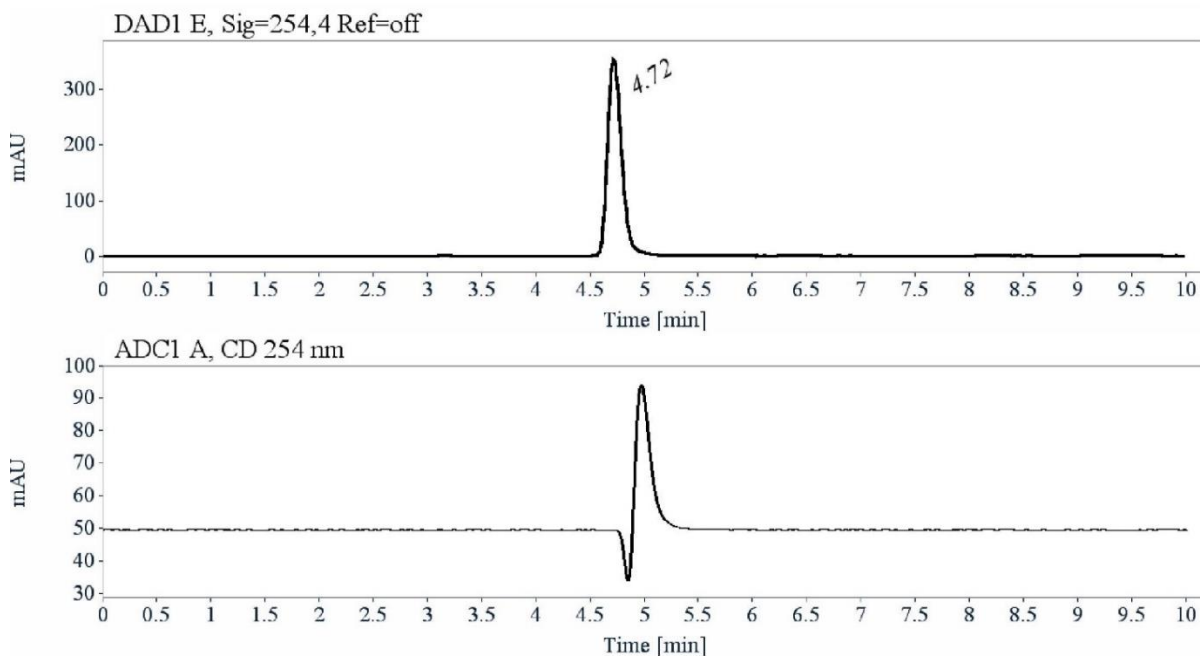
Signal: DAD1 E, Sig=254,4 Ref=off

RT [min]	Area	Area%	Capacity Factor	Enantioselectivity	Resolution (USP)
5.38	1561	48.30	0.82		
5.63	1671	51.70	0.91	1.10	1.04
Sum	3232	100.00			

Data file: C:\CHEM32\1\DATA\ACHERAR\SA2\SA2_IF_8.D
Injection date: 10/19/2018 9:49:57 PM **Injection volume:** 20.000
Acq. method: E-2-CD254NM.M **Analysis method:** E-2-CD254NM.M
Last changed: 1/28/2019 10:13:40 AM **Location:** Vial 20
Column void time (min): 2.950

Chiral HPLC report

Sample name: SA2
Column: (S,S)-Whelk-O1
Temperature:
Mobile phase: Heptane/ethanol (98/2), 1 mL/min



Signal: DAD1 E, Sig=254,4 Ref=off

RT [min]	Area	Area%	Capacity Factor	Enantioselectivity	Resolution (USP)
4.72	3271	100.00	0.60		
Sum	3271	100.00			

Data file: C:\CHEM32\1\DATA\ACHERAR\SA2\SA2_WHELK_8.D
Injection date: 10/19/2018 10:36:57 PM **Injection volume:** 20.000
Acq. method: E-2-CD254NM.M **Analysis method:** E-2-CD254NM.M
Last changed: 1/28/2019 10:13:40 AM **Location:** Vial 20
Column void time (min): 2.950

SYNTHESIS OF ENANTIOPURE 3,4-DIHYDRO-2H-1,4-BENZOXAZINE ANALOGUES FOR POTENTIAL BIOLOGICAL APPLICATION

Key words: 1,4-benzoxazine, enantioselective synthesis, chiral HPLC, racemization, pseudopeptides, conformational analysis

This work describes the synthesis and conformational analysis of enantiopure 1,4-benzoxazine-based pseudodipeptides and pseudotripeptides.

Enantiomers of ethyl 2,3-dibromopropionate and ethyl 3,4-dihydro-2H-1,4-benzoxazine-2-carboxylate are obtained by two strategies (i) *via* enantioselective synthesis and (ii) *via* preparative HPLC enantioseparation of racemate on multigram scale. Because of the racemization process during the enantioselective synthesis, preparative HPLC enantioseparation on racemates are successfully applied to afford enantiomers with high enantiomeric purities ($ee \geq 99.5\%$). Both enantiomers of the 1,4-benzoxazine compound are used to design new 1,4-benzoxazine-based pseudopeptides *via* peptide coupling reactions on C- and N-terminal extremities. Their conformational behaviour in solution and solid states are investigated by spectroscopic (IR, NMR) and X-Ray diffraction analyses. The results indicate (i) a predominant C₅ pseudocycle involving a lone pair of electrons of oxygen in 1,4-benzoxazine ring with NH group from C-extremity elongation and (ii) a slight influence of the absolute configuration at C2 position of 1,4-benzoxazine scaffold and the side chains of amino acids.

SYNTHÈSE D'ANALOGUES 3,4-DIHYDRO-2H-1,4-BENZOXAZINE ÉNANTIOPURES POUR DES APPLICATIONS BIOLOGIQUES POTENTIELLES

Mots clés : 1,4-benzoxazine, synthèse énantiosélective, HPLC chirale, racémisation, pseudopeptides, analyse conformationnelle

Ce travail décrit la synthèse et l'analyse conformationnelle de pseudodipeptides et pseudotripeptides à base d'un motif 1,4-benzoxazinique énantio pur.

Les énantiomères du 2,3-dibromopropionate d'éthyle et du 3,4-dihydro-2H-1,4-benzoxazine-2-carboxylate d'éthyle sont obtenus par deux stratégies (i) synthèse énantiosélective et (ii) énantioséparation des racémiques par HPLC préparative à l'échelle du multigramme. En raison de processus de racémisation au cours des synthèses énantiosélectives, l'énantioséparation des racémiques par HPLC préparative est réalisée avec succès pour accéder aux différents énantiomères avec une pureté énantiomérique élevée ($ee \geq 99,5\%$). Les deux énantiomères du composé 1,4-benzoxazine sont utilisés pour concevoir de nouveaux pseudopeptides à base d'un motif 1,4-benzoxazinique *via* des réactions de couplage peptidique au niveau des extrémités C- et N-terminales. Leur préférence conformationnelle en solution et à l'état solide sont étudiées par analyses spectroscopiques (IR, RMN) et diffraction des rayons X. Les résultats indiquent (i) la prédominance d'un pseudocycle C₅ impliquant un doublet non liant de l'oxygène du cycle 1,4-benzoxazinique avec un groupement NH au niveau de l'élongation de l'extrémité C-terminale et (ii) une légère influence de la configuration absolue en position C2 sur le motif 1,4-benzoxazinique et des chaînes latérales des acides aminés.